Durham E-Theses

In vivo stability of radiolabelled macrocycle complexes

Royle, Louise

IN VIVO STABILITY OF RADIOLABELLED

MACROCYCLE COMPLEXES.

by

Louise Royle, B.Sc.(Hons.)

University of Manchester.

A Thesis submitted for the degree of

Doctor of Philosophy at the University of Durham

Department of Chemistry.

1995

DECLARATION

The content of this thesis represents the work of the author unless indicated otherwise or acknowledged by reference. This thesis describes work carried out in the Department of Chemistry of the University of Durham and the Medical Research Council Radiobiology Unit, Didcot, Oxon., between October 1992 and June 1995. It has not been submitted for a higher degree in any other academic institution.

STATEMENT OF COPYRIGHT

The copyright of this thesis rests with the author. No quotation from it should be published without her prior written consent and information derived from it should be acknowledged.

DEDICATION

This thesis is dedicated to Liz and Ron Warburton.

ACKNOWLEDGEMENTS

IN VIVO STABILITY OF RADIOLABELLED MACROCYCLE COMPLEXES.

ABSTRACT

The gadolinium (^{153}Gd) complexes of 21 aza-phosphinic and aza-carboxylic acid macrocycles based on 1,4,7,10-tetraazacyclododecane were studied as possible contrast agents for magnetic resonance imaging. The acid dissociation rates and partition coefficients of gadolinium complexes were measured and related to their in vivo stability and route of elimination in mice. The anionic aza-phosphinic acids had low acid dissociation rates (24-78 x 10^{-6} sec^{-1} at pH 1) which correlated with high in vivo stability (<0.025% dose in the skeleton at 24 hours). [Gd.12N4P4Bz4]$^-$ shows potential as a gall bladder, bile duct contrast imaging agent at doses of 0.1 to 10 μmol/kg , and for tumour detection within the hepatobiliary system at doses of 100 to 200 μmol/kg .

Macrocycles based on 1,4,7,10-tetraazacyclododecane can be used to complex yttrium (^{90}Y) for tumour therapy. ^{90}Y complexes of aza-phosphinic and aza-carboxylic acid derivatives showed slow acid catalysed dissociation rates of 1-14 x 10^{-6} sec^{-1} at pH 1, and rapid association kinetics of greater than 80% yttrium uptake within 30 minutes at 5 μM ligand. A tetraaza-carboxylic acid and a tri-phosphinic acid derivative modified with maleimide were linked to monoclonal antibodies and labelled with ^{90}Y. Both were highly stable in vivo with <0.01% ^{90}Y dose in the mouse femur shaft at 48 hours.

Seven aza-phosphinic and aza-carboxylic acid macrocycles based on 1,4,7,-triazacyclononane were labelled with radioactive gallium or indium. Gallium complexes were generally more stable in vivo than the corresponding indium complexes. Three ^{67}Ga and two ^{111}In complexes showed potential as imaging agents and one gallium complex as a hepatobiliary imaging agent. Several complexes were examined as possible tumour localisation agents, [Ga.9N3] giving a tumour to blood ratio of 22:1 at 4 hours after injection.

LOUISE ROYLE (1995).

ABBREVIATIONS

12N4, (DOTA)	1,4,7,10-tetraazacyclododecane-N,N^1,N^2,N^3-tetraacetic acid
9N3, (NOTA)	1,4,7-triazacyclononane-N,N^1,N^2-triacetic acid
EDTA	Ethylenediamine-tetraacetic acid
DTPA	Diethylenetriamine-pentaacetic acid
CaDTPA	DTPA cyclic anhydride
CT	Computed tomography
MRI	Magnetic resonance imaging
NMR	Nuclear magnetic resonance
SPECT	Single photon emission computerised tomography
PET	Positron emission tomography
HPLC	High performance liquid chromatography
PBS	Phosphate buffered saline pH 7.4
BSP	Bromosulphophthalein
NMG	N-methylglucamide
McAb	Monoclonal antibody
$t^1/_2$	Physical half life
α	Alpha particle
β^-	Beta particle or electron
β^+	Positron
γ	Gamma photon
Ci	Curie, equivalent to 3.7×10^{10} becquerels

CONTENTS

FIGURES AND TABLES CONTENTS.

CHAPTER ONE

INTRODUCTION

1.1 MEDICAL IMAGING.

Medical imaging is used to study human internal organs and to demonstrate pathological lesions. The most basic imaging technique involves X-rays. It is 100 years since Roentgen first discovered the X-ray, and simple radiography is still the most routinely used imaging technique today. However, the last 40 years have seen great advances in medical imaging techniques with the introduction into clinical practice of radioisotope imaging in the 1950s, ultrasound in the 1960s, computed tomography (CT) in the 1970s and magnetic resonance imaging (MRI) in the 1980s[1].

All of these imaging techniques rely in one way or another on electromagnetic radiation:-

1. **X-rays.** The simple X-ray image is produced by passing externally produced X-rays through a patient onto a photographic plate. The visibility of structures depends on their absorption of X-rays. Calcified tissues such as bone absorb X-rays most strongly and therefore show up white on the photographic plate.

2. **Radioisotope imaging.** The radioisotope is detected by virtue of the gamma photons which it emits during radioactive decay. The imaging method depends on certain radiolabelled substances concentrating in particular parts of the body. This can be a simple chemical form of the radioisotope e.g. iodine concentrates in the thyroid when injected as iodide. However the radioisotope is usually attached to a pharmaceutical the chemistry of which determines the fate of the radiolabel in vivo.

3. **Ultrasound.** Images are produced following the passage of high frequency sound waves through the body. When these waves encounter an object or a surface of different density, they are reflected. This reflected echo is detected, converted to an electrical signal and an image is constructed.

4. **Computed Tomography.** CT relies on externally produced X-rays which are picked up by gas or crystal detectors which are much more sensitive than simple photographic plates. A far higher resolution of different density tissues is obtained than from a conventional X-ray image. Sophisticated computing tomography methods are employed to construct high resolution 2-dimensional images of slices through the body.

5. **Magnetic Resonance Imaging.** MRI is based on the fact that certain nuclei behave like tiny magnets. The most abundant of these nuclei in the human body are the protons in water. A strong magnetic field is applied externally to the body causing all these protons to align in the same direction. A pulse of radio waves is then applied at the appropriate frequency to cause the protons to be displaced from alignment with the field. When the radiofrequency pulse is stopped, the nuclei realign and emit the absorbed radiofrequency. This radio-signal is then detected, the intensity of the signal being proportional to the concentration of protons. This allows an image to be constructed mapping the water content of tissues. MRI uses similar computing methods to CT to construct 2-dimensional slices through the body.

The techniques of MRI and radioisotope imaging along with radioisotope therapy will be dealt with in greater detail in the following sections.

1.2. RADIOACTIVITY.[2,3]

Radioactive isotopes are those isotopes which possess an unstable ratio of protons to neutrons. The isotope decays to a stable configuration by emitting energy in the form of charged particles, electromagnetic radiation or both. This emitted radiation may be:-

(i) Alpha particles. These consist of 2 neutrons and 2 protons. Alpha-particles are heavy, slow moving, densely

3

ionising radiation capable of inflicting severe biological damage.

(ii) Beta particles. These are energetic electrons (β^-) or positrons (β^+). Beta particles are less dense than alpha-particles, consequently they can penetrate tissue further and deliver their dose over a longer range. Positrons have a range in tissue similar to that of electrons of the same energy, but at the end of its path the positron combines with an electron (annihilates) and two 511 keV γ-rays are created.

(iii) Auger electrons[4]. These electrons are sometimes emitted from an atom due to the filling of a vacancy in an inner electron shell after the process of electron capture or internal conversion, they lose their energy over a very short range(nm to a few μm).

(iv) Gamma rays or X rays. These are electromagnetic, not particle radiations. They can travel much further distances than charged particles, with little dose loss to their surroundings. Gamma rays can be produced along with any particle radiation or alone from electron capture (where a proton captures an orbital electron and is thereby converted into a neutron), or from an internal transition (this is the decay of a nucleus from an excited state).

1.2.1. Radioisotopes for Imaging

For diagnostic imaging the following properties are desirable of a radionuclide :-

1. Emission of γ-rays in high abundance
2. The γ-rays should be of sufficient energy to penetrate the body, but low enough in energy to allow for efficient detection, (100 to 300 keV)[5]
3. Have a low abundance (preferably zero) of particle emissions in order to minimise the radiation dose to the patient.
4. Have a short half life in order to keep the radiation dose to a minimum.

4

5. Have a sufficiently long half life to permit time for the radiolabelling, injection and targeting of the pharmaceutical.
6. Decay to a stable daughter product.
7. Be cheap and readily available
8. Be carrier free
9. Possess chemical properties which permit attachment to pharmaceuticals.

Table 1.1 lists some radioisotopes which have γ-emissions suitable for imaging. The most widely used isotope is ^{99m}Tc, its γ-emission being ideal for detection by an Anger camera. ^{99m}Tc labelled pharmaceuticals are used for imaging brain, liver, lung, skeleton, thyroid, kidneys and heart tissues[5,6]. However the 6 hour half life of ^{99m}Tc is too short for the labelling of pharmaceuticals which require lengthy preparation or those which take time to target within the body (e.g. radiolabelled antibodies). This is where the longer half life ^{111}In and ^{67}Ga isotopes prove useful. Both ^{111}In and ^{67}Ga emit abundant γ-rays suitable for imaging and have different chemical properties from technetium, making them more attractive candidates for pharmaceutical labelling.

^{131}I has been widely used for imaging, but its physical properties are not ideal. The beta emission giving a high patient dose, the gamma emissions being too energetic for efficient counting, and a long half life of 8 days. ^{123}I is more suitable for imaging of the thyroid, having an appropriate γ emission and short 13 hour half life. Iodine has been used for labelling pharmaceuticals but these are susceptible to dehalogenation in vivo.

The isotopes ^{64}Cu, ^{82}Rb and ^{68}Ga are all positron emitters suitable for PET imaging. The dose to the patient from the positron is usually outweighed by the production of a high definition image. The short half lives of ^{82}Rb and ^{68}Ga make them unsuitable for the labelling of pharmaceuticals which take a long time to prepare or to localise in the target tissue.

5

Table 1.1. *Radioisotopes for Imaging*[3,7,8]

Isotope	Half life	Type of decay	Average particle energy* MeV (%)	Principle gamma energies MeV (%)	Method of production
^{99m}Tc	6 hr	I.T.		0.141 (89)	Generator
^{123}I	13 hr	E.C.		0.159 (83)	Cyclotron
^{111}In	67 hr	E.C.		0.171 (91) 0.245 (94)	Cyclotron
^{67}Ga	78 hr	E.C.		0.093 (38) 0.185 (21) 0.300 (17)	Cyclotron
^{131}I	193 hr	β^-	0.19 (89)	0.080 (3) 0.284 (6) 0.364 (81)	Reactor
^{64}Cu	13 hr	β^- β^+ E.C. (41%)	0.19 (37) 0.28 (18)	 0.511 (36) 1.346 (0.5)	Reactor
^{82}Rb	75 min	β^+ E.C. (4%)	1.16 (12) 1.52 (83)	0.511 (191) 0.777 (13)	Generator
^{68}Ga	68 min	β^+ E.C. (10%)	0.35 (1) 0.84 (88)	0.511 (178) 1.077 (3)	Generator

I.T.= Isomeric transition from upper to lower isomeric state.

E.C.= Orbital electron capture.

* The average beta particle energy is about a third of its maximum.

1.2.2. Radioimaging Techniques.

Single Photon Emission Tomography (SPECT)[9,10].

A SPECT image of the distribution of a gamma emitting radioisotope within a patient is obtained by means of an Anger camera (also known as a gamma or scintillation camera). The gamma radiation needs to be of sufficient energy to

penetrate body tissues, but of low enough energy to be detected by the Anger camera. Thus gamma energies in the range 100 to 300 keV are the most suitable for imaging[11]. An Anger camera consists of a 0.25 to 0.5 inch thick NaI(Tl) crystal in front of an array of photomultiplier tubes. When a gamma photon strikes the NaI(Tl) crystal, a photon of light is produced which is then amplified in the photomultiplier tubes and counted as an electrical pulse. The Anger camera detects the radiation from the whole field simultaneously. Spatial resolution is provided by the use of multiple photomultiplier tubes, the tube nearest the incident gamma radiation producing the largest signal.

In order to limit gamma photons from outside the field of view entering the detector, a collimator is employed. A collimator ensures that only gamma photons arising from the field of view and travelling parallel to the axis of the collimator reach the detector. Collimators therefore increase the definition of the image, but at the expense of sensitivity. The sensitivity and resolution of the Anger camera is also depth dependent as the gamma photons are absorbed and scattered by body tissue (the number of gamma photons with an energy of 100 keV reaching the detector is halved by 5 cm of tissue[11]). Thus the ability to detect small or low contrast structures is reduced with depth, the effective resolution of SPECT is about 1 cm.

In order to obtain a three-dimensional image, the Anger camera is mounted on a gantry which rotates longitudinally around the patient at 3 to 10° increments. This allows slices through the patient to be imaged from many angles then, by the process of computerised tomography, these images can be reconstructed into a three-dimensional image. By mounting up to three cameras on the gantry, several projections can be monitored simultaneously thereby reducing the total imaging time.

Positron Emission Tomography (PET)[9,12,13].

Positrons travel only a short distance in the body before being annihilated by an electron. This process results in the emission of two 511 keV gamma photons at 180° to each other. It is the production of these two anti-parallel photons which endows PET with its ability to produce such high resolution images.

To detect these annihilation photons, a pair of scintillation detectors (NaI, BaF_2, or $Bi(GeO_4)_3$)[14] are mounted in coincidence mode on opposite sides of the patient. Only photons which are recorded by both detectors simultaneously are accepted for imaging. This coincident detection acts as a sort of collimator, as only information from unattenuated radiation is processed. The result is that the sensitivity and resolution in the field of view does not vary with depth. By mounting pairs of detectors in a ring or hexagonal array around the patient, the sensitivity is increased. The information gathered by this array of detectors is then processed by computers and a tomographic three-dimensional image of a slice through a patient is produced. As no physical collimator is needed with PET, a resolution of 3 to 5 mm is obtained in all directions[14]. This resolution is greater than with SPECT.

The only disadvantage of PET over SPECT is the radiation dose to the patient. As positrons are particulate radiation they deposit a large amount of energy at their source in tissue before they are annihilated. However the increased sensitivity and resolution gained from the use of PET has to be weighed up against this.

1.2.3. Radioisotopes for Therapy.[8,15-18]

Many of the previously listed desirable properties of radioisotopes for imaging (section 1.2.1) are also applicable to therapy. Radioisotopes for therapy are also required to:- decay to a stable daughter product; be readily available and not too expensive; be carrier-free; and to have chemical

properties which permit attachment to pharmaceuticals. The major difference between isotopes used in therapy and imaging, is the requirement in therapy of a large component of particle radiation capable of delivering a high localised radiation dose with little or no accompanying gamma radiation. However the presence of a small percentage of gammas can be useful for monitoring the location of the therapeutic isotope within the patient.

In therapy the half life of the isotope needs to be such that the major part of the radiation dose is delivered during the residence time of the labelled pharmaceutical in the target tissue. The choice of particle emission and its range in tissue will vary depending on the type of tumour being treated. Cancerous tissue can exist as large masses (g-kg), or as small nodules (mg), or as single cells from metastatic tumours or cancers of the haemopoetic system such as leukaemia. A list of some radioisotopes suitable for therapy is given in table 1.2. These isotopes are listed according to their type of decay particle and estimated range in soft tissue.

Radionuclides for therapy fall into three major categories:- beta-emitters, alpha-emitters, and Auger electron emitters. These different types of radiation have different ranges and intensities of energy deposition (the energy deposition is measured as linear energy transfer or LET). Beta-particles have the longest range, the beta-emitters listed in table 1.2 have average ranges of 0.1 to 3.9 mm. Alpha particles have shorter ranges of ~50 to 90 μm, and a high LET of ~100 KeV/μm. Because of its high LET an alpha-particle can cause irreparable damage to any DNA through which it passes by causing double strand breaks. It is estimated that only 3 to 6 hits per cell nucleus are needed to reduce the percentage of surviving cells by 73%[15]. The lower LET of beta-particles (~0.2 KeV/μm) means that about 400 times more hits are required per cell nucleus to produce the same effect. To be effective in therapy, an alpha-emitter needs to be attached to every cell, but because of their short range, non-specific irradiation of distant

tissues is eliminated. Thus, alpha-emitters are best suited
to the treatment of single cells or small tumour masses. The

Table 1.2. *Radioisotopes for Therapy*[7]

Isotope	Half life	Type of decay	Average particle energy* MeV (%)	Principle photon energies MeV (%)	Method of production	Mean range in tissue
^{90}Y	64 hr	β^-	0.94 (100)	none	Generator	3.9 mm
^{188}Re	17 hr	β^-	0.73 (25) 0.79 (72)	0.155 (15)	Generator	3.3 mm
^{186}Re	89 hr	β^-	0.31 (21) 0.36 (76)	0.137 (9)	Reactor	1.1 mm
^{111}Ag	179 hr	β^-	0.36 (93)	0.245 (1) 0.342 (7)	Reactor	1.1 mm
^{109}Pd	13.4hr	β^-	0.36 (100)	0.088 (4)	Reactor	1.1 mm
^{77}As	39 hr	β^-	0.23 (97)	0.239 (1.6) 0.250 (0.4) 0.521 (0.6)	Cyclotron	0.5 mm
^{131}I	193 hr	β^-	0.19 (89)	0.080 (3) 0.284 (6) 0.364 (81)	Reactor	0.4 mm
^{161}Tb	166 hr	β^-	0.14 (23) 0.15 (67) 0.18 (10)	0.026 (22) 0.049 (17) 0.075 (10)	Reactor	0.3 mm
^{177}Lu	161 hr	β^-	0.05 (12) 0.11 (9) 0.15 (79)	0.113 (6) 0.208 (11)	Reactor	0.3 mm
^{67}Cu	62 hr	β^-	0.12 (57) 0.15 (22) 0.19 (20)	0.091 (7) 0.093 (16) 0.185 (49)	Cyclotron	0.2 mm
^{199}Au	76 hr	β^-	0.07 (19) 0.08 (66) 0.13 (15)	0.049 (0.3) 0.158 (37) 0.208 (8)	Reactor	0.1 mm
^{212}Bi	1 hr	β^- (64%) α (36%)	0.83 (48) 0.53 (8) 0.23 (3) 0.19 (3) 6.05 (25) 6.09 (10)	0.727 (12) 0.785 (2) 1.621 (3)	Generator	50 to 90 μm
^{211}At	7.2 hr	α (42%) E.C,α(58%)	5.87 (42) 7.45 (58)	0.687 (0.2) 0.079 (21)	Cyclotron	50 to 90 μm

E.C.= Orbital electron capture.

* The average beta particle energy is about a third of its maximum.

longer range of beta-particles is more effective in the treatment of larger tumour masses where the radiopharmaceutical may not have been able to penetrate through the whole mass, or where there is heterogeneity in the uptake of radiopharmaceutical by the tumour cells[15,19].

Auger electrons are high LET radiations[4] which usually only have a very short range in the order of nm to μm. In order to deliver a lethal dose to DNA, the Auger emitter must be within the cell nucleus in very close proximity with the DNA. Auger emitter labelled DNA intercalators[20] are being investigated as possible therapy agents, but the short range of these electrons makes them unsuitable for most radiotherapy applications.

The choice of alpha-emitters suitable for therapy is limited as most are heavy elements which decay to unstable daughters. Suitable alpha emitters are astatine-211 and bismuth-212. Astatine-211 labelled monoclonal antibodies[21] (McAbs) have been use for the treatment of lymphoma in mice[22,23], or as [211]At-methylene blue in the treatment of metastatic melanoma in mice[24]. Bismuth-212 labelled McAbs[25,26] have been used to treat human lymphoma xenografts in mice[27] and acsitic tumours in mice[28].

There is a much wider choice of beta-emitters giving more flexibility in choice of particle range, half life and chemistry. The most widely used isotope for radioimmumotherapy to date has been iodine-131. ^{131}I-labelled McAbs have been used to treat patients with lymphoma[29-31] neuroblastoma[32]. and melanoma[33]. This popularity has been due to the ready availability, low cost and ease of chemical labelling. However, ^{131}I is not an ideal isotope for therapy as it has a high yield of gamma radiation, a rather long half life, and iodine labelled pharmaceuticals tend to dehalagonate in vivo giving an even higher non-specific radiation dose.

The introduction of bifunctional complexing agents has opened up the field to the use of radiometal ions as labels for pharmaceuticals. Of these, yttrium-90 has shown the most promise. It is readily available from a strontium-90

generator, has a shorter half life than ^{131}I and is a pure beta emitter with no accompanying gammas. The high energy of its beta particle, with a mean range of 3.9 mm in tissue, makes ^{90}Y suitable for the treatment of tumour masses. Several treatments with ^{90}Y-McAbs of human colonic cancer[34-38], lymphoma[39], hepatoma[40] and glioma[41] xenografts in mice have proved successful. ^{90}Y labelled McAbs are being used in clinical trials on patients with ovarian cancer[42-46], lymphoma[47] and breast cancer[48].

Of the other beta-emitters, ^{186}Re labelled McAbs have produced a partial response in the treatment of metastatic epithelial carcinoma in patients[49], having shown promise in animal therapy experiments[50-52]. Copper-67 labelled McAbs are being used to treat lymphoma patients[53] following successful animal experiments[54-58]. The rest of the isotopes in table 1.2 have not been studied in as much detail:- Rhenium-188 labelled McAbs have been studied for in vivo stability[52]; Palladium-109 McAbs have been shown to target human melanoma xenografts[59]; Lutetium-177 McAbs have been used in therapy in colonic cancer xenografts in mice[60]; and silver-111 is being investigated as a possible label for McAbs[61].

For all of these isotopes used in therapy, the dose limiting factor is proving to be bone marrow toxicity[62]. As free metal ions are known to accumulate in bone tissue, this makes the in vivo stability of any radiolabelled pharmaceutical of paramount importance.

1.2.4. Targeting of Radiopharmacuticals.

The radioisotopes discussed above for imaging and therapy need to be targeted to specific organs or tissues. For successful imaging or therapy, a high target to non-target ratio is needed. So although it is desirable to get as much label as possible in the target tissue, this has to be balanced against the overall pharmacokinetics of the labelled compound. It is important that the labelled pharmaceutical should bind quickly and with high affinity to the target tissue, and that this is followed by rapid clearance from

non-target tissues especially from circulating blood. A few isotopes target specific tissues in their simple chemical forms, for example:- anionic iodine isotopes concentrate in thyroid tissue and are utilised for the imaging and therapy of thyroid cancer[63,64]; and radiometal cations concentrate in bone tissue, strontium-89 (β^-, $t^1/_2$ 51 days) can be used for the relief of pain in metastatic cancer in the bone[65,66]. In order to expand the scope of imaging and therapy, methods of altering the biodistribution and pharmacokinetics of these isotopes need to be developed.

Simple complexes of metals with DTPA or DOTA which are hydrophilic and have an overall negative charge are distributed around the body into the extracellular spaces and then quickly excreted into the urine following intravenous injection[67]. As such, they are used to assess blood flow, to detect any breakdown in the blood-brain barrier which occurs with brain tumours, as well as to assess renal function. Chemically altering the overall charge and lipophilicity of a metal complex can change its route of excretion from renal to hepatobiliary, thus enabling the imaging of liver and gut function. Examples of this are the indium and gallium complexes of HBED and PLED derivatives (figure 4.1), the most lipophilic of these exhibit the most hepatobiliary clearance[68]. Another example of the effect of lipophilicity is with a group of ^{99m}Tc labelled iminoacetic acids. Here, hepatobiliary clearance has been shown to be directly proportional to the natural log of the molecular weight of the complex divided by the molecular charge[69]. The ability of small molecular weight compounds (<400 daltons) to cross the blood-brain barrier has also been related to the lipophilicity of the compound[70]. These examples illustrate that relatively simple changes to the chemistry of the complexing agent can be utilised to target different organs.

A more direct approach to targeting is the use of analogues to naturally occurring biomolecules. [68]Ga-[Desferrioxamine B-Succinyl-(D)Phe[1]]-Octroetide is a somatostatin analogue which is used for the imaging of somatostatin positive tumours[71], and fluorine-18 labelled

oestrodiol is used to assess the presence of oestrogen receptors in breast tumours before treatment with oestrogen-receptor blocking drugs[72] (^{18}F has a half life of 110 min and is imaged by PET).

The most promising approach to targeting so far has been through the use of target specific antibodies. By targeting McAbs to tumour specific antigens such as CEA (carcino-embrionic antigen), AFP (α-fetoprotein), and HCG (human chorionic gonadotropin), the imaging and therapy of tumours should be possible. Selective localisation of an iodine-131 labelled anti-CEA antibody was first demonstrated for xenografts of human colonic cancer in hamsters in 1973[73].Since then, the development of monoclonal antibodies[74] has led to the production of high affinity antibodies which can be raised against specific antigens. This was heralded as 'the magic bullet' for the targeting of cancers. ^{131}I labelled anti-CEA monoclonal antibodies were first use in the clinic in 1981[75], but there have been problems with these 'magic bullets'. Firstly, the tumour specific antigens are rarely truly tumour specific although the tumour has higher concentrations of antigen than normal tissues. Secondly, the whole antibodies are fairly large with molecular weights of about 160,000. These whole antibodies can have problems penetrating throughout a tumour mass, and have a long circulating half life in the blood giving low tumour to blood contrast. Smaller fragments of antibodies which retain the antigen binding capacity of the antibody, can penetrate further into tumour masses, and have a shorter circulating lifetime are currently being investigated. There are also however, problems with patients developing their own immune response to these foreign antibodies which are made from animal proteins. Humanised monoclonal antibodies are being developed to help overcome this immune response. (Other problems are that the iodine label is proving to be unstable in vivo and this dehalagonation leads to increased radiation doses to normal tissues and high background levels in imaging studies). Methods of labelling antibodies with bifunctional complexing agents[76,77] have been developed for use with

radiometals such as ^{111}In, ^{67}Ga and ^{90}Y, which as well as increasing the scope of isotopes which may be used, should also provide much more stable radiolabelled monoclonal antibodies.

1.2.5. In Vivo Stability of Radiolabelled Pharmaceuticals.

When targeting radiolabelled pharmaceuticals it is important that the radiolabel stays attached to the pharmaceutical which is responsible for its targeting properties. If the radiolabel becomes detached, then this leads to a lower target to non-target ratio. This results in increased irradiation of normal tissue and a less clearly defined picture in imaging studies.

The nature of the released radioisotope determines its fate. Dehalogenation of iodinated antibodies leads to a build up of radioactive iodine in the thyroid. But for antibodies with a radiometal label it depends on whether the metal is still attached to the ligand. If the metal-ligand is detached from the antibody intact, then rapid renal clearance is likely to follow thus removing any radioactivity from the body[78]. However, if the metal ion itself becomes dissociated from its ligand, then there will be problems with metal ions concentrating in the bone[79-81] and liver causing radiation damage[78]. For any metal-ligand used in targeting, either as a simple complex or attached to a larger biomolecule such as an antibody, its success is largely dependent on its in vivo stability.

1.2.6. Factors Influencing the In Vivo Stability of Macrocyclic and Acyclic Complexes.

Metal ions such as Ga^{3+} and In^{3+} have small ionic radii (0.62 and 0.80 Å)[82] and form hexadentate complexes[87], whereas metal ions such as Y^{3+} and Gd^{3+} have larger ionic radii (1.02 and 1.05 Å)[82] and prefer to form octadentate complexes[84]. Of the ligands pictured in figure 1.1, 9N3 and EDTA have six donor atoms for forming hexadentate complexes, whereas DOTA

15

and DTPA both have eight donor atoms for forming octadentate complexes. Closed ring macrocycle ligands exhibit size-match selectivity, i.e. the most stable complexes are formed where the size-match between the metal ion and the cavity in the ligand is closest[85], whereas the more flexible acyclic EDTA and DTPA can accommodate a range of ion sizes[86].

Figure 1.1. *Macrocyclic and Acyclic Ligands.*

9N3 (NOTA)	EDTA	DOTA	DTPA
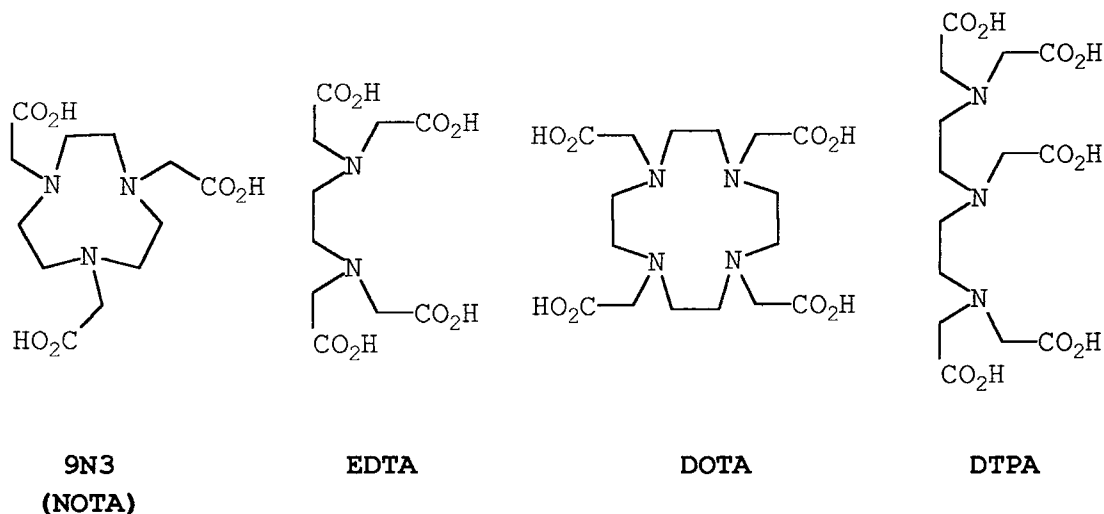
Although all the ligands in figure 1.1 have high thermodynamic stability constants in vitro, the situation in vivo is very different. In an animal these complexes encounter many challenging environments. Amongst these are acid conditions in the stomach, endogenous metal ions such as Zn^{2+}, Ca^{2+}, Mg^{2+} and Cu^{2+} in the plasma[84,87], as well as natural ligands such as citrate, albumin and transferrin[87,88]. These components in principle may all compete with the complex for either the metal ion or the ligand, and in doing so contribute towards dissociation of the complex.

Several thermodynamic considerations can affect the stability of these metal complexes[88-90]. For example, the thermodynamic stability constant (K_{therm}) is a measure of the affinity of the metal ion and ligand for each other[87,91]. However, a better measure of stability under physiological conditions is the conditional stability constant (K_{cond})

which takes into account the pK_a values of the complex and hence the basicity and extent of protonation of the ligand. Even so, the correlation between both these values and in vivo stability of metal complexes is poor[87,92]. A more important consideration is that of transmetallation. This is measured by the selectivity constant (K_{sel}) which measures the selectivity of the ligand for the bound metal over competing endogenous metal ions in the plasma (Zn^{2+}, Ca^{2+}, Mg^{2+} and Cu^{2+})[87].

Although all these thermodynamic parameters contribute towards in vivo dissociation of the complex, it is <u>kinetic</u> considerations which are the main contributors to in vivo stability. Acyclic ligands such as DTPA and EDTA have high rates of transmetallation[87,92] and thermodynamic equilibrium is reached before the complex has been excreted from the body. In this case a correlation holds between K_{sel} and in vivo stability for acyclic ligands[87,82]. However, macrocyclic ligands such as DOTA can have poor selectivity[87] for their complexed metal ion e.g. Gd^{3+} over endogenous ions such as Zn^{2+}, which, from thermodynamic considerations alone, would indicate that they would be susceptible to transmetallation. But this is not the case. Due to the rigid conformational stability of macrocyclic ligands the rate of cation promoted dissociation is extremely slow so there is enough time for in vivo elimination of metal macrocycle complexes to occur before any dissociation takes place[89]. This kinetic factor imparts these macrocyclic complexes with their high in vivo stability.

The in vitro measurement which has been shown to correlate best with the actual in vivo stability of metal-complexes is their acid catalysed dissociation rate (k_{obs})[84,93]. Regions of low pH are encountered in the body particularly in the stomach. Under strongly acidic conditions protonation of the metal-complex occurs. Electrostatic considerations also affect the rate of acid or cation promoted dissociation. A charge neutral complex will protonate at a lower pH than a negatively charged complex,

and should therefore be more resistant towards acid catalysed dissociation[8].

1.3. NUCLEAR MAGNETIC RESONANCE

The basic phenomenon of NMR was discovered in 1946[94,95] and gave rise to NMR spectroscopy. This became a valuable tool for analytical chemistry as well as a means of studying the metabolism of biochemicals in vitro. Magnetic resonance imaging (MRI) emerged in 1980 with the development of instrumentation capable of whole body imaging[96]. This relied on powerful magnets capable of producing stable magnetic field gradients as well as advances in computing methods for tomography.

More recently developments have been made in the use of paramagnetic contrast agents to expand and improve the diagnostic ability of MRI. The first of these agents to be developed was $[Gd-DTPA]^{2-}$, which in 1984 was shown to distribute in extracellular water and to be excreted by the kidneys in rats[97]. $[Gd-DTPA]^{2-}$ was first used clinically in 1981 for liver and brain imaging[98-100]. Since then other more stable contrast agents[101] have been developed, notably $[Gd-DOTA]^-$ which is also in current clinical use. At present there is much interest in the development of contrast agents which can be directed to specific targets e.g. the liver and gastrointestinal tract ($[Gd.BOPTA]^{102}$, $[Mn.DPDP]^{103}$, $[Gd.EOB-DTPA]^{104}$, $[Fe.5-Br-EHPG]^{105}$ and $[Fe.PGDF]^{106}$), calcified soft tissue $(Gd-EDTMP)^{107}$ or tumours (Gd-monoclonal antibodies)[108,109].

The major advantages of MRI over other imaging techniques are that it is non invasive, does not use ionising radiation and is without known hazard.

1.3.1. Principles of Nuclear Magnetic Resonance.[110-113]

All NMR systems measure the characteristic absorption and re-emission of quanta of energy by nuclei in atoms of body

tissues. The nucleus which is most often studied by magnetic resonance imaging (MRI) is the hydrogen atom or proton. Hydrogen is the most abundant element in the human body. The proton can be studied by NMR because it possesses a nuclear spin, which means that it can be considered to behave like a tiny bar magnet.

In the absence of an external magnetic field these tiny magnets are pointing in all directions and there is no resultant net magnetism. When these protons are placed in an external magnetic field they align themselves in the direction of that field. For protons there are two orientations which they can take. The first is in the direction of the applied field, and this state has the lowest energy level. The second orientation is at 180° to the field (upside-down), and has a slightly higher energy state. In effect more protons take the lower energy orientation (aligned with the direction of the field) than the higher energy orientation. This leads to a net magnetism in the direction of the applied magnetic field. An NMR experiment involves inducing transitions between these two energy states by the absorption and emission of quanta.

If an alternating field of a specific radiofrequency is applied whilst the static field also exists, the spin system will absorb energy and the population at the higher energy level will increase, whilst that of the lower level will decrease. The applied radiofrequency must be of a value specific to the difference in energy levels ,this is called the Larmor frequency. It is this effect which is the resonant process in NMR. The difference between energy levels changes with the environment in which the proton is situated, thus the Larmor frequency is dependent on the chemical state in which the proton finds itself.

When the radiofrequency pulse is stopped, the system returns to equilibrium with a resultant loss of energy. There are two ways in which this energy can be lost. Firstly it can be lost by gradual transfer to nuclei and electrons in the environment (or lattice) resulting in transition of nuclei from the higher energy state to the lower energy state. This

is termed spin-lattice relaxation and is characterised by the time constant T_1. Secondly the energy can be redistributed within the spin system by the transition of a nuclei from the higher to lower energy level being accompanied by the transition of a nuclei from the lower to the higher energy level. This is called spin-spin relaxation and is characterised by the time constant T_2.

Figure 1.2.
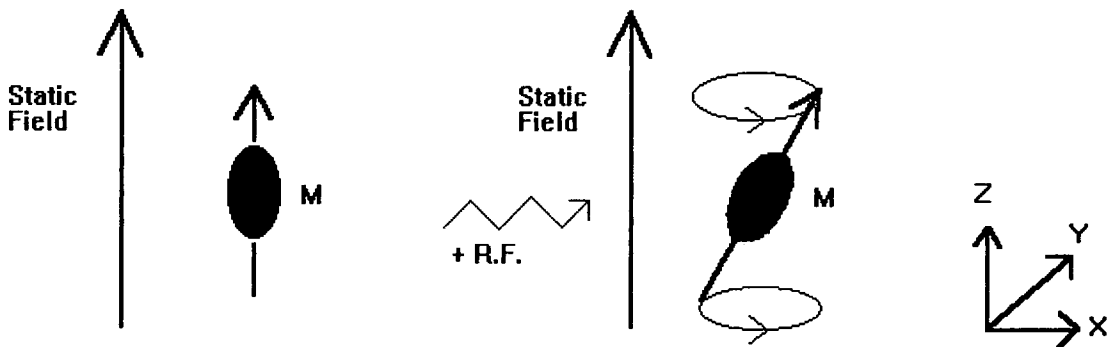
(a) At equilibrium the net magnetism (M) is aligned with the applied static field

(b) After application of a radiofrequency pulse (R.F.), the net magnetism rotates at an angle about the Z axis

To measure these relaxivities a static field is applied in the Z direction (figure 1.2), and all the protons align themselves with this field. A radiofrequency pulse is applied at 90° to the main field (in the XY direction), causing the net magnetism to flip out of the Z direction and rotate around the Z axis, the angle of rotation being proportional to the direction and duration of the applied pulse (figure 1.2). The relaxation time T_1 is a measure of how fast energy can be transferred from the spinning nuclei to the lattice. T_2 is a measure of how long the resonant nuclei hold this temporary magnetism.

The angular precession of the magnetism around the Z axis will generate an electromagnetic force (by Faraday's law of electromagnetic induction) in a coil which has been wrapped around the sample. This gives a means of detection of the resonant frequency, the magnitude of which depends on the

concentration of the nuclei of interest. In practice there is a range of frequencies detected as not all nuclei experience exactly the same magnetic field. This is due to the shielding effect of the chemical environment on the nucleus. By performing a spectral analysis of the total induced signal, the signal strength at different frequencies can be measured. Then the relative amounts of nuclei of the same type but in different chemical environments can be calculated. This is the basis of NMR spectroscopy and the underlying principle of MRI.

1.3.2. NMR Using Nuclei Other Than Protons.

Although protons are the most abundant nuclei suitable for NMR found in biological systems, they are not the only ones. Any nucleus which contains an odd number of protons or neutrons, or both, will possess spin and a magnetic moment[110]. Examples of such nuclei are ^1H, ^2H, ^7Li, ^{13}C, ^{14}N, ^{17}O, ^{19}F, ^{23}Na, ^{31}P, ^{35}Cl, ^{63}Cu, ^{71}Ga and ^{127}I.

If high field strengths are employed (higher than those used for proton MRI), measurements can be made on the chemical state of a specific nucleus. For example measurements of ^{31}P NMR spectra can be used to determine the relative amounts of ATP and inorganic phosphate in vivo[111].

1.3.3. Magnetic Resonance Imaging[110-112]

Although many nuclei possess the properties required for MRI, it is the proton which is utilised for the imaging of patients. This is because hydrogen is the most abundant element in living tissue. In fact MRI relies mostly on the protons of water as the body is composed of approximately 60% water.

Images are obtained by measuring the signal intensity of water protons which is a sensitive function of their T_1 and T_2 relaxation times. Firstly a magnetic field gradient is set up across the patient, then radiofrequency pulses are applied at an angle to this field. Because the frequency of the

absorbed and emitted radiofrequency is dependent on the strength of the local magnetic field, this gradient makes the absorption and emission frequency position dependent. The imager is able to apply magnetic field gradients in three directions enabling three dimensional images to be constructed. Analysis of the spectrum of frequencies obtained is achieved by the mathematical process of Fourier Transformation which provides the information needed to construct an image.

Tissue contrast is provided from the differences in proton T_1 and T_2 relaxation times within differing local environments. The easier it is for protons to pass their energy to neighbouring molecules, the more quickly they can relax to their original state and the faster the fall in the T_1 signal. Thus protons which are closely bound to proteins in tissues such as liver and muscle, have short T_1 values, whereas protons in fluids such as urine, ascitic and cerebrospinal fluid have longer T_1 values[99].

For example, MRI is able to differentiate between the grey and white matter of the brain. White matter has a higher proportion of its water content bound to fats and large molecules than grey matter. This, along with its lower water content, gives white matter a shorter T_1 value than grey matter[100]. Differentiation can also be detected between normal, cystic and tumour tissue in organs such as the liver[99]. Cancerous tissue tends to have a lower degree of organisation and less water structure than normal tissue, leading to an increase in proton relaxation times[113]. Moving blood usually has no detectable signal. There is a waiting time between excitation and emission of the radiofrequency, if water molecules move out of the field during this time, no signal will be detected. The ability of MRI to provide high quality images with good soft tissue contrast and spatial resolution enables the diagnosis of abnormalities in many body parts to be made.

1.3.4. Paramagnetic Contrast Agents

The contrast between tissues in MRI is generated by variations in the relaxation times T_1 and T_2. In some cases the differences between healthy and diseased tissue is small or the relaxation times may overlap. In these cases, an agent that could alter the relaxation times would increase the contrast. This has lead to the development of paramagnetic contrast agents to improve the diagnostic utility and precision of MRI[88,114].

Paramagnetic metal ions have magnetic dipole moments that are about a 1,000 times greater than that of protons[115]. These produce large local magnetic fields and so enhance the relaxation rates of water protons which are in their vicinity. Paramagnetic agents which are likely to be of the most use clinically are those based on the metals gadolinium (III), manganese (II) or iron (III) owing to their high magnetic moments and long relaxation times[88]. These metal ions are highly toxic and need to be in a complexed form before they can be used for MRI. As well as reducing the toxicity, complexation alters the biodistribution and elimination route of the metal ion.

Orally administered Fe^{3+} has been investigated as a means of enhancing the gastrointestinal tract[118,119], and complexes of Mn^{2+} are being developed as hepatobiliary contrast agents[103,118,119]. However, at present only complexes containing Gd^{3+} are in general clinical use.

The first paramagnetic agent in wide use was $[Gd.DTPA]^{2-}$. The lanthanide gadolinium has 7 unpaired outer-shell electrons which are potent promoters of T_1 and T_2 relaxation[120]. The complex $[Gd.DTPA]^{2-}$ rapidly diffuses into the extracellular interstitial spaces after intravenous injection[97,121]. This causes enhancement of contrast within tissues which have a high proportion of fluid content (e.g. oedema), as well as identifying any breakdown of the blood brain barrier which occurs in tumours such as glioblastoma[112]. $[Gd.DTPA]^{2-}$ is almost completely eliminated by glomerular filtration, enabling abnormalities in kidney

function to be diagnosed[114,122]. [Gd.DOTA]$^-$ was the second
gadolinium complex to come into widespread clinical use in
1988[122]. This complex also distributes rapidly into the
extracellular interstitial spaces, and is eliminated by
glomerular filtration[122], but has the added advantage of
being less toxic than [Gd.DTPA]$^{2-}$ due to its slower kinetics
of dissociation[101].

When the relaxation times T_1 and T_2 are decreased by the
presence of a paramagnetic agent, they have the opposite
effect on signal intensity. A decrease in T_1 increases the
signal intensity, whereas a decrease in T_2 decreases the
signal intensity. This enables images with different
contrasts to be constructed depending on the pulse sequences
employed and the type of relaxation time measured.

1.3.5. Relaxivity of Gadolinium Complexes.

The presence of the paramagnetic gadolinium complex
decreases the relaxation time of the protons of water
molecules in the vicinity. The relaxivity of different types
of gadolinium complexes depends on the interaction of the
metal ion with the water protons. Water molecules which are
coordinated directly to the metal ion via an oxygen are
referred to as inner sphere water. Due to this close
proximity, the gadolinium has most effect on the relaxivity
of these inner sphere waters. There is also a direct
relaxation effect on water molecules that are close in space
but are not directly bound to the complex. These are referred
to as 'outer sphere water'. For the uncomplexed ion Gd^{3+}, 90%
of its relaxivity effect comes from inner sphere water.
However, in gadolinium complexes this contribution is much
reduced, and the contribution from the outer sphere water
becomes much more important. It is estimated that one bound,
inner sphere water contributes about as much to the overall
relaxivity as all of the outer sphere waters[88,114].

The complexation of the Gd^{3+} ion is fundamental to its
safe use in MRI. This complexation however displaces a number
of coordinated water molecules, and consequently reduces the

effective relaxivity of the Gd^{3+} ion. Gadolinium has a total co-ordination number of nine, and the number of donor atoms in the ligand will reduce the number of bound water. The ligands DTPA and DOTA are octadentate, thus leaving room for one bound water[88]. As the chemical structures of the ligands are modified to reduce the toxicity of the complex and alter its biodistribution and elimination, the amount of bound water will change[123].

Other factors which contribute to the overall relaxivity are the correlation times. These describe the time dependence of motions of the metal complex on relaxivity[115]. Of specific interest is the rotational correlation time, which is dependent on the Brownian molecular rotation of the metal complex. The rotational correlation time increases as a function of molecular volume and leads to increased relaxivity[114]. For example, the attachment of the gadolinium complex to macromolecules such as proteins can increase the molecular volume and thus the rotational correlation time. As a consequence there is a substantial (2 to 10 fold) increase in relaxivity[124]. Molecular volume can be taken into account in the design of gadolinium complexes which target specific sites.

One approach is to use gadolinium complexes covalently bound to monoclonal antibodies[109]. Problems associated with this approach are firstly the difficulty in delivering sufficient quantities of gadolinium to the site of interest (this requires a high saturation of the antigenic sites and a large number of gadolinium atoms per antibody), and secondly the need for the antibody to be metabolised before the gadolinium can be eliminated from the body.

A more promising approach is the use of a simple gadolinium ligand complex in combination with a specific carrier mediated transport system. In this case binding of the complex to a carrier molecule is noncovalent, but is still accompanied by an increase in the rotational correlation time and relaxivity. This can be achieved by modifying the gadolinium complex to be eliminated from the body by the hepatobiliary route. This involves the gadolinium

complex binding to carrier molecules in the liver hepatocytes[88,125], and thus increasing the molecular volume and relaxivity of the complex at this specific site. Whilst targeting the hepatocytes the complex is also en route to being eliminated from the body without the need of preliminary metabolism.

With the use of contrast agents in MRI, the intensity of the final image is related to the amount of agent present. However, due to relaxivity considerations, this is not a simple relationship as is the case in radioisotope imaging.

1.3.6. Hepatobiliary Imaging Contrast agents for MRI

Hepatobiliary contrast agents are specifically targeted at the liver and hepatobiliary excretion pathway. This targeting results in an increase in the relaxivity of the water molecules, enabling imaging of the liver, biliary tree and intestines. Contrast is also seen between normal and malignant liver tissue where the function of the transport system within the tumour cells is different from normal.

Hepatocytes are the cells in the liver which are responsible for the production of bile and the elimination of certain xenobiotics from the blood into the bile[126]. This latter function is the one utilised by MRI contrast agents. The hepatocytes contain different transport mechanisms for the transport of organic anionic, cationic and neutral compounds from the blood into the bile[126]. The anion transport system appears to be active, and a wide range of compounds are eliminated by this route, demonstrating a low degree of specificity. Certain anionic compounds have been shown to compete for this carrier[126,127].

Within the liver, blood plasma comes into direct contact with the hepatocytes which are capable of extracting chemicals from the blood in one pass through the liver. This is called the first pass effect[126]. The amount of chemical removed per pass is dependent on its extraction ratio. If the extraction ratio is low, then only a small amount will be extracted per pass. If the extraction ratio is high and the

carrier system is not saturated, then the chemical may all be extracted in the first pass. However, if there are large amounts of chemical and the carrier system becomes saturated, then the rate of extraction of the chemical from the blood will depend on the kinetics of the carrier system[126,127].

Figure 1.3. *MRI Hepatobiliary Contrast Agents.*
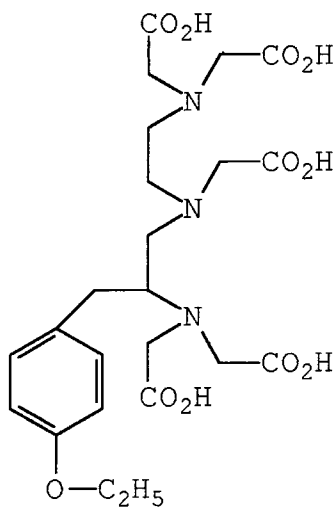
EOB-DTPA
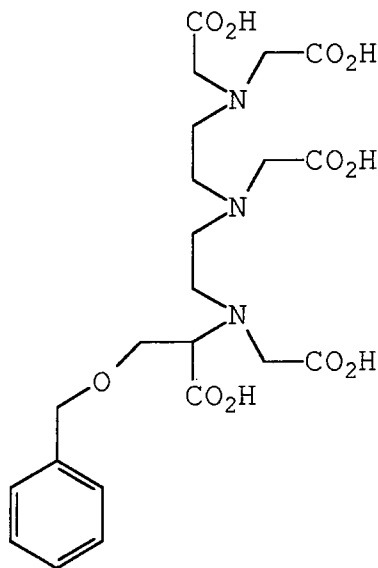
BOPTA

5-Br-EHPG

PGDF

27
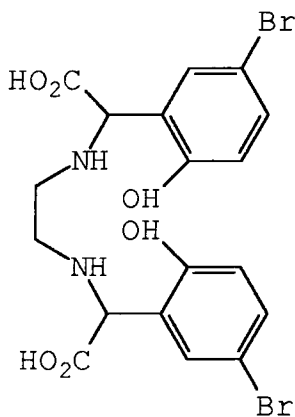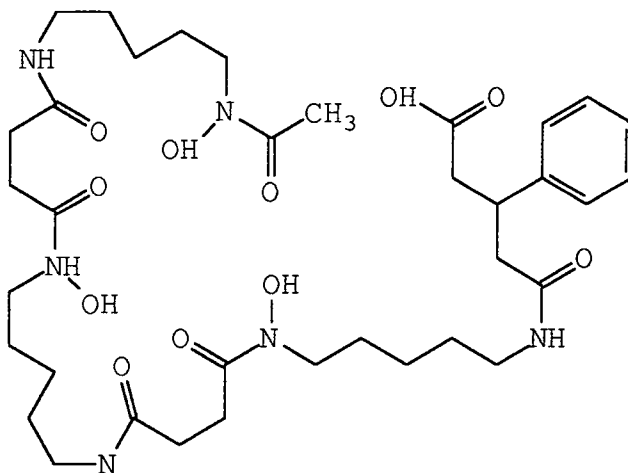
The MRI contrast agents [Gd.EOB-DTPA]$^{2-}$, [Gd.BOPTA]$^{2-}$ and
[Fe.5-Br-EHPG]$^-$ and [Fe.PGDF]$^-$ (figure 1.3) have all been
shown to be eliminated from the blood to some extent by the
hepatobiliary system[128-131]. These contrast agents are
distributed throughout the extracellular spaces and undergo
renal as well as hepatobiliary elimination. The transport
system within the liver utilised by these agents is referred
to as 'the organic anion transport system'[104,128]. This
system is based on transport proteins such as glutathione-s-
transferase[128] within the hepatocytes and can be inhibited by
bromosulphophthalein (BSP)[88,106,128]. Although exhibiting
broad specificity, this carrier system requires the substrate
to be, (i) anionic, (ii) have some lipophilicity imparted
from an aromatic ring, and (iii) have some hydrophilic sites
for water solubility. The aromatic rings are thought to be
important in plasma protein binding, which shows some
correlation with hepatobiliary elimination, as well as for
binding to the carrier molecule within the hepatocytes[88,126].
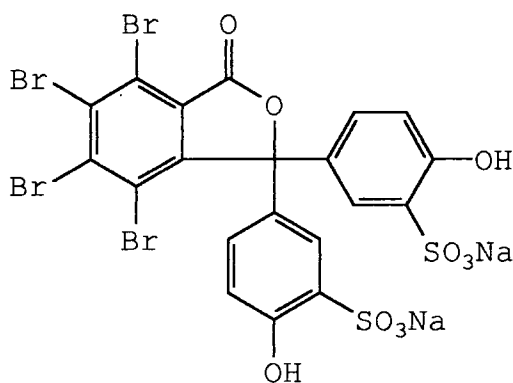
BSP

The contrast agent [Mn.DPDP] also exhibits hepatobiliary
elimination, however it is designed to use a different
transport system from the three complexes mentioned
previously, that used by the coenzyme pyridoxal-5'-
phosphate[103,118,119].

DPDP
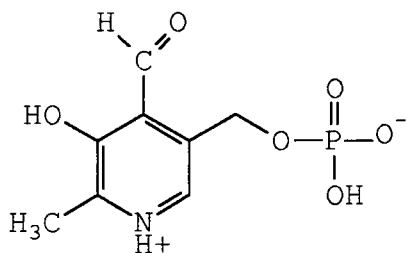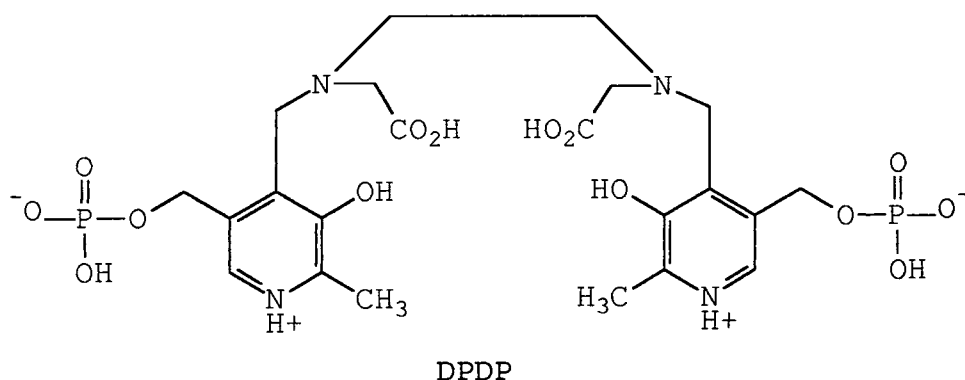
Pyridoxal-5'-phosphate

These four contrast agents show varying degrees of hepatobiliary uptake. Measurements of T_1 relaxivities show increased contrast within the liver and bile[102,104,118,131-133]. The binding to transport proteins increases the relaxivity due to the lengthening of the rotational correlation times. Because of this effect and the specific uptake by the hepatocytes, lower doses of contrast agents (10-30 μmol/kg) can be used in comparison to those used for traditional abdominal imaging (100 μmol/kg)[132]. If larger doses of contrast agents are used, saturation of the hepatobiliary transport system occurs leading to higher doses of circulating contrast agent. This then leads to competition by the kidneys which results in a larger percentage clearing renally.

The hepatobiliary contrast agents studied so far are acyclic compounds. The stability of these compounds in vivo would be expected to be lower than could be obtained from the use of macrocyclic contrast agents. The complexes [Gd.EOB-DTPA]$^{2-}$ and [Gd.BOPTA]$^{2-}$ both show good hepatobiliary imaging properties but possess a double negative charge. A contrast

agent with a single negative or zero charge would possess a lower osmolality and hence should give rise to less pain on injection and a reduced tendency to crenate red blood cells close to the site of injection.

1.4. THE SCOPE OF THIS WORK.

The major theme of this thesis is that of the in vivo stability and route of elimination of metal macrocycle complexes.

In chapter 2 a series of 21 12N4 macrocyclic and 4 acyclic complexes are studied with a view to their use as contrast agents in MRI. The effect of both charge and lipophilicity on the pharmacokinetics and stability of these complexes is assessed. Measurements of in vitro acid dissociation rates and partition coefficients of these complexes are compared to the in vivo stabilities and routes of elimination.

Chapter 3 is concerned with yttrium-90 12N4 macrocycles for the labelling of monoclonal antibodies for tumour therapy. In vitro measurements of acid dissociation rates and association rates of both ^{90}Y-macrocycles and ^{90}Y-macrocycle-maleimide bifunctional complexing agents are examined. The in vivo stability of an ^{90}Y-monoclonal antibody is assessed from biodistribution and detailed bone studies.

In chapter 4 gallium and indium complexes of seven 9N3 substituted macrocycles are examined. The effect of the charge and lipophilicity on the in vivo stability and route of elimination of the complexes is evaluated. Gallium and indium 9N3 are further studied as possible tumour localisation agents as is a gallium-9N3-misonidazole conjugate.

1.5. REFERENCES

1.   D. Sutton. *Radiology and Imaging for Medical Students.*
     Sixth Edition, 1994. Churchill Livingstone.

2. 'Radioisotopes in Biology. A Practical Approach'.Ed. R.J. Slater.1990, Oxford Uni. Press.

3. *The Radiochemical Manual. 2nd Ed,*1966. The Radiochemical centre, Amersham.

4. E. Pomplun, J. Booz and D.E. Charlton, *Radiat. Res.,* 1987, 111, 533-332.

5. H.N. Wagner. *Medical Radionuclide Imaging*, 1980 I, IAEA-SM-247/200, 1-26.

6. W.C. Eckelman and S.M. Levenson, *Int.J. App. Radiat. and Isotopes*, 1977, 28, 67-82.

7. 'Radionuclide Transformations'.Annals of the ICRP, publication 38, 1983, Vol 11-13.

8. D.Parker, *Chem. Soc. Rev.*, 1990, **19**, 271-291.

9. R. Weissleder and J. Wittenberg, *'Primer of Diagnostic Imaging'*, 1994, Mosby.

10. G.B.Saha, *'Physics and Radiobiology of Nuclear Medicine'*, 1993, Springer-Verlag.

11. V.R. McCready and N.G. Trott, *'Tumour Localization with Radioactive Agents'*, (IAEA-MG-50/10), 1974, 1-18.

12. M.M. Ter-Pogossian, M.E. Phelps, E.J. Hoffmann and N.A. Mullani, *Radiology,* 1975, 114, 89-98.

13. P.V. Harper. *Int.J. App. Radiat. and Isotopes*, 1977, 28, 5-11.

14. S.M. Tilyou, *J. Nucl. Med.*, 1991, 32, vol 4, 15N-26N.

15. J.L. Humm, *J. Nucl. Med.*, 1986, 27, 1490-1497.

16. W.A Vilkert, W.F. Goeckeler, G.J. Ehrhardt and A.R. Ketring, *J. Nucl. Med.*, 1991, 32, 174-185.

17. D.E. Troutner, *Nucl. Med. Biol. Int. J. Radiat. Appl. Instrum. Part B*, 1987, 14, 171-176.

18. B.W. Wessels and R.D. Rogus, *Med. Phys.*, 1984, 11, 638-645.

19. J.L. Humm, R.M. Macklis, Y. Yang, K. Bump and L.M. Chin, *J. Nucl. Med.*, 1994, 35, 1217-1225.

20. A.I. Kassis, F. Fayad, B.M. Kinsey, K.S.R. Sastry and S.J. Adlestein, *Radiat. Res.*, 1989, 118, 283-294.

21. A. Harrison, L. Royle, *Int. J. Appl. Radiat. Isot.*, 1984, 35, 1005-1008.

22. A. Harrison and L. Royle, *NCI. Monogr.*, 1987, 3, 157-158.

23. A. Harrison, *Radiochimica Acta*, 1989, 47, 157-161.

24. E.M. Link and R. Carpenter, *Cancer Res.*, 1990, 50, 2963-2967.

25. Y-C.C. Lee, L.C. Washburn, T.T.H. Sun, B.L. Bird, J.E. Crook, E.C. Holloway and Z. Steplewski, *Cancer Res.*, 1990, 50, 4546-4551.

26. S.H. Kurtzman, A. Russo, J.B. Mitchell, W. Degroff, M.W. Brechbiel, O.W. Gansow, A.M. Friedman, J.J. Hines, J. Gamson and R.W. Atcher, *J. Nat. Canc. Inst.*, 1988, 80, 449-452.

27. F. Hartman, E.M. Horak, K. Garmestani,C. Wu, W. Brechbeil, R.W. Kozak, J. Tso, S.A. Kosteiny, O.W. Gansow, D.L. Nelson and T.A. Waldmann, *Cancer Res.*, 1994, 54, 4362-4370.

28. R.M. Macklis, B.M. Kinsey, A.I. Kassis, J.L.M. Ferrara, R.W. Atcher, J.J. Hines, C.N. Coleman, S.J. Adelstein and S.J. Burakoff, *Science*, 1988, 240, 1024-1026.

29. S.T. Rosen, A.M. Zimmer, R. Goldman-Leiken *et. al.*, *J. Clin. Oncol.*, 1987, 5, 562.

30. O.W. Press, J.F. Eary and C.C. Badger, *J. Clin. Oncol.*, 1989, 7, 1027-1038.

31. S.J. DeNardo, S.V. Deshpande, M.K. Moi, G.P. Adams, M.K. McCall, G.L. DeNardo and C.F. Meares, *Front. Radiat. Ther. Oncol., Basel, Karger*, 1990, 24, 142-150.

32. S.M. Larson, *Cancer*, 1991, 67, 1253-1260.

33. S.M. Larson, *J. Nucl. Med.*, 1985, 26, 538-545.

34. R.M. Sharkey, F.A. Kaltovich, L.B. Shih, I. Fand, G.
.Govelitz and D.M. Goldenberg, *Cancer Res.*, 1988, <u>48</u>,
3270-3275.

35. R.M. Sharkey, C. Motta-Hennessy, D. Pawlyk, J.A. Siegel
and D.M. Goldenberg, *Cancer Res.*, 1990, <u>54</u>, 2330-2336.

36. Y-C.C. Lee, L.C. Washburn, T.T.H. Sun, B.L. Bird, J.E.
Crook, E.C. Holloway and Z. Steplewski, *Cancer Res.*,
1990, <u>50</u>, 4546-4551.

37. L.C. Washburn, Y.C.C. Lee, T.T.H. Sun, B.L. Bird, E.C.
Holloway, J.E. Cook and Z. Steplewski, *Antibod.
Immunoconj. Radiopharm.*,1991, <u>4</u>, 729-728.

38. D.J. Buchsbaum, T.S. Lawrence, P.L. Roberson, D.B.
Heidorn, R.K. TenHaken and Z. Staplewski, *Int. J.
Radiation Oncology Biol. Phys.*, 1993, <u>25</u>, 629-638.

39. H. Schmidberger, D.J. Buchsbaum, B.R. Blazer, P. Everson
and D.A. Vallera, *Cancer Res.*, 1991, <u>51</u>, 1883-1890.

40. J.L. Klein, T.H. Nguyen, P. Laroque, K.A. Kopher, J.R.
Williams, B.W. Wessels, L.E. Dillehay, J. Frincke, S.E.
Order and P.K. Leichner, *Cancer Res.*, 1989, <u>49</u>, 6383-
6389.

41. J.A. Williams, J.L. Klein, M.D. Wharam, B.W. Wessels and
S.E. Order, *J. Neurosurg.*, 1989, <u>70</u>, 312A.

42. D.J. Hnatowich, G. Mardirossian, P.G. Rose, B. Kinders,
M. Rusckowski, S. Stevens, R. Hunter, T. Griffin and
A.B. Brill, *Antibod. Immunoconj. Radiopharm.*,1991, <u>4</u>,
359-371.

43. D.J. Hnatowich, M. Chinol, D.A. Siebecker, M. Gionet, T.
Griffin, P.W. Doherty, R. Hunter and K.R. Base, *J. Nucl.
Med.*, 1988, <u>29</u>, 1428-1434.

44. A. Maraveyas, D. Snook, V. Hird, C. Kosmas, C.F. Meares,
H.E. Lambert and A.A. Epenetos, *Cancer*, 1994, <u>73</u>, 1067-
1075.

45. J.S.W. Stewart, V. Hird, D.Snook, M. Sullivan, M.J.
Myers and A.A. Epanatos, *Int. J. Cancer*, 1988, <u>suppl.3</u>,
71-76.

46. J.S.W. Stewart, V. Hird, D. Snook, B. Dhokia, G. Sivolapenko, G. Hooker, J.Taylor Papadimitriou, G. Rowlinson, M. Sullivan, H.E. Lambert, C. Coulter, W.P. Mason, W.P. Soutter and A.A. Epenetos, *J. Clin. Oncol.*, 1990, <u>8</u>, 1941-1950.

47. B.A. Parker, A.A. Vassos, S.E. Halpern, R.A. Miller, H. Humpf, D.G. Amox, J.L. Simoni, R.J. Starr, M.R. Green and I. Royson, *Cancer Res. (suppl.)*, 1990, <u>50</u>, 1022s-1028s.

48. S.J. DeNardo, E.L. Kramer, C.M. Richman, Q.A. Salako, E.A. Perez, L.F. O'Grady, M.B. Rippon, S.D. Glenn, G.M. Butchko, J.C. Couto, R.L. Ceriani and G.L. DeNardo, *J. Nucl. Med.*, 1993, <u>34</u>, 53P.

49. H.B. Breitz, P.L. Weiden, J-L Vanderheyden, J.W. Appelbaum, M.J. Bjorn, M.F. Fer, S.B. Wolf, B.A. Ratliff, C.A. Seiler, D.C. Foisie, D.R. Fisher, R.W. Schroff, A.R. Fritzberg and P.G. Abrams, *J. Nucl. Med.*, 1992, <u>33</u>, 1099-1109.

50. P.C. Beaumier, P. Venkatesan, J.L. Vanderheyden, W.D. Burgua, L.L. Kunz, A.R. Fritzberg, P.G. Abrams and A.C. Morgan Jr., *Cancer Res.*, 1991, <u>51</u>, 676-681.

51. G.W.M. Visser, M. Gerretsen, J.D.M. Herscheid, G.B. Snow and G. van Dogen, *J. Nucl. Med.*, 1993, <u>34</u>, 1953-1963.

52. G.L. Griffiths, D.M. Goldenberg, F.F. Knapp Jr.,A.P. Callahan, C-H Chang and H.J. Hansen, *Cancer Res.* 1991, <u>51</u>, 4594-4602.

53. G.L. DeNardo, S.J. DeNardo, C.F. Meares *et. al.*, *Antibod. Immunoconj. Radiopharm.*,1991, <u>4</u>, 777-785.

54. S.V. Despande, S.J. DeNardo, C.F. Meares, M.J. McCall, G.P. Adams, M.K. Moi and G.L. DeNardo, *J. Nucl. Med.*, 1988, <u>29</u>, 217-225.

55. E.K. John, A.J. Bott and M.A. Green, *J. Pharmacutical Sciences*, 1994, <u>83</u>, 587-590.

56. D.Z. Kukis, H. Diril, D.P. Greiner, S.J. DeNardo, G.L. DeNardo, Q.A. Salako and C.F. Meares, *Cancer Res.*, 1994, <u>73</u>, 779-786.

57. P.M. SmithJones, R. Fridrich, T.A. Kaden, I. Novakhofor, *et. al.*, *Clinical Pharmacy*, 1991, 10, 359-375.

58. S.V. Deshpande, S.J. DeNardo, C.F. Meares, M.J. McCall, G.P. Adams, M.K. Moi and G.L.DeNardo, *J. Nucl. Med.*, 1988, 29, 217-225.

59. R.A. Fawwaz, T.S.T. Wang, S.C. Srivastava, J.M. Rosen, S. Ferrone, M.A. Hardy and P.O. Alderson, *J. Nucl.Med.*, 1984, 25, 796-799.

60. M.E. Schott, J. Schlom, K. Siler *et. al.*, *Cancer*, 1994, 73, 993-998.

61. D.K. Hazra, V.L. Lahiri, M. Kumari, P. Khanna and B. Arvind, *British J. Cancer*, 1989, 5, 317.

62. J.D. Beatty, *Cancer*, 1992, 70, 1425-1433.

63. J.G. Hamilton, *Am. J. Physio.*, 1938, 127, 667.

64. S. Hertz, *Proc. Soc. Exp. Biol. Med.*, 1938, 38, 510.

65. P.M. Mauch and M.A. Drew, 1985, 2132-2145, in *'Cancer-Principles and Practice in Oncology'*, 2nd *Ed*. V.T. DeVita et al, Lippincot pub.

66. S.E. Order, *Int. J. Radiat. Oncol. Biol. Phys.*, 1990, 18, 981-992.

67. M.J. Welch, M.R. Kilbourn and M.A. Green, *Radioisotopes*, 1985, 34, 170-179.

68. C.J. Mathias, Y Sun, M.J. Welch, M.A. Green, J.A. Thomas, K.R. Wade and A.E. Martell, *Nucl. Med. Biol.*, 1988, 15, 69-81.

69. H.N. Wagner Jr., *Medical Radionuclide Imaging*, 1980, I, IAEA-SM-147/200, 3-26.

70. V.A. Levin, *J. Med. Chem.*, 1980, 23, 682-684.

71. P.M. Smith-Jones, B. Stolz, C. Bruns, R. Albert, H.W. Reist, R. Fridrich and H.R. Mäcke, *J. Nucl. Med.*, 1994, 35, 317-325.

72. H.N. Wagner, Jr., *J. Nucl. Med.*, 1991, 32, 561-564.

73. F.J. Primus, R.H. Wang, D.M. Goldenberg and H.J. Hansen, *Cancer Res.*, 1973, 33, 2977.

74. G. Köhler and C. Milstein, *Nature*, 1975, 256, 495.

75. J.P. Mach, F. Buchegger, M. Forni *et. al.*, *Immunol. Today*, 1981, 2, 239-249.

76. G.E. Krejcarek and K.L. Tucker, *Biochem. Biophys. Res. Comm.*, 1977, 77, 581-585.

77. J.P.L. Cox, A.S. Craig, I.M. Helps, K.J. Jankowski, D. Parker, M.A.W. Eaton, A.T. Millican, K. Millar, N.R.A. Beeley and B.A. Boyce, *J. Chem. Sos. Perkin, Trans. 1*, 1990, 2567-2576.

78. A. Harrison, C.A. Walker, D. Parker, K.J. Jankowski, J.P.L. Cox, A.S. Craig, J.M. Sansom, N.R.A. Beeley, R.A. Boyce, L. Chaplin, M.A.W. Eaton, A.P.H. Farnsworth, K. Millar, A.T. Millican, A.M. Randall, S.K. Rhind, D.S. Secher and A. Turner, *Nucl. Med. Biol.*, 1991, **18**, 469-476.

79. *'Metals in Bone'*, 1984, Ed. N.D. Priest, MTP press Ltd.

80. R.E. O'Mara, J.G. McAfee and G. Subramanian, *J. Nucl. Med.*, 1968, 10, 49-51.

81. J. Jowsey, R.E. Rowland and J.H. Marshall, *Rad. Res.*, 1958, 8, 490-501.

82. *'CRC Handbook of Chemistry and Physics'*, 74 th edition, 1993-94, Ed. D.R. Lide.

83. E.T. Clarke and A.E. Martell, *Inorganica Chimica Acta*, 1991, 181, 273-280.

84. R.D. Hancock and A.E. Martell, *Chem. Rev.*, 1989, 89, 1875-1914.

85. W.P. Cacheris, S.K. Nickle and A.D. Sherry, *Inorg. Chem.*, 1987, 26, 958-960.

86. W.P. Cacheris, S.C. Quay, and S.M. Rocklage, *Magn. Reson. Imaging*, 1990, 8, 467-481.

87. C.J. Broan, J.P.L. Cox, A.S. Craig, R. Kataky, D. Parker, A.Harrison, A. Randall, and G. Ferguson, *J. Chem. Soc. Perkins Trans. 2*, 1991, 87-99.

88. R.B. Lauffer, *Chem Rev.,* 1987, <u>87</u>, 901-927.

89. S.M. Rocklage, D. Worah and S-H. Kim, *Magn. Reson. Med.,* 1991, <u>22</u>, 216-221.

90. Chang, K. Kumar, J.M. Garrison, H.G.Brittain, M.F. Tweedle, *Soc.Mag Res in Medicine, 9th Annual Conference.* 1990, 729.

91. D.Fornasiero, J.C. Bellen, R.J. Baker and B.E. Chatterton. 1987, *Invest. Radiol.,* <u>22</u>, 322-327.

92. M.F. Tweedle, J.J. Hagan, K. Kumar, S. Mantha, and C.A. Chang, *Magn. Reson. Imaging*, 1991, <u>9</u>, 409-415.

93. P.Wedeking, K. Kumar and M.F. Tweedle, *Magn Reson Imaging,* 1992, <u>10</u>, 641-648.

94. E.M. Purcell, H.C. Torrey, R.V. Pound..*Phys. Rev.,* 1946, <u>69</u>, 37-38.

95. F. Bloch, W.W. Hansen, M. Packard. *Phys. Rev.,* 1946, <u>69</u>, 127.

96. J.M.S. Hutchinson, W.A. Edelstein, G.Johnson. *J. Phys(E) Sci. Instrum.,* 1980, <u>13</u>, 947-955.

97. R.C. Brasch, H-J Weinmann and G.E. Wesbey, *American Journal of Radiology*, 1984, <u>142</u>, 625-630.

98. F.W. Smith, J.R. Mallard, J.M.S. Hutchinson, A. Reid, G. Johnson, T.W. Redpath and R.D. Selbie, 1981, *Lancet* <u>I</u>, 78-79.

99. F.W. Smith, J.R. Mallard, A. Reid, J.M.S. Hutchinson. *Lancet,* 1981, <u>I</u>, 963-965.

100. F.H. Doyle, J.C. Gore, J.M. Pennock, G.M. Bydder, J.S. Orr, R.E. Steiner, I.R. Young, M. Burl, H. Clow, D.J. Gilderdale, D.R. Bailes and P.E. Walters, *Lancet,* 1981, <u>II</u>, 53-57.

101. J-C. Bousquet, S. Saini, D.D. Stark, P.F. Hahn, M.Nigam, J. Wittenberg, and J.T. Ferrucci, *Radiology*, 1988, <u>166</u>, 693-698.

102. F. Cavagna, M. Daprà, F. Maggioni, C. DeHaën, E. Felder, *Magn. Reson. Med.*, 1991, <u>22</u>, 329-333.

103. M.E. Bernardino. *Magn. Reson. Med.*, 1991, <u>22</u>, 334-338.

104. A. Mühler, O. Clément, V. Vexter, Y. Berthzène, W. Rosenau and R. Brasch. *Radiology*, 1992, <u>184</u>, 207-213.

105. R.B. Lauffer, A.C. Vincent, S. Padmanabhan, A. Villringer, S. Saini, D.R. Elmaleh and T.J. Brady, *Magn. Reson. Med.*, 1987, <u>4</u>, 582-590.

106. B-A. Hoener, A.A. Tzika, B.L. Englestand and D.L. White, *Magn. Reson. Med.*, 1991, <u>17</u>, 509-515.

107. I.K. Adzamli, M. Blau. *Magn. Reson. Med.*,1991, <u>17</u>, 141-148.

108. W.T. Anderson-Berg, M. Strand, T.E. Lempert, A.E. Rosenbaum, P.M. Joseph. *J. Nucl.Med.*, 1986, <u>27</u>, 829-833.

109. W.C. Eckelman, M.F. Tweedle, M.J. Welch. *'Radiolabeled Monoclonal Antibodies for Imaging and Therapy - Potential Problems and Prospects.'* NATO Advanced Studies Institute. Ed. S. Scrivastava, 1987, 571-579.

110. E.R. Andrew. *'Scientific basis of Medical Imaging'*. Ed. P.N.T. Wells. Pub. Churchill Livingston, 1982, Chapter 6, 212-236.

111. J.C. Gore. *'Recent Advances in Radiology and Medical Imaging'*.Ed. R.E. Steiner, 1983, No. 7, Chapter 1, 1-13.

112. R.R. Edelman and S. Warach. New England J. of Medicine, 1993, vol 328, No.10, 709-716.

113. R. Damadian. 1971, *Science*, <u>171</u>, 1151-1153.

114. M.F. Tweedle. *'Lanthanide Probes in Life, Chemical and Earth Sciences'*, Eds. J-C.G. Bunzli and G.R. Choppin, Elsevier, Amsterdam, 1989, Chapter 5, 127-173.

115. D.G. Gadian, J.A. Payne, D.J. Bryant, I.R. Young, D.H. Carr, G.M. Bydder. *Journal of Computer Assisted Tomography*, 1985, 9, 242-251.

116. G.E. Wesbey, R.C. Brasch, B.L. Engelstand, A.A. Moss, L.E. Crooks, A.C. Brito, *Radiology*, 1983, 149, 175-180.

117. T.Liebig, C.Stoupis, P.R.Ros, J.R. Ballinger and R.W.Briggs. *Magn. Reson. Med*, 1993, 30, 646-649.

118. G. Elizondo, C.J. Fretz, D.D. Stark, S.M. Rocklage, S.C. Quay, D. Worah, Y-M. Tsang, M.C-M. Chen J.T. Ferrucci. *Radiology*, 1991, 178, 73-78.

119. K.O. Lim, D.D. Stark, P.T. Leese, A. Pfefferbaum, S.M. Rocklage, S.C. Quay. *Radiology*, 1991, 178, 79-82.

120. H-J. Weinmann, R.C. Brasch, W-R. Press, G.E. Wesbey. *American Journal of Radiology*, 1984, 142, 619-624.

121. H.P. Niendorf, J. Haustein, I. Cornelius, A. Alhassan and W. Clau. *Magn. Reson. Med.*, 1991, 22, 222-228.

122. M.F. Bellin, G. Deray, U. Assogba, E. Auberton, F. Ghany, E. Dion-Voirin, C. Jacobs and J. Grellet, *Magn. Reson. Imag.*, 1992, 10, 115-118.

123. D. Parker, in *'Comprehensive Supramolecular Chemistry'* Volume 10, Ed. D.N. Reinhoudt and J.M. Lehn, Chapter 17, Pergamon press, 1995.

124. R.B. Lauffer, *Magn. Reson. Imag.*, 1991, 22, 339-342.

125. H.-J. Wienmann, G. Schuhmann-Giampieri, H. Schmitt-Willich, H. Vogler, *Magn. Reson. Imag.*, 1991, 22, 233-237.

126. C.D. Klaassen, J.B. Watkins III, *Pharmacological Reviews*, 1984, 36, 1-67.

127. M. Rowland and T.N. Tozer, *Clinical Pharmocokinetics: Concepts and Applications*, 1989, Second Edition, Lea and Febiger, 148-173.

128. G. Schuhmann-Giampieri, H. Schmitt-Willch, W-R. Press, C. Negishi, H-J. Weinmann, U. Speck. *Radiology*, 1992, 183, 59-64.

129. A. Davies, C. de Haën. *Drugs of the Future*, 1991, <u>16</u>, 1001-1003.

130. G. Vittadini, E. Felder, P. Tirone, V. Lorusso. *Invest. Radiol.*, 1988, <u>23</u>, 246-248.

131. R.B. Lauffer, A.C. Vincent, S. Padmanabhan, A. Villringer, S. Saini, D.R. Elmaleh, T.J. Brady. *Magn. Reson. Med.*, 1987, <u>4</u>, 582-590.

132. H.-J. Wienmann, G. Schuhmann-Giampieri, H. Schmitt-Willich and H. Vogler, *Magn. Reson. Imag.*, 1991, <u>22</u>, 233-237.

133. P. Pavone, G. Patrizio, C. Buoni, E. Tettamamti, R. Passarello, C. Musu, P. Tirone and E. Felder. *Radiology*, 1990, <u>176</u>, 61-64.

CHAPTER TWO

GADOLINIUM MACROCYCLE COMPLEXES

2.1 INTRODUCTION

2.1.1. Gadolinium Complexes as Contrast Agents for Magnetic Resonance Imaging

The two major MRI contrast agents in present clinical use are [Gd.DTPA]$^{2-}$ and [Gd.DOTA]$^{-}$. Both these agents rapidly distribute exracellularly following intravenous injection, and are subsequently eliminated from the body via glomerular filtration[1]. This allows for contrast enhancement of tissues with a high proportion of fluid content (e.g. oedema), and for identification of any breakdown of the blood brain barrier[2-4]. The elimination of [Gd.DTPA]$^{2-}$ and [Gd.DOTA]$^{-}$ by the renal route also allows the imaging of kidney function[5].

There is also much interest in developing contrast agents for imaging the liver/gall bladder/ intestine[6-8]. This imaging of the hepatobiliary elimination route is achieved by agents which are specifically taken up by liver hepatocytes and eliminated into the bile (section 1.3.6). Contrast agents which are being developed for hepatobiliary imaging include [Gd.EOB-DTPA]$^{2-}$ and [Gd.BOPTA]$^{2-}$. Both these agents show rapid extracellular distribution and considerable hepatobiliary elimination along with some renal elimination[8-14].

Factors which may influence the transport of a given metal complex by hepatocytes into the bile are its charge, lipophilic and hydrophilic characteristics[15,16].

2.1.2. Toxicity of Gadolinium Complexes.

The amount of gadolinium contrast agent administered to a patient tends to be large, typically about 10 grams, (0.1 to 0.2 mmol per kg). Thus it is of paramount importance that the toxicity of any complex is as low as possible. Toxicity can arise from three sources, (i) the intact metal-ligand complex, (ii) free metal, and (iii) free ligand. LD$_{50}$ values (the dose at which 50% of the animals would die) in mice for metal-ligand complexes are in the order of 5 mmol/kg for the acyclic[1,12,17] gadolinium complexes [Gd.DTPA]$^{2-}$ and

[Gd.BOPTA]$^{2-}$, and 11 mmol/kg for the macrocyclic[1,17] gadolinium complex [Gd.DOTA]$^-$.

The toxicity of the intact metal-ligand complex is related to its osmolality. This is of particular importance in MRI as large doses of 0.1 to 0.2 mmol/kg are administered[18]. Due to their charged nature the complexes [Gd.DTPA]$^{2-}$ and [Gd.DOTA]$^-$ have to be injected in solution with a counter ion, usually NMG (N-methylglucamide). The larger the number of solute particles (a total of 3 for NMG$_2$[Gd.DTPA] and 2 for NMG[Gd.DOTA]) the greater the osmolality of the injection solution[19]. Injection of a hyperosmolar solution causes osmotic shock to the patient. This can lead to crenation of the blood cells, shrinkage and shrivelling due to loss of internal water, as well as a reduction in blood pressure and elevation of blood volume[16,20,21].

The data listed in table 2.1 shows that the osmolality values for these contrast agents are higher than that of blood, whose osmolality is 0.3 Osmol/kg-water[22]. Moreover, it is clear that the smaller the number of counter ions needed, the lower the osmolality of the injection solution. Hence [Gd.DOTA]$^-$ with a single negative charge will be less toxic than [Gd.DTPA]$^{2-}$ with its double negative charge. The complex [Gd.HP-DO3A] which is neutral in charge, is being developed as a low osmolality contrast agent because of these considerations[19].

Table 2.1. *Osmolalities of Gadolinium Contrast Agents 37°C 0.5M* [17,14].

Complex	Osmolality. Osmol/kg-H$_2$O
NMG$_2$[Gd.DTPA]	1.96
NMG$_2$[Gd.BOPTA]	1.9
NMG[Gd.DOTA]	1.4
[Gd.HP-DO3A]	0.60

Figure 2.1. *Chemical Structures of Gadolinium Contrast Agents.*
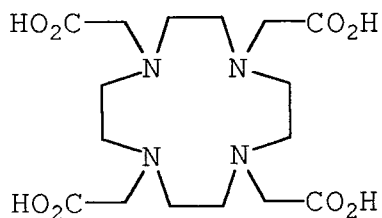
DOTA
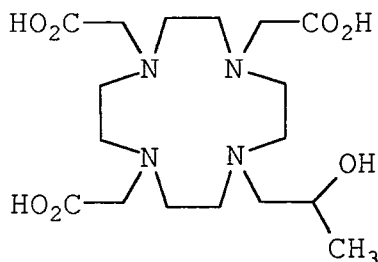
HP-DO3A
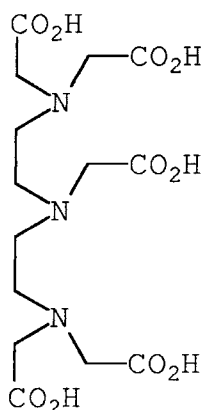
DTPA
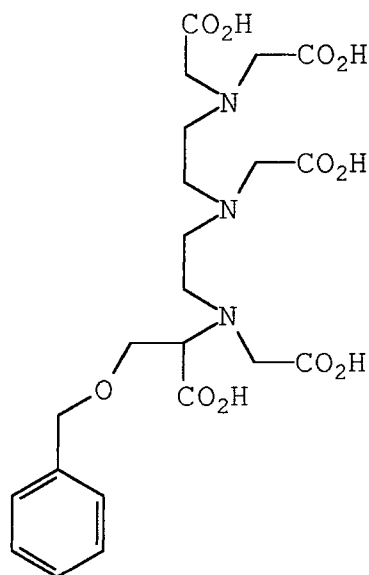
BOPTA

Dissociation of gadolinium contrast agent leads to both free metal and free ligand. Uncomplexed Gd^{3+} has an LD_{50} value of between 0.3 and 0.5 mmol/kg for mice[16,17]. The free Gd^{3+} ion is taken up by complexing agents which are naturally present in the serum such as citrate, albumin and transferrin[21]. The Gd^{3+} then accumulates in the body at such sites as the liver and bone[2] causing toxicity[20]. (Gd^{3+} at about 20 μM, has been shown to inhibit Ca^+ binding to mammalian sarcoplasmic reticulum[21]). Equally toxic are any free ligands which have LD_{50} values of between 0.1 and 0.5 mmol/kg in mice[23]. Toxicity of the free ligands is due to their ability to complex naturally occurring essential metal

44

ions from the blood, such as Zn^{2+}, Ca^{2+}, Mg^{2+} and Cu^{2+} , and the subsequent loss of these metals by elimination of the complex from the body[23].

2.1.3. In Vivo Stability of Gadolinium Complexes.

For a gadolinium complex to be of use as a MRI contrast agent it needs to be kinetically stable in vivo (section 1.2.6). In animals the complex will encounter many challenging environments. Amongst these are acid conditions as low as pH 2 in the stomach, endogenous metal ions such as Zn^{2+}, Ca^{2+}, Mg^{2+} and Cu^{2+} in the plasma[21,24], as well as natural ligands such as citrate, albumin and transferrin[16,21]. These components all compete with the complex for gadolinium ion or ligand, and so contribute towards dissociation of the complex.

There are several thermodynamic considerations which can effect the stability of the gadolinium complex[16,20,21]. However, it is kinetic considerations (the acid catalysed dissociation rates (k_{obs})) which are the most relevant measurements[24,25]. These have been shown to correlate well with in vivo stability for both acyclic and macrocyclic gadolinium complexes[25]. Due to the rigid conformational stability of macrocyclic ligands such as DOTA, these complexes are much more resistant to both acid and cation attack than the open chain acyclic ligands such as DTPA.

The macrocyclic ligand complex [Gd.DOTA]$^-$ and the acyclic ligand complex [Gd.DTPA]$^{2-}$ are both used in the clinic as MRI contrast agents. However, the kinetic stability of [Gd.DOTA]$^-$ is clearly superior to that of [Gd.DTPA]$^{2-}$, the rate of dissociation at pH 1 of [Gd.DOTA]$^-$ being 1,000 times slower[19] than that of [Gd.DTPA]$^{2-}$.

2.1.4. The use of Radioactively Labelled Gadolinium Complexes.

Although these gadolinium complexes are intended for use in MRI, nuclear magnetic resonance signal intensities are not

a simple function of complex concentration in vivo[26]. A direct and sensitive approach is via the use of radioactive label. The isotope ^{153}Gd ($T^1/_2$ 242 days, γ = 97-103 KeV, X rays = 41-47 KeV) is easily detected by means of its gamma radiation. In this series of experiments all of the gadolinium complexes are labelled with a mixture of stable ^{157}Gd and radioactive ^{153}Gd.

2.1.5. The Scope of Work in This Chapter.

A total of 25 gadolinium complexes were studied. The chemical structures of these ligands are listed in figures 2.2a and 2.2b, and they can be separated into the following nine groups:-

    I.   Hydrophilic anionic aza-carboxylic and aza-phosphinic acids

    II.   Lipophilic anionic aza-phosphinic acids

    III. Neutral monoamide aza-phosphinic acids

    IV.   Neutral monoamide aza-carboxylic acids

    V.   Cationic monoamide aza-phosphinic acids

    VI.   Cationic monoamide aza-carboxylic acids

    VII.   Neutral 7 co-ordinate aza-phosphinic acid

    VIII. Acyclic carboxylic acids

    IX.   Citrate

Figure 2.2a. *Chemical Structures of the Ligands Used to Complex Gadolinium.*
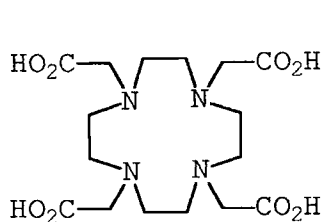
DOTA
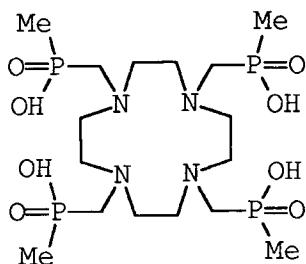
12N4P4Me4
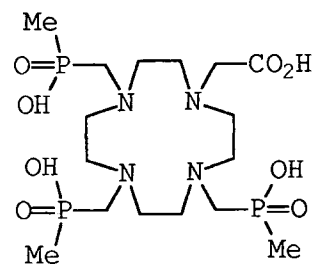
12N4P3Me3C
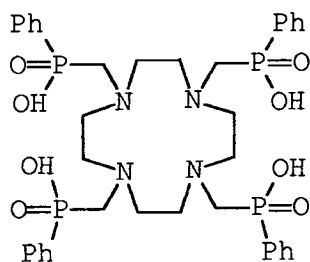
12N4P4Ph4
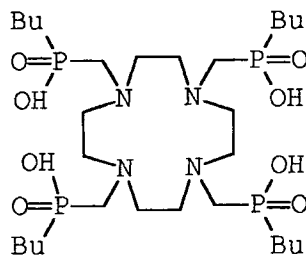
12N4P4Bu4
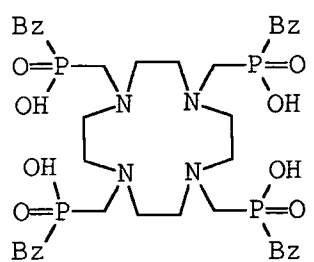
12N4P4Bz4
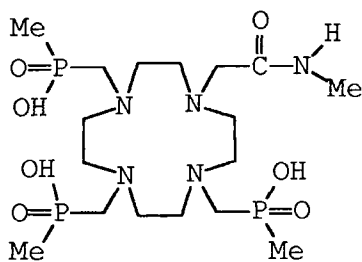
12N4P3Me3NHMe
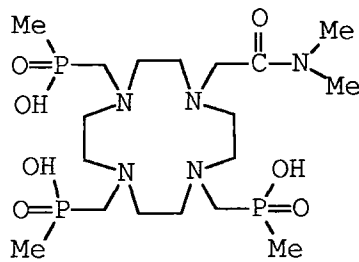
12N4P3Me3NMe2
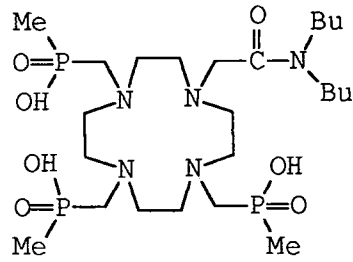
12N4P3Me3NBu2
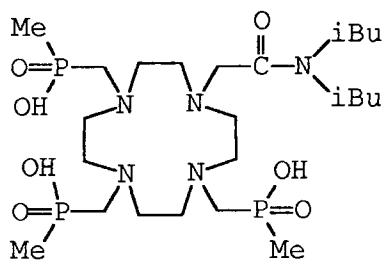
12N4P3Me3N(IBu2)
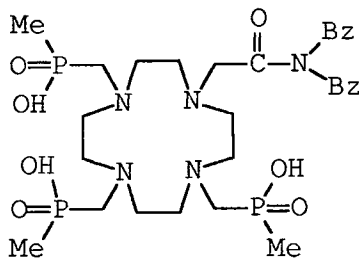
12N4P3Me3NBz2
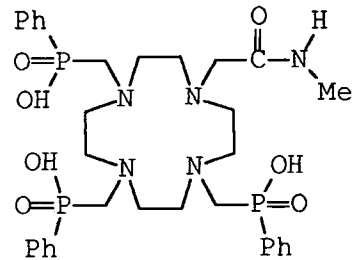
12N4P3Ph3NHMe

Figure 2.2b. *Chemical Structures of the Ligands Used to Complex Gadolinium.*
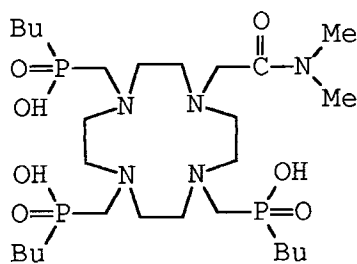
12N4P3Bu3NMe2
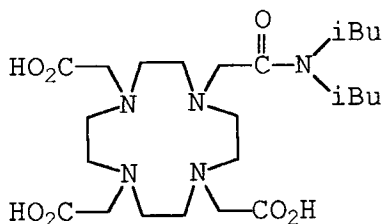
12N4C3N(IBu2)
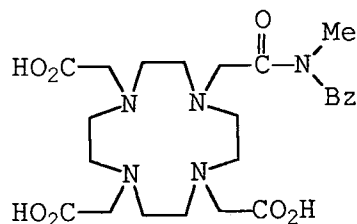
12N4C3NMeBz
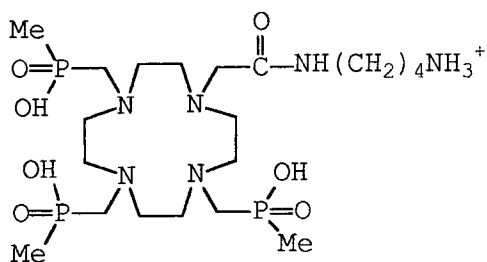
12N4P3Me3NH(CH2)4NH3+
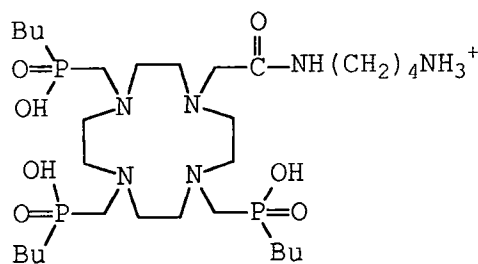
12N4P3Bu3NH(CH2)4NH3+
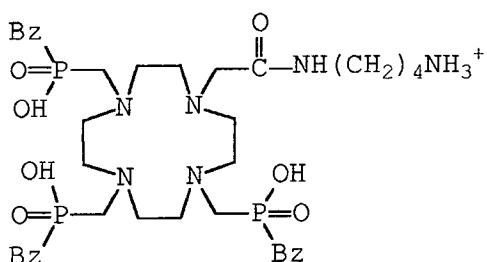
12N4P3Bz3NH(CH2)4NH3+
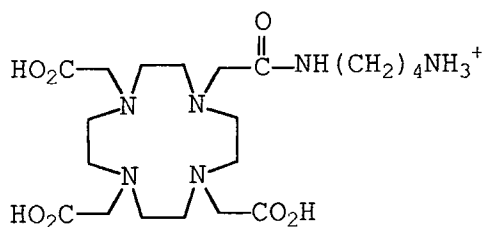
12N4C3NH(CH2)4NH3+
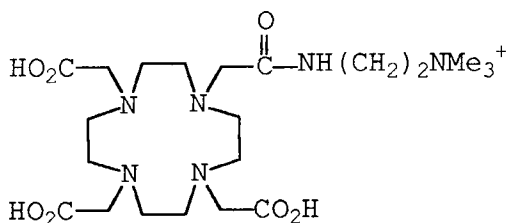
12N4C3NH(CH2)2NMe3+
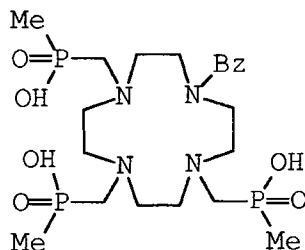
12N4P3Me3Bz

Figure 2.2c. *Chemical Structures of the Ligands Used to Complex Gadolinium.*

| DTPA(NHBz)2 | DTPA | BOPTA | Citrate |
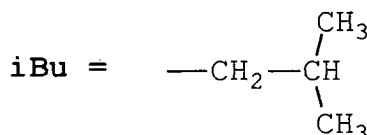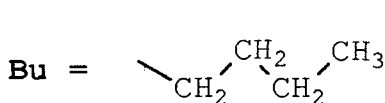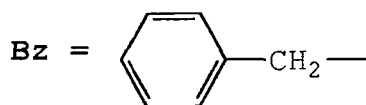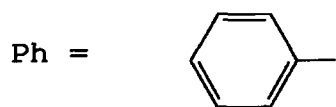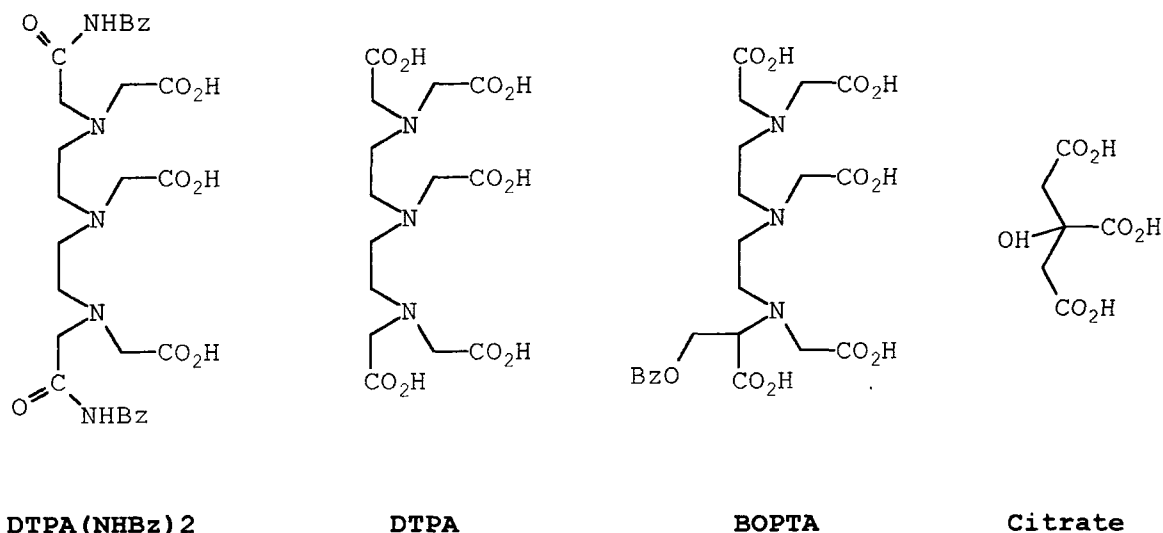
In Vitro Measurements

Acid catalysed dissociation measurements were performed on the following eight complexes and then related to their kinetic stability in vivo :-

Group I,   [Gd.DOTA]⁻ and [Gd.12N4P4Me4]⁻, hydrophilic
             anionic.

Group II,   [Gd.12N4P4Ph4]⁻, [Gd.12N4P4Bu4]⁻ and
             [Gd.12N4P4Bz4]⁻, lipophilic anionic.

Group III,   [Gd.12N4P3Me3NBu2], [Gd.12N4P3Me3NBz2] and
             [Gd.12N4P3Bu3NMe2], neutral.

Partition coefficient measurements were performed as a means of determining the relative lipophilicities of the gadolinium complexes. These measurements were then compared to the animal distribution data to determine whether any relationship exists between the lipophilicity of the complex and its route of elimination from the mouse. Partition coefficients were determined for eleven gadolinium complexes:-

Group I,   [Gd.DOTA]$^-$ and [Gd.12N4P4Me4]$^-$, hydrophilic
             anionic.
Group II,   [Gd.12N4P4Ph4]$^-$, [Gd.12N4P4Bu4]$^-$ and
             [Gd.12N4P4Bz4]$^-$, lipophilic anionic.
Group III,   [Gd.12N4P3Me3NBu2], [Gd.12N4P3Me3NBz2],
             [Gd.12N4P3Ph3NMe2] and [Gd.12N4P3Bu3NMe2],
             neutral.
Group IV,   [Gd.DTPA]$^{2-}$ and [Gd.BOPTA]$^{2-}$.

In Vivo Experiments

Biodistributions of all 25 gadolinium complexes were examined in order to assess their suitability for MRI. In the first study all 25 complexes were given to mice at a low dose of 0.1 μmol/kg to assess the in vivo stability of the complexes and to establish the principle route of elimination of the complex from the body (hepatobiliary vs. renal).

Following on from this study one complex [Gd.12N4P4Bz4]$^-$, which exhibited properties which could make it a favourable agent for use in hepatobiliary imaging by MRI, was studied in greater detail. This included examining not only its biodistribution over an extended time period and at higher doses, but also its behaviour in another species (rats) and the effect of co-administration of the drug bromosulphophthalein (section 1.3.6).

The effect of increasing the dose a thousand fold to 100 μmol/kg, corresponding to the levels used in the clinic, on the route of excretion and in vivo stability of three

selected complexes [Gd.12N4P4Bz4]⁻, [Gd.12N4P4Me4]⁻ and [Gd.DTPA]$^{2-}$ was also studied.

The Overall Aims.

The overall aims of this study were to determine the principle route of excretion (hepatobiliary or renal) of the groups of gadolinium complexes (page 46) and to assess their in vivo stability. It was also of particular interest to determine whether any chemical properties of the complexes (i.e. cyclic vs. acyclic, charge, lipophilicity, and acid dissociation rate constant (k_{obs})) could be correlated with their in vivo stability and route of elimination.

The two gadolinium complexes in common use in MRI, [Gd.DOTA]⁻ (group I) and [Gd.DTPA]$^{2-}$(group VIII), were included in this study to illustrate the behaviour of complexes which are known to be cleared almost exclusively by the kidneys[1]. The complex [Gd.Citrate] (group IX), is known to be unstable in vivo and has been included in order to pinpoint those tissues in which uncomplexed gadolinium is deposited.

2.2. DISSOCIATION OF GADOLINIUM MACROCYCLE COMPLEXES

Experimental details are given in section 2.6.

Dissociation measurements using HPLC radiometry were carried out on the following eight gadolinium macrocycle complexes:-

Group I,   [Gd.DOTA]⁻ and [Gd.12N4P4Me4]⁻, hydrophilic anionic.

Group II,   [Gd.12N4P4Ph4]⁻, [Gd.12N4P4Bu4]⁻ and [Gd.12N4P4Bz4]⁻, lipophilic anionic.

Group III, [Gd.12N4P3Me3NBu2], [Gd.12N4P3Me3NBz2] and [Gd.12N4P3Bu3NMe2], neutral.

2.2.1. Stabilities of Gadolinium Aza-phosphinic Acid Macrocycles

The results given in Table 2.2 show that in the pH range 1 to 2, all of these gadolinium aza-phosphinic acid macrocyclic complexes are between 15 and 1,000 times more stable than [Gd.DTPA]$^{2-}$ (k_{obs}= 1.1 x 10^{-3} s^{-1} at pH 1)[19].

The most stable of the new [Gd.macrocycle] compounds are the neutral compounds [Gd.121N4P3Me3NBu2], [Gd.12N4P3Bu3NHMe] and [Gd.12N4P3NBz2]. These exhibit similar stabilities to [Gd.DOTA]$^-$ with respect to acid catalysed dissociation. Indeed [Gd.12N4P3Me3Bu2] is more stable than [Gd.DOTA]$^-$ at pH 1.0, as might be expected on the basis of coulombic attraction. Neutral complexes should be the least sensitive to acid catalysed dissociation and their k_{obs} values also show a less steep dependence on pH than do the anionic complexes (figure 2.3).

Of the negatively charged [Gd.macrocycles], [Gd.DOTA]$^-$ is the most stable with [Gd.12N4P4Me4]$^-$ not far behind followed by [Gd.12N4P4Bz4]$^-$, [Gd.12N4P4Bu4]$^-$ and lastly [Gd.12N4P4Ph4]$^-$. These compounds also follow the same order when it comes to stability dependence on pH (figure 2.3). For [Gd.12N4P4Ph4]$^-$ the plot of k_{obs} vs. pH shows a steep slope, this complex having the greatest increase in k_{obs} with decrease in pH. The more lipophilic compounds appear to be more sensitive to attack by H$^+$ at low pH.

Table 2.2. *Dissociation Data for Gadolinium Complexes*

Gadolinium complex	pH	$k_{obs}/$ * 10^{-6} sec^{-1}	Half Life Hours
DOTA	1.0	3.16	60.2
	1.3	1.73	111
	1.5	0.898	214
	2.0	0.0490	3930
12N4P4Me4	1.0	10.4	18.5
	1.3	7.37	26.1
	1.5	4.63	41.6
	2.0	1.13	171
12N4P4Ph4	1.0	77.6	2.48
	1.5	36.4	5.29
	2.0	14.7	13.1
12N4P4Bu4	1.0	36.9	5.22
	1.5	20.1	9.59
	2.0	7.08	27.2
12N4P4Bz4	1.0	23.9	8.06
	1.5	9.14	21.1
	2.0	2.81	68.5
12N4P3Me3NBu2	1.0	1.26	152
	1.5	0.494	389
	2.0	0.204	943
12N4P3Me3NBz2	1.0	4.28	44.9
	1.5	1.64	118
	2.0	1.00	192
12N4P3Bu3NHMe	1.0	4.14	46.5
	1.5	1.52	127
	2.0	0.451	427

*Standard Errors are listed in Table 2.33.

Figure 2.3.

Variation of kobs with pH for Gadolinium Macrocycles

(y-axis: kobs/10 -6 s-1; x-axis: pH; curves labelled 12N4P4Ph4, 12N4P4Bu4, 12N4P4Bz4, 12N4P4Me4, 12N4P3Me3NHBz2, 12N4P3Bu3NHMe, DOTA, 12N4P3Me3NBu2)
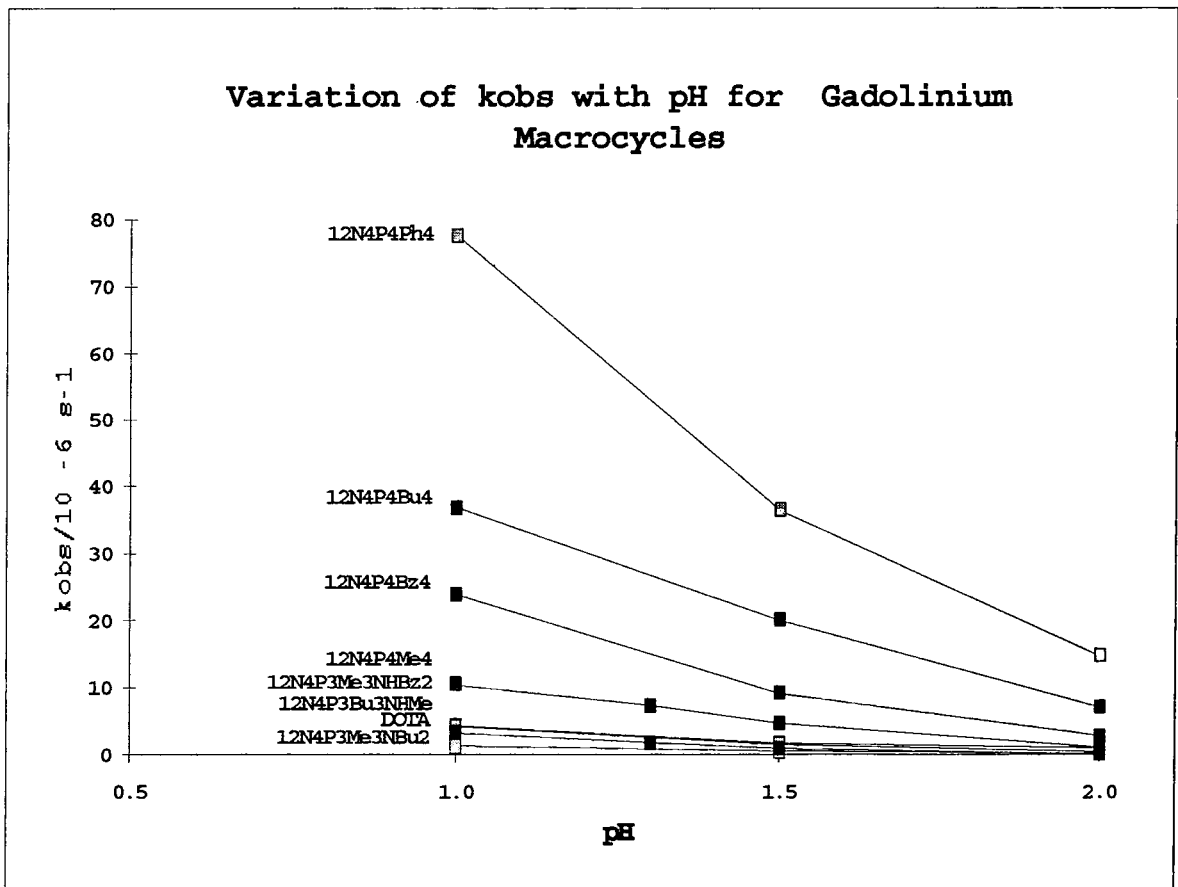
2.3. PARTITION COEFFICIENTS OF GADOLINIUM MACROCYCLE COMPLEXES

Experimental details are given in section 2.6.3.

The partition coefficient P is a measure of the amount of a compound dissolved in one solvent phase relative to another solvent phase under equilibrium conditions.

Here, the partition coefficients between octanol and water, octanol and phosphate buffered saline, pH 7.4 (PBS), butanol and water, and butanol and PBS are measured as a means of comparing the lipophilicities of the gadolinium complexes. PBS was used as well as water as PBS is more comparable with physiological conditions i.e. buffered at pH 7.4.

A high (more positive) Log P value relates to increased lipophilicity. Lipophilic compounds are more likely to be eliminated from the body via the hepatobiliary route than the renal route. Hence it was hoped to establish a correlation between the Log P values and the route of elimination from a mouse that had been injected with the corresponding radiolabelled complex.

Log P values were determined for eleven gadolinium complexes:-

Group I,   [Gd.DOTA]⁻ and [Gd.12N4P4Me4]⁻, hydrophilic anionic.

Group II,   [Gd.12N4P4Ph4]⁻, [Gd.12N4P4Bu4]⁻ and [Gd.12N4P4Bz4]⁻, lipophilic anionic.

Group III, [Gd.12N4P3Me3NBu2], [Gd.12N4P3Me3NBz2], [Gd.12N4P3Ph3NMe2] and [Gd.12N4P3Bu3NMe2], neutral.

Group IV,   [Gd.DTPA]²⁻ and [Gd.BOPTA]²⁻, acyclic anionic.

Table 2.3. *Gadolinium Macrocycle Partition Coefficients*

Gadolinium Complex	Octanol/ water	Log P Octanol/ PBS	Butanol/ water	Butanol/ PBS
12N4P4Me4	-4.75	-4.47	-3.03	-3.15
DTPA	-4.18	-4.59	-3.96	-3.87
BOPTA	-3.63	-3.79	-2.50	-2.18
DOTA	-3.40	-4.16	-2.39	-3.01
12N4P3Me3NBu2	-2.00	-1.91	-0.05	-0.53
12N4P3Me3NBz2	-1.36	-1.33	-0.13	-0.15
12N4P4Ph4	-1.54	-1.14	0.41	0.35
12N4P4Bu4	-1.09	-1.05	0.58	0.52
12N4P4Bz4	-0.66	-0.48	0.71	0.61
12N4P3Ph3NMe2	-0.36	-0.37	0.54	0.51
12N4P3Bu3NHMe	-0.35	-0.34	0.57	0.58

These results are shown graphically in figure 2.4.

The complexes [Gd.12N4P3Bu3NHMe] and [Gd.12N4P3Ph3NMe2] have the highest Log P values with [Gd.12N4P4Bz4]⁻, [Gd.12N4P4Bu4]⁻ and [Gd.12N4P4Ph4]⁻ next. These complexes all have positive Log P values when measured in butanol/water and butanol/PBS.

The low Log P value for [Gd.BOPTA]$^{2-}$ can be attributed to its double negative charge.

For all the complexes there is no significant difference between the Log P values for water or PBS, showing that the buffering action of the PBS does not change Log P. Complexes follow the same pattern of solubility in octanol and butanol. Log P values are generally higher in butanol than octanol.

Figure 2.4. *Log P Values for Gadolinium Complexes.*
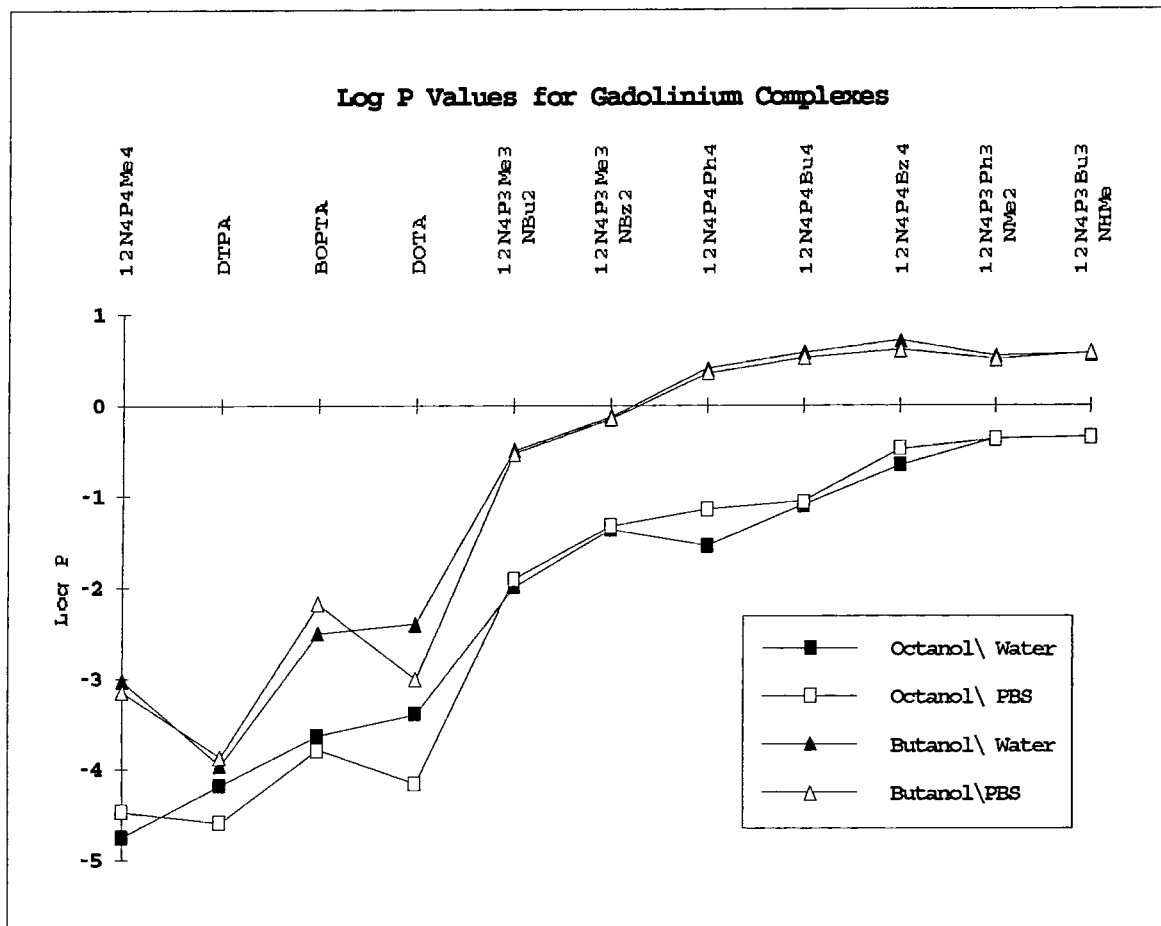
2.4. BIODISTRIBUTION STUDIES.

2.4.1. Biodistribution of Gd Complexes at a Dose of 0.1 μmol/kg.

The aims of this study were to determine the principle route of excretion (hepatobiliary or renal) of all 25 gadolinium complexes and to assess their in vivo stability.

Presentation of results

Figures 2.5 to 2.11 show the % dose in 5 tissues at 5 minutes post injection for the groups I to IX. These 5 tissues are blood, kidneys, liver, gall bladder and gut, where the gut represents the total intestinal tract from the stomach to the large intestine inclusive. More precise data for individual tissues are shown in section 2.4.1.6. Figures 2.12 to 2.21 each show the % dose for each of the 25 complexes in a single tissue.

Key to Figures in this section.

Number in Figures	Group	Complex
1.	I	[Gd.DOTA]⁻
2.	I	[Gd.12N4P4Me4]⁻
3.	I	[Gd.12N4P3Me3C]⁻
4.	II	[Gd.12N4P4Ph4]⁻
5.	II	[Gd.12N4P4Bu4]⁻
6.	II	[Gd.12N4P4Bz4]⁻
7.	III	[Gd.12N4P3Me3NHMe]
8.	III	[Gd.12N4P3Me3NMe2]
9.	III	[Gd.12N4P3Me3NBu2]
10.	III	[Gd.12N4P3Me3N(IBu)2]
11.	III	[Gd.12N4P3Me3NBz2]
12.	III	[Gd.12N4P3Ph3NHMe]
13.	III	[Gd.12N4P3Bu3NMe2]
14.	IV	[Gd.12N4C3N(IBu)2]
15.	IV	[Gd.12N4C3NMeBz]
16.	V	[Gd.12N4P3Me3NH(CH2)4NH3]⁺
17.	V	[Gd.12N4P3Bu3NH(CH2)4NH3]⁺
18.	V	[Gd.12N4P3Bz3NH(CH2)4NH3]⁺
19.	VI	[Gd.12N4C3NH(CH2)4NH3]⁺
20.	VI	[Gd.12N4C3NH(CH2)2NMe3]⁺
21.	VII	[Gd.12N4P3Me3Bz]
22.	VIII	[Gd.DTPA(NHBz)2]
23.	VIII	[Gd.DTPA]²⁻
24.	VIII	[Gd.BOPTA]²⁻
25.	IX	[Gd.Citrate]

2.4.1.1. Biodistribution Data for the Different Groups of Gd Complexes

Figure 2.5. *Group I. Hydrophilic Anionic Aza-carboxylic and Aza-phosphinic Acids*
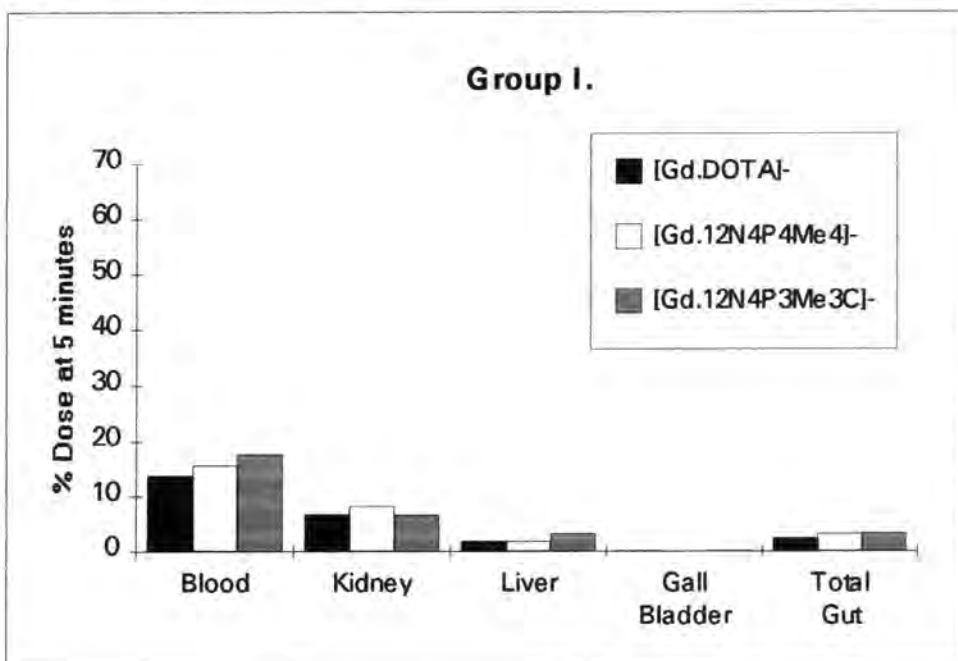
Figure 2.6. *Group II. Lipophilic Anionic Aza-phosphinic Acids*
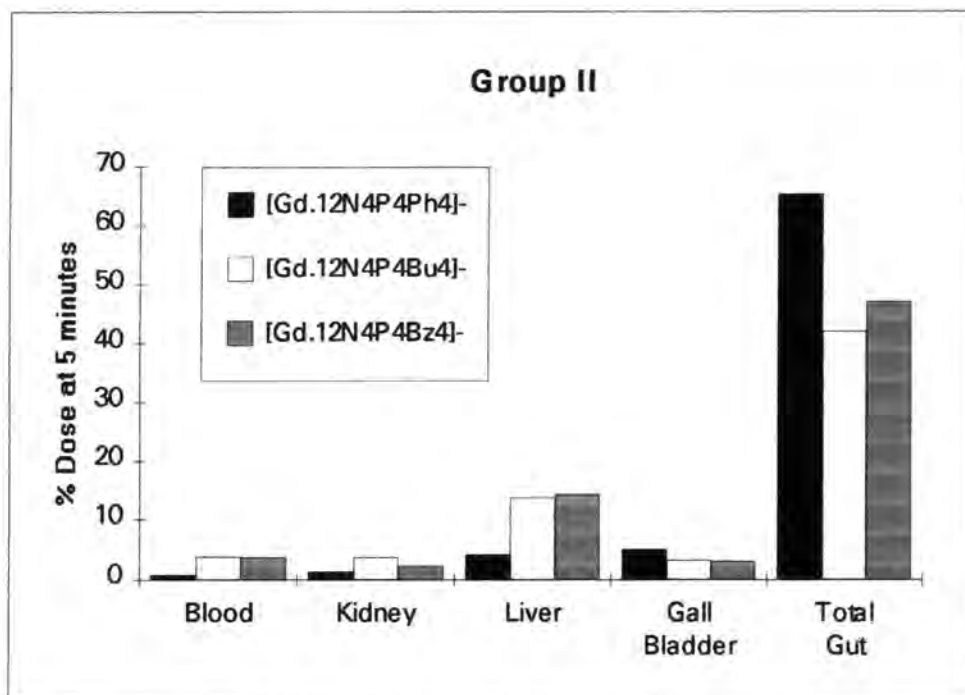
Figure 2.7. *Group III. Neutral Monoamide Aza-phosphinic Acids*

Group III

Legend:
- [Gd.12N4P3Me3NHMe]
- [Gd.12N4P3Me3NMe2]
- [Gd.12N4P3Me3NBu2]
- [Gd.12N4P3Me3N(IBu)2]
- [Gd.12N4P3Me3NBz2]
- [Gd.12N4P3Ph3NMe2]
- [Gd.12N4P3Bu3NHMe]

Y-axis: % Dose at 5 minutes

X-axis: Blood, Kidney, Liver, Gall Bladder, Total Gut
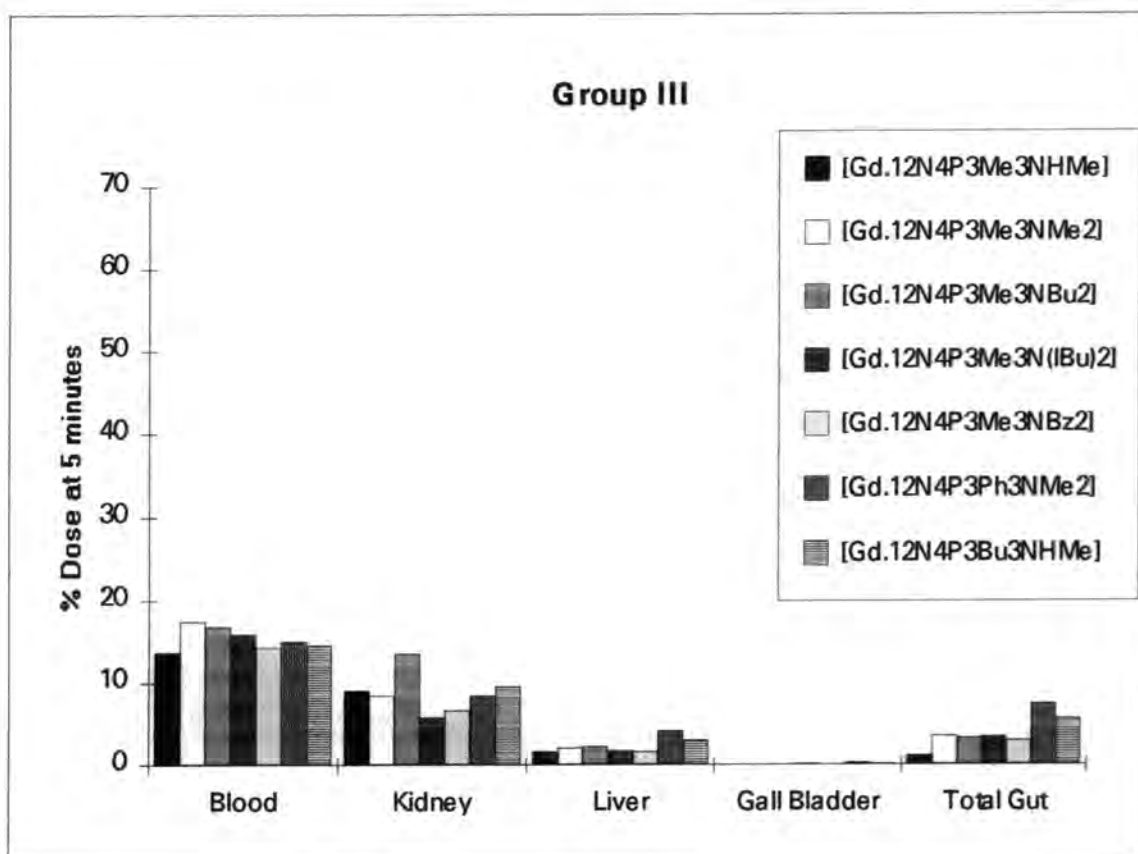
Figure 2.8. *Group IV. Neutral Monoamide Aza-carboxylic Acids*

Group IV

Legend:
- [Gd.12N4C3N(IBu)2]
- [Gd.12N4C3NMeBz]

Y-axis: % Dose at 5 minutes

X-axis: Blood, Kidney, Liver, Gall Bladder, Total Gut
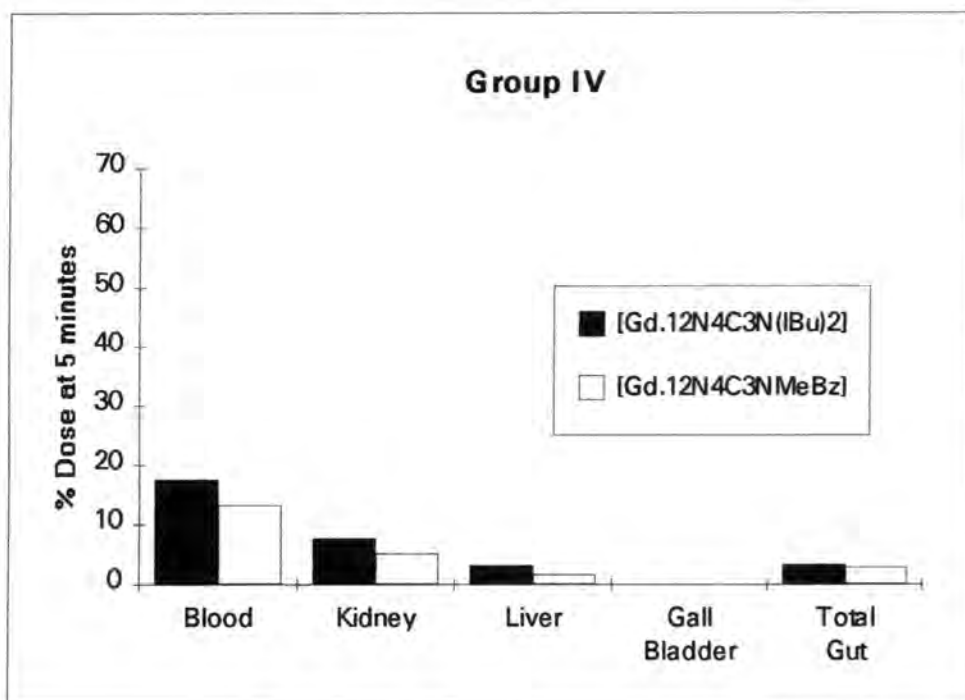
Figure 2.9. *Group V. Cationic Monoamide Aza-phosphinic Acids*
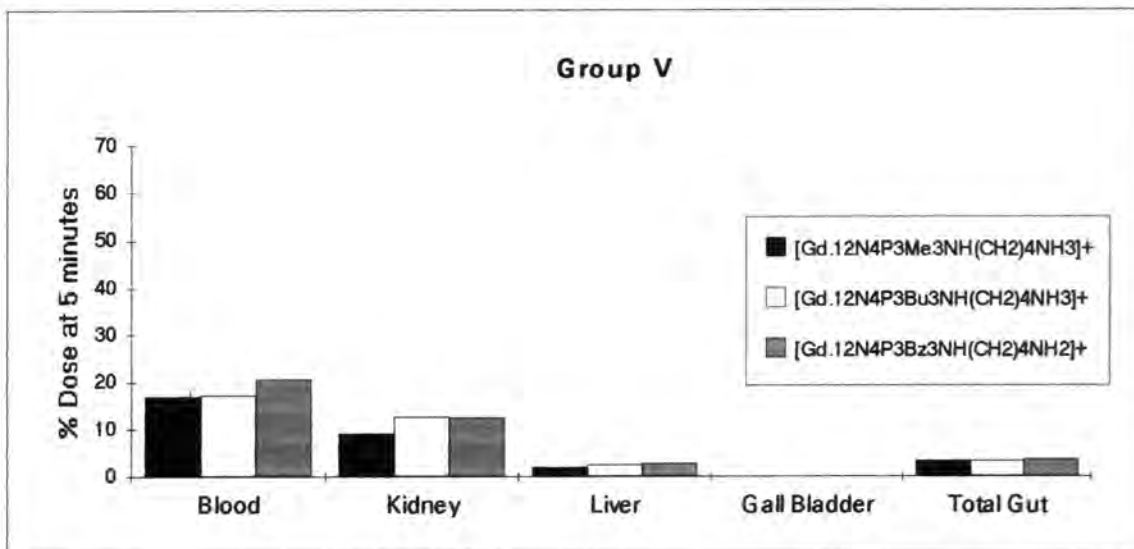
Figure 2.10. *Group VI. Cationic Monoamide Aza-carboxylic Acids and Group VII Neutral 7 Co-ordinate Aza-phosphinic Acid.*
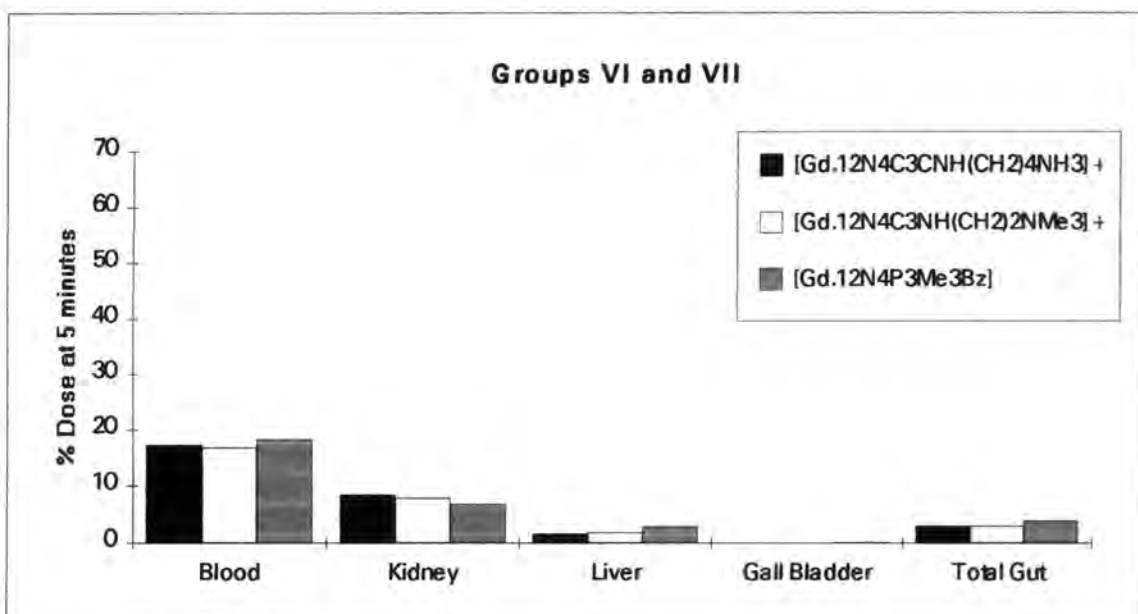
Figure 2.11. *Group VIII. Acyclic Carboxylic Acids and Group IX Citrate.*

Groups VIII and IX
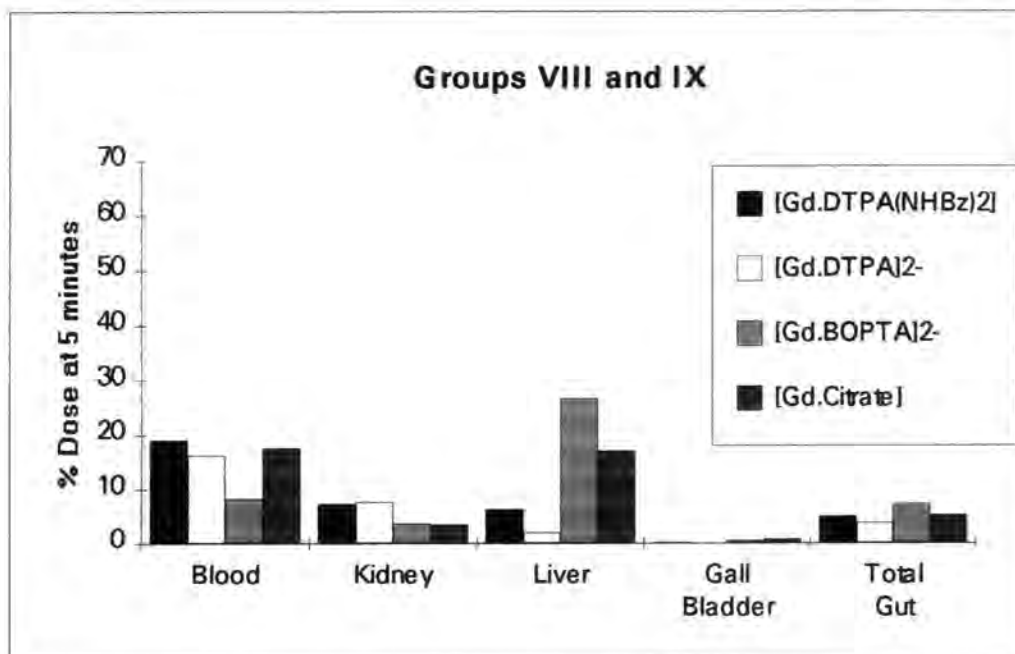
2.4.1.2. **Summary of the Biodistribution of Groups I to IX at a Dose of 0.1 μmol/kg.**

Group I

The three hydrophilic anionic aza-carboxylic and aza-phosphinic acids in group I (numbers 1, 2 and 3) are excreted renally. (figure 2.5). The biodistributions of [Gd.12N4P4Me4]⁻ and [Gd.12N4P3Me3C]⁻ (numbers 2 and 3) are comparable at 5 minutes to that of [Gd.DOTA]⁻ (number 1) which is known to be excreted predominantly via the kidneys. These similarities indicate that renal excretion is the main route of clearance for [Gd.12N4P4Me4]⁻ and [Gd.12N4P3Me3C]⁻

In respect of in vivo stability, [Gd.12N4P3Me3C]⁻ is less stable than [Gd.DOTA]⁻ and [Gd.12N4P4Me4]⁻. [Gd.12N4P3Me3C]⁻ having an elevated retention of ¹⁵³Gd in the blood, liver and skeleton at 24 hours (figures 2.13, 12.17 and 2.19). This is a clear indication of the dissociation of ¹⁵³Gd from this complex.

Group II

This group of lipophilic anionic aza-phosphinic acids (numbers 4, 5 and 6) shows principally hepatobiliary clearance. This is indicated by the very high levels, by 5 minutes post injection, of complex in the liver, gall bladder and gut compared with levels of the other 22 complexes in these tissues (figures 2.16, 2.18 and 2.20). Most of the dose present in the gut at 5 minutes is in the first few centimetres of the small intestine into which the gall bladder empties.

From figure 2.12 it is clear that the group II complexes are being cleared from the blood more quickly by the liver than the other complexes which clear by the kidneys.

Levels of ^{153}Gd in the blood, liver and skeleton at 24 hours are low and comparable to levels with [Gd.DOTA]$^-$ indicating that group II complexes are stable in vivo.

The data in figure 2.6 illustrate the differences within the group. The complex [Gd.12N4P4Ph4]$^-$ (number 4) has the lowest dose in the liver and the highest dose in the gut at 5 minutes. This complex also has the highest Log P value for lipophilicity (section 2.3). Thus there may be some correlation between Log P values of the anionic macrocycle complexes and their rate of clearance through the hepatobiliary system.

Group III

Within this group of seven neutral monoamide aza-phosphinic acid complexes (numbers 7 to 13), two complexes [Gd.12N4P3Ph3NHMe] and [Gd.12N4P3Bu3NMe2] (numbers 12 and 13), were found to behave differently from the other five (figure 2.7).

Complexes [Gd.12N4P3Me3NHMe], [Gd.12N4P3Me3NMe2], [Gd.12N4P3Me3NBu2], [Gd.12N4P3Me3N(IBu)2] and [Gd.12N4P3Me3NBz2] (numbers 7, 8, 9, 10 and 11), are all showing primarily renal clearance. Also, judging by the low

levels of ^{153}Gd in the blood, liver and skeleton at 24 hours (figures 2.13, 2.17 and 2.19), they are stable in vivo.

These complexes could be useful for MRI imaging in the same way as [Gd.DOTA]$^-$ and [Gd.DTPA]$^{2-}$ are used at present with the added advantage that they are neutral complexes. This means that they would have a much more favourable, lower osmolality.

The complexes [Gd.12N4P3Ph3NHMe] and [Gd.12N4P3Bu3NMe2] (numbers 12 and 13) show some clearance by the hepatobiliary route. By 5 minutes a total of 11.7% and 8.8% dose respectively were present in the combined liver, gall bladder and gut of mice given [Gd.12N4P3Ph3NHMe] and [Gd.12N4P3Bu3NMe2]. These values compare with less than 6% of the injected dose in the corresponding tissues of mice given the other 5 neutral complexes. At 24 hours after injection of [Gd.12N4P3Ph3NHMe] or [Gd.12N4P3Bu3NMe2] the level of ^{153}Gd in the blood, liver and skeleton is about twice as great as the levels in the rest of the group (figures 2.13, 2.17 and 2.19). This may indicate a degree of dissociation but is more likely to reflect the rather slower clearance of these neutral lipophilic complexes from the body.

Group IV

The two neutral monoamide aza-carboxylic acids (numbers 14 and 15, figure 2.8) show similar tissue distributions to the neutral monoamide aza-phosphinic acid complexes (numbers 7 to 11) in group III (figures 2.7). Again their is no significant retention of ^{153}Gd in the blood, liver or skeleton at 24 hours (figures 2.13, 2.17 and 2.19) indicating good in vivo stability. Both complexes show primarily renal clearance and could prove useful in MRI for the same reasons as numbers 7 to 11 in group III.

Group V

These cationic monoamide aza-phosphinic acids (numbers 16 to 18) are all showing primarily renal clearance (figure

2.9). Only [Gd.12N4P3Bu3NH(CH2)4NH3]$^+$ (number 17), shows any
indication of dissociation with a slightly elevated level in
the skeleton at 24 hours of 0.46% dose, in comparison to
<0.05% for [Gd.DOTA]$^-$ (figure 2.19). Complexes
[Gd.12N4P3Me3NH(CH2)4NH3]$^+$ and [Gd.12N4P3Bz3NH(CH2)4NH3]$^+$
appear to be stable in vivo, based upon the lack of ^{153}Gd
deposition in the skeleton.

Group VI

These two cationic monoamide aza-carboxylic acids
(numbers 19 and 20), show primarily renal clearance (figure
2.10) and no significant retention of ^{153}Gd at 24 hours in
the liver or skeleton(figures 2.17 and 2.19) consistent with
good in vivo stability.

Group VII

This neutral 7 co-ordinate aza-phosphinic acid (number
21), is showing primarily renal clearance at 5 minutes
(figure 2.10). However by 24 hours it is obvious that this
complex is highly unstable in vivo with large amounts of
^{153}Gd retained in the liver (8% dose) and skeleton (10.8%
dose) as well as elevated levels in blood and gut (figures,
2.17, 2.19, 2.13 and 2.21).

Group VIII

This group of acyclic carboxylic acids (figure 2.11)
includes a neutral complex, [Gd.DTPA(NHBz)2] (number 22), an
anionic hydrophilic complex, [Gd.DTPA]$^{2-}$ (number 23), and a
lipophilic anionic complex, [Gd.BOPTA]$^{2-}$ (number 24).
At 5 minutes [Gd.DTPA(NHBz)2] (number 22), shows
primarily renal clearance, but the % dose in the liver (6.3%)
and gut (4.9%), is about twice that found in the
corresponding tissues of the mice given stable, renally
cleared, neutral macrocyclic complexes (group III numbers 7
to 11). By 24 hours the amount of radiolabel remaining in the

liver, skeleton and gut (figures 2.13, 2.17, 2.19 and 2.21) is about 10 times that remaining after treatment with one of the stable, renally cleared, neutral complexes (group III numbers 7 to 11). Although it is difficult to say precisely to what extent this can be accounted for by some hepatobiliary clearance as opposed to dissociation of the complex, it is clear that the complex does dissociate significantly.

The complex $[Gd.DTPA]^{2-}$ (number 23), is clearing primarily by the renal pathway. There is a slight elevation in the % dose in the skeleton at 24 hours, and 0.3% of the injected dose was found there compared to less than 0.05% of the dose for $[Gd.DOTA]^-$. This suggests that $[Gd.DTPA]^{2-}$ is more susceptible to dissociation in vivo than $[Gd.DOTA]^-$ in accordance with their relative rates of acid-catalysed dissociation (section 2.2).

The lipophilic anionic complex $[Gd.BOPTA]^{2-}$ (number 24), also shows hepatobiliary clearance. In common with the behaviour of the lipophilic macrocycle complexes in group II, $[Gd.BOPTA]^{2-}$ clears rapidly from the blood into the liver (22% dose), gall bladder and gut with only about 5% dose in the kidneys at 5 minutes. The rate of passage through the hepatobiliary system is not as fast as for the group II lipophilic anionic aza-phosphinic acids. This could be related to the double negative charge on $[Gd.BOPTA]^{2-}$ and therefore its lower Log P value.

By 24 hours the % dose/g retained in the skeleton is slightly elevated at 0.22% dose compared to <0.05% dose for $[Gd.DOTA]^-$, suggesting that $[Gd.BOPTA]^{2-}$ is less stable in vivo than $[Gd.DOTA]^-$.

Group IX

$[Gd.Citrate]$ is known to be highly unstable in vivo. This can be seen from the elevated levels in the liver (22% dose) and skeleton (52% dose) at 24 hours (figures 2.17 and 2.19). There are also elevated levels in the blood (figure 2.13) caused by the dissociated ^{153}Gd binding to blood proteins

such as transferrin, and in the gut (figure 2.21) where dissociated ^{153}Gd is being slowly eliminated from the liver.

Other tissues

The distribution of these complexes was also examined in various other tissues i.e. brain, fat, lungs, heart muscle, skeletal muscle, spleen, salivary glands and skin.

Of particular interest was whether the lipophilic complexes were crossing the blood/brain barrier or being concentrated in the fat. The salivary glands and skin were examined to see if there was any excretion of complexes by these routes. There was no evidence of accumulation of lipophilic complexes in the brain, fat, salivary glands or the skin.

Some slight increases in the % dose in the tissues listed below were seen for [Gd.Citrate] (number 25) and [Gd.12N4P3Me3Bz] (number 21). Both of these complexes are highly unstable and are showing high blood levels of ^{153}Gd (figure 2.13). The complex no. 23 [Gd.DTPA]$^{2-}$, appears to have about twice the % dose in the brain and lung as most of the other stable complexes measured.

(a) % Dose in Brain.

The % dose in the brain at 5 minutes was less than 0.15% for all the gadolinium complexes. After 24 hours all the complexes had less than 0.002% dose in the brain, with the exceptions of numbers 21 (0.006%), 23 (0.004%) and 25 (0.028%).

(b) % Dose/g Fat

The % dose/g fat was less than 1% dose/g at 5 minutes and less than 0.005% dose/g at 24 hours for all complexes.

(c) % Dose Lung

The % dose in the lung was measured for complexes numbers 1, 2 ,4, 5, 6, 7, 17, 18, 21, 22, 23 and 25. There was less than 1% dose at 5 minutes and less than 0.005% dose at 24 hours in the lungs with the exceptions of numbers 21, 23 and 25 with 0.06, 0.01 and 0.25% dose respectively at 24 hours.

(d) % Dose/g Heart Muscle

The % dose/g of heart muscle was measured for complexes numbers 4, 5, 6, 7, 18, 21, 22 and 25. The % dose/g was less than 1.5% at 5 minutes and less than 0.002% at 24 hours for these complexes measured except for number 25 (2.5% at 5 min and 0.98% at 24 hr).

(e) % Dose Spleen

For the complexes 1, 2, 4, 6, 7, 17 ,18, 22, 23 and 25 the amount of radiolabel in the spleen was measured. The % dose was less than 0.3% for these complexes at 5 minutes, and less than 0.005% at 24 hours except for numbers 23 (0.02%) and 25 (0.07%).

(f) % Dose in the Salivary Glands.

The dose in the salivary glands was measured for complexes 1, 2, 4, 7, 23 and 25. All had doses of less than 0.6% at 5 minutes and less than 0.01% at 24 hours except number 25 (0.14% at 24 hr).

(g) % dose/g Skin

The % dose/g of skin was measured for complexes 1, 2, 4, 7, 23 and 25. The % dose/g were less than 0.6% at 5 minutes and less than 0.1% at 24 hours except for number 25 (0.34% at 24 hr).

2.4.1.3. Biodistributions of 25 Gadolinium Complexes at 0.1 μ mol/kg.

% Dose in Blood

Figure 2.12. % *Dose ^{153}Gd in Blood at 5 Minutes.*
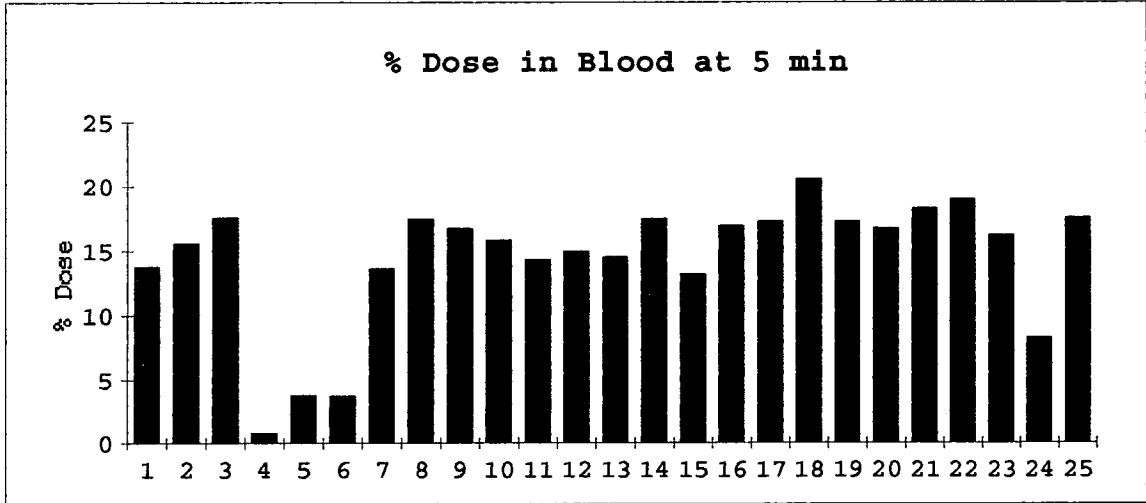
Figure 2.13. % *Dose ^{153}Gd in Blood at 24 Hours.*
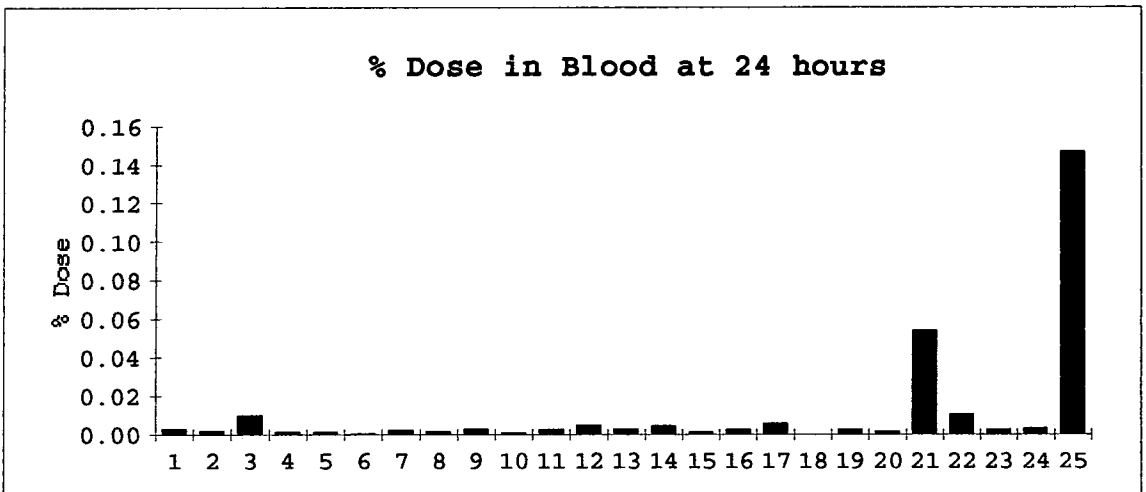
% Dose in Kidneys

Figure 2.14. % Dose ^{153}Gd in Kidneys at 5 Minutes.

% Dose in Kidney at 5 min
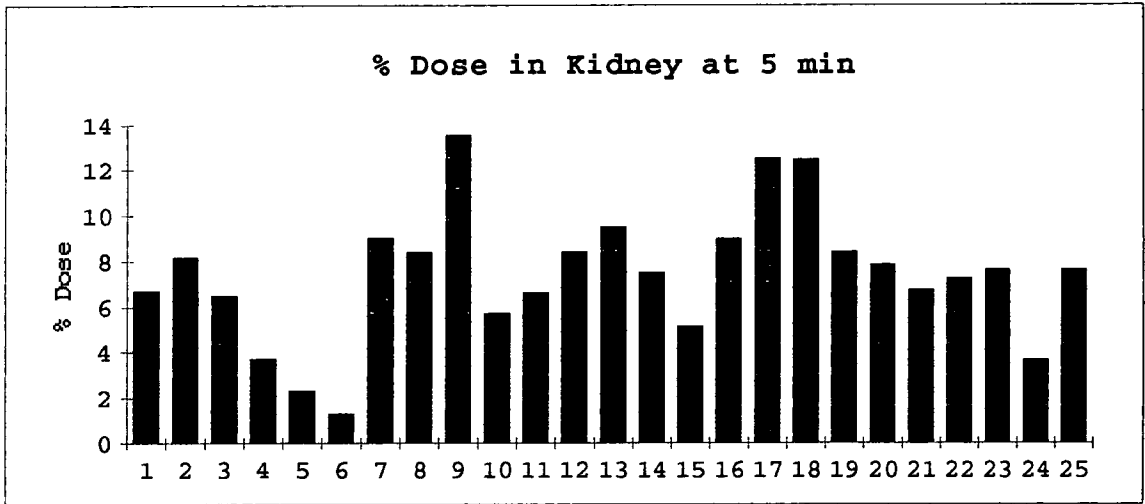
Figure 2.15. % Dose ^{153}Gd in Kidneys at 24 Hours.

% Dose in Kidneys at 24 hours
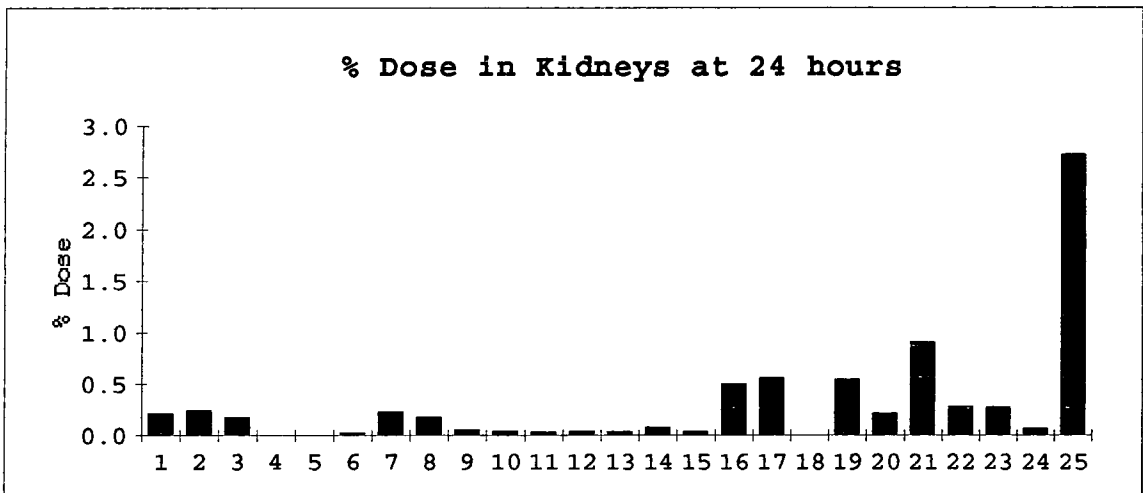
% Dose in Liver

Figure 2.16. % Dose ^{153}Gd in Liver at 5 Minutes.

% Dose in Liver at 5 min
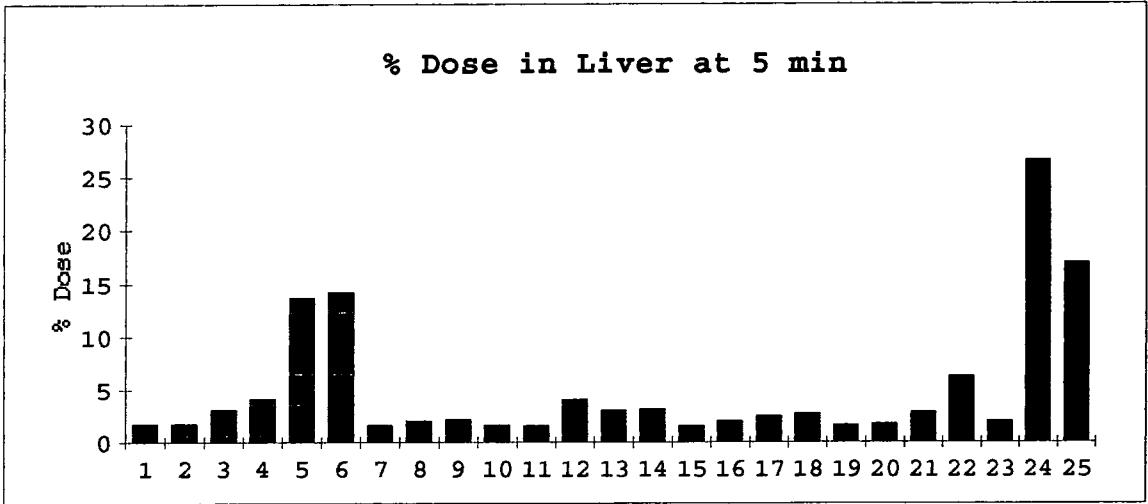
Figure 2.17. % Dose ^{153}Gd in Liver at 24 Hours.

% Dose in Liver at 24 hours
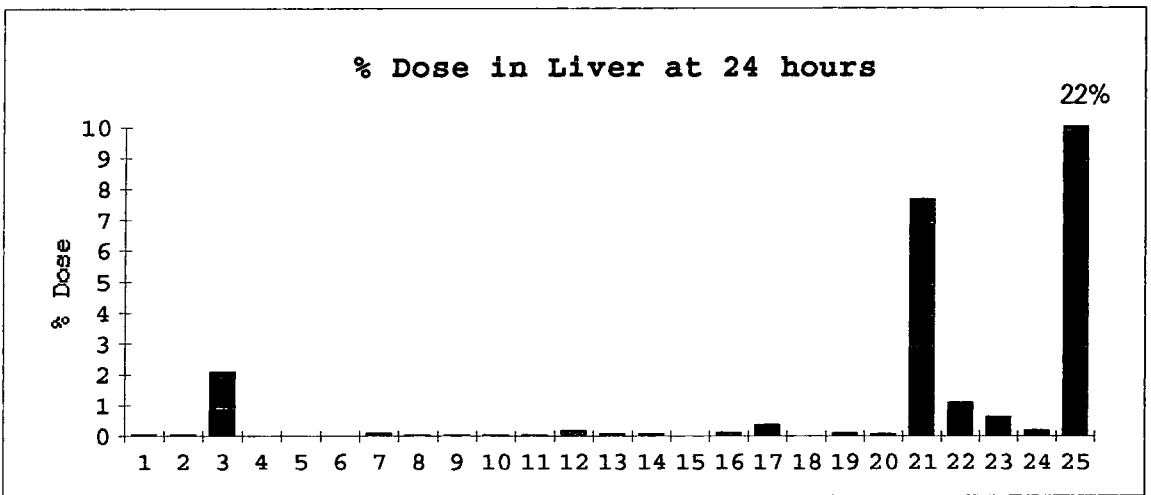
% Dose in Gall Bladder.

Figure 2.18. % Dose ^{153}Gd in Gall Bladder at 5 Minutes

% Dose in Gall Bladder at 5 min
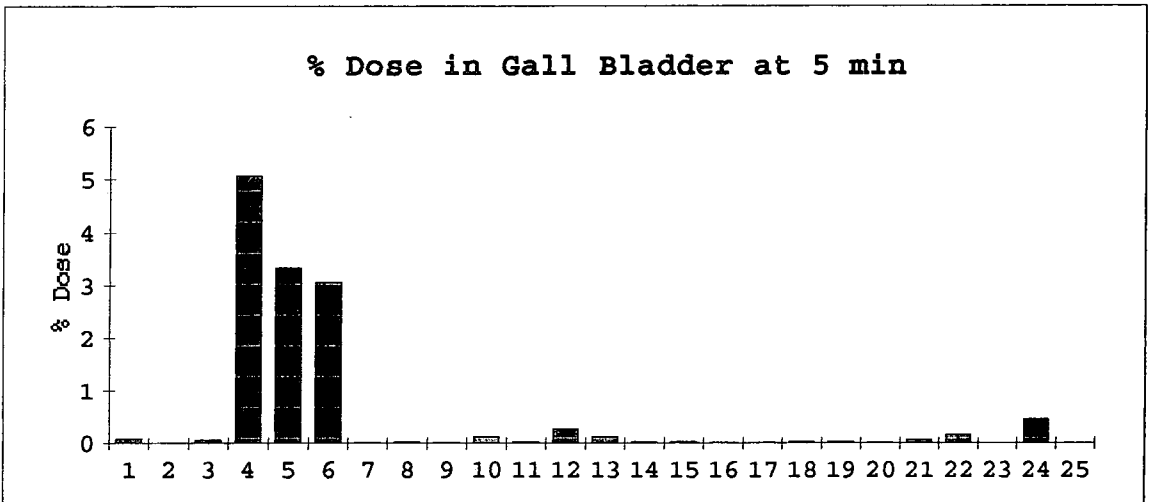
% Dose/g in Skeleton.

Figure 2.19. % Dose ^{153}Gd in Skeleton at 24 Hours.

% Dose in Skeleton at 24 hours
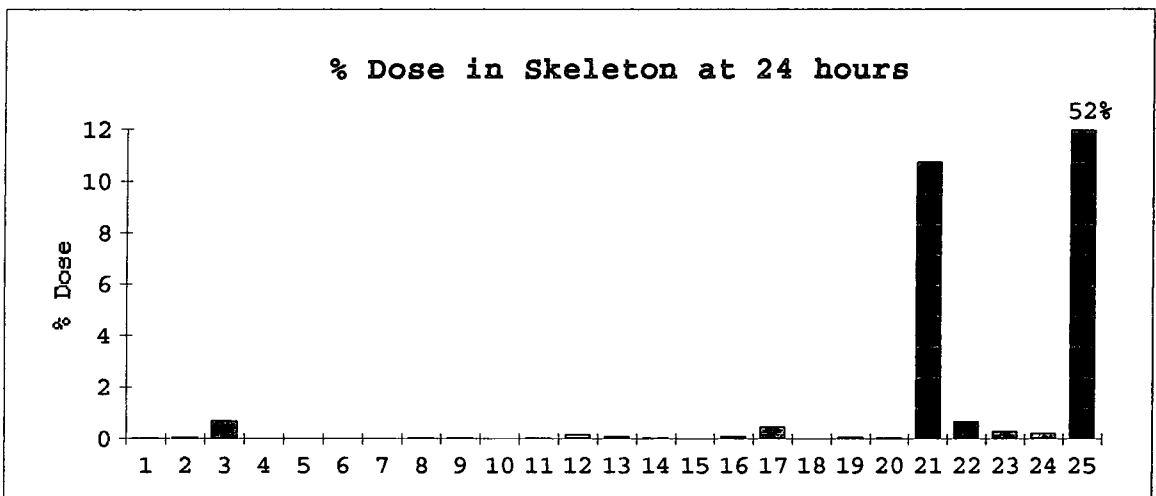
% Dose in the Gut.

Figure 2.20. % Dose ^{153}Gd in Total Gut at 5 Minutes

% Dose in Total Gut at 5 min
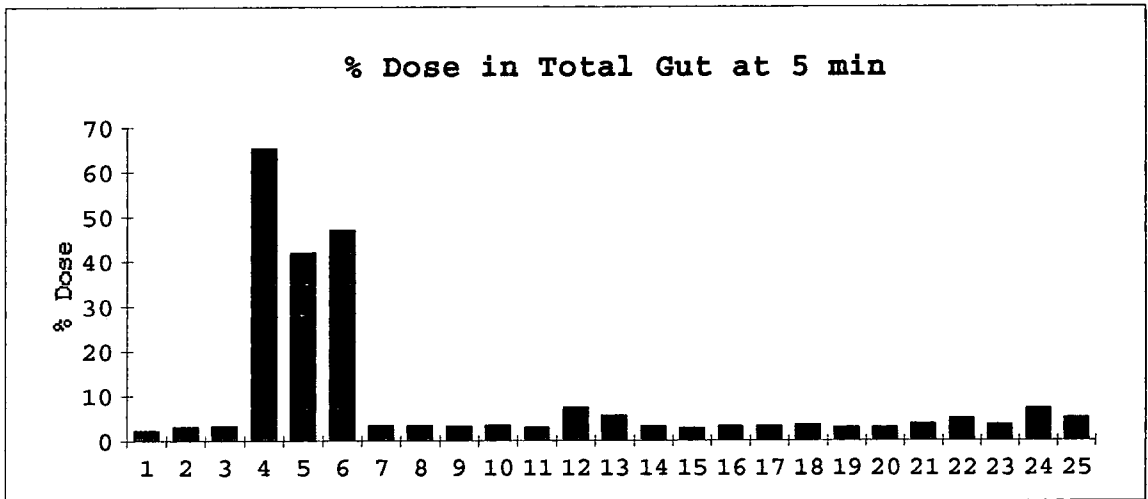
Figure 2.21. % Dose ^{153}Gd in Total Gut at 24 Hours

% Dose in Total Gut at 24 hours
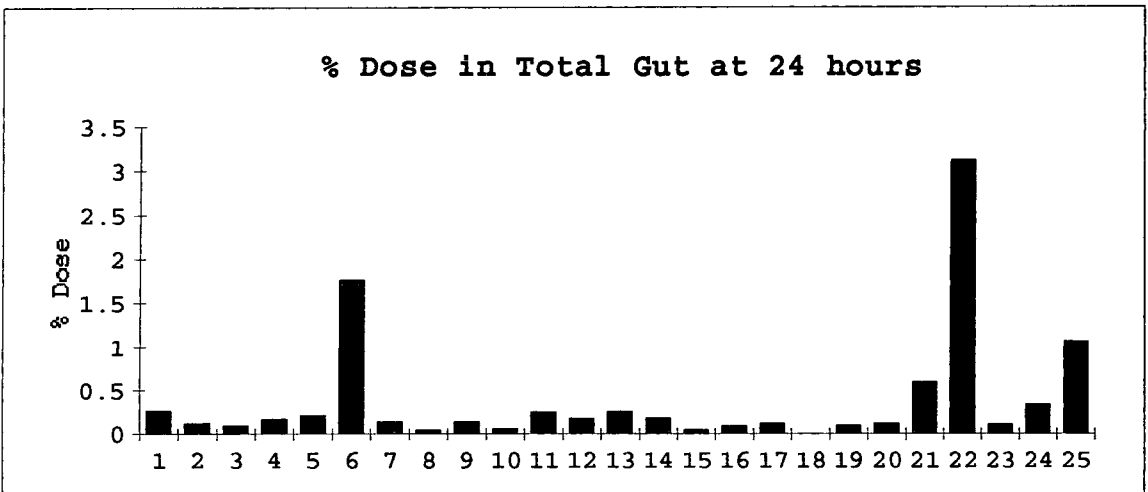
2.4.2. Further Biodistribution Studies on the Complex [Gd.12N4P4Bz4]⁻

Further studies at higher doses were carried out with [Gd.12N4P4Bz4]⁻ as it was showing properties which suggested that it was a candidate for hepatobiliary imaging by MRI. The properties which influenced this choice were :-

1. A high specific clearance through the hepatobiliary system (section 2.4.1).
2. It was the most stable of the anionic lipophilic macrocycles with respect to acid catalysed dissociation (section 2.2).
3. It was the most water soluble of the anionic lipophilic macrocycles. The solubility[27] of H_3O^+[Gd.12N4P4Bz4]⁻ is 40 mmol dm⁻³.
4. Ease of synthesis and purification[28].

The biodistribution of [Gd.12N4P4Bz4]⁻ was firstly studied in more detail over 24 hours with a dose of 0.1 μ mol/kg. This included 2 and 4 hour time points. Higher doses of [Gd.12N4P4Bz4]⁻, 2, 70 and 100 μmol/kg were then studied at 5 minute, and doses of 2, and 100 μmol/kg at 24 hour time points. These higher doses are in line with doses currently used in the clinic for [Gd.DTPA]²⁻.

The biodistribution of [Gd.12N4P4Bz4]⁻ was also examined in two rats at 10 and 20 minutes to see if the clearance pattern was similar in the two species. Lastly the effect of the drug bromosulphophthalein was examined. This compound inhibits liver uptake of the complex by the 'organic anion transporter' (section 1.3.6).

2.4.2.1. Biodistribution of [Gd.12N4P4Bz4]⁻ at a Dose of 0.1 μmol/kg.

Figure 2.22. *[Gd.12N4P4Bz4]⁻ at a Dose of 0.1 μmol/kg*
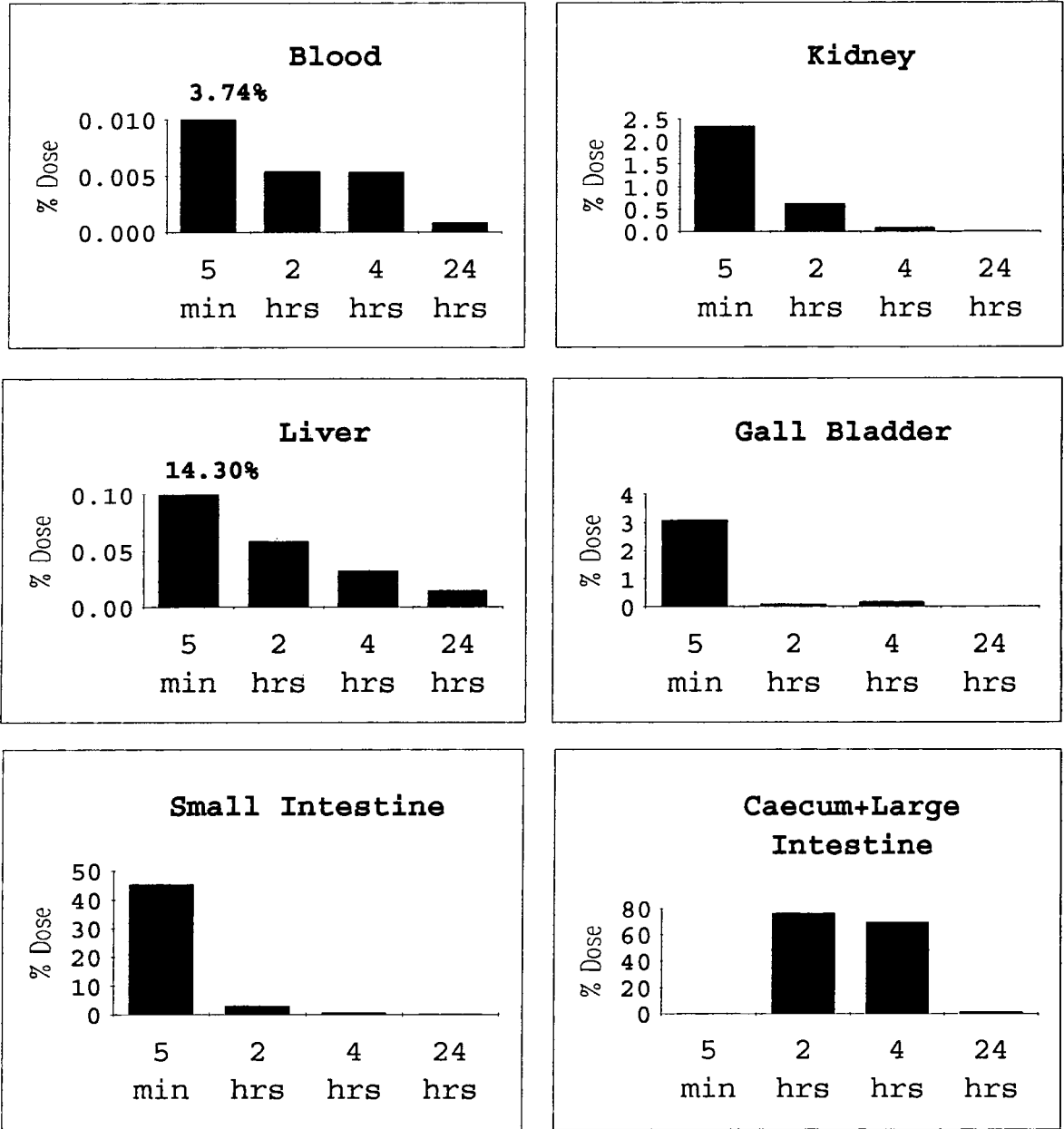
The data shown in figure 2.22 demonstrate the rapid clearance of [Gd.12N4P4Bz4]⁻ from the blood through the hepatobiliary system. By 5 minutes 14.3% of the dose is in the liver, 3% in the gall bladder and 45% is already present in the small intestine.

By 2 hours there is less than 0.005% dose left in the blood and only 0.05% dose in the liver. 80% of the dose has entered the intestine and can be seen to have moved down the intestine into the caecum and large intestine.

After 4 hours some complex has been excreted in the faeces, and by 24 hours the majority of the complex has left the mouse with only very small amounts remaining in the elimination pathway.

The role of the kidneys in renal clearance is also evident from figure 2.22. There is a low % clearance by this route, <2.5% dose being in the kidneys at 5 minutes and this amount decreases steadily thereafter. However the % dose in the kidneys is not a measure of the total dose cleared renally, as even by 5 minutes some dose has passed through the kidneys and into the urine.

2.4.2.2. The Effect on Biodistribution of Increasing Doses of [Gd.12N4P4Bz4]⁻

Figure 2.23. % *Dose [Gd.12N4P4Bz4]⁻ at 5 Minutes*.
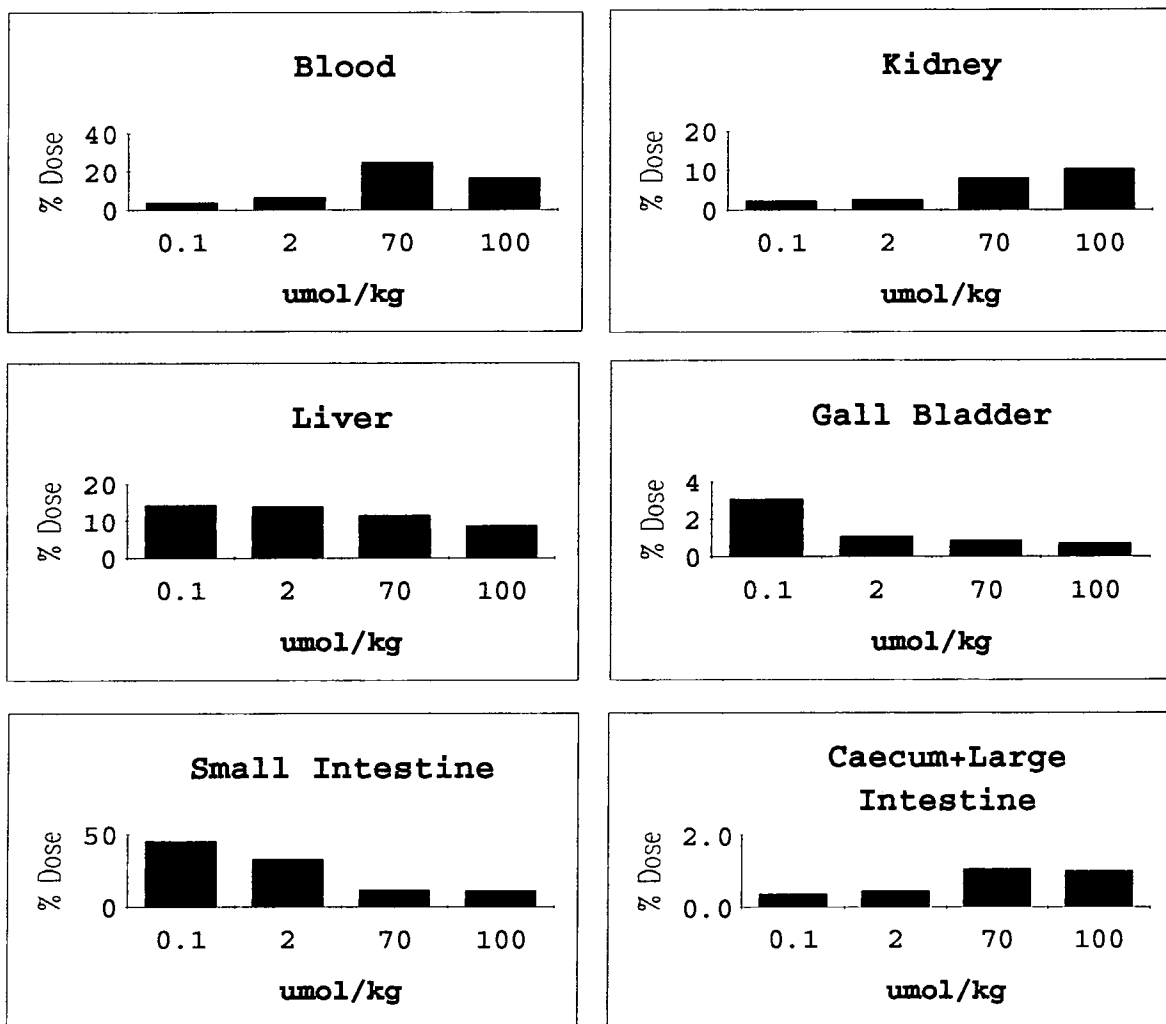
Clear differences in the biodistribution of [Gd.12N4P4Bz4]⁻ with increasing dose of complex can be seen 5 minutes after injection of the complex (figure 2.23). This dose dependence is characterised by an increase in the % dose in the blood and kidneys, and by a decrease in the % dose in the gall bladder and small intestine as the dose of [Gd.12N4P4Bz4]⁻ is increased.

The % dose of [Gd.12N4P4Bz4]⁻ present in the liver at 5 minutes is from both hepatobiliary clearance and liver blood content. This total % dose does not vary much with the dose

of the complex, only dropping from 14% dose at 0.1 μmol/kg to 9% dose at 100 μmol/kg

The % dose in the caecum and the large intestine is less than 1% at all doses. The slightly higher amounts in the 70 and 100 μmol/kg doses can be attributed to their higher % dose in the blood.

Figure 2.24. % *Dose [Gd.12N4P4Bz4]⁻ at 24 Hours.*
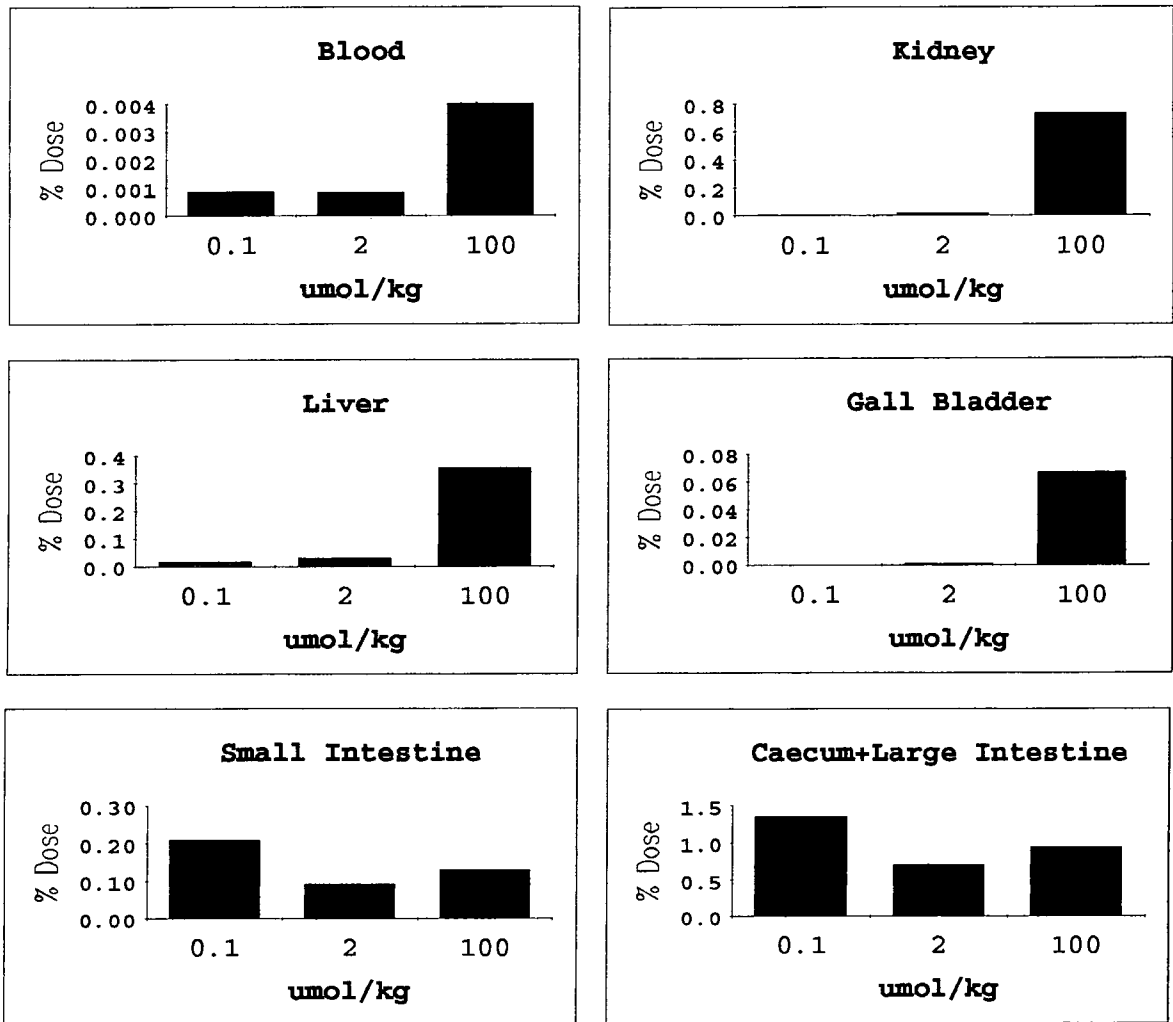
Although there are only very small amounts of [Gd.12N4P4Bz4]⁻ remaining in the excretion pathways at 24 hours, it is evident that the larger the dose given to the mouse, the longer it takes to clear the complex from the body. In section 2.4.3 the retention of [Gd.12N4P4Bz4]⁻ from

the highest dose of 100 μmol/kg is examined at 7 days post injection. This data shows that the vast majority of the complex has been eliminated by 7 days with less than 0.05% of the injected dose remaining in the kidneys, liver, gut or skeleton.

The Effect of Dose Increases

As the dose of [Gd.12N4P4Bz4]$^-$ is increased from 0.1 to 100 μmol/kg saturation of the transporter sites in the liver appears to be occurring. This has the effect of slowing down the rate of clearance of the complex via the hepatobiliary route. This has the added effect of increasing the % dose cleared by the renal route due to the higher circulating levels of complex in the blood.

2.4.2.3. The Biodistribution of [Gd.12N4P4Bz4]$^-$ in the Rat.

Figure 2.25 illustrates the similarity in biodistribution of [Gd 12N4P4Bz4]$^-$ in the mouse and the rat. The primary route of elimination of the complex is via the hepatobiliary route, and the % dose cleared by this route is similar in both species.

The rat is a larger animal with a slower metabolic rate than the mouse, and appears to clear the complex at a slightly slower rate than the mouse (the % dose in the blood of the mice at 5 minutes is between the amount in the blood of the rats at 10 and 20 minutes).

Figure 2.25. *Biodistribution of [Gd.12N4P4Bz4]⁻ in the Rat and Mouse.*
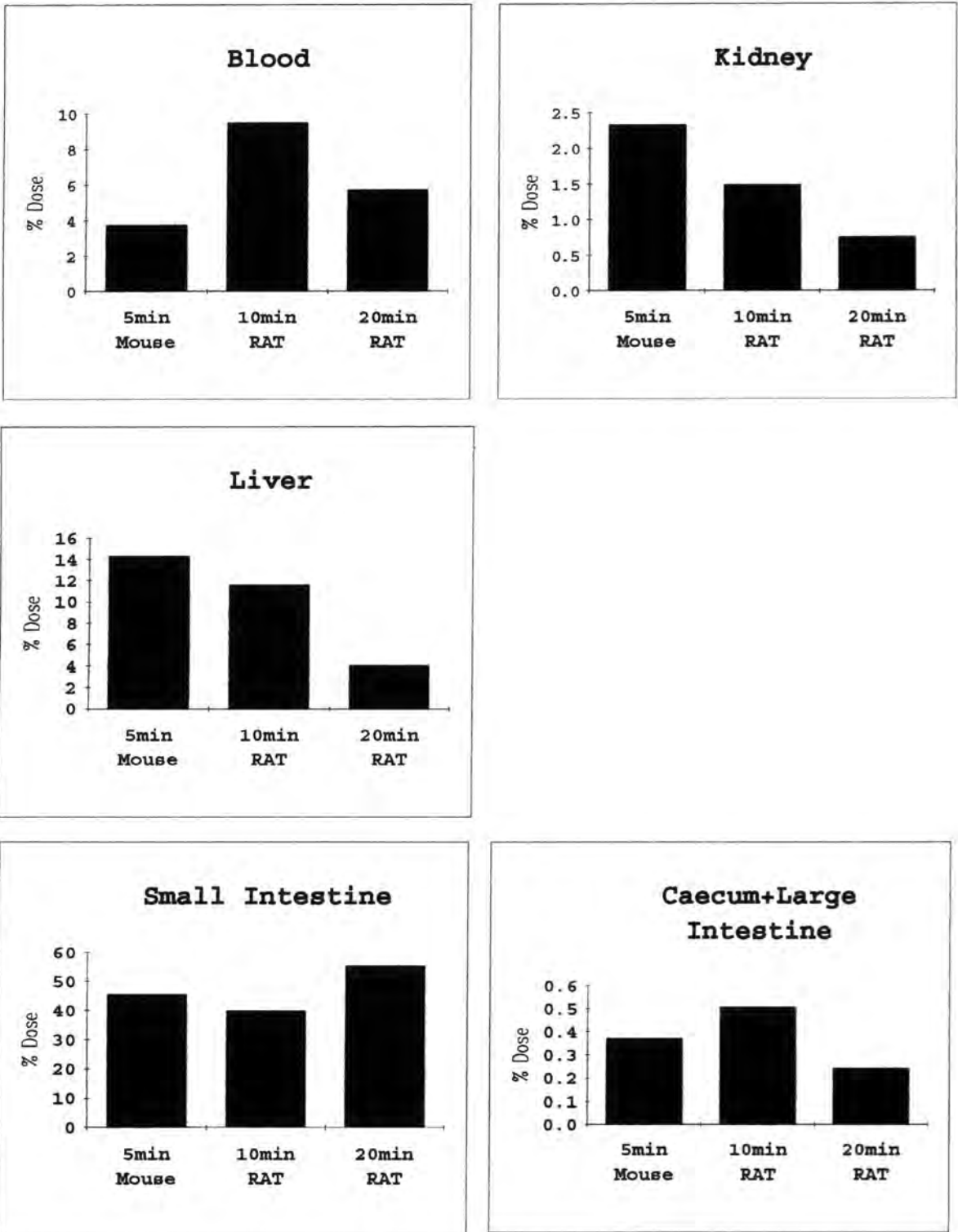
2.4.2.4. The Effect of Bromosulphophthalein on Hepatobiliary Clearance.

Figure 2.26. *The Effect of BSP on the Biodistribution of [Gd.12N4P4Bz4]⁻ at 100 µmol/kg.*
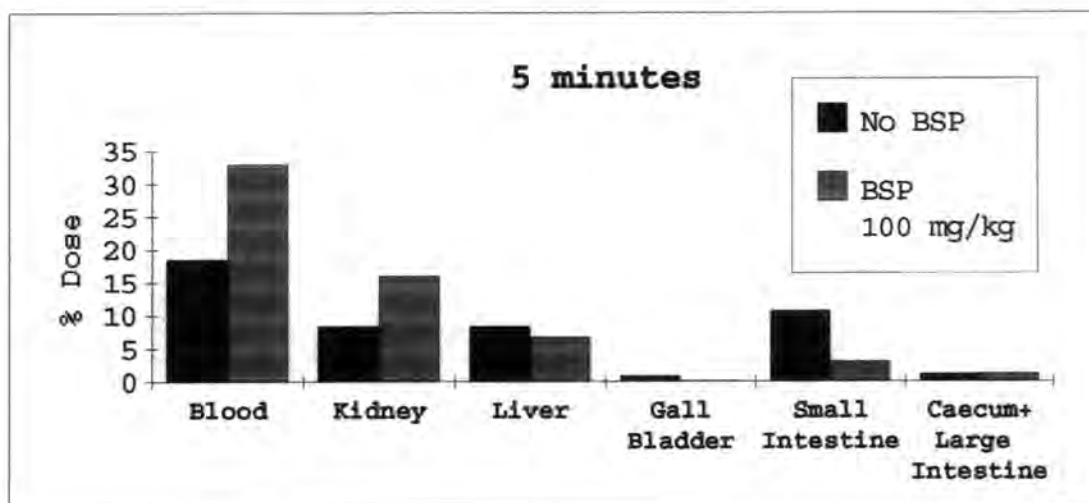
Figure 2.26 shows the effect of 100 mg/kg of bromosulphophthalein (BSP) which was administered intra venously to mice 2 minutes before injection of 100 µmol/kg [Gd.12N4P4Bz4]⁻. Five minutes after the injection of [Gd.12N4P4Bz4]⁻ there is a decrease in the % dose of [Gd.12N4P4Bz4]⁻ present in all tissues in the hepatobiliary clearance route, i.e. liver, gall bladder and intestines. As a consequence, the amount of [Gd.12N4P4Bz4]⁻ in the blood is greater and there is an increase in the proportion of renal elimination.

BSP blocks the receptors in the liver which are responsible for the transport of anionic lipophilic complexes[15,16]. Because the rate of passage of [Gd.12N4P4Bz4]⁻ through the liver is slowed down by BSP, it can be concluded that the same receptors in the liver are responsible for the transport of [Gd.12N4P4Bz4]⁻.

2.4.3. Comparison of the Biodistribution of [Gd.12N4P4Bz4]⁻, [Gd.12N4P4Me4]⁻ and [Gd.DTPA]²⁻ at High (100 μmol/kg) and Low (0.1 μmol/kg) Doses.

The dose of a typical gadolinium contrast agent used in clinical MRI is of the order of 100 μmol/kg. In the previous section 2.4.1, the dose levels used were only 0.1 μmol/kg due to the small amounts of these new complexes which were available.

The effect of increasing the dose of [Gd.12N4P4Bz4]⁻ on the % cleared by the hepatobiliary and renal routes was studied in section 2.4.2. This showed that the % dose cleared by the hepatobiliary route decreased with increasing dose of [Gd.12N4P4Bz4]⁻.

In this section comparisons are made between the biodistributions of three gadolinium complexes [Gd.12N4P4Bz4]⁻, [Gd.12N4P4Me4]⁻ and [Gd.DTPA]²⁻, at high and low doses (100 and 0.1 μmol/kg). As well as examining changes in the % elimination by the different routes, the long term retention of the complexes in the skeleton was also studied to see if there were any changes in the stability of the complexes at the higher dose.

Biodistributions

Figure 2.27. *Biodistributions at 0.1 μmol/kg Dose.*
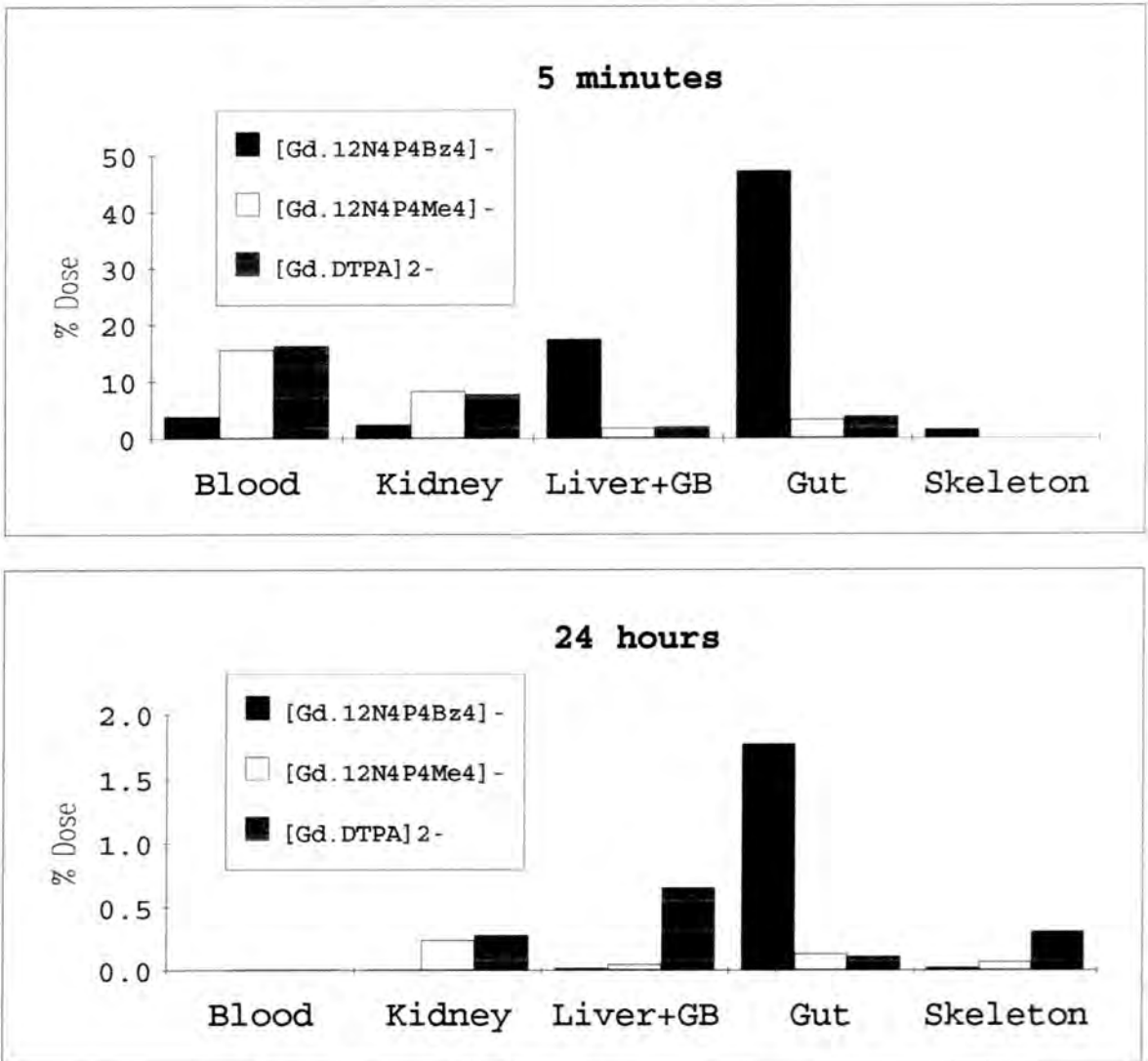
Figure 2.28. *Biodistributions at 100 μmol/kg Dose.*
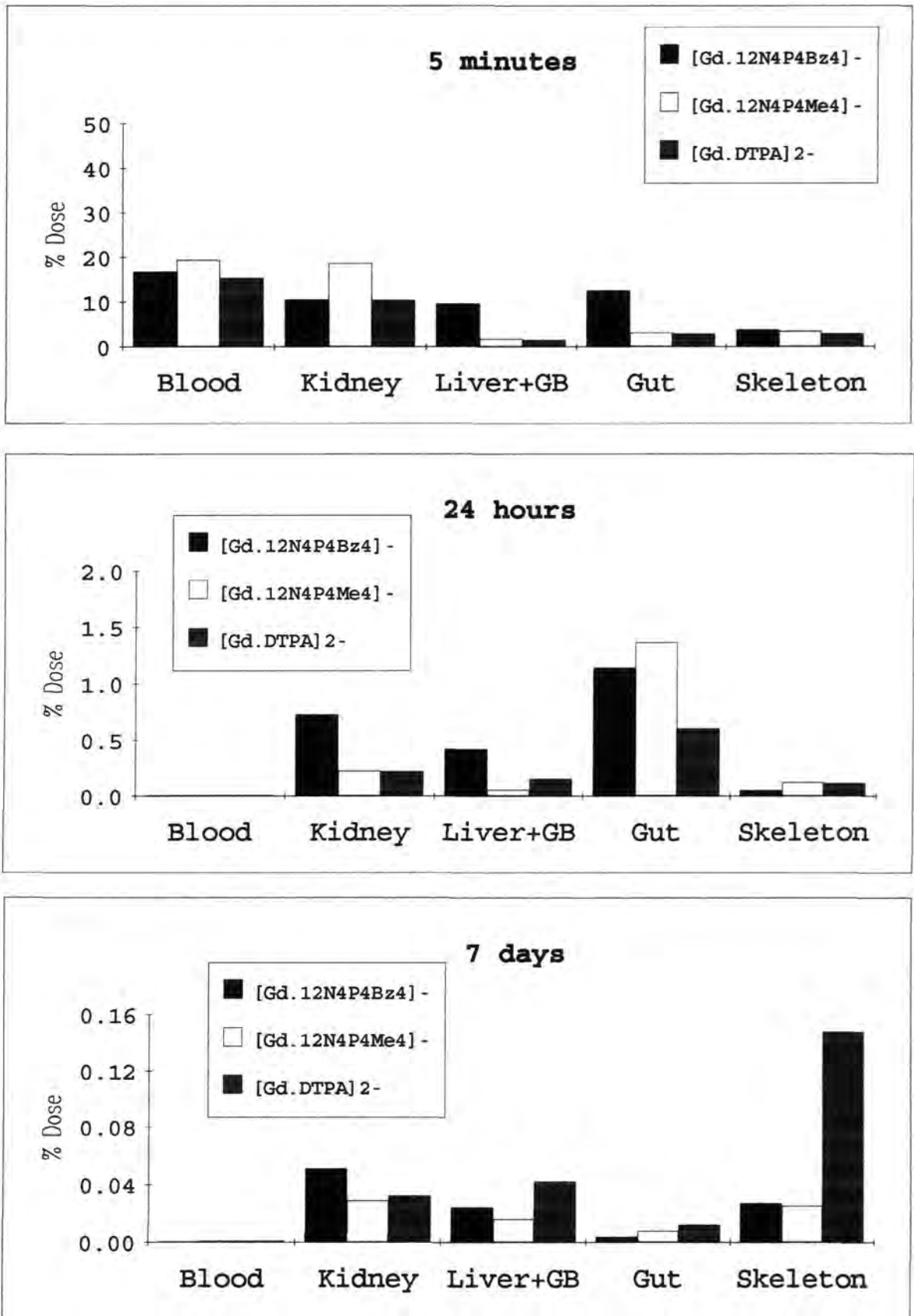
[Gd.12N4P4Bz4]⁻

The data shown in figures 2.27 and 2.28 illustrate that
at 5 minutes when a higher dose of [Gd.12N4P4Bz4]⁻ is given
(100 μmol/kg versus 0.1 μmol/kg), less of the complex clears
through the gut. However the amount of the complex in the
intestine at 5 minutes, (12.5% dose), is still 4 times
greater than that for [Gd.12N4P4Me4]⁻ or [Gd.DTPA]$^{2-}$.

After 5 minutes, the % of the complex found in the liver
at a high dose (100 μmol/kg) is about half that at a low
dose (0.1 μmol/kg). After 24 hours, four times as much of the
complex is in the liver at the high dose. This is as a result
of the longer time taken to clear a larger amount of complex.

The % dose in both the blood and the kidneys at 5 minutes
is higher from the 100 μmol/kg dose and is of the same order
as for [Gd.12N4P4Me4]⁻ and [Gd.DTPA]$^{2-}$. At 24 hours there is
still some renal clearance from the high dose, as the % dose
in the kidneys is about 7 times that from the low dose.

The % dose retained in the skeleton from the 100 μmol/kg
dose (0.05%) is about twice that retained from the low dose
at 24 hours . This % dose had further reduced to only 0.03%
after 7 days indicating that [Gd.12N4P4Bz4]⁻ is a highly
stable complex in vivo.

[Gd.12N4P4Me4]⁻

At 5 minutes the biodistribution of [Gd.12N4P4Me4]⁻ at
both doses is very similar. By 24 hours there is about ten
times more %[Gd.12N4P4Me4]⁻ in the gut and three times more
in the liver from the 100 μmol/kg dose. This implies that at
the higher dose, small amounts of [Gd.12N4P4Me4]⁻ clear
through the alternative hepatobiliary route.

The % dose retained in the skeleton at 24 hours is 0.07%
from the high dose and is about twice that retained from the
low dose. By 7 days this has reduced to 0.03% dose indicating
that like the analogous macrocyclic complex [Gd.12N4P4Bz4]⁻,
the complex [Gd.12N4P4Me4]⁻ is highly stable in vivo.

[Gd.DTPA]$^{2-}$

The biodistribution of [Gd.DTPA]$^{2-}$ at 5 minutes is very similar at both doses (100 and 0.1 μmol/kg).

At 24 hours there is about 5 times the % dose in the gut from the high dose of [Gd.DTPA]$^{2-}$. This again indicates that at a high dose some complex is passed through the alternative excretion pathway as the preferred renal pathway becomes overloaded.

The amount of radiolabel retained in the skeleton and liver at 24 hours from the high dose is 0.11% and 0.15% of the injected dose compared to 0.30% and 0.65% respectively from the low dose of [Gd.DTPA]$^{2-}$. This increased % retention in both the liver and skeleton from the lower dose of [Gd.DTPA]$^{2-}$ could be due to its susceptibility to cation promoted dissociation[21]. At the low dose of [Gd.DTPA]$^{2-}$, 0.1 μmol/kg, the concentration of [Gd.DTPA]$^{2-}$ relative to the concentration of cations (e.g. Zn^{2+} and Cu^{2+}) in the blood would be low, so a higher proportion would dissociate than at the high dose (100 μmol/kg) where the relative concentration of [Gd.DTPA]$^{2-}$ to cations would be high.

The amount of ^{153}Gd in the skeleton at 7 days is 0.15% of the injected dose. Unlike the situation with the macrocyclic complexes where the % dose reduces over 7 days, the % dose in the skeleton remains constant (possibly even increasing a little). This indicates that [Gd.DTPA]$^{2-}$ is less stable in vivo than [Gd.12N4P4Bz4]$^-$. and [Gd.12N4P4Me4]$^-$.

2.5. CONCLUSIONS

The Relationship Between Acid Dissociation constants and In Vivo Stability.

All the gadolinium aza-phosphinic acid macrocycles which had acid dissociation constant measurements taken were shown to be 15 to 1,000 times more stable than [Gd.DTPA]$^{2-}$ in the

range of pH 1 to 2.(table 2.2). This high in vitro stability
is also mirrored in vivo as all of these complexes
demonstrate high in vivo stability in the mouse as
demonstrated by very low % doses in the skeleton 24 hours
after injection (figure 2.19).

The Relationship Between Lipophilicity and Hepatobiliary Clearance.

Figures 2.29 to 2.31 are plots of the relationship
between the gadolinium macrocycle Log P values for
butanol/water and **[A.]** % Dose in the Intestine (figure 2.29),
[B.] % Dose in the Liver + gall bladder (figure 2.30) and
[C.] % Dose in the Intestine + liver + gall bladder , 5
minutes after an injection of 0.1 μmol/kg (figure 2.31).
These figures show the extent of elimination of these
complexes by the hepatobiliary pathway in the mouse.

The anionic gadolinium macrocycle complexes
([Gd.12N4P4Bz4]$^-$, [Gd.12N4P4Bu4]$^-$ and [Gd.12N4P4Ph4]$^-$) have
positive butanol/water Log P values and all clear by the
hepatobiliary route. For these complexes there is a
correlation between a high butanol/water Log P value and a
high total amount of complex in the hepatobiliary pathway
(figure 2.31).

The complexes [Gd.12N4P3Bu3NHMe] and [Gd.12N4P3Ph3NMe2]
which have the most positive Log P values in butanol/water
but are neutral in charge, show some elimination by the
hepatobiliary route, but this is much less than the anionic
lipophilic macrocycle complexes.

[Gd.BOPTA]$^{2-}$ has a low (negative) Log P value for
butanol/water, but shows a high concentration in the liver +
gall bladder. The elimination picture for this anionic
acyclic complex is different from that of the anionic
lipophilic macrocycles in that at 5 minutes after intravenous
injection there is 27% in the liver + gall bladder but only
7% in the intestine compared with 17% and 47% respectively
for [Gd.12N4P4Bz4]$^-$.This indicates that [Gd.BOPTA]$^{2-}$ is taken
up by the liver but is not passed through the gall bladder

into the intestine as quickly as the anionic lipophilic macrocycle complexes.

Gadolinium Macrocycle Complexes Suitable for use as MRI Contrast Agents.

From the range of gadolinium complexes studied the following macrocycle complexes all have properties which make them possible new candidates for MRI contrast agents. The properties which make a gadolinium complex suitable for MRI contrast are :- (i) rapid extracellular distribution, (ii) high in vivo stability, (iii) specific clearance by the kidneys or liver, with no long term body retention, and (iv) low charge, so as to reduce osmotic shock.

From group I the complex [Gd.12N4P4Me4]$^-$ has properties very similar to [Gd.DOTA]$^-$ which would make it a suitable extracellular contrast agent.

The group II complexes all exhibited rapid extracellular distribution and high in vivo stability with a combination of hepatobiliary and renal elimination. This makes them suitable for use as general extracellular and specific liver/gall bladder/intestine contrast imaging.

Groups III and IV, the neutral aza-phosphinic and aza-carboxylic acid macrocycles, all show rapid extracellular distribution, high in vivo stability and renal clearance. They also have the added advantage of neutral charge which eliminates the need for counter ions in the injection solution, thus lowering the osmolality of the solution. Thus these two groups of gadolinium complexes could be less toxic and hence safer to use than the present contrast agents, [Gd.DTPA]$^{2-}$ and [Gd.DOTA]$^-$.

Figure 2.29. *Plot of Butanol/Water Log P Values vs. % Dose of Complex in the Intestines at 5 Minutes Post Injection*
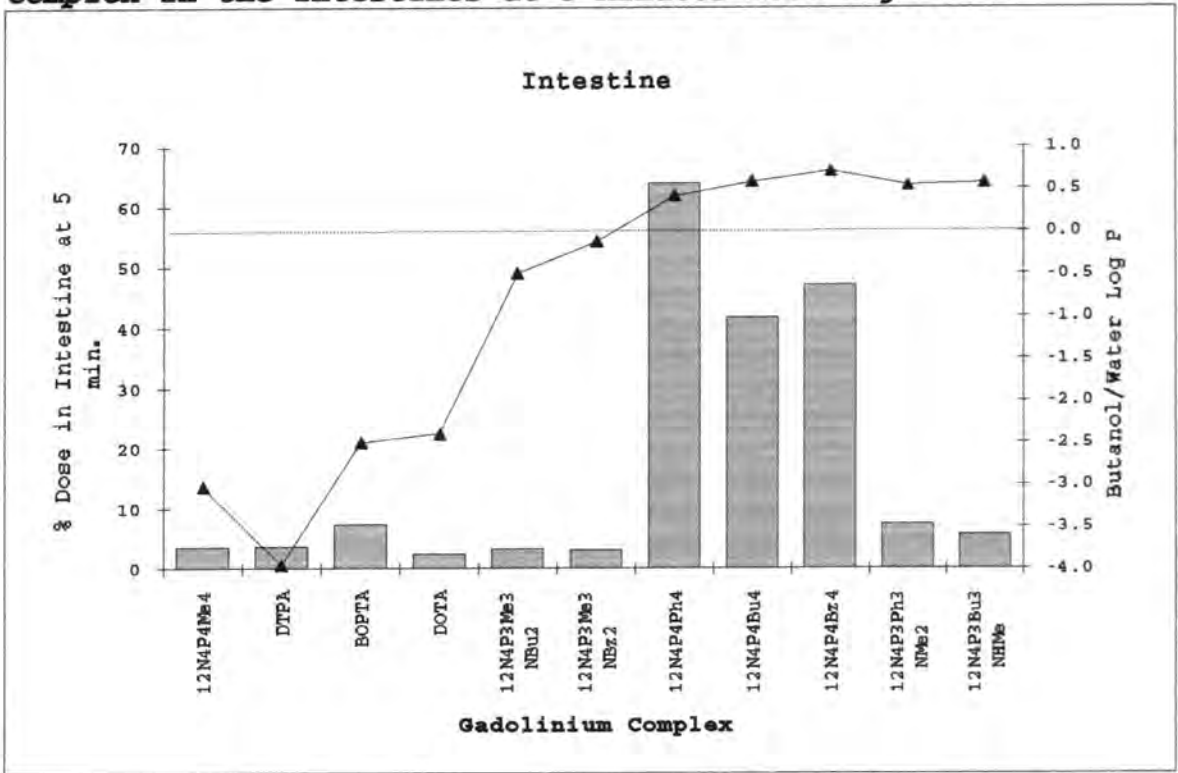
Figure 2.30. *Plot of Butanol/Water Log P Values vs. % Dose of Complex in the Liver + Gall Bladder at 5 Minutes Post Injection*
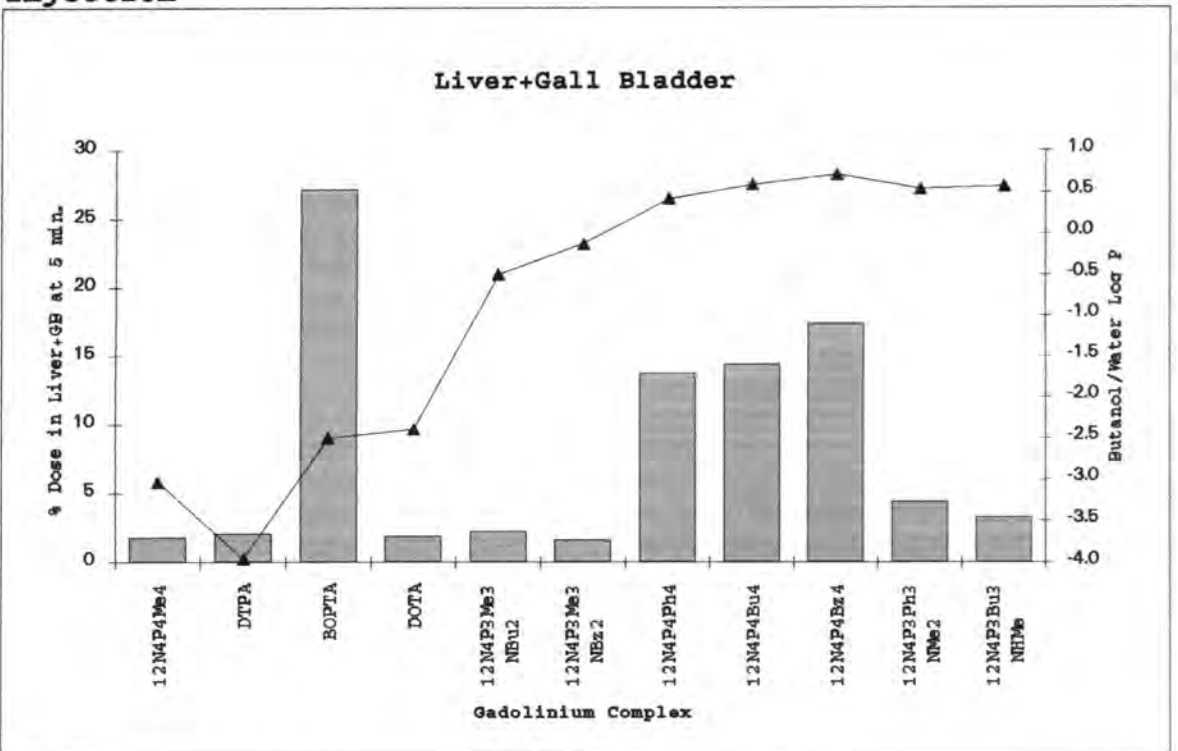
Figure 2.31. *Plot of Butanol/Water Log P Values vs. % Dose of Complex in the Intestine + Liver + Gall Bladder at 5 Minutes Post Injection*
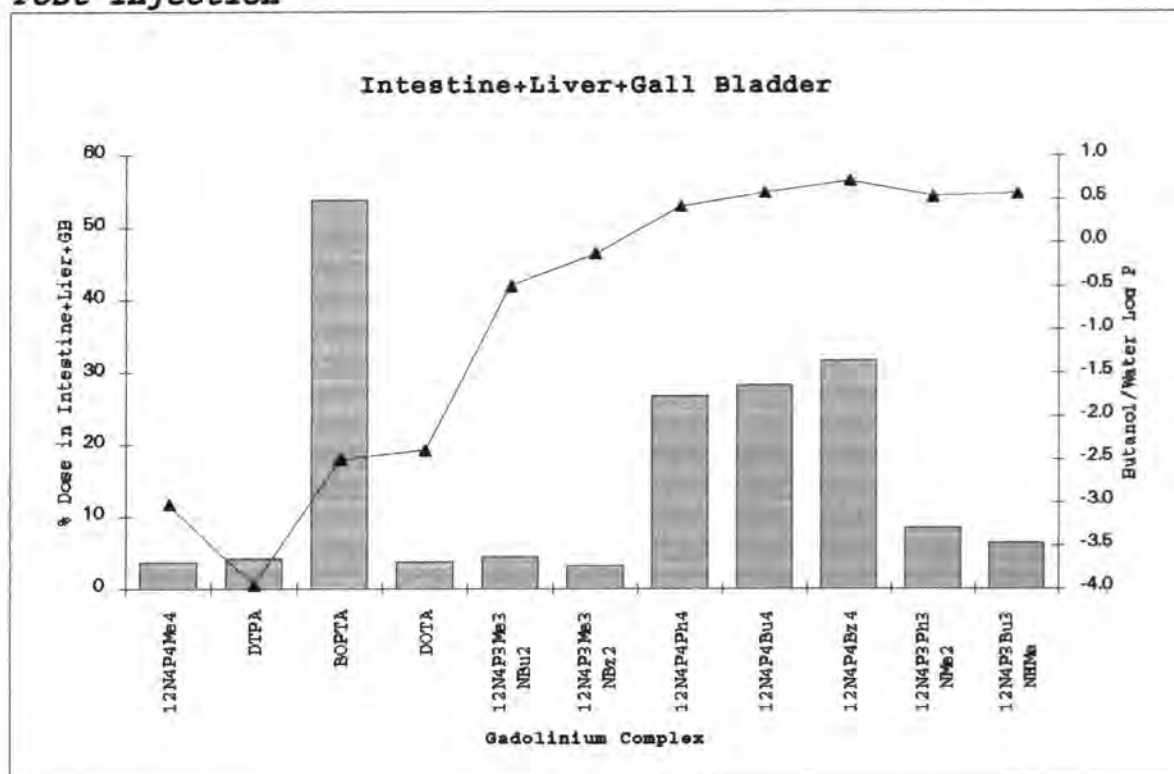
Suitability of Gadolinium Complexes For MRI Hepatobiliary Imaging

The group II anionic lipophlic macrocycles [Gd.12N4P4Ph4]⁻, [Gd.12N4P4Bu4]⁻ and [Gd.12N4P4Bz4]⁻ all have properties making them suitable candidates for MRI hepatobiliary contrast agents. All have high percentage clearances (42-65% dose at 5 minutes) by this route, and high in vivo stability as indicated by low percentage doses retained in the skeleton at 24 hours (less than 0.025%) and low acid dissociation rate values (24-78 x 10^6 sec⁻¹ at pH 1).

[Gd.12N4P4Bz4]⁻ was the most promising complex from this group and was studied in further detail. The factors which contributed to this choice were the high hepatobiliary clearance, stability, and water solubility of [Gd.12N4P4Bz4]⁻ This complex was shown to be eliminated by the same transport mechanism in liver hepatocytes as BSP. This transport

mechanism can be saturated at high doses of complex. High
doses of 100 μmol/kg were shown to have cleared almost
completely from the mouse in 7 days, indicating long term
stability and safety.

The [Gd.12N4P4Bz4]⁻ complex is being further studied by
Dr. I.J. Rowland at the Royal Marsden Hospital by direct MRI
measurements of rats. [Gd.12N4P4Bz4]⁻ is showing potential as
a tumour detection agent when administered at doses of 100-
200 μmol/kg, and as an agent for cholangiography when
administered at doses as low as 0.1 to 10 μmol/kg (when liver
transport sites are not saturated).

Figure 2.32. *MRI Image of the Abdomen of a Rat, 6 Hours After
Administration of 0.2 mmol/kg [Gd.12N4P4Bz4]⁻.*

Figure 2.32 shows enhancement of the gut and bladder of a
rat. This MRI image is a fat suppressed FLASH image taken 6
hours after administration of 0.2 mmol/kg [Gd.12N4P4Bz4]⁻.
Figure 2.32 courtesy of I.J. Rowland.

2.6. GADOLINIUM EXPERIMENTAL.

Throughout the following experimental procedures, gold label quality chemicals and metal free plastic ware were used to reduce any metal contamination. The suppliers of apparatus and reagents used, together with the purity of reagents are listed in Appendix I. Gadolinium-153 was supplied as gadolinium chloride in 0.1M HCl, 0.5-5 mCi/mg Gd.(18.5-185 MBq/mg Gd), $t^1/2=$ 242 days, $\gamma=$ 97-103 KeV, X-rays= 41-47 KeV.

2.6.1. Preparation of Gadolinium Macrocycle Complexes for Biological Use

In the following preparations the amount of carrier added was usually 10%, but in order to achieve the maximum percentage labelling the amount of carrier was reduced in some cases. This was because the macrocycle solutions contained small amounts of contaminating cations. Any contaminating cations from either the ^{153}Gd, the macrocycle preparation or in any of the buffer solutions used will limit the final yield of [Gd.macrocycle]. Hence, throughout, high purity (e.g. Aldrich 'gold label') chemicals and metal free plastics where used.

The ^{153}Gd used was 0.5-5 mCi/mg Gd, i.e. a 100 μCi sample of ^{153}Gd contained 20-200 μg ^{157}Gd (0.13-1.3 μmoles). This compares with 0.5 μmoles of macrocycle in 250 μl of a 2 mM solution. Usually the ^{153}Gd gave good labelling results >90% with 10% added carrier, suggesting that the ^{153}Gd was of the higher purity (i.e. 0.13 μmoles/100 μCi).

Before the reaction mixture was separated by HPLC, unreacted Gd^{3+} was mopped up by adding DTPA. Formation of the [Gd.DTPA]$^{2-}$ complex not only prevented contamination of the HPLC column with ^{153}Gd^{3+}, but also provided the means by which the percentage labelling of [Gd.macrocycle] could be measured accurately. A 10 fold molar excess of DTPA over macrocycle was sufficient to complex all unreacted Gd^{3+} and any other cations which may have been present. When testing very small amounts e.g. 1 μl of 2 mM macrocycle solution, a

50 times molar excess of DTPA over macrocycle was used because of any small absolute amounts of contaminating cations. It had previously been established that the macrocycles were stable with respect to trans-complexation by DTPA in the pH range used[24].

All the gadolinium complexes were prepared by methods similar to those employed for the preparation of [Gd.DOTA]⁻ This method is set out below with any variations used in the other preparations listed in table 2.4.

The only exception to this was the preparation of [Gd.Citrate]. [Gd.Citrate] was prepared by adding ^{153}GdCl$_3$ to a solution containing 1.8 mg sodium citrate and 6.8 mg NaCl per ml.

Preparation of [Gd.DOTA]⁻

250 μl of a solution containing 200 mM ammonium acetate pH 6.5, 2 mM DOTA, 0.2 mM GdCl$_3$ (10% carrier) + 50-150 μCi ^{153}Gd, was incubated at 310K (37°C) for 30-90 minutes.

The formation of [Gd.DOTA]⁻ and other complexes was measured firstly at 30 minutes by adding 1 μl of the reaction mixture to 50 times molar excess of DTPA over macrocycle(2 μl of 100 mM DTPA). This was then made up to 100 μl with HPLC running buffer (0.2 M ammonium acetate pH 6.8, 10% acetonitrile with AX300 column, or 0.15 M ammonium acetate pH 6.8 with Poros Q/M column) and incubated for 5 minutes. The percentage labelling was then analysed by HPLC anion exchange. If the % of [Gd.DOTA]⁻ or of the other complexes was >90% the reaction mixture was quenched with DTPA. If the labelling was less than 90% the reaction mixture was incubated for a further period at 37°C and the percentage complex formation re-examined. When there was no further increase in complex formation the reaction mixture was quenched by adding 10 μl of 500 mM DTPA (10 times molar excess over macrocycle). This mixture was then separated by HPLC, the [Gd.DOTA]⁻(or other complex) peak being collected manually (dropwise into a polyethylene tube).

For [Gd.DOTA]⁻ the labelling efficiency was usually
greater than 98%. On an AX300 anion exchange column run at 1
ml/min with 0.2 M ammonium acetate pH 6.8, 10% acetonitrile
running buffer, [Gd.DOTA]⁻ elutes at 4.6 min followed by
[Gd.DTPA]²⁻ at about 12 min.

On a Poros Q/M anion exchange column run at 2 ml/min with
0.15 M ammonium acetate pH 6.8 running buffer, [Gd.DOTA]⁻
elutes at 0.9 min followed by [Gd.DTPA]²⁻ at 2 to 3 min.

Before any preparation was used further, an aliquot was
challenged by DTPA and checked by HPLC to make sure that it
was free from ¹⁵³Gd labelled contaminants and uncomplexed
¹⁵³Gd.
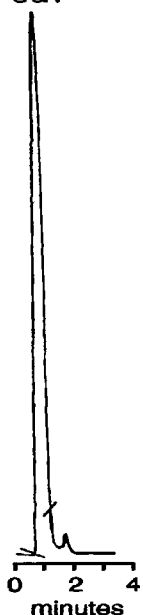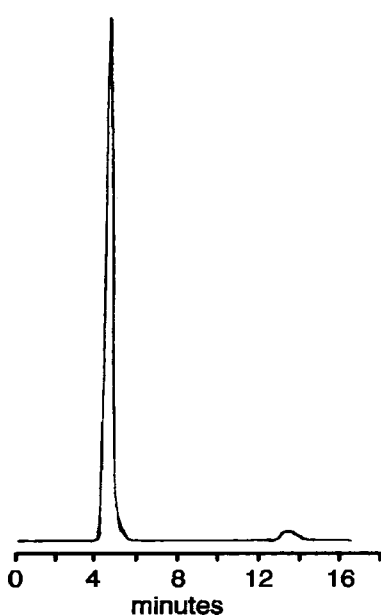
Figure 2.33.   **Figure 2.34.**   **Figure 2.35.**
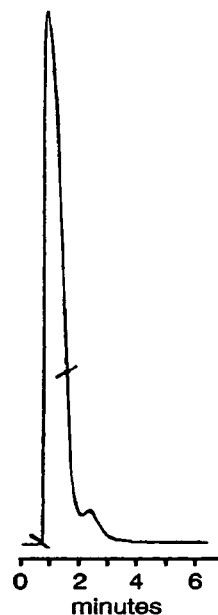
Figures 2.33 to 3.35 are typical HPLC traces from
gadolinium-labelled macrocycles. Figure 2.33 is a
radioactivity trace of [Gd.12N4P4Me4]⁻ purified by a Poros
Q/M anion exchange column. This preparation achieved 98%
labelling efficiency, the section of the peak between the two
marks was the fraction collected for animal studies. Figure
2.34 shows [Gd.12N4P4Me4]⁻ purified on an AX300 anion
exchange column, in this case 95% labelling was achieved, and
the [Gd.DTPA]²⁻ eluted much later than on the Poros Q/M
column. Figure 2.35 is a radioactivity trace of a
[Gd.12N4P4Bz4]⁻ preparation separated by a Poros Q/M anion

exchange column. The section between the two marks is the fraction taken for animal studies.

Table 2.4. *Part 1. Preparation of Gadolinium Complexes.*

Gadolinium Complex	Variation from [Gd.DOTA]⁻ prep.	% labelling	Elution time (min)	
			AX300	Poros Q/M
DOTA		98	4.6	0.9
12N4P4Me4	KOH added to adjust pH to 6.5	95	4.0	0.9
12N4P4Me3C	5% carrier	98	3.9	
12N4P4Bu4	no carrier	70	4.9	
12N4P4Ph4	no carrier	98	7.3	
12N4P4Bz4		90	9.0	1.57 (with DTPA at 3.5)
12N4P3Me3NHMe	no carrier	99	3.7	
12N4P3Me3NMe2		94	4.1	
12N4P3Me3NBu2		93	3.6	
12N4P3Me3(IBu)2	5% carrier	98	3.6	
12N4P3Me3NBz2	1.2% carrier	92	3.6	
12N4P3Bu3NHMe	18 hour incubation	95	3.8	
12N4P3Ph3NMe2		80	4.7	

Table 2.4. *Part 2. Preparation of Gadolinium Complexes.*

Gadolinium Complex	Variation from [Gd.DOTA]$^-$ prep.	% labelling	Elution time (min) AX300	Poros Q/M
12N4C3N(IBu)2	0.5% carrier. 18 hour incubation	97	3.8	
12N4C3NMeBz		95	3.9	0.85
12N4P3Me3 NH(CH2)4NH3$^+$		60	3.5	
12N4P3Bu3 NH(CH2)4NH3$^+$		80	4.0	0.91
12N4P3Bz3 NH(CH2)4NH3$^+$	pH adjusted to 6.5	80	4.0	0.95
12N4C3 NH(CH2)4NH3$^+$	20% carrier	60	3.4	
12N4C3 NH(CH2)2NMe3$^+$	2% carrier	65	3.4	
12N4P3Me3Bz	no carrier	65	6.9 (dissociated by 50% in 24 hours)	
DTPA(NHBz)2	not DTPA quenched		3.7	
DTPA	not DTPA quenched		14.2	2.0
BOPTA	not DTPA quenched		15.2	

2.6.2 Gadolinium Labelled Macrocycles Dissociation Experiments

Preparation of Gadolinium Labelled Macrocycles for Dissociations.

As high a labelling efficiency as possible was required for these dissociation measurements. To achieve this the amount of non radioactive $GdCl_3$ (carrier) used in these preparations varied depending on the purity of the macrocycles (i.e. freedom from contaminating cations).

[Gd.DOTA]⁻

250 μl of a solution containing 200 mM ammonium acetate pH 7, 40 mM DOTA, 30 mM $GdCl_3$ (75% carrier) + 63 μCi ^{153}Gd, was incubated at 333K (60°C) for 30 minutes.

The formation of [Gd.DOTA]⁻ was measured by removing 2 μl of the above solution and incubating with 50 times molar excess DTPA over macrocycle in HPLC running buffer (0.2 M ammonium acetate pH 6.8, 10% acetonitrile with AX300 column, or 0.15 M ammonium acetate pH 6.8 with Poros Q/M column) for 5 minutes. This was then analysed by HPLC anion exchange to determine the percentage of ^{153}Gd in the [Gd.DOTA]⁻ and [Gd.DTPA]⁻ peaks by radiometry (section 2.6.1).

[Gd.12N4P4Me4]⁻

250 μl of a solution containing 200 mM ammonium acetate pH 7, 25 mM 12N4P4, 88 μCi ^{153}Gd (no carrier) and KOH to adjust to pH 7 was incubated at 333K (60°C) for 2.5 hours.

The formation of [Gd.12N4P4Me4]⁻ was tested as for [Gd.DOTA]⁻.

[Gd.12N4P4Bu4]⁻

250 μl of a solution containing 200mM ammonium acetate pH 6.5, 40 mM 12N4P4Bu4, 4 mM GdCl$_3$ (10% carrier)+65 μCi ^{153}Gd was incubated at 333K (60°C) overnight.

The formation of [Gd.12N4P4Bu4]⁻ was tested as for [Gd.DOTA]⁻

[Gd.12N4P4Ph4]⁻

The preparation was the same as for [Gd.12N4P4Bu4]⁻.

[Gd.12N4P4Bz4]⁻

The preparation was the same as for [Gd.12N4P4Bu4]⁻ with KOH having been added to adjust the pH to 7.

[Gd.12N4P3Me3NBz2]

The preparation was the same as for [Gd.12N4P4Bu4]⁻ except only 0.4 mM (1% carrier) was added.

[Gd.12N4P3Me3Bu2]

The preparation was the same as for [Gd.12N4P4Bu4]⁻.

[Gd.12N4P3Bu3NHMe]

The preparation was the same as for [Gd.12N4P4Bu4]⁻.

Buffers for Dissociation Measurements

A solution of glycine (0.1 mol dm^{-3}) was adjusted to pH 1.0, 1.3, 1.5 and 2.0 with HCl. The pH (+/- 0.1 units) was measured by a Horiba pH meter on each dissociation. The same buffers were used throughout.

Dissociation Measurements

An aliquot of a stock solution of [Gd.macrocycle] was added to 1.0 or 1.5 mls of buffer (at 310K (37°C)) to give a final concentration of 2 mM [Gd.macrocycle], (except [Gd.12N4P4]$^-$ which was 1.27 mM). These were incubated at 310K (37°C).

Three 35 μl samples were removed at each time point and added to a mixture of 7 μl, 500 mM DTPA (50 times molar excess over macrocycle) and 59 μl of HPLC running buffer (0.2 M ammonium acetate pH 6.8, 10% acetonitrile with AX300 column, or 0.15 M ammonium acetate pH 6.8 with Poros Q/M column) to make up to 100 μl total volume. The mixtures were vortexed, centrifuged and then frozen at 253K (-20°C) immediately, or run on the HPLC within 5-20 minutes. Similarly, samples were run on the HPLC within 5-20 minutes of defrosting.

Radiometric HPLC analysis of [Gd.DOTA]$^-$ and [Gd.12N4P4]$^-$ was carried out using an AX300 anion exchange column. A Poros Q/M anion exchange column was used for analysis of the rest of the gadolinium complexes.

Calculation of k_{obs}.

The rate of dissociation was calculated by first measuring the relative amounts of complexed [Gd.macrocycle] and unbound Gd^{3+}. Each sample taken had a 50 times molar excess of DTPA added to scavenge any unbound Gd^{3+}. The [Gd.macrocycle] and [Gd.DTPA]$^{2-}$ were then separated by HPLC radiometry, the relative amounts of each species being given by the areas of the corresponding peaks.

A typical data set is given below for
[Gd.12N4P3Me3NBu2]:-

Time hours	% [Gd.12N4P3Me3NBu2] Run 1	Run 2	Run 3	Average
0	89.05	89.35	89.30	89.23
1	87.32	87.44	87.37	87.38
3	85.55	85.70	85.84	85.70
6.67	83.55	83.63	83.68	83.55
24	73.96	74.44	74.96	74.42
30	71.87	71.85	72.18	71.97
48	66.23	66.38	66.95	66.52
72.86	59.80	59.68	59.71	59.73
143.67	44.12	44.55	44.43	44.37
168	40.04	40.70	40.46	40.40
192	37.04	36.80	37.08	36.97
216	33.48	33.52	33.38	33.46
336	18.09	18.14	17.91	18.05

The observed rate of dissociation (k_{obs}) was calculated from the slope of a plot of Log C_t/C_O vs. time (seconds) [plots 1-8], where C_O is the concentration of [Gd.macrocycle] at time zero and C_t is the concentration at a given time point.

C_t/C_O was calculated from % [Gd.macrocycle] at time t divided by % [Gd.macrocycle] at t=0.

k_{obs} = slope x -2.303

Assuming a first-order dependence on the gadolinium complex, the half life of the [Gd.macrocycle] is given by:-

$t^1/_2 = 0.693/k_{obs}$

A summary of all the gadolinium macrocycle dissociation data is given in table 2.5. Figures 2.36 to 2.43 are the plots for each macrocycle. The slopes were determined by linear regression analysis.

Table 2.5. *Summary of Gadolinium Dissociation Data.*

Gadolinium Complex	pH	Slope of -Log Ct/Co vs time (sec)	SE on Slope	R^2	kobs 10^{-6} s^{-1}	% SE	Half life hours
DOTA	1.0	1.39E-06	1.26E-08	0.999	3.16	0.91	60.2
	1.3	7.51E-07	6.83E-09	0.999	1.73	0.91	111
	1.5	3.90E-07	1.83E-09	1.000	0.898	1.47	214
	2.0	2.13E-08	2.06E-09	0.883	0.0490	9.68	3930
12N4P4Me4	1.0	4.52E-06	4.43E-08	0.999	10.4	0.98	18.5
	1.3	3.20E-06	3.07E-08	0.999	7.37	0.96	26.1
	1.5	3.01E-06	1.28E-08	1.000	4.63	0.64	41.6
	2.0	4.90E-07	1.18E-08	0.996	1.13	2.41	171
12N4P4Ph4	1.0	3.37E-05	2.69E-07	1.000	77.6	0.80	2.48
	1.5	1.58E-05	1.19E-07	1.000	36.4	0.75	5.29
	2.0	6.38E-06	8.88E-08	0.998	14.7	1.39	13.1
12N4P4Bu4	1.0	1.60E-05	2.61E-07	0.998	36.9	1.63	5.22
	1.5	8.72E-06	1.17E-07	0.999	20.1	1.34	9.59
	2.0	3.07E-06	4.22E-08	0.999	7.08	1.37	27.2
12N4P4Bz4	1.0	1.04E-05	9.54E-07	0.937	23.9	9.19	8.06
	1.5	3.97E-06	3.87E-07	0.917	9.14	9.52	21.1
	2.0	1.22E-06	6.16E-08	0.977	2.81	5.05	68.5
12N4P3Me3NBu2	1.0	5.48E-07	1.03E-08	0.996	1.26	1.88	152
	1.5	2.15E-07	1.02E-08	0.980	0.494	4.75	389
	2.0	8.86E-08	6.74E-09	0.956	0.204	7.61	943
12N4P3Me3NBz2	1.0	1.86E-06	3.65E-08	0.995	4.28	1.96	44.9
	1.5	7.10E-07	3.97E-08	0.967	1.64	5.59	118
	2.0	4.35E-07	2.53E-08	0.973	1.00	5.81	192
12N4P3Bu3NHMe	1.0	1.80E-09	4.01E-08	0.996	4.14	2.23	46.5
	1.5	6.59E-07	1.64E-08	0.994	1.52	2.49	127
	2.0	1.96E-07	8.68E-09	0.954	0.451	4.43	427

Figure 2.36.
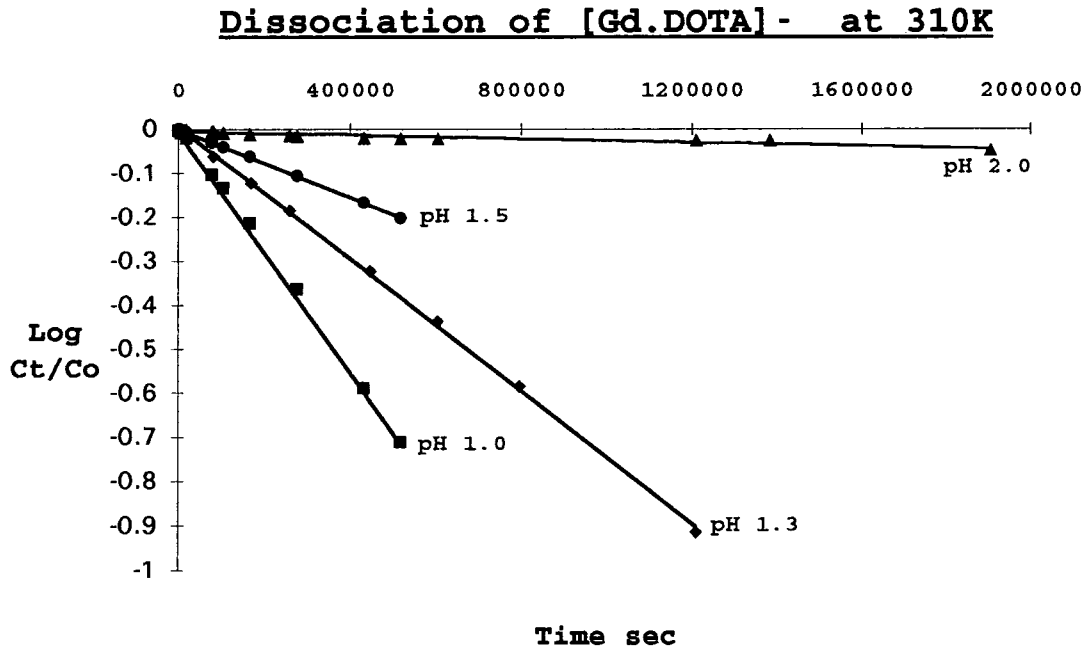
Dissociation of [Gd.DOTA]- at 310K

Figure 2.37.

Dissociation of [Gd.12N4P4Me4]- at 310K

Figure 2.38.

Dissociation of [Gd.12N4P4Ph4]- at 310K

Figure 2.39.

Dissociation of [Gd.12N4P4Bu4]- at 310K

Figure 2.40.

Dissociation of [Gd.12N4P4Bz4]- at 310K

Figure 2.41.

Dissociation of [Gd.12N4P3Me3NBu2] at 310K

Figure 2.42.

Dissociation of [Gd.12N4P3Me3NBz2]   at 310K

Time sec

Figure 2.43.

Dissociation of [Gd.12N4P3Bu3NHMe] at 310K

Time sec
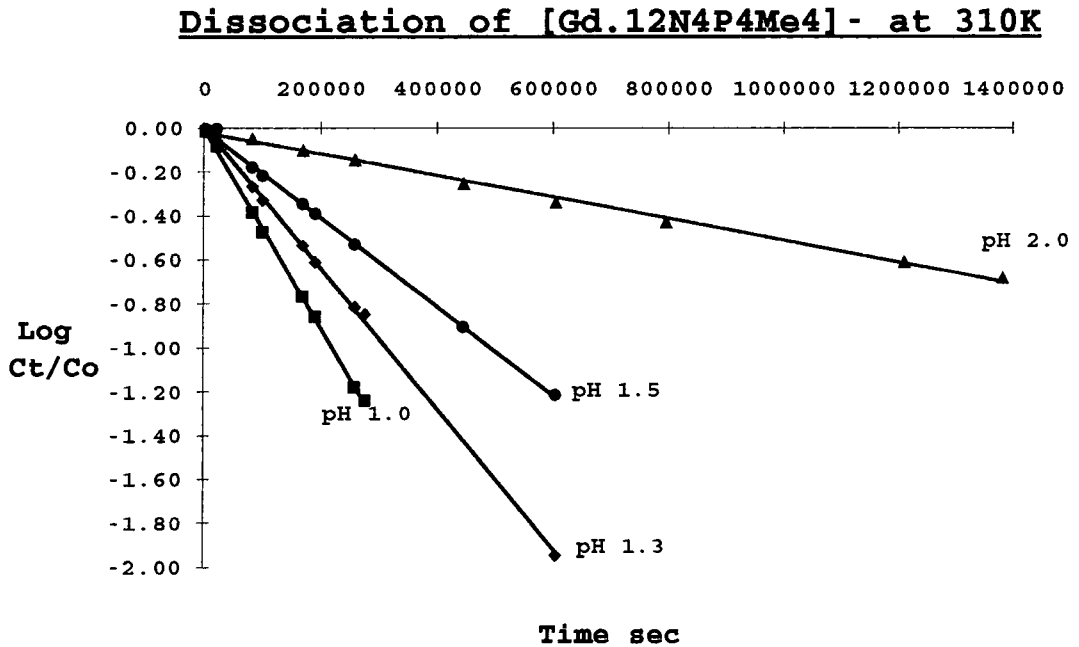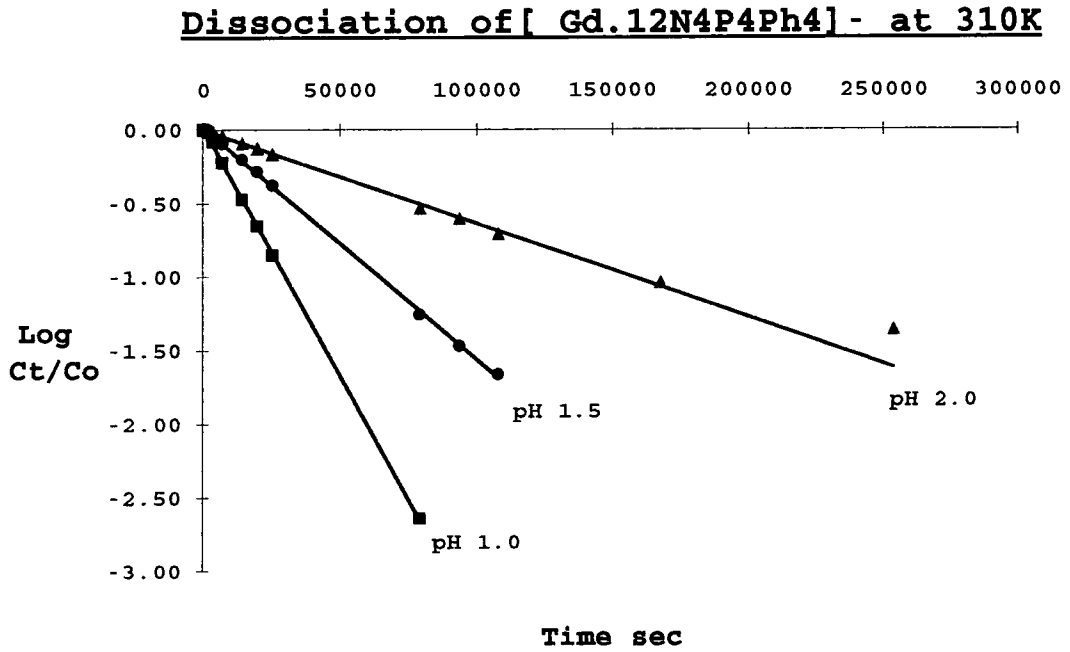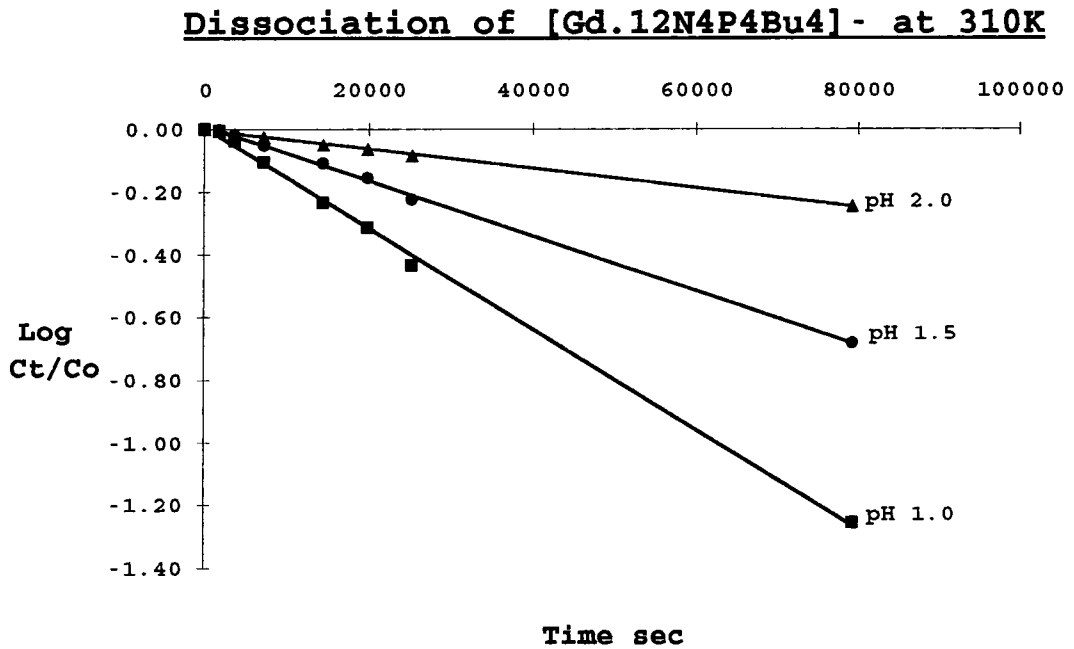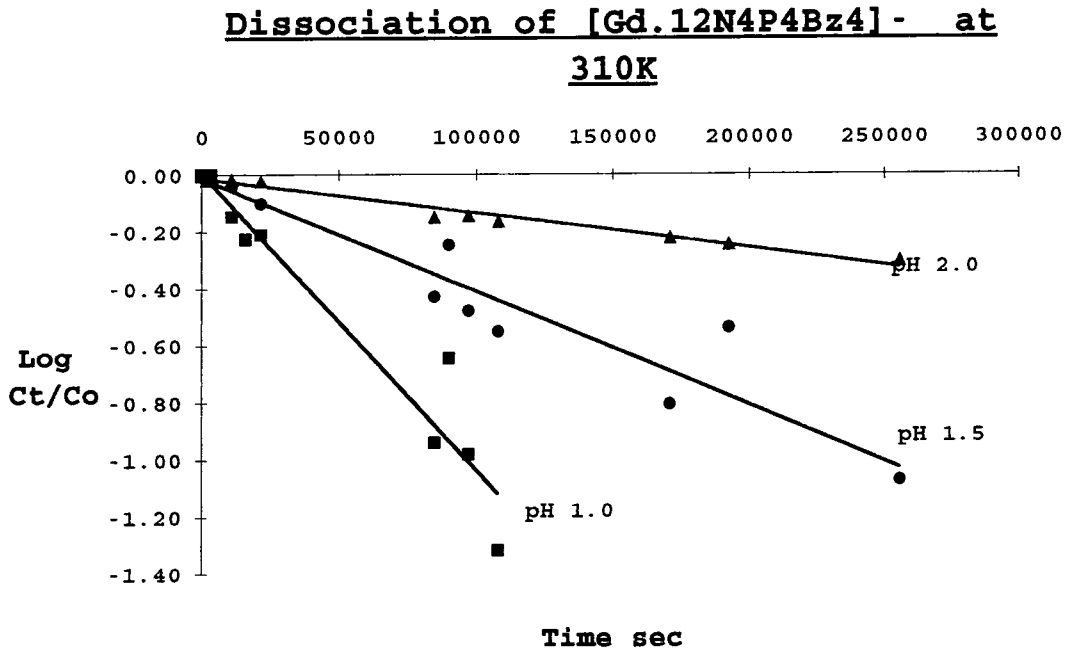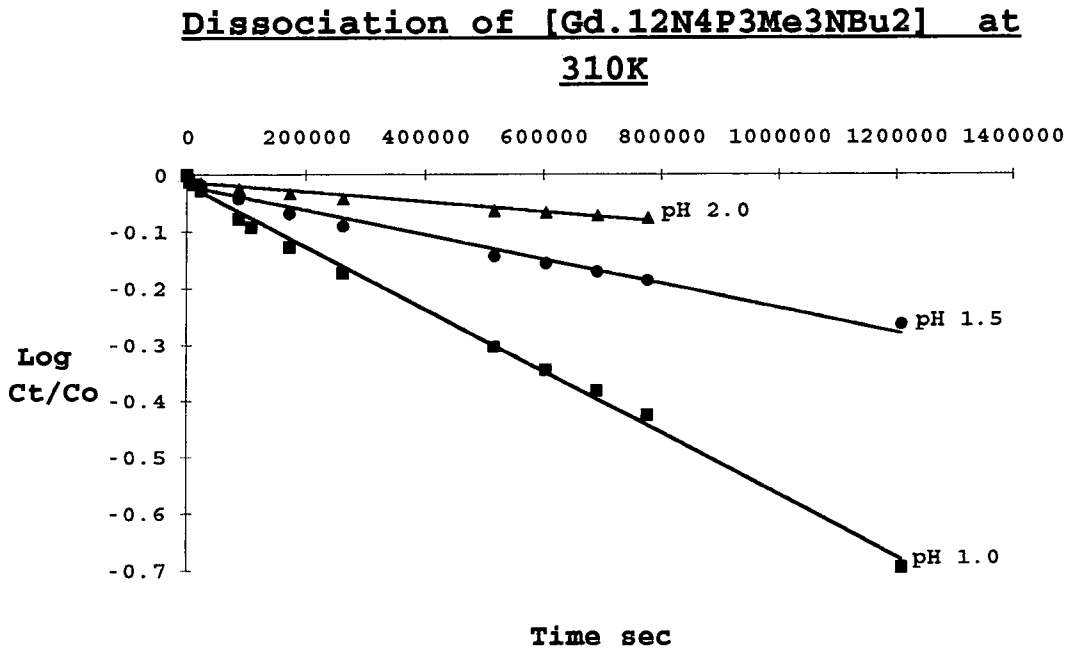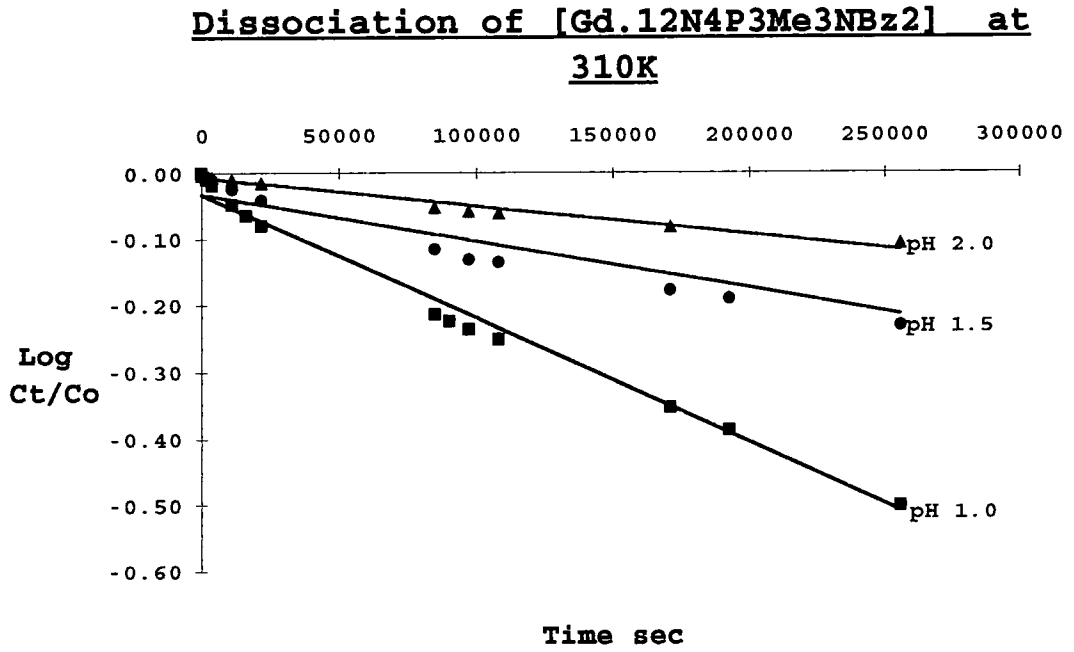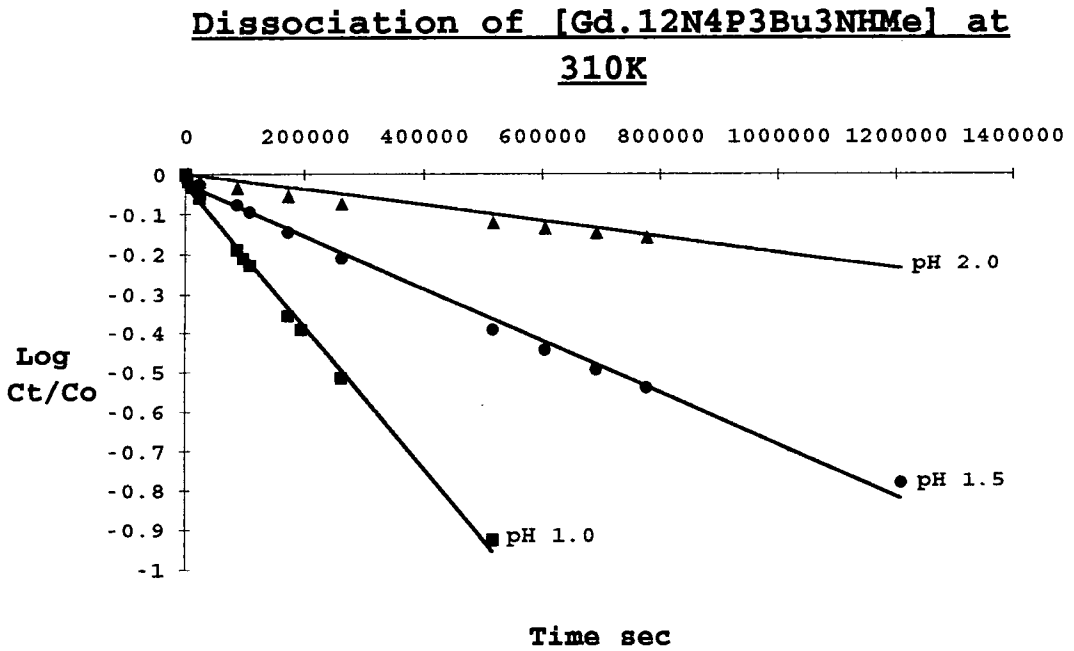
2.6.3 Partition Coefficients of Gadolinium Complexes

The gadolinium macrocycle complexes were prepared as described in section 2.6.1.

Four solvent mixtures were prepared :-

1.   Octanol/Water
2.   Octanol/PBS
3.   Butanol/Water
4.   Butanol/PBS

All solvents were saturated with their partner (e.g. octanol was saturated with water, and water was saturated with octanol for (1). Dulbeccos A pH 7.3 phosphate buffered saline (PBS) was used.

For each of the above mixtures, 3 different volume ratios were set up.

A.   0.50 ml/0.50 ml
B.   0.75 ml/0.25 ml
C.   0.25 ml/0.75 ml

To each of these 12 mixtures, 5 or 10 μl of radiolabelled gadolinium macrocycle in 0.15 M ammonium acetate pH 6.8, was added. These were shaken for 1 hour on a vertical turntable, then centrifuged for 2 min to separate the phases. Duplicate samples (100 μl) were taken from each phase of each tube. These samples were then counted for radioactivity using an LKB compugamma.

Calculation of Log P values

The ratio of the cpm in the solvent phase to the cpm in water was used to calculate the P values

$$P = \frac{\text{cpm in 100 } \mu\text{l Octanol or Butanol}}{\text{cpm in 100 } \mu\text{l Water or PBS}}$$

This calculation is the same for each volume ratio i.e. 1:1, 3:1, or 1:3.

A typical data set is given below for [Gd.12N4P4Bz4]⁻

	P	Log P		P	Log p
Octanol/Water	0.20	-0.70	Octanol/PBS	0.32	-0.50
0.5 ml/0.5 ml	0.23	-0.64	0.5 ml/0.5 ml	0.35	-0.45
Octanol/Water	0.22	-0.65	Octanol/PBS	0.31	-0.51
0.75 ml/0.25 ml	0.25	-0.61	0.75 ml/0.25 ml	0.32	-0.49
Octanol/Water	0.20	-0.70	Octanol/PBS	0.34	-0.46
0.25 ml/0.75 ml	0.21	-0.68	0.25 ml/0.75 ml	0.36	-0.44
Average	0.22	-0.66	**Average**	0.33	-0.48
SD	*0.02*	*0.04*	SD	*0.02*	*0.03*

	P	Log P		P	Log p
Butanol/Water	4.99	0.70	Butanol/PBS	4.20	0.62
0.5 ml/0.5 ml	4.77	0.68	0.5 ml/0.5 ml	4.44	0.65
Butanol/Water	3.23	0.51	Butanol/PBS	2.19	0.34
0.75 ml/0.25 ml	3.51	0.55	0.75 ml/0.25 ml	2.26	0.35
Butanol/Water	8.23	0.92	Butanol/PBS	7.40	0.87
0.25 ml/0.75 ml	8.71	0.94	0.25 ml/0.75 ml	7.07	0.85
Average	5.57	0.71	**Average**	4.60	0.61
SD	*2.35*	*0.18*	SD	*2.26*	*0.23*

Table 2.6. *Summary of Gadolinium Macrocycle Partition Coefficient Data.*

Gadolinium Complex	Octanol\Water		Octanol\PBS		Butanol\Water		Butanol\PBS	
	LOG P	SD	LOG P	SD	LOG P	SD	LOG P	SD
12N4P4Me4	-4.75	*0.55*	-4.47	*0.77*	-3.03	*0.03*	-3.15	*0.06*
DTPA	-4.18	*0.56*	-4.59	*0.34*	-3.96	*0.43*	-3.87	*0.49*
BOPTA	-3.63	*0.36*	-3.79	*0.57*	-2.50	*0.08*	-2.18	*0.03*
DOTA	-3.40	*0.26*	-4.16	*0.73*	-2.39	*0.18*	-3.01	*0.04*
12N4P3Me3NBu2	-2.00	*0.38*	-1.91	*0.05*	-0.50	*0.01*	-0.53	*0.01*
12N4P3Me3NBz2	-1.36	*0.03*	-1.33	*0.04*	-0.13	*0.04*	-0.15	*0.04*
12N4P4Ph4	-1.54	*0.15*	-1.14	*0.02*	0.41	*0.01*	0.35	*0.01*
12N4P4Bu4	-1.09	*0.05*	-1.05	*0.04*	0.58	*0.17*	0.52	*0.20*
12N4P4Bz4	-0.66	*0.04*	-0.48	*0.03*	0.71	*0.18*	0.61	*0.23*
12N4P3Ph3NMe2	-0.36	*0.03*	-0.37	*0.02*	0.54	*0.02*	0.51	*0.02*
12N4P3Bu3NHMe	-0.35	*0.04*	-0.34	*0.03*	0.57	*0.09*	0.58	*0.09*

2.6.4. Biodistribution Studies

Biodistribution studies were carried out on 25 gadolinium complexes whose preparations are described in section 2.6.1. All complexes had their purity checked by HPLC before injection into animals.

The biodistributions were conducted on congenitally athymic nude male mice (MFI-nu/nu/Ola/Hsd) aged 13 to 16 weeks with an average weight of 36 g. Between three and five mice were killed for each complex at each time point.

Gadolinium-153 complexes were administered intra venously via the tail vein at a dose of approx. 0.1 μmol/kg, 7.5 μCi ^{153}Gd/mouse. The dose of [Gd.Citrate] was approx. 2 nmol/kg, 0.8 μCi ^{153}Gd/mouse.

Further studies were undertaken with [Gd.12N4P4Me4]$^-$ and [Gd.DTPA]$^{2-}$ at a dose of 100 μmol/kg, 7.5 μCi ^{153}Gd/mouse and with [Gd.12N4P4Bz4]$^-$ at doses of 2, 70 and 100 μmol/kg, 7.5 μCi ^{153}Gd/mouse. At these higher doses the injection consisted of a mixture of radioactive(^{153}Gd) and non radioactive (^{157}Gd) complex which had been left to equilibrate for 24 hours. The non radioactive complexes used were 0.5M [Gd.DTPA]$^{2-}$ Magnevist (Schering HealthCare), and [Gd.12N4P4Me4]$^-$ (Celltech Ltd.) and [Gd.12N4P4Bz4]$^-$ (Durham University).

The biodistribution of [Gd.12N4P4Bz4]$^-$ was also examined in two Fischer rats (body weigh approx. 300g) at a dose of 0.01 μmol/kg, 7.5 μCi ^{153}Gd per rat.

Mice were killed at 5 minutes post injection by cervical dislocation, and at later times by an intra peritoneal injection of pentobarbitone. A sample of cardiac blood was taken and the following tissues dissected:- brain, both femurs, both kidneys, liver, gall bladder, lungs, heart muscle, salivary glands, spleen, stomach, small intestine (from the pyloric sphincter to the start of the caecum), caecum, large intestine, samples of fat, skeletal muscle and skin.

All samples were weighed with the exception of the gut. For calculations of total tissue dose, the mass of both the

blood and the skeleton were taken as 10% of the body weight. Tissue samples were placed in polyethylene vials and had their volume made up to 1 ml with formal saline in order to keep the geometry constant for gamma counting. Larger samples such as liver and intestines were divided between several tubes for analysis. Samples were assayed for ^{153}Gd by a Compugamma equipped with a 3" well type NaITl crystal. Each sample was counted for 5 or 20 minutes depending on the level of ^{153}Gd present. The limit of detection based on a 20 min count, was 100 cpm. This is approx. 0.0006% of the dose assuming a dose of 22 x 10^6 cpm, 7.5 μCi ^{153}Gd.

Rat tissues were removed and assayed as in the mice experiments with the exception of the gall bladder, as the rat does not possess one.

Summary tables are presented in Chapter 2.4

2.7. REFERENCES

1. M. Allard, D. Doucet, P. Kein, B. Bonnemain, J.M. Caillé. *Invest. Radiol.*, 1988, 23, 271-274.

2. R.R. Edelman and S. Warach. *New England J. of Medicine*, 1993, 328, 709-716.

3. V.M. Runge, S. Jacobson, M.L. Wood, D. Kaufman, L.S. Adelman, *Radiology*, 1988, 166, 835-838.

4. R.C. Brasch H-J Weinmann, G.E. Wesbey, *American Journal of Radiology*, 1984, 142, 625-630.

5. M.F. Bellin, G. Deray, U. Assogba E. Auberton, F. Ghany, E. Dion-Voirin, C. Jacobs, J. Grellet. *Magn. Reson. Imag.*, 1992, 10, 115-118.

6. M.E. Bernardino. *Magn. Reson. Med.*, 1991, 22, 334-338.

7. D.D. Stark. *Magn. Reson. Med.*, 1991, 22, 324-328.

8. G. Schuhmann-Giampieri, H. Schmitt-Willch, W-R. Press, C. Negishi, H-J. Weinmann, U. Speck. *Radiology*, 1992, 183, 59-64.

9.   H.-J. Wienmann, G. Schuhmann-Giampieri, H. Schmitt-
      Willich, H. Vogler, *Magn. Reson. Imag.*, 1991, <u>22</u>, 233-
      237.

10.   A. Mühler, O. Clément, V. Vexter, Y. Berthzène, W.
      Rosenau and R. Brasch, *Radiology*, 1992, <u>184</u>, 207-213.

11.   G. Vittadini, E. Felder, P. Tirone, V. Lorusso. *Invest.
      Radiol.*, 1988, <u>23</u>, 246-248.

12.   P. Pavone, G. Patrizio, C. Buoni, E. Tettamamti, R.
      Passarello, C. Musu, P. Tirone and E. Felder, *Radiology*,
      1990, <u>176</u>, 61-64.

13.   F. Cavagna, M. Daprà, F. Maggioni, C. DeHaën, E. Felder,
      Magn. Reson. Med., 1991, <u>22</u>, 329-333.

14.   A. Davies, C. de Haën, *Drugs of the Future*, 1991, <u>16</u>,
      1001-1003.

15.   C.D. Klaassen, J.B. Watkins III. *Pharmacological
      Reviews*, 1984, <u>36</u>, 1-67.

16.   R.B. Lauffer, *Chem Rev.*, 1987, <u>87</u>, 901-927.

17.   J-C. Bousquet, S. Saini, D.D. Stark, P.F. Hahn, M.Nigam,
      J. Wittenberg, and J.T. Ferrucci, *Radiology*, 1988, **166**,
      693-698.

18.   H.P. Niendorf, J. Haustein, I. Cornelius, A. Alhassan
      and W. Clau. *Magn. Reson. Med.*, 1991, <u>22</u>, 222-228.

19.   C.A. Chang, K. Kumar, J.M. Garrison, H.G.Brittain, M.F.
      Tweedle, *Soc.Mag Res in Medicine,* 9th *Annual Conference.*
      1990,729.

20.   S.M. Rocklage, D. Worah and S-H. Kim, *Magn. Reson. Med.*,
      1991, <u>22</u>, 216-221.

21.   M.F. Tweedle. *'Lanthanide Probes in Life, Chemical and
      Earth Sciences'*, Eds. J-C.G. Bunzli and G.R. Choppin,
      Elsevier, Amsterdam, 1989, Chapter 5, 127-173.

22.   W.P. Cacheris, S.C. Quay, and S.M. Rocklage, *Magn Reson
      Imaging*, 1990, **8**, 467-481.

23.   M.F. Tweedle, J.J. Hagan, K. Kumar, S. Mantha, and C.A.
      Chang, *Magn Reson Imaging*, 1991, **9**, 409-415.

24. C.J. Broan, J.P.L. Cox, A.S. Craig, R. Kataky,D. Parker, A. Harrison, A. Randall, and G. Ferguson, *J.Chem. Soc. Perkin Trans. 2*, 1991, 87-99.

25. P.Wedeking, K. Kumar and M.F. Tweedle, *Magn Reson Imaging*, 1992, **10**, 641-648.

26. P.Wedeking and M. Tweedle, *Nucl. Med. Biol.* 1988,**4**,395-402.

27. D. Parker. *Personal Communication*.

28. K.P. Pulukkody, T.J. Norman, D. Parker, L. Royle, and C.J. Broan, *J.Chem. Soc. Perkin Trans. 2*, 1993, 605-620.

CHAPTER THREE

YTTRIUM MACROCYCLES

3.1. INTRODUCTION.

3.1.1. Radioimmunotherapy.

The aim of radioimmunotherapy is to deliver a sterilising dose of radiation selectively to tumour cells by using the targeting properties of antibodies which recognise tumour specific antigens.

In order to achieve the maximum tumour killing effect with as little damage to normal tissue as possible, a high tumour to background ratio is needed. For this the following requirements should be met:-

1. An antibody which will bind selectively, tightly and quickly to a tumour specific antigen.
2. Rapid clearance from the circulation of any unbound antibody.
3. A radioisotope which emits particle radiation.
4. A radioisotope with a half life which is matched to the time scale of antibody uptake by the tumour and clearance of any unbound antibody, so that the major part of the radiation dose is delivered to the tumour.
5. A radioisotope which is readily available, carrier-free, decays to a stable daughter, and has chemical properties which enable it to be attached to an antibody.
6. The radioisotope should be bound tightly to the antibody so that it does not accumulate in tissues other than those to which the antibody directs it.

3.1.2. Antibodies for Targeting.

In 1957 Pressman[1] first proposed the use of antibodies for the targeting of radioactivity to tumours. However, it was not until the development of monoclonal antibodies (McAb) by Köhler and Milstein[2] in 1975 that antibodies of a high enough specificity to a single antigen became available to make clinical radioimmunotherapy feasible. McAbs are highly specific, high affinity antibodies which can be raised against specific antigens. McAbs have been raised against

several tumour associated antigens. These antigens can be
expressed in high levels in tumours but are not usually
totally tumour specific, as the antigens can be present in
some normal tissues[3]. Two such McAbs are B72.3 and HMFG1.
B72.3 binds to the antigen TAG-72 which is a high molecular
weight glycoprotein expressed in over 90% of colorectal,
gastric and ovarian cancers, and 70% of breast cancers[4,5].
HMFG1 McAb binds to 'human milk fat globule antigen' which is
expressed in normal lactating breast and is also found in
many cancers including ovarian cancer[6]. Both these McAbs have
been labelled with yttrium-90 and used in clinical trials for
the therapy of colorectal[4] and ovarian [6-8] cancers.

One problem with the use of McAbs in humans has been the
development of an immunogenic response by patients to the
mouse McAb[4,6-9], which can lead to potentially lethal serum
sickness. In order to overcome this HAMA (human anti-mouse
antigen) response, techniques have been developed through
genetic engineering to produce chimeric and humanised
antibodies[9].

Another problem has been the difficulty experienced by
the relatively high molecular weight McAb (160,000 daltons)
penetrating into solid tumours[10]. Antibodies can be split
into smaller fragments, Fab or Fab' (molecular weight 50,000)
or Fab'$_2$ (molecular weight 100,000) and still retain their
antigen binding capacity. The smaller the molecule, the
easier it is for it to enter the extravascular space and from
there to enter tumours. Smaller molecules also show more
rapid blood clearance[9]. Labelled McAb fragments have been
used in xenografts of human colonic tumour in mice to give
higher tumour to blood ratios than have been obtained by
using whole McAb[11]. However, this higher tumour to blood
ratio was at the expense of less antibody (or fragments) in
total being delivered to the tumour. To overcome the problem
of the penetration of McAbs into tumours or any heterogeneity
of antigen expression within the tumour[12], an isotope
emitting beta particle radiation capable of delivering a
sterilising dose over many cell diameters can be used.

3.1.3 Yttrium in Radioimmunotherapy.

A range of radioisotopes and their decay characteristics for possible use in radioimmunotherapy use have been discussed in section 1.2.3. The most widely used isotope for radioimmunotherapy is iodine-131 [13-17], followed by yttrium-90 [18-24]. Iodine -131 is not an ideal isotope for therapy as it has a high yield of gamma radiation, a rather long half life (193 hours) and a tendency to dehalogenate from the McAb in vivo. Yttrium-90 is more suited to radioimmunotherapy due to being a pure beta-emitter with a better suited half life of 64 hours. The yttrium-90 beta particle has a mean range of 3.9 mm in tissue, making it suitable for the treatment of tumour masses where total and uniform penetration can be difficult[10,12]. ^{90}Y is also readily available from a strontium-90 generator in carrier free form, suitable for labelling of bifunctional complexing agents.

Several treatments with ^{90}Y-McAbs of human colonic cancer[18-21], lymphoma[22], hepatoma[23] and glioma[24] xenografts have resulted in inhibition of tumour growth and in some cases complete remission. Following on from these successes in animal studies, ^{90}Y-McAbs have been used in clinical trials on patients with B cell lymphoma[25], breast cancer[26] and ovarian cancer[6-8,27,28]. The success of ^{90}Y-McAbs in clinical therapy has been limited by bone marrow toxicity (myelosuppression) with ^{90}Y doses being limited to less than 20 to 25 mCi per patient[6-8,26,28]. This has been due to the release of free yttrium-90 from the McAb. Uncomplexed yttrium is known to be a bone seeker and to deposit on bone surfaces[29,30] where it can irradiate the bone marrow thereby causing myelosuppression. The problem of irradiation of the bone marrow from yttrium-90 on the bone surface is worse in humans than has been suggested from pre-clinical studies in mice, because more of the radiation dose is absorbed in the marrow of larger species. In order to minimise this bone marrow toxicity, bifunctional complexing agents need to be developed with high in vivo stabilities with respect to metal release.

3.1.4. Bifunctional Complexing Agents.

A bifunctional complexing agent has the dual properties of binding a metal ion and attaching to an antibody. This bifunctional complexing agent plays a critical role in the in vivo stability and hence effectiveness in therapy of the radioimmunoconjugate. The bifunctional complexing agent should fulfil the following criteria:-

1. The attachment of the bifunctional complexing agent to the McAb should not alter its immunoreactivity. This usually means a maximum of 3 complexing agents per McAb[31].
2. The metabolism of the McAb should not be altered by the labelling procedure. Thus any labelling should be performed in aqueous solution between pH 4 and 8 at no greater than 37°C.
3. Following the catabolism of the McAb, the bifunctional complexing agent should help to clear the radiometal from the body. The complexes $[Y.DOTA]^-$ and $[Y.DTPA]^{2-}$ and their bifunctional complexing agents are all cleared rapidly from the body via the kidneys[32].
4. The complexing agent should not release the radiometal in vivo.

The most common failure of the bifunctional complexing agent is that it does not hold the radiometal securely enough in vivo which leads to the premature release of ^{90}Y and consequent bone marrow toxicity[6,7,27].

3.1.5. In Vivo Stability of Yttrium Complexes.

In experiments on the stability of yttrium-macrocycle complexes yttriim-88 is sometimes used instead of yttrium-90. This is because ^{90}Y has a relatively short half life of 64 hours, and is detected by measuring the Bremsstrauhlung radiation from its β-emission. Yttrium-88 has a longer half life of 107 days and emitts gamma-radiation (0.51 and 3.62

MeV) which is easier to detect than Bremsstrauhlung radiation.

Yttrium -90 was first linked to McAbs by using DTPA cyclic anhydride (CaDTPA) which was linked to the McAb via one of its carboxylic acid groups[33,34]. Yttrium has a co-ordination number of 8 and thus needs an octodentate ligand[35]. The loss of one carboxylic acid group from the DTPA ligand for linking to the antibody leads to loss in the stability of the yttrium-DTPA complex. This was seen as:- the loss of 8 to 9% of ^{90}Y per day[36] from the ^{90}Y-CaDTPA-McAb complex in serum stability experiments; the accumulation in bone of 13% of the injected yttrium dose per gram at 3 days (^{90}Y)[37], 11 to 12% at 5 days (^{88}Y)[38,39] and 9% at 8 days (^{90}Y)[32] post injection; and as bone marrow toxicity in therapy trials with ^{90}Y-McAbs both in mice[18,19,40] and patients[7,27].

Figure 3.1. *Bifunctional Complexing Agents Based on DTPA.*

| CaDTPA | SCN-Bz-DTPA | MX-DTPA | CHX-A-DTPA |
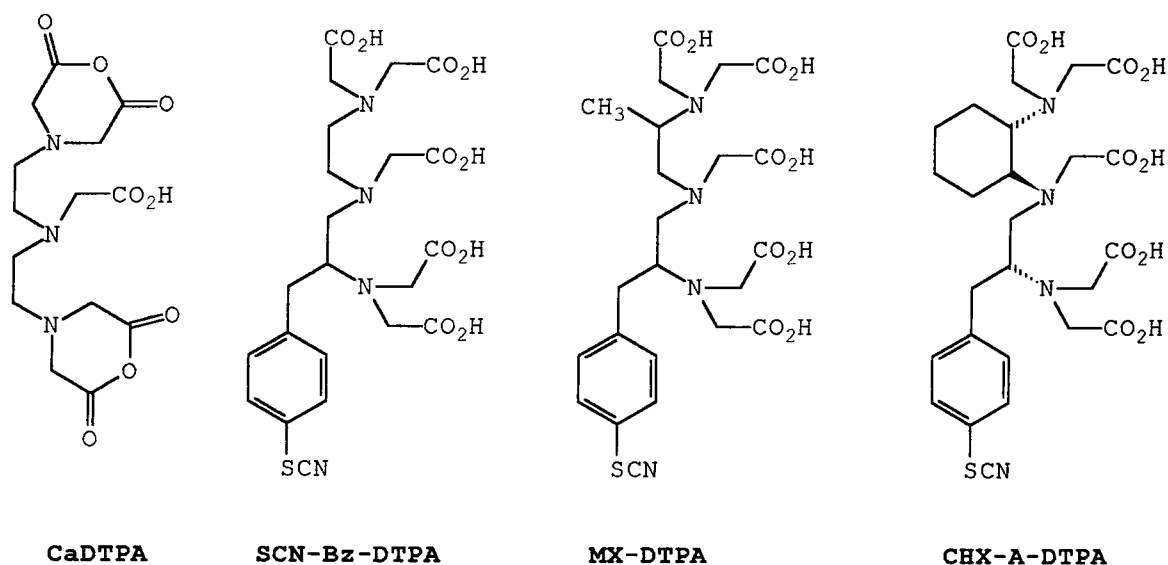
In order to improve on the in vivo stability of CaDTPA labelled McAbs, backbone substituted derivatives of DTPA were synthesised. The derivatives in figure 3.1 use an isothiocyanate group for antibody linkage, leaving all the DTPA carboxylic acid groups available for the co-ordination of yttrium. Alternatively a NH_2 group has be used in place of

the SCN group[37] of SCN-Bz-DTPA and MX-DTPA, or a maleimide linker group has been attached to the DTPA backbone in place of the benzylisothiocyanate group of SCN-Bz-DTPA to give the bifunctional complexing agent CT-DTPA.

Yttrium-labelled McAbs made with these backbone substituted DTPA derivatives all showed increased stability over those made with CaDTPA. In serum stability studies ^{88}Y-MX-DTPA lost 6.6% and ^{88}Y-CHX-A-DTPA 4.2% of ^{90}Y over 17 days[41]. In animal studies less yttrium accumulated in the bone. Only about 3% dose/g was found in the bone of mice given Y-McAbs labelled via the backbone substituted DTPA derivatives(^{90}Y)[21,32,37] (^{88}Y)[38,39,41] compared to between 9 and 13% dose/g in bone from Y-Ca-DTPA labelled McAbs at 3 to 7 days post injection. The nature of the chemical linkage between the backbone substituted DTPA and the McAb did not appear to alter the ^{90}Y bone uptake[37]. The higher in vivo stability of the backbone substituted DTPA conjugates was simply a result of all five carboxylic acid groups on the DTPA being available for complexing the yttrium. In therapy studies with ^{90}Y-MX-DTPA-McAbs in both mice[19-21] and humans[6], less bone marrow toxicity was seen.

Although these backbone-substituted DTPA labelled McAbs are more stable in vivo than the original cyclic anhydride linked DTPA McAbs, there is still a measurable loss of yttrium. It is well established that macrocyclic ligands such as DOTA form much more stable metal complexes in vivo[42] (section 1.3.6) than acyclic ligands such as DTPA. The rate of trasmetallation of DTPA metal complexes with endogenous metal ions in the plasma is high[43], whereas [Y.DOTA]$^-$ shows no measurable loss of ^{88}Y over 18 days incubation in serum[44]. [Y.DOTA]$^-$ is also less susceptible to acid catalysed dissociation showing no loss of stable yttrium over 3 months at pH 3.6[45], or ^{90}Y over 10 days at pH >2.6, 37°C[46]. Even at pH values as low as 1.0 the loss of ^{90}Y from [Y-DOTA]$^-$ is still only 50% over 12.8 hours[47]. This high kinetic inertness of [Y.DOTA]$^-$ which is an advantage in reducing the loss of ^{90}Y in vivo, also results in a slower rate of forward binding of yttrium with DOTA than with DTPA[48]. However, the rate of

forward binding of yttrium by DOTA is still sufficiently
rapid (84% uptake in 30 minutes at pH 5.5, 37°C, at 5 μM
DOTA)[46] for efficient radiolabelling of McAbs.

When bifunctional complexing agents based on the
macrocycle DOTA (figure 3.2) are used to link yttrium-90 to
McAbs, the high in vivo kinetic stability associated with
[Y.DOTA]$^-$ was retained. In serum stability studies the ligand
p-nitrobenzyl DOTA showed no measurable loss of ^{88}Y over 18
days[44], 2B-DOTA showed no loss of ^{88}Y over 17 days[41], and BAD
showed no loss of ^{88}Y over 25 days[49]. Animal studies on bone
uptake of yttrium from Y-McAb conjugated with the ligands 2B-
DOTA and DOTA-Mal gave only 2.1% injected dose/g (^{88}Y) at 5
days[41] and 1.5% injected dose/g (^{90}Y) after 8 days[33]
respectively. When ^{90}Y-BAD-McAb and ^{90}Y-MX-DTPA-McAb were
used in toxicity experiments (LD$_{50}$) in mice, ^{90}Y-MX-DTPA-McAb
was shown to be more toxic and by implication the less stable
of the two. The LD$_{50}$'s were 220 μCi of ^{90}Y-MX-DTPA-McAb and
307 μCi of ^{90}Y-BAD-McAb[50].

Figure 3.2. *Bifunctional Complexing Agents Based on DOTA.*

DOTA-Mal

p-nitrobenzyl DOTA

BAD

2B-DOTA
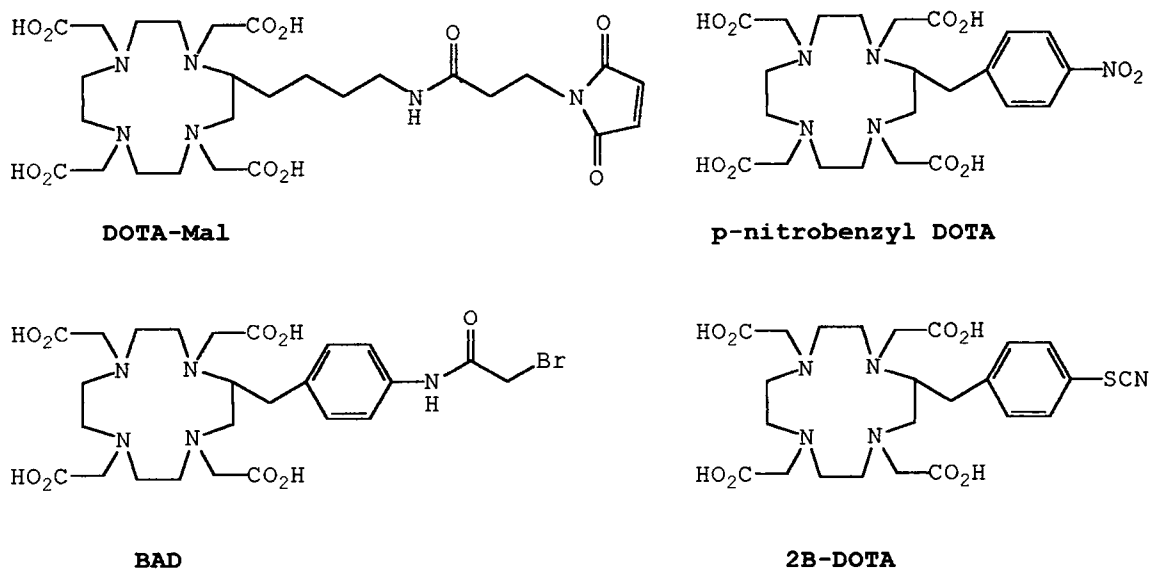
Further evidence of the improved in vivo stability of
yttrium-DOTA conjugated McAbs over yttrium-DTPA conjugated
McAbs comes from studies on the distribution of yttrium
within the mouse femur. Free yttrium is known to concentrate

in cortical bone[29,30], and studies by both Camera et.al[41] and Harrison et.al[32] have shown that substantially more yttrium is found in the cortical bone of the femur than in the bone marrow of mice given yttrium-DTPA conjugated McAbs as opposed to yttrium-DOTA conjugated McAbs. This clearly demonstrates the greater in vivo stability of ^{90}Y-immunoconjugates which have been labelled via a macrocyclic DOTA ligand over than of ^{90}Y-immunoconjugates labelled via the acyclic DTPA ligand. Because less yttrium-90 is being released from ^{90}Y-DOTA-McAbs than from ^{90}Y-DTPA-McAbs, the use of the DOTA ligand should result in less bone marrow toxicity to patients undergoing radioimmunotherapy.

3.1.6. The Scope of the Work in This Chapter.

In this chapter, the acid dissociation constants are measured for three tetraaza-phosphinic acid macrocycles and two bifunctional complexing agents, DOTA-maleimide and an aza-phosphinic acid-maleimide. These acid dissociation measurements are then compared to those of gadolinium labelled macrocycles from chapter 2. The association rates for a range of 9 anionic, neutral, and cationic aza-carboxylic and aza-phosphinic acids are also measured

Finally the McAb B72.3 is radiolabelled with ^{90}Y via the bifunctional complexing agents DOTA-maleimide or 12N4P3Me3-maleimide. The biodistributions of these labelled McAbs in normal mice are measured to assess their in vivo stabilities. The bones of these mice are examined in detail to assess the amounts of ^{90}Y deposited in the bone as opposed to ^{90}Y in the bone marrow from circulating ^{90}Y-McAb.

3.2. DISSOCIATION OF YTTRIUM MACROCYCLE COMPLEXES.

Experimental details are given in section 3.5.

Dissociation measurements using HPLC radiometry were carried out on one anionic yttrium aza-phosphinic acid

complex [Y.12N4P4Me4]⁻, and two neutral yttrium aza-
phosphinic acid complexes [Y.12N4P3Me3NBu2] and
[Y.12N4P3Me3NBz2].

Dissociation measurements were also performed on two
yttrium labelled bifunctional complexing agents [Y.DOTA-Mal]
and [Y.12N4P3Me3-Mal].

Figure 3.3. *Chemical Structures of the Ligands Used to
Complex Yttrium.*

12N4P4Me4   12N4P3Me3NBu2   12N4P3Me3NBz2

DOTA-Mal

Bu= CH₂ CH₂ CH₂ CH₃

Bz= —CH₂—⟨phenyl⟩
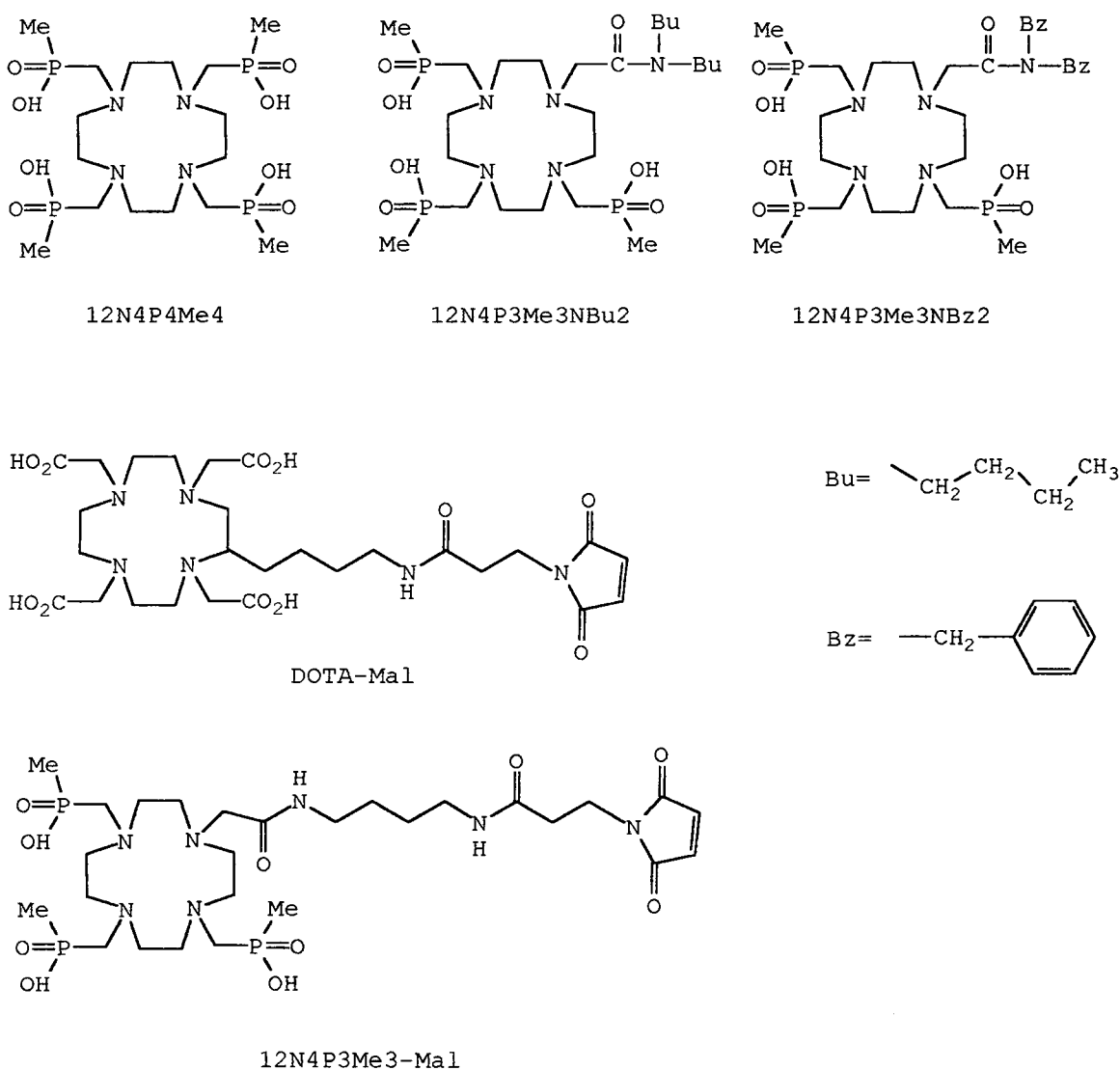
12N4P3Me3-Mal

3.2.1. Stability of yttrium macrocycles.

A summary of the results of the acid catalysed dissociation constants for the yttrium labelled macrocycles is given in table 3.1. The two neutral yttrium complexes [Y.12N4P3Me3NBu2] and [Y.12N4P3Me3NBz2] are more stable in acid solution than the anionic [Y.12N4P4Me4]$^-$, as would be expected on the basis of coulombic attraction. The k_{obs} values of the neutral complexes also show a less steep dependence on pH than the anionic complex [Y.12N4P4Me4]$^-$. However, considering that the physical half life of yttrium-90 is only 64 hours, even [Y.12N4P4Me4]$^-$ is stable for twice this amount of time at pH 2.

The two bifunctional complexing agents both show high stability under acid conditions, [Y.DOTA-Mal]$^-$ being more stable than [Y.12N4P3Me3-Mal]. This augurs well for their use in antibody labelling for in vivo use.

Table 3.1. *Dissociation Data for Yttrium Complexes.*

Yttrium complex	pH	$k_{obs}/$ * 10^{-6} sec^{-1}	Half Life Hours
12N4P4Me4	1.0	13.9	13.8
	1.5	5.74	33.6
	2.0	1.67	116
12N4P3Me3NBu2	1.0	1.89	102
	1.5	0.699	276
	2.0	0.267	721
12N4P3Me3NBz2	1.0	1.33	145
	1.5	0.507	379
	2.0	0.195	989
DOTA-Mal	1.0	2.72	70.8
	1.5	0.758	254
	2.0	0.141	1370
12N4P3Me3-Mal	1.0	6.56	29.3
	1.5	2.11	91.2
	2.0	0.520	370

* Standard errors are listed in table 3.5

Figure 3.4.

Variation of kobs with pH for Yttrium Macrocycles
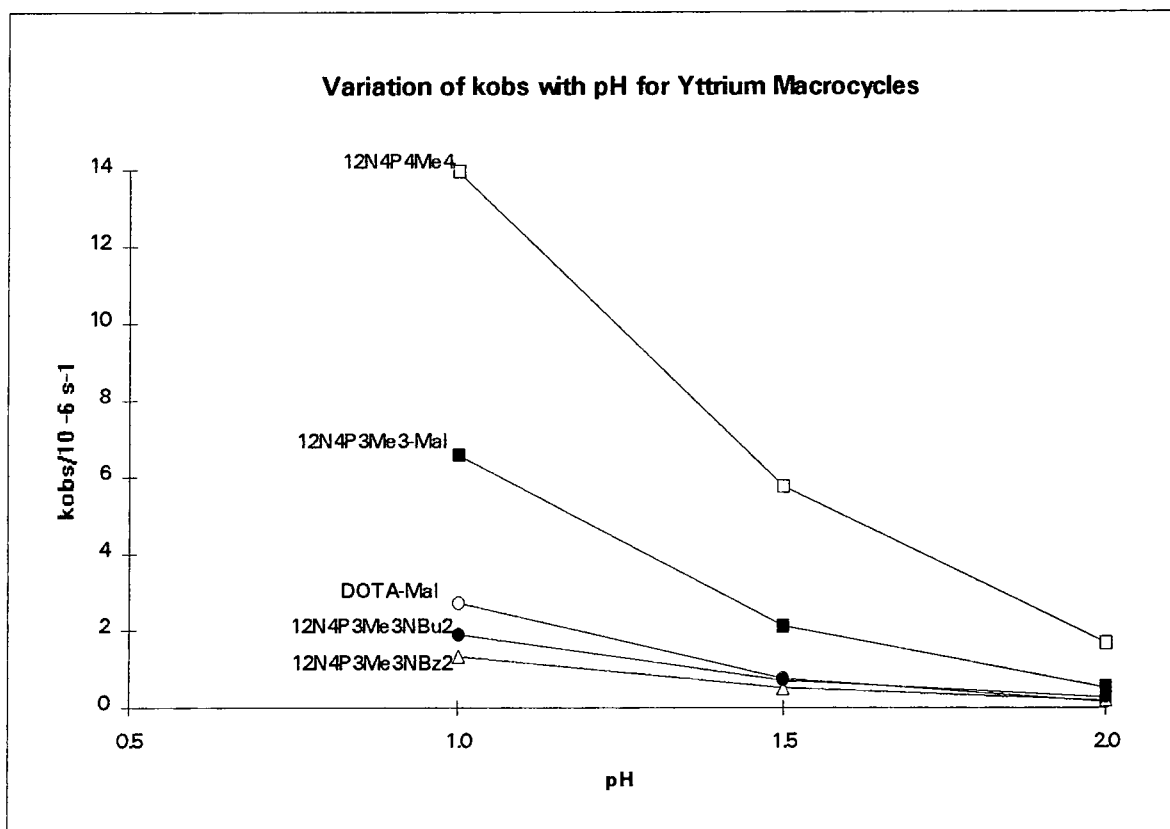
3.2.2. Comparison of Acid Catalysed Dissociation Constants for Yttrium and Gadolinium Complexes.

Table 3.2 lists the acid dissociation constants for the yttrium complexes together with those of their corresponding gadolinium complexes. Yttrium and gadolinium have ionic radii of 1.02 and 1.05 Å respectively[51], and both have tripositive ions which form octodentate complexes.

The yttrium complex of DOTA is not as resistant to acid catalysed dissociation as [Gd.DOTA]⁻. The yttrium complexes [Y.12N4P4Me4]⁻ and [Y.12N4P3Me3NBu2] are also a little less stable than the corresponding gadolinium complexes, but [Y.12N4P3Me3NBz2] which is the most stable of the yttrium complexes is more stable than the corresponding gadolinium complex. All of the neutral complexes show less acid catalysed dissociation than the anionic complexes as well as a less steep dependence of k_{obs} on pH.

Table 3.2. *Acid Dissociation Rates of Yttrium and Gadolinium Macrocycles*

		$K_{obs}/10^{-6}$ s^{-1}			Half life hours		
pH	1.0	1.5	2.0	1.0	1.5	2.0
[Gd.DOTA]$^-$	3.16	0.898	0.049	60.2	214	3930
*[Y.DOTA]$^-$	15.0	1.88	0.33	12.8	102	583
[Y.DOTA-Mal]$^-$	2.72	0.758	0.141	70.8	254	1370
[Gd.12N4P4Me4]$^-$	10.4	4.63	1.13	18.5	41.6	171
[Y.12N4P4Me4]$^-$	13.9	5.74	1.67	13.8	33.6	116
[Y.12N4P3-Mal]	6.56	2.11	0.520	29.3	91.2	370
[Gd.12N4P3Me3NBu2]	1.26	0.494	0.204	152	389	943
[Y.12N4P3Me3NBu2]	1.89	0.699	0.267	102	276	721
[Gd.12N4P3Me3NBz2]	4.28	1.64	1.00	44.9	118	192
[Y.12N4P3Me3NBz2]	1.33	0.507	0.195	145	379	989

* Data from K.P.Pulukkody et al[47].

The two bifunctional complexing agents [Y.DOTA-Mal]$^-$ and [Y.12N4P3Me3-Mal] have higher stability than their non functionalised anionic parent complexes [Y.DOTA]$^-$ and [Y.12N4P4Me4]$^-$.

All of the yttrium and gadolinium macrocycle complexes listed above have much better resistance to acid catalysed dissociation than the acyclic complex [Gd.DTPA]$^{2-}$. Even the k_{obs} of 1.39 x10^{-5} for [Y.12N4P4Me4]$^-$ is two orders of magnitude greater than the k_{obs} of 1.1 x 10^{-3} for [Gd.DTPA]$^{2-}$ at pH 1[52].

In conclusion, the acid catalysed dissociation rates of the yttrium macrocycle complexes measured are much lower than those of acyclic complexes. This should correspond to high in vivo stabilities for all of the above macrocycle complexes. Proteins labelled with the macrocyclic bifunctional complexing agents [Y.DOTA-Mal]$^-$ and [Y.12N4P3Me3-Mal], should have much higher in vivo stability than those labelled with bifunctional DTPA, leading to less release of free ^{90}Y and consequently less toxicity.

3.3. KINETICS OF YTTRIUM ASSOCIATION WITH MACROCYCLES

Experimental details are given in section 3.5.2.

The use of ^{90}Y-labelled antibodies for radioimmunotherapy requires a quick and reliable labelling protocol. To this end, the complexing agent which is to be attached to the antibody should undergo efficient and rapid radiolabelling under conditions which will not cause denaturation of the antibody. In these experiments low concentrations of ligand (5 μM) were used to reflect the concentration of macrocycle which would be expected when labelling conjugated antibody. The ^{90}Y used was of high purity, essentially carrier free, and relatively free of other metal ions. At these low concentrations any small amount of contaminating metal ions will severely alter the labelling efficiency.

3.3.1. Rates of Yttrium Uptake.

Association kinetics were carried out on the following macrocycles (see figure 3.6) with respect to yttrium-90 uptake:-

    anionic complexes: DOTA, 12N4P4Me4, 12N4P3Me3C,
                        12N4P4Bz4.
    neutral complexes: 12N4P3NHMe, 12N4P3Me3NBu2,
                        12N4C3(IBu)2.
    cationic complexes: 12N4P3Me3NH(CH2)4NH3^{+},
                        12N4C3NH(CH2)4NH3^{+}.

Table 3.3 and figure 3.6 summarise the data for yttrium uptake by the range of macrocycles pictured in figure 3.5 at concentrations of 5 μM. DOTA has the fastest rate of ^{90}Y uptake, achieving 80% uptake within 2 minutes. This level of uptake (80%) is achieved within 5 minutes for 12N4P3Me3NH(CH2)4NH3^{+}; 10 minutes for 12N4P4Me4; 15 minutes for 12N4P4Bz4 and 12N4P3Me3NBu2; 30 minutes for 12N4P3Me3C

Figure 3.5. *Chemical Structures of the Ligands Used for Yttrium Uptake*

DOTA

12N4P4Me4

12N4P3Me3C

12N4P4Bz4

12N4P3Me3NHMe

12N4P3Me3NBu2

12N4C3N(IBu)2

12N4P3Me3NH(CH2)4NH3+

12N4C3NH(CH2)4NH3+

Bz=   —CH2— (phenyl)

Bu=   —CH2—CH2—CH2—CH3

iBu=   —CH2—CH(CH3)2
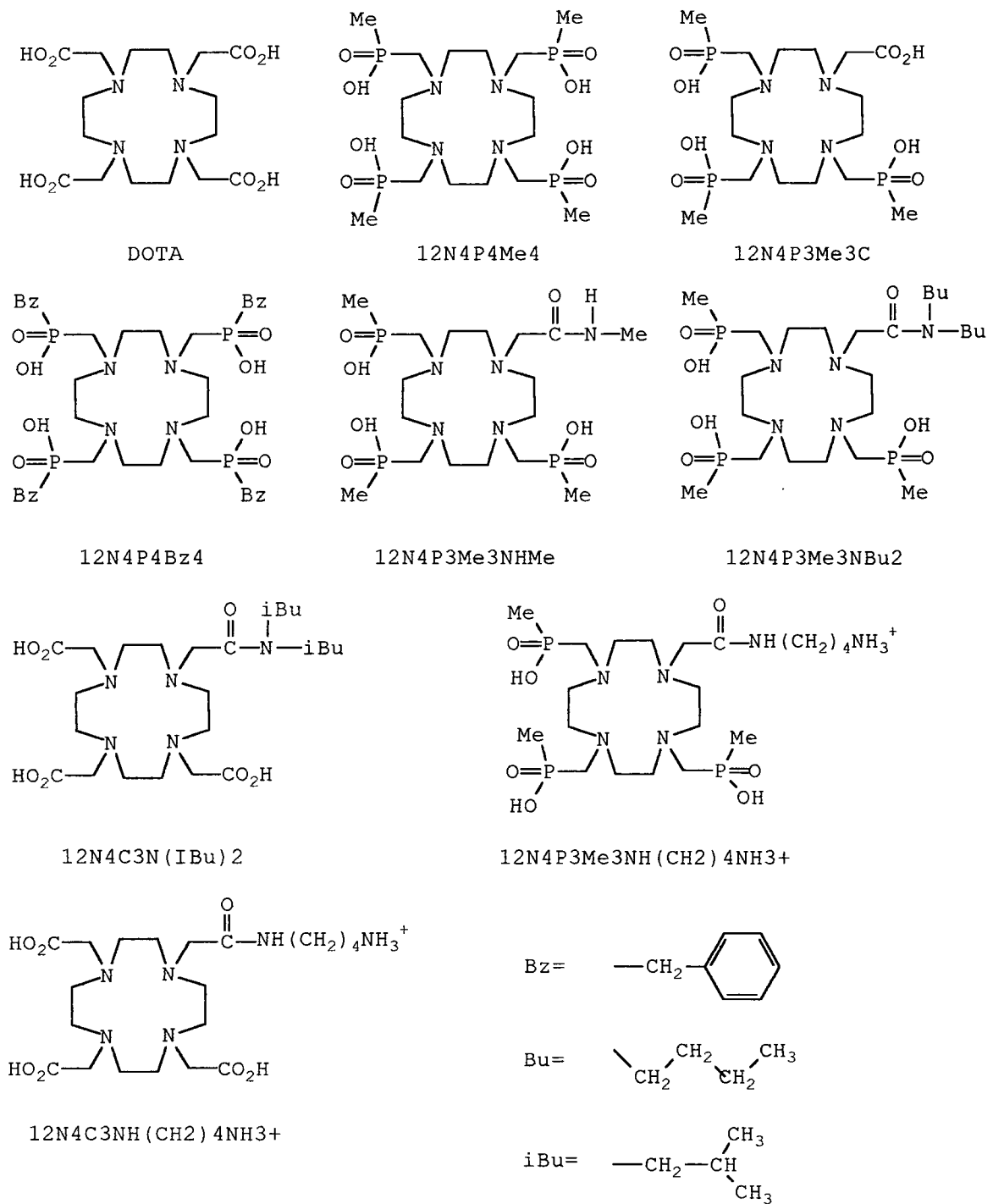
and 12N4C3NH(CH2)4NH3$^+$; and 60 minutes for 12N4P3NHMe. The ligand 12N4C3(IBu)2 shows very little uptake of yttrium within 60 minutes at a concentration of 5 μM. This is probably due to metal ion contamination of the sample examined rather than a lack of affinity of the ligand for yttrium.

Table 3.3. *Summary of Percentage ⁹⁰Y Uptake @ 5 µM Macrocycle, 200 mM NH₄OAc, pH 6.5, 310K.*

Time min	DOTA	12N4P4 Me4	12N4P3 Me3C	12N4P4 Bz4	12N4P3 Me3NHMe	12N4P3 Me3NBu2	12N4C3N (IBu)2	12N4P3 Me3NH (CH2)4NH3$^+$	12N4C3 NH (CH2)4NH3$^+$
1	54.36	8.83	5.55	5.46	2.01	5.91	0.28	17.36	3.40
2	80.51	18.26	11.43	14.86	4.11	11.97	0.39	36.18	8.86
5	98.49	55.15	29.03	43.37	12.64	35.17	0.48	78.54	23.62
10	99.67	85.27	51.74	68.59	24.67	61.08	0.60	90.19	42.82
15	99.59	87.11	66.01	82.32	35.78	78.65	0.68	97.35	59.88
20	99.76	92.55	73.40	83.53	45.38	86.77	0.78	90.31	67.55
30	99.30	93.35	84.22	88.17	58.38	90.23	0.93	95.91	81.25
60	99.02	95.05	94.67	87.22	79.75	82.97	1.54	95.11	91.78

Figure 3.6. *Percentage ⁹⁰Y Uptake With Time.*
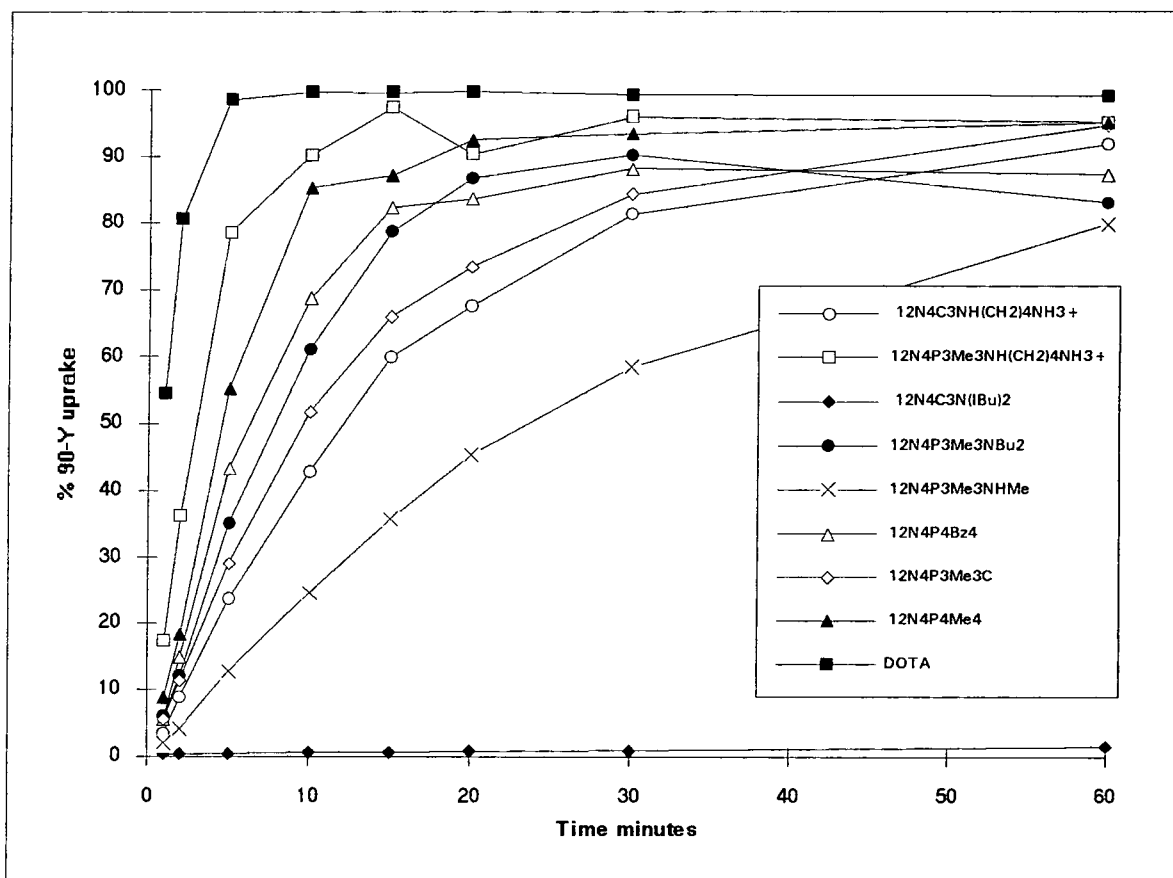
The five macrocycles which take less than 15 minutes to reach 80 % yttrium uptake (i.e. DOTA, 12N4P3Me3NH(CH2)4NH3$^+$, 12N4P4Me4, 12N4P4Bz4 and 12N4P3Me3NBu2) would all be suitable

to attach to monoclonal antibodies via a bifunctional group for labelling with ^{90}Y for immunotherapy experiments.

3.3.2. Yttrium Macrocycles for Which Both the Kinetics of Association and Dissociation Have Been Measured.

Table 3.4. *Kinetics of association and Dissociation of Yttrium Macrocycles.*

Macrocycle	Time taken for 80% Y uptake	Dissociation half life (hr) at pH 1.0	Dissociation half life (hr) at pH 2.0
[Y.DOTA]$^-$	2	12.8	583
[Y.12N4P4Me4]$^-$	10	13.8	116
[Y.12N4P3Me3NBu2]	15	102	721

All three yttrium macrocycle complexes (table 3.4) exhibit high rates of yttrium uptake and low rates of dissociation at acid pH. The neutral complex [Y.12N4P3Me3NBu2] has the highest stability in acid but the rate of yttrium uptake is slightly slower, both these rates will be dependent on electrostatic charges for opposing reasons. The bifunctional complexes derived from DOTA and 12N4P4Me4 (DOTA-Mal and 12N4P3Me3-Mal) have also been shown to have high stability in acid conditions (section 3.2.1)

In conclusion, [Y.DOTA]$^-$, [Y.12N4P4Me4]$^-$ and [Y.12N4P3Me3NBu2] should prove suitable for ^{90}Y labelling of antibodies for radioimmunotherapy.

3.4. YTTRIUM MACROCYCLE MALEIMIDE LINKED MONOCLONAL ANTIBODY.

3.4.1. Labelling of Monoclonal Antibody.

The monoclonal antibody B72.3 is a mouse IgG_1 type antibody with a high affinity for tumour-associated glycoprotein (TAG-72) found in human colonic and breast

cancers[4,5]. Labelling of this antibody with yttrium was achieved by means of the bifunctional complexing agents DOTA-Mal and 12N4P3Me3-Mal (figure 3.3). These two bifunctional complexing agents have a macrocyclic group for binding yttrium and a maleimide group for attachment to the antibody. The maleimide group combines with thiol groups on a protein to form a stable linkage between the macrocycle and the antibody[53]. As the B72.3 has no free thiol groups, Traut's reagent (2-iminothiolane) was used to introduce thiol groups by reaction with lysine ε-amino groups. The macrocycle maleimide was then conjugated to the antibody by reaction with these thiol groups (figure 3.7).

Figure 3.7. *Labelling of Antibody With Bifunctional Ligand.*

Ab = Antibody

Mac = Macrocycle
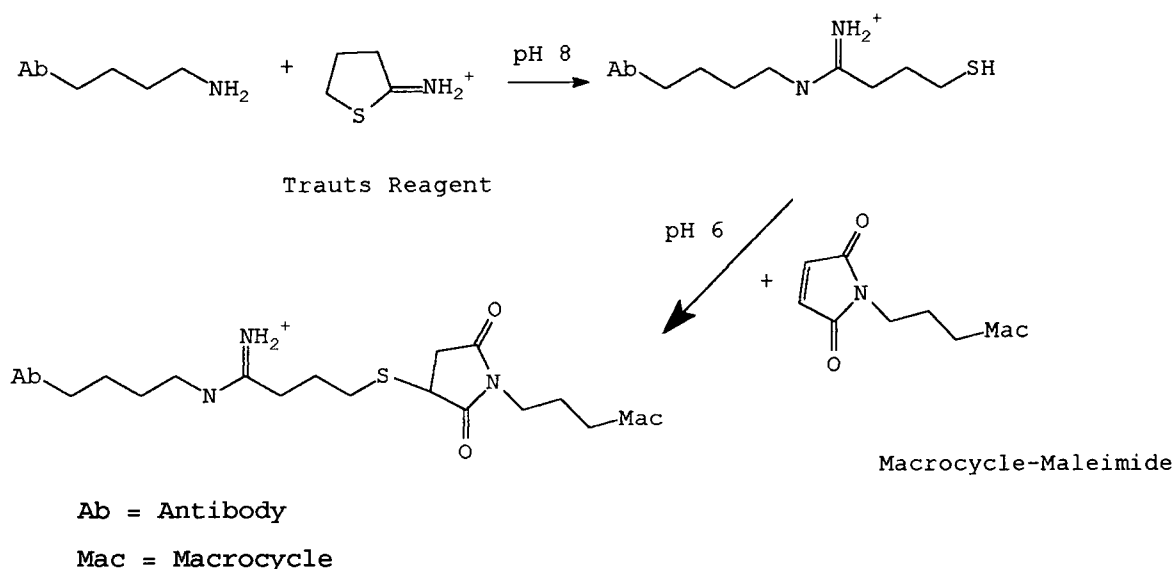
Any unreacted thiols were capped with N-ethylmaleimide before purification of the antibody conjugate by gel filtration. The antibody was then incubated with yttrium-90 for 15 minutes at 37°C (310K) in 0.1M ammonium acetate buffer pH 6. After the addition of DTPA to complex any unbound ^{90}Y, the ^{90}Y-labelled antibody was purified by means of size exclusion HPLC. This separated any high molecular weight protein aggregates and any low molecular weight [Y-DTPA]$^{2-}$ from the labelled antibody. Both DOTA-B72.3 and 12N4P3Me3-B72.3 showed labelling efficiencies of 30 % with ^{90}Y. Figures 3.8 and 3.9 show the elution profiles of ^{90}Y-labelled B72.3

antibody from HPLC. The sections marked were the fractions of the eluents taken for use in biodistribution studies (section 3.4.2). The number of thiols estimated to have been introduced per antibody was 2.2, so the number of macrocycles per antibody will have been less than this.

The macrocycles DOTA-Mal and 12N4P3Me3-Mal have already shown high stability under acid conditions, and fast rates of yttrium uptake (sections 3.2 and 3.3) in vitro. The attachment of these macrocycles to the antibody B72.3 enables the in vivo stability of these yttrium macrocycle conjugates to be assessed.

Figure 3.8. HPLC Elution Profile of ^{90}Y-DOTA-B72.3.
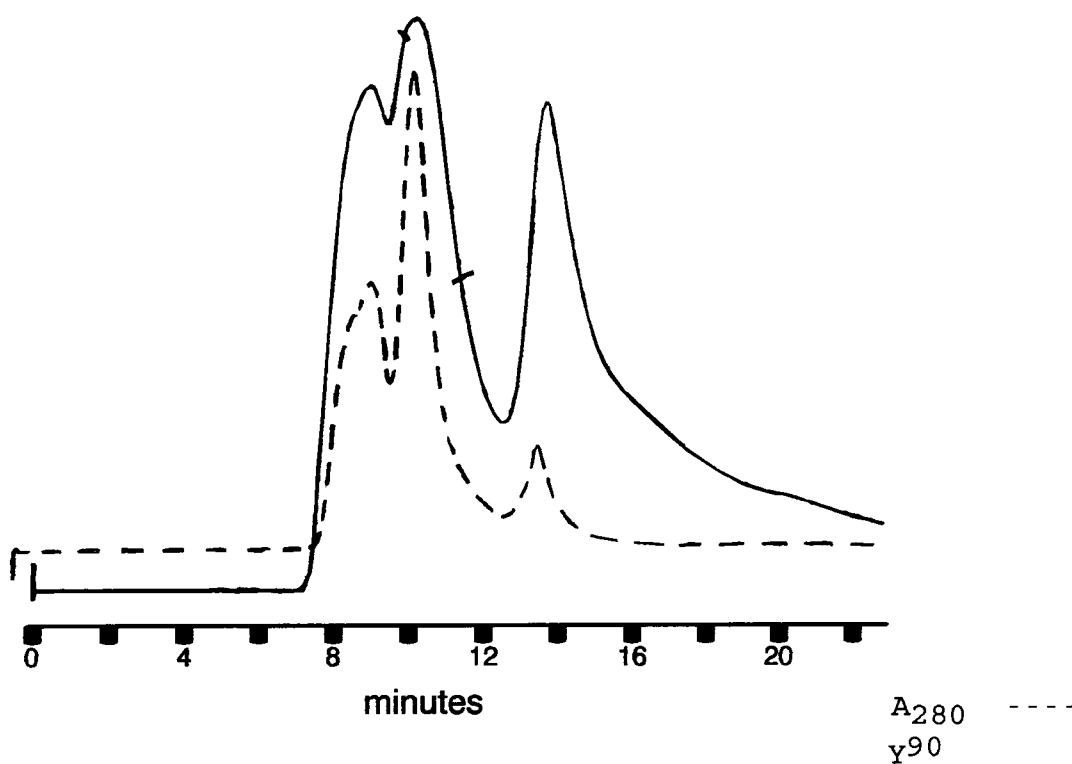
A solution of the monoclonal antibody B72.3 labelled with ^{90}Y via either a DOTA or 12N4P3Me3 macrocycle was injected intravenously into mice. A general tissue biodistribution was performed for both types of labelled antibody to assess the in vivo stability of the whole conjugate. A more detailed biodistribution of ^{90}Y in the bone was also performed to ascertain if there had been any release of free ^{90}Y from the macrocycle antibody conjugate.

Figure 3.9. HPLC Elution Profile of ^{90}Y-12N4P3Me3-B72.3.

A_{280}	----
Y^{90}	____
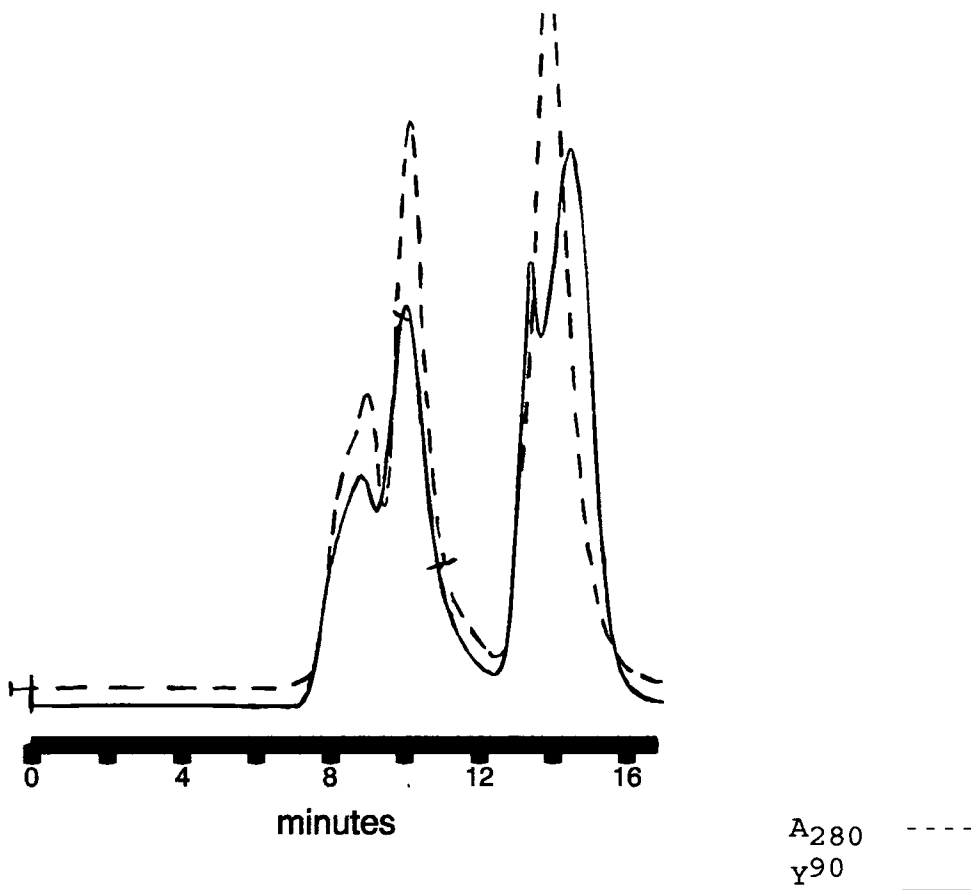
3.4.2. Biodistribution of ^{90}Y-Labelled Monoclonal Antibody

Tissue distributions are given in figures 3.10 to 3.13 as % dose/g and % dose per tissue for both ^{90}Y-DOTA-B72.3 and ^{90}Y-12N4P3Me3-B72.3. These results are the mean values taken from five mice for each conjugate at 48 hours post injection. All the tissues examined contain less ^{90}Y-DOTA-B72.3 than ^{90}Y-12N4P3Me3-B72.3, due to the more rapid excretion of the former. The overall pattern of distribution between the tissues is similar from both conjugates. The higher excretion rate by the DOTA-B72.3 group was probably due to the inclusion of some [^{90}Y.DTPA]$^{2-}$ in the injection dose (figures 3.8 and 3.9 show that there was less separation between the ^{90}Y-antibody and [^{90}Y.DTPA]$^{2-}$ in the ^{90}Y-DOTA-B72.3 than in the ^{90}Y-12N4P3Me3-B72.3 HPLC separation) or from a less satisfactory conjugation of the ^{90}Y-DOTA-Mal to the antibody. Any ^{90}Y-macrocycle-maleimide which is released during

metabolism of the antibody conjugate would be excreted very quickly (greater than 98% excretion in 24 hours)[32] as would any [Y.DTPA]$^{2-}$.

The results of the bone analysis are presented as % dose/g (figures 3.12 and 3.14), % dose (figures 3.11 and 3.15) and as tissue to blood ratios (figures 3.14 and 3.16). For all animals the right and left femurs were analysed separately. The femurs each had their ends (epiphyses) cut off and the bone marrow washed from the shaft to give three separate samples (i) the shaft - bone only, (ii) the marrow - no bone, and (iii) the epiphyses - both bone and marrow. From the data in figures 3.12 and 3.14 it can be seen that there is very little difference between the left and right femur samples, but that there is more ^{90}Y dose in all the bone tissues from ^{90}Y-12N4P3Me3-B72.3 than from ^{90}Y-DOTA-B72.3. When the data are presented as tissue to blood ratios (figure 3.16), the higher amount of ^{90}Y-12N4P3Me3-B72.3 in the blood is taken into account, and there is very little difference between the two samples. Free ^{90}Y is known to concentrate in bone tissue[29,30], so any concentration of ^{90}Y in the femur shaft over that of circulating ^{90}Y-B72.3 would be an indication of dissociation of ^{90}Y from the macrocycle. The % dose of yttrium in the femur shaft is less than 0.01% from both preparations. The ratio of yttrium in the shaft to that in the marrow is 0.27 from ^{90}Y-DOTA-B72.3 and 0.24 from ^{90}Y-12N4P3Me3-B72.3. These low ratios compare favourably with those measured by Harrison et al[32], of 0.24 for stable ^{90}Y-DOTA-B72.3 and 3.5 for the less stable ^{90}Y-cyclic anhydride DTPA-B72.3. The yttrium dose in the bone marrow is from circulating labelled antibody. The concentration(% dose/g) of ^{90}Y in the epiphyses is similar to that in the whole femur because the epiphyses consist of both bone and marrow.

Figure 3.10. *% Dose/g of ^{90}Y-DOTA-B72.3 at 48 Hours.*
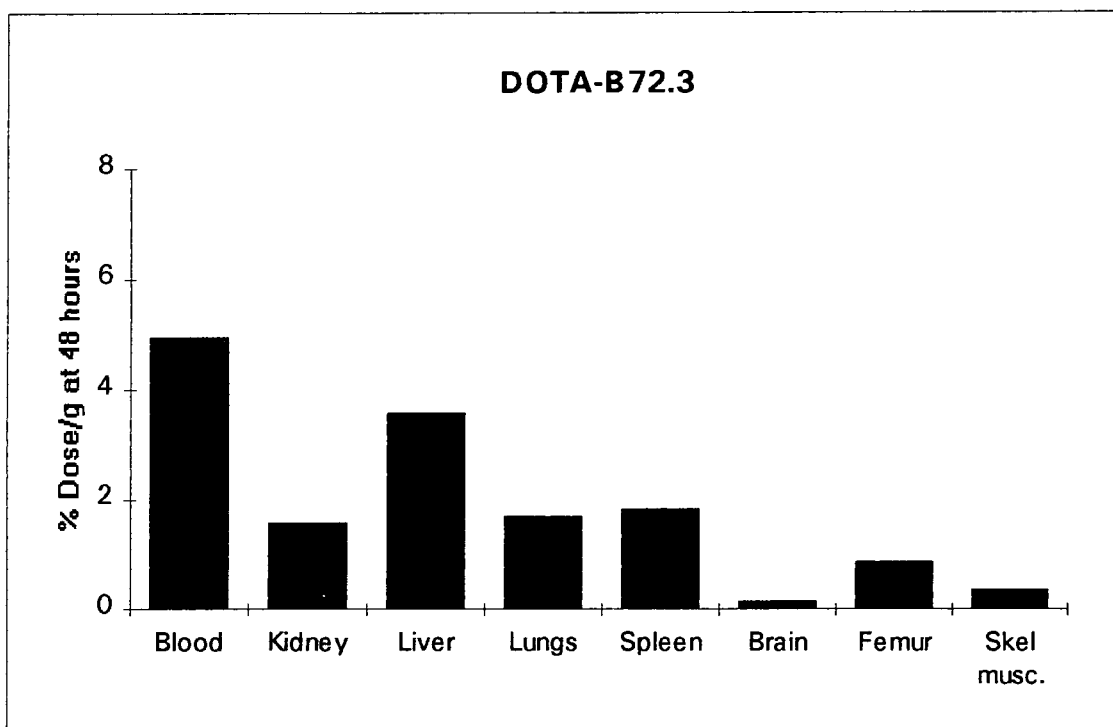
DOTA-B72.3

Figure 3.11. *% Dose of ^{90}Y-DOTA-B72.3 at 48 Hours.*

DOTA-B72.3
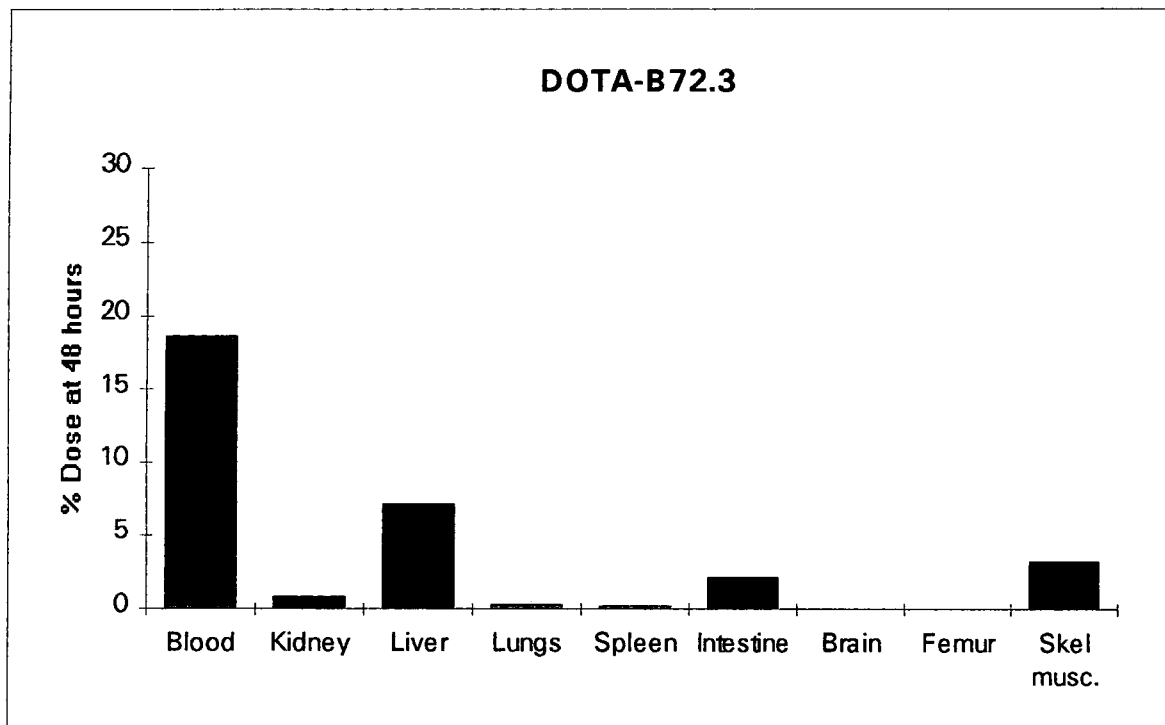
Figure 3.12. % *Dose/g* ^{90}Y-*12N4P3Me3-B72.3 at 48 Hours.*
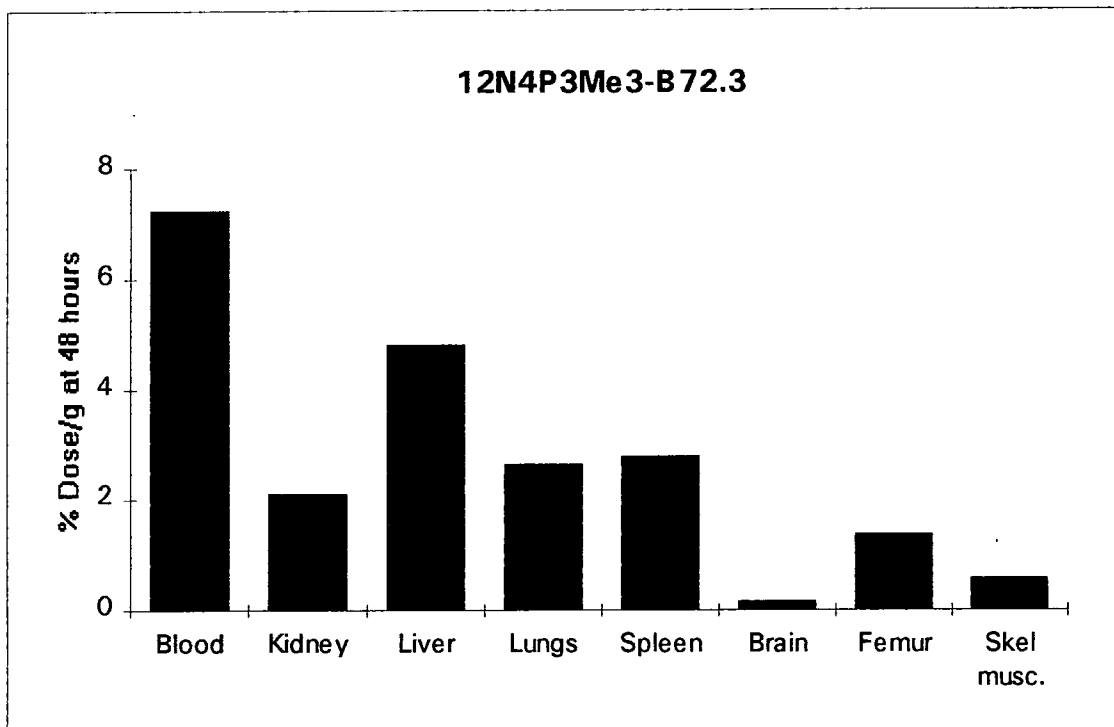
12N4P3Me3-B72.3

Figure 3.13. % *Dose* ^{90}Y-*12N4P3Me3-B72.3 at 48 Hours.*
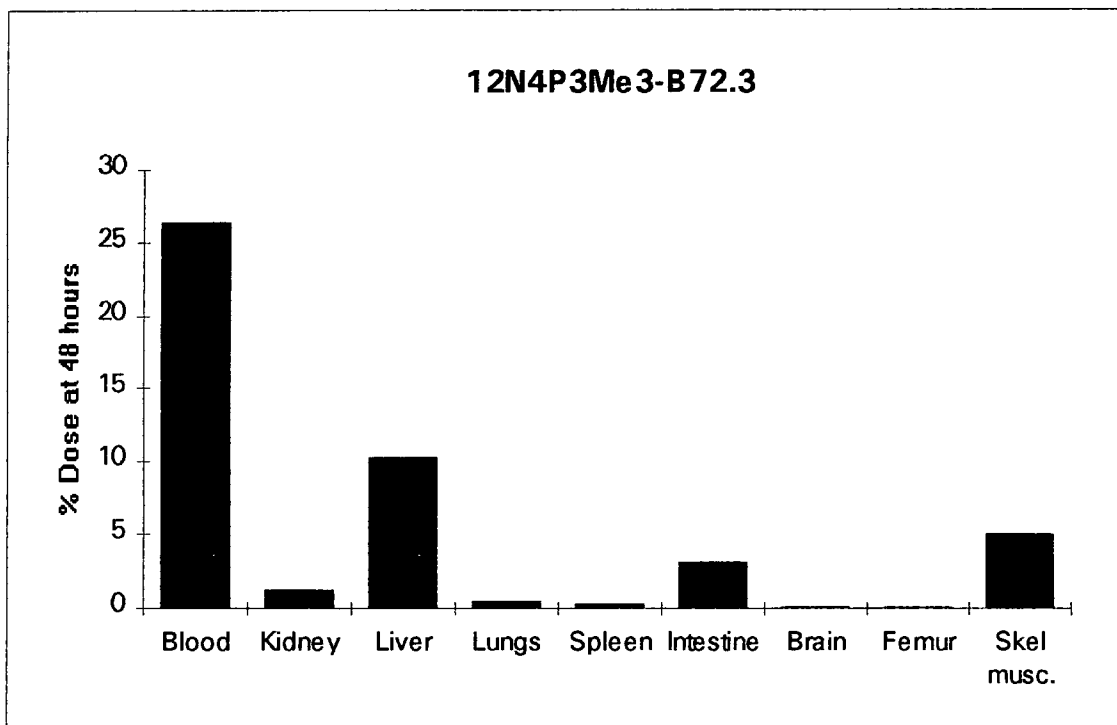
12N4P3Me3-B72.3

Figure 3.14. % Dose/g in Bone Tissues at 48 Hours.
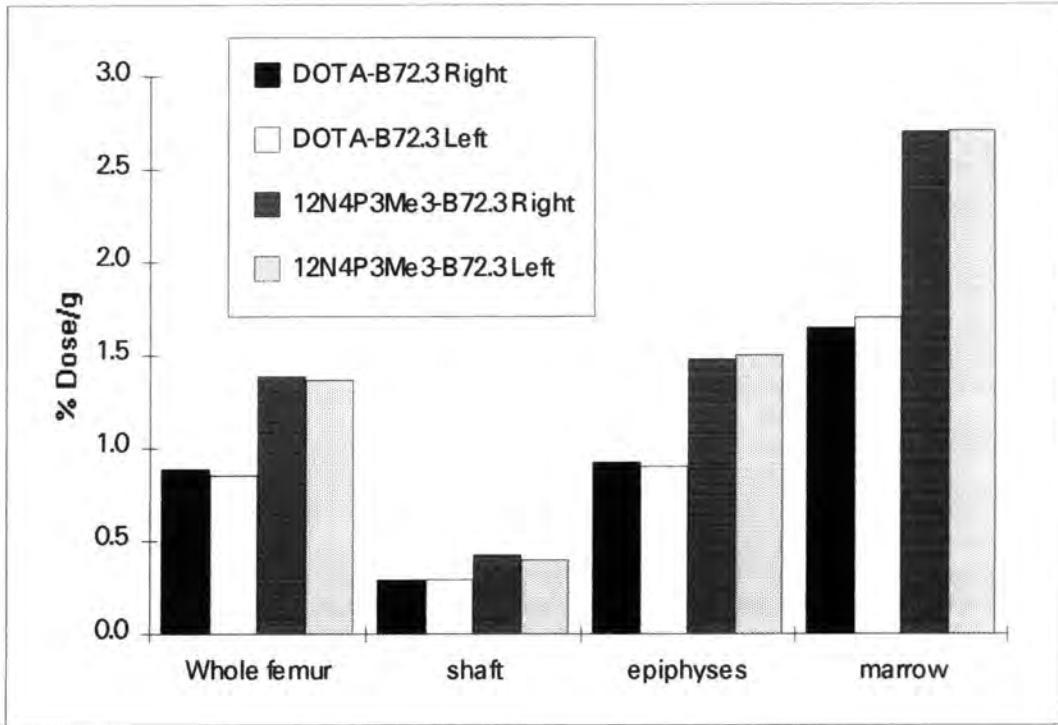
Figure 3.15. % Dose in Bone Tissues at 48 Hours.
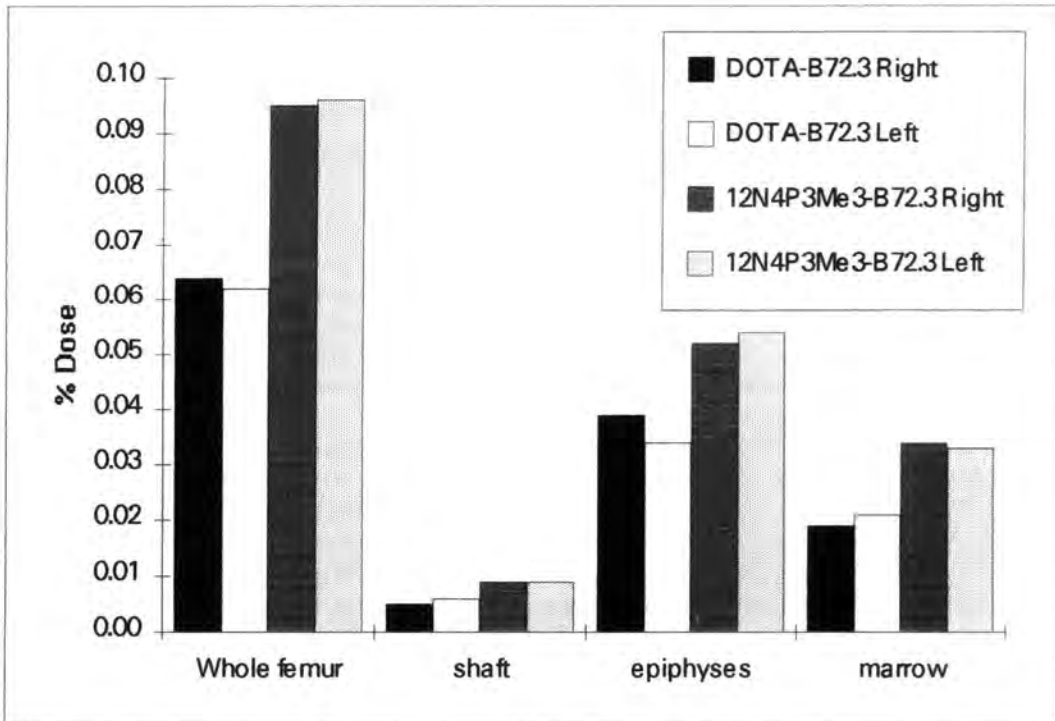
Figure 3.16. *Tissue to blood ratios for bone tissues.*
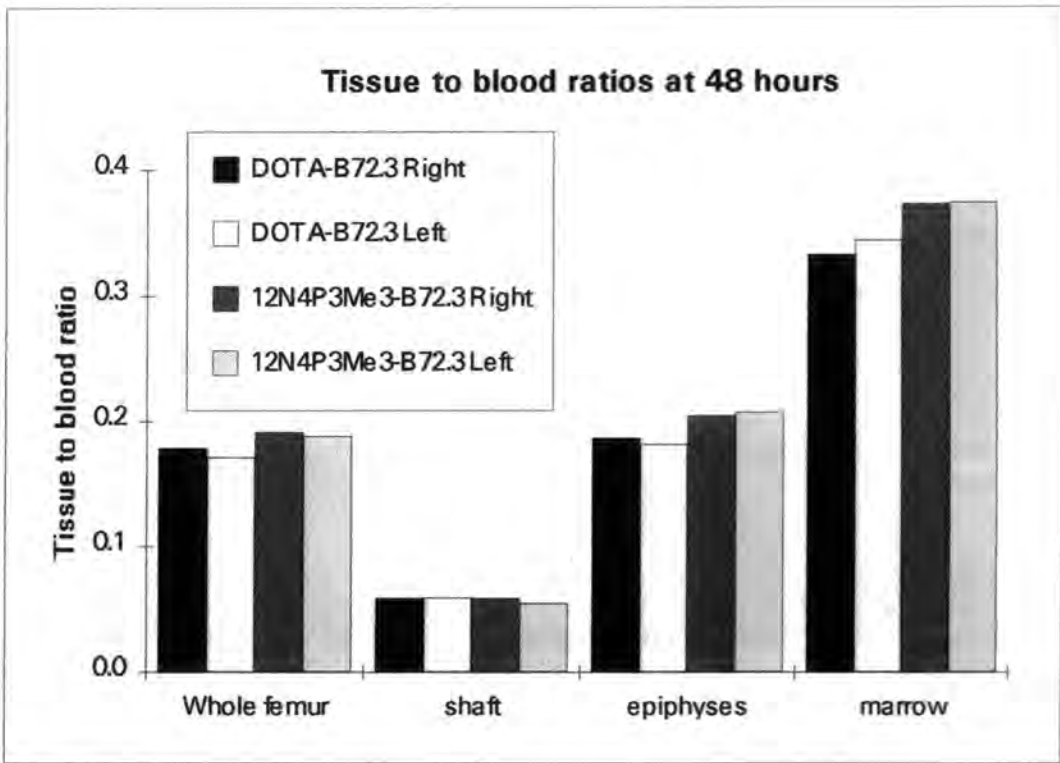
In conclusion, the amounts of circulating antibody are greatest from ^{90}Y-12N4P3Me3-B72.3 with 26.4% dose in the blood at 48 hours compared to 18.7% dose for ^{90}Y-DOTA-B72.3. Both of the labelled antibody preparations, ^{90}Y-DOTA-B72.3 and ^{90}Y-12N4P3Me3-B72.3, are highly stable in vivo as indicated by the very low yttrium doses in bone tissue at 48 hours post injection.

3.5. YTTRIUM EXPERIMENTAL.

Throughout the following experimental procedures, gold label quality chemicals and metal free plastic ware were used to reduce any metal contamination. The suppliers of apparatus and reagents used, together with the purity of reagents are listed in Appendix I. Yttrium-90 was supplied as yttrium-90 chloride in 0.02 M HCl ($t^1/_2$= 64 hours, β^- average energy 0.935 MeV),.and was essentially carrier free. All ^{90}Y-labelled macrocycles or conjugates were purified by HPLC

before use. Prior to purification by HPLC, all mixtures were incubated with DTPA to complex any unreacted ^{90}Y in order to prevent contamination of the HPLC column and also to provide a means by which the percentage labelling could be monitored. It has previously been established that Y-labelled macrocycles are stable with respect to transcomplexation by DTPA in the pH range used[46].

3.5.1. Yttrium Labelled Macrocycles Dissociation Experiments

Preparation of Yttrium Labelled Macrocycles

[Y.12N4P4Me4]⁻

250 μl of a solution containing 200 mM ammonium acetate pH 6.5, 40 mM 12N4P4Me4, 4 mM YCl$_3$ (10% carrier) + 500 μCi ^{90}Y and KOH to adjust to pH 6.5, was incubated at 333K (60°C) for 1 hour.

The formation of [Y.12N4P4Me4]⁻ was measured by removing 2 μl of the above solution and incubating with 50 times molar excess DTPA over macrocycle in HPLC running buffer (0.15 M ammonium acetate pH 6.8) for 5 minutes. This was then analysed by HPLC anion exchange using a Poros Q/M column with 0.15 M ammonium acetate pH 6.8 buffer run at 2 ml/min, to determine the proportion of ^{90}Y in the macrocycle peak by radiometry .

[Y.12N4P3Me3NBu2], [Y.12N4P3Me3NBz2]⁻, [Y.DOTA-Mal] and [Y.12N4P3Me3-Mal]

The method of preparation of these complexes was the same as for [Y.12N4P4Me4]⁻ except that no KOH was added.

Buffers for Dissociation Measurements

A solution of glycine (0.1 mM) was adjusted to pH 1.0, 1.5 and 2.0 with HCl. The pH (+/- 0.1 units) as measured by

Horiba pH meter on each dissociation. The same buffers were used throughout.

Dissociation Measurements

A 75 μl aliquot of the 40 mM stock solution of [Y.macrocycle] was added to 1.5 mls of each buffer to give a final concentration of 2 mM [Y.macrocycle]. These were incubated at 310K (37°C).

Three samples (20 or 35 μl) were removed at each time point and added to a mixture of 50 times molar excess DTPA over macrocycle (4 or 7 μl of 500 mM) and HPLC running buffer (0.15 M ammonium acetate pH 6.8) to make up to 100 μl total volume. The mixtures were vortexed, centrifuged and then frozen at 253K (-20°C) immediately, or run on the HPLC within 5-20 minutes. Similarly, defrosted samples were run on the HPLC within 5-20 minutes.

Radiometric HPLC analysis was performed with a Poros Q/M anion exchange column run at a speed of 2 ml/min with 0.15 M ammonium acetate pH 6.8 buffer. Figures 3.17 and 3.18 show typical HPLC radiometric analysis traces from ^{90}Y-macrocycles. Figure 3.17 is a HPLC trace of ^{90}Y.12N4P3Me3NBz2 showing 14% dissociation after 212 hours incubation at pH 2.0, 310K (37°C). Figure 3.18 is a HPLC trace of ^{90}Y-12N4P3Me3-Mal showing 30% dissociation after 18 hours at pH 1.0.
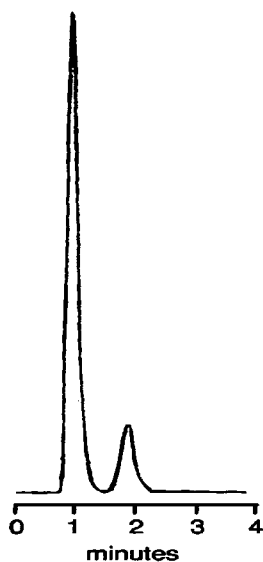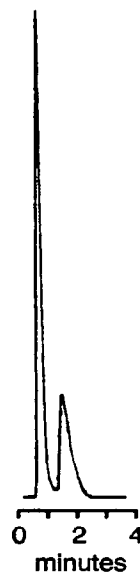
Figure 3.17.   **Figure 3.18.**

Calculation of k_{obs}

The rate of dissociation was calculated by measuring the relative amounts of complexed [Y.macrocycle] and unbound Y^{3+}. Each sample taken had a 50 times molar excess of DTPA added to scavenge any unbound Y^{3+}. The [Y.macrocycle] and $[Y.DTPA]^{2-}$ were then separated by HPLC anion exchange using a Poros Q/M column with 0.15 M ammonium acetate pH 6.8 buffer run at 2 ml/min, the relative amounts of each species being given by the areas of the corresponding peaks.

The observed rate of dissociation (k_{obs}) was calculated from the slope of a plot of Log Ct/Co vs. time (seconds), where Co is the concentration of [Y.macrocycle] at time zero and Ct is the concentration at a given time point (figures 3.19-3.23).

Ct/Co was calculated from % [Y.macrocycle] at time t divided by % [Y.macrocycle] at t=0.

$$k_{obs} = \text{slope} \times -2.303$$

The dissociation half life of the [Y.macrocycle] is given by:-

$$t^1/_2 = 0.693/k_{obs}$$

A typical data set is given below for $[Y.12N4P4Me4]^-$:-

Time hours	% $[Y.12N4P4Me4]^-$ Run 1	Run 2	Run 3	Average
0	100	100	100	100
1	95.96	96.06	95.94	95.99
3	88.04	87.87	87.96	87.96
20.75	35.02	35.06	35.40	35.16
24	30.03	29.78	29.69	29.83
27.25	25.97	25.70	25.97	25.88
46.08	9.89	10.05	9.83	9.92
116.5	0.32	0.31	0.25	0.29

A summary of all the yttrium macrocycle dissociation data is given in table 3.5. Figures 3.19 to 3.23 are the plots for

each macrocycle. The slopes were determined by linear regression analysis.

Figure 3.19.

Dissociation of [Y.12N4P4Me4]⁻ at 310K
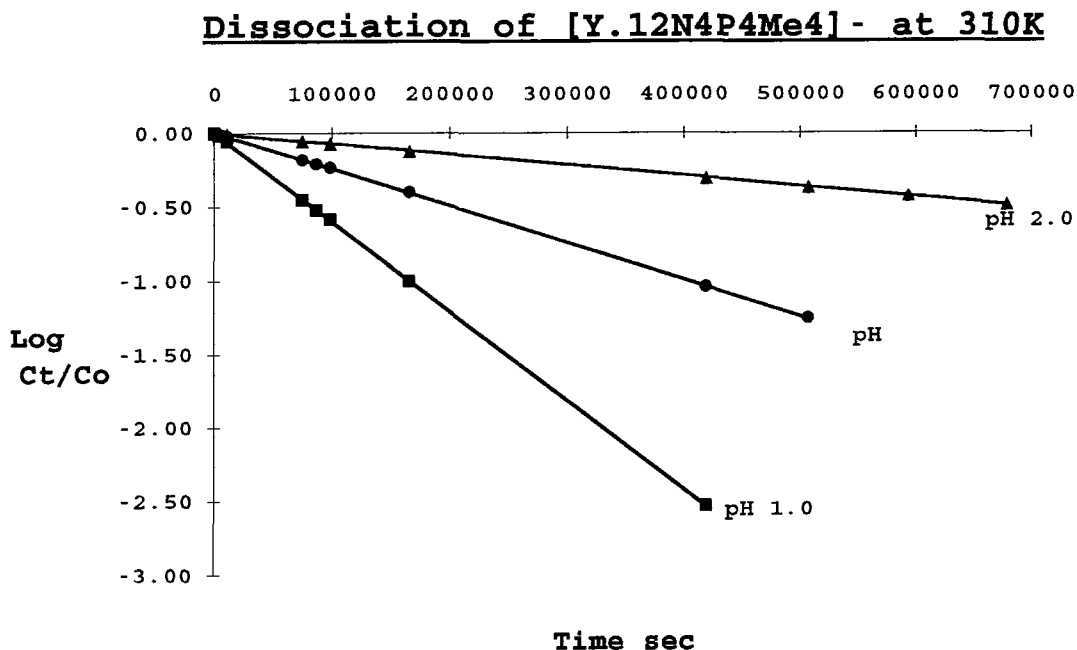
Time sec

Table 3.5. *Summary of Yttrium Dissociation Data.*

Yttrium Complex	pH	Slope of -Log Ct/Co vs. time (sec)	SE on Slope	R^2	k_{obs} 10^{-6} s^{-1}	% SE	Half life hours
12N4P4Me4	1.0	6.05E-06	1.27E-08	1.000	13.9	0.21	13.8
	1.5	2.49E-06	8.67E-08	1.000	5.74	0.35	33.6
	2.0	7.24E-07	4.37E-08	1.000	1.67	0.60	116
12N4P3Me3NBu2	1.0	8.21E-07	1.11E-08	0.998	1.89	1.35	102
	1.5	3.03E-07	8.77E-09	0.993	0.699	2.89	276
	2.0	1.16E-07	3.99E-09	0.989	0.267	3.44	721
12N4P3Me3NBz2	1.0	5.76E-07	1.14E-08	0.996	1.33	1.98	145
	1.5	2.20E-07	7.74E-09	0.989	0.507	3.51	379
	2.0	8.45E-08	3.08E-09	0.988	0.195	3.65	989
DOTA-Mal	1.0	1.18E-06	2.83E-08	0.997	2.72	2.40	70.8
	1.5	3.29E-07	9.69E-09	0.995	0.758	2.95	254
	2.0	6.11E-08	2.89E-09	0.987	0.141	4.73	1370
12N4P3Me3-Mal	1.0	2.85E-06	6.24E-08	0.997	6.56	2.19	29.3
	1.5	9.17E-07	1.96E-08	0.997	2.11	2.14	91.2
	2.0	2.26E-07	9.27E-09	0.990	0.520	4.10	370

Figure 3.20.

Dissociation of [Y.12N4P3Me3NBu2] at 310K

Figure 3.21.

Dissociation of [Y.12N4P3Me3NBz2] at 310K

Figure 3.22.

Dissociation of [Y.DOTA-Mal]- at 310K

Figure 3.23.

Dissociation of [Y.12N4P3Me3-Mal] at 310K
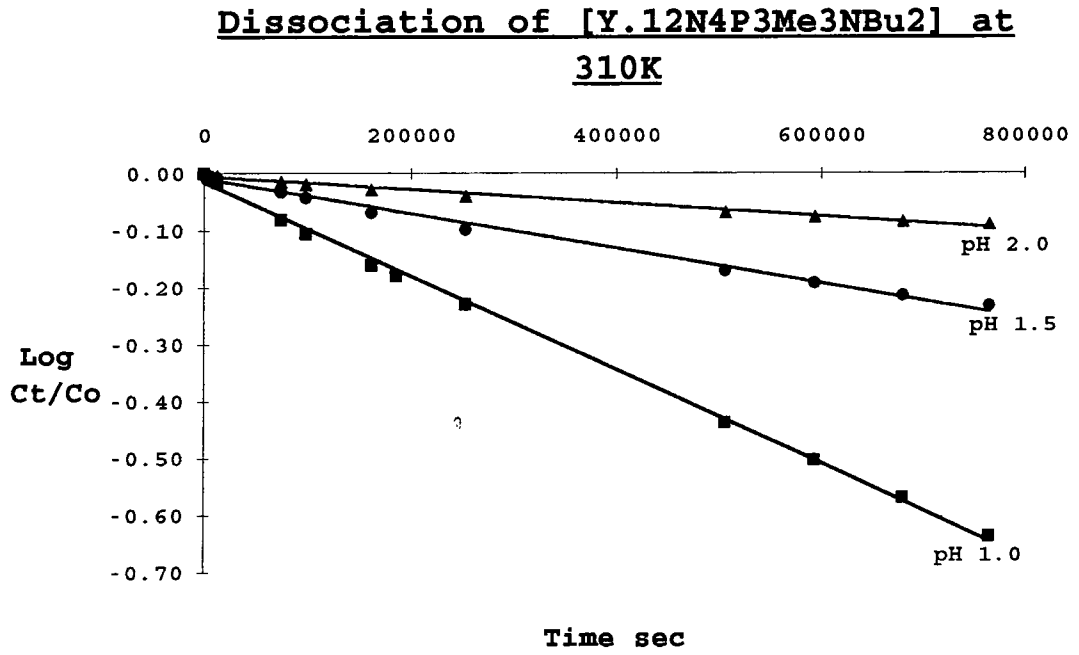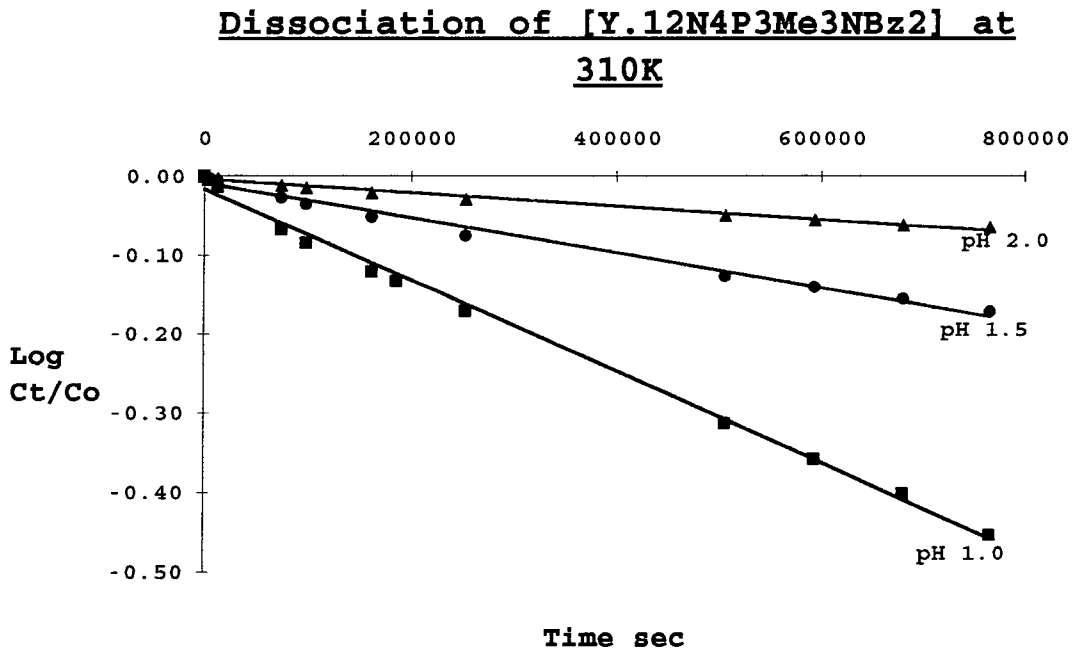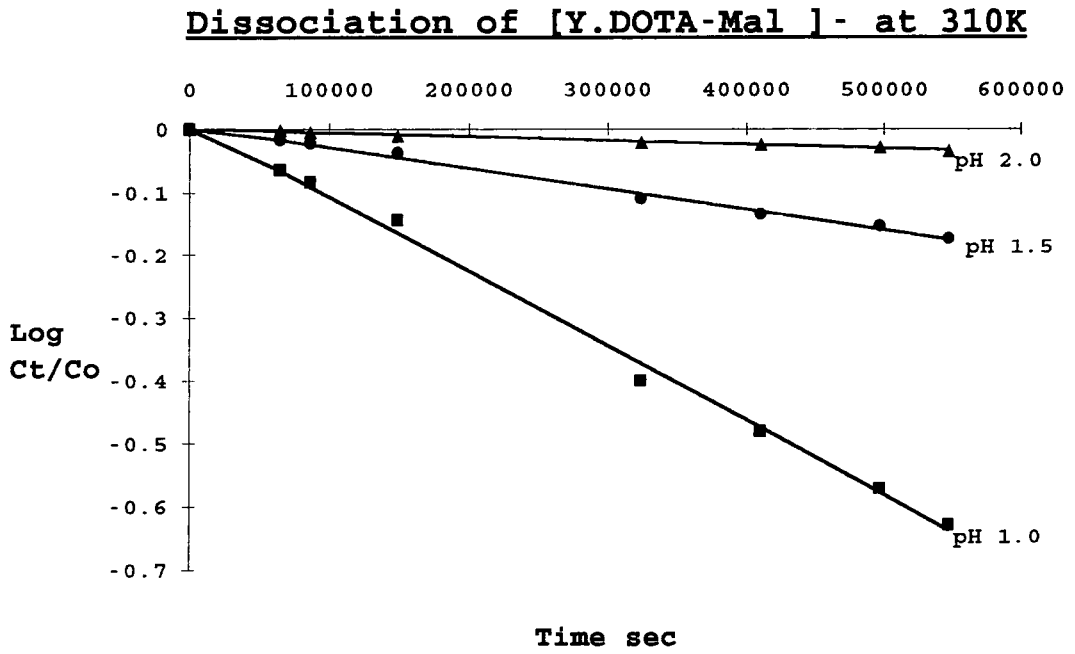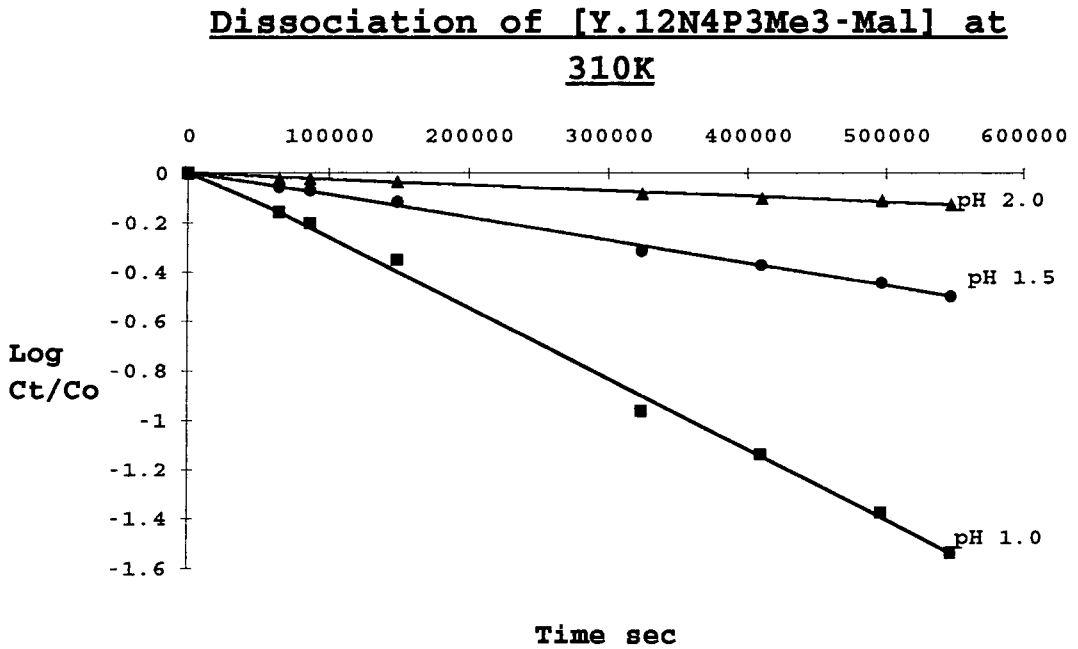
3.5.2. Yttrium Uptake Experiments.

A 1 μl aliquot of ^{90}Y (70 μCi) was added to a solution containing 25 μl of a 50 μM solution of macrocycle; 125 μl of 400 mM NH$_4$OAc pH 6.5; and 99 μl H$_2$O, which had been warmed to 37$^{\mathrm{O}}$C (310K). This 5 μM solution of macrocycle in 200 mM NH$_4$OAc pH 6.5 was incubated at 37$^{\mathrm{O}}$C (310K). Duplicate 10 μl samples were removed at time intervals of up to 1 hour and added to a solution of 5 μl 500 μM DTPA with 85 μL 0.15 M NH$_4$OAc pH 6.8, vortexed and spun down. The 50 fold excess of DTPA bound any uncomplexed yttrium whilst leaving any yttrium-macrocycle complex intact[46]. These samples were analysed by anion exchange HPLC using a Poros Q/M column with 0.15 M NH$_4$OAc pH 6.8 running buffer at 2 ml/min.

All samples were run within 5 to 40 minutes of sampling. The proportion of ^{90}Y in the macrocycle peak was determined by radiometry. The yttrium-macrocycle complex eluted at about 1 min with [Y.DTPA]$^-$ eluting at about 3 min.

3.5.3. Biodistribution Studies

Biodistribution studies were carried out on ^{90}Y-DOTA-B72.3 and ^{90}Y-12N4P3Me3-B72.3 as described in section 3.4.2. The biodistributions were conducted on congenitally athymic nude male mice (MFI-nu/nu/Ola/Hsd) aged 13 to 16 weeks with an average weight of 37.6 g.

Yttrium complexes were administered intra venously via the tail vein at a dose of 10 to 15 μCi and 10 to 15 μg antibody per mouse. Five mice were used per complex and were killed at 48 hours by an intra-peritoneal injection of pentobarbitone. A sample of cardiac blood was taken and the following tissues dissected:- brain, both femurs, both kidneys, liver, lungs, spleen, stomach, small intestine (from the pyloric sphincter to the start of the caecum), caecum, large intestine, and a sample of skeletal muscle. For all animals the right and left femurs were analysed separately. The femurs each had their ends (epiphyses) cut off and the bone marrow washed from the shaft to give three separate

samples (i) the shaft - bone only, (ii) the marrow - no bone, and (iii) the epiphyses - both bone and marrow.

All samples were weighed with the exception of the gut. For calculations of total tissue dose, the mass of both the blood and the skeleton were taken as 10% of the body weight. Large tissues were divided into 0.5g or less fractions. Tissues were minced in the vial in which they were weighed and had their volume made up to 1 ml with formol saline. The weighed epiphyses and femur shafts were placed in individual 2 ml quartz thimbles and ashed in a muffle furnace at 600°C for three hours. This ashed bone was then dissolved in 100 μl 1M HCl and transferred to a counting vial, then made up to 1 ml. Attention was paid to the even distribution of tissue in 1 ml of liquid for consistent counting of the Bremsstrahlung radiation from ^{90}Y. An LKB Compugamma with a 3'' well type NaITl crystal was used to assay the tissue samples for ^{90}Y.

Summary tables are presented in section 3.4.2.

3.6. REFERENCES

1.   D. Pressman, *Ann. N. Y. Acad. Sci.*, 1957, <u>69</u>, 644.

2.   G. Köhler and C. Milstein, *Nature*, 1975, <u>256</u>, 495.

3.   S.E. Order, *Int. J. Radiat. Oncol. Biol. Phys.*, 1990, <u>18</u>, 981-992.

4.   D. Colcher, D.E. Milenic, P. Ferroni, J.A. Carrasquillo, J.C. Reynolds, M. Roselli, S.M. Larson and J. Schlom, *J. Nucl. Med.*, 1990, <u>31</u>, 1133-1142.

5.   D. Colcher, P. Horand Hand, M. Nuti and J.A. Schlom, *Proc. Nat. Acad. Sci. USA.*, 1981, <u>78</u>, 3199-3203.

6.   A. Maraveyas, D. Snook, V. Hird, C. Kosmas, C.F. Meares, H.E. Lambert and A.A. Epenetos, *Cancer*, 1994, <u>73</u>, 1067-1075.

7.   J.S.W. Stewart, V. Hird, D. Snook, B. Dhokia, G. Sivolapenko, G. Hooker, J.Taylor Papadimitriou, G. Rowlinson, M. Sullivan, H.E. Lambert, C. Coulter, W.P.

Mason, W.P. Soutter and A.A. Epenetos, *J. Clin. Oncol.*, 1990, <u>8</u>, 1941-1950.

8.   J.S.W. Stewart, V. Hird, D.Snook, M. Sullivan, M.J. Myers and A.A. Epenatos, *Int. J. Cancer*, 1988, <u>suppl.3</u>, 71-76.

9.   A.N. Serafini, *J. Nucl. Med.*, 1993, <u>34</u>, 533-536.

10.   R.K. Jain, *Cancer Res. (suppl.)*, 1990, <u>50</u>, 814s-819s.

11.   R.M. Sharkey, C. Motta-Hennessy, D. Pawlyk, J.A. Siegel and D.M. Goldenberg, *Cancer Res.*, 1990, <u>54</u>, 2330-2336.

12.   W.A Volkert, W.F. Goeckeler, G.J. Ehrhardt and A.R. Ketring, *J. Nucl. Med.*, 1991, <u>32</u>, 174-185.

13.   S.T. Rosen, A.M. Zimmer, R. Goldman-Leiken *et. al.*, *J. Clin. Oncol.*, 1987, <u>5</u>, 562.

14.   O.W. Press, J.F. Eary and C.C. Badger, *J. Clin. Oncol.*, 1989, <u>7</u>, 1027-1038.

15.   S.J. DeNardo, S.V. Deshpande, M.K. Moi, G.P. Adams, M.K. McCall, G.L. DeNardo and C.F. Meares, *Front. Radiat. Ther. Oncol., Basel, Karger*, 1990, <u>24</u>, 142-150.

16.   S.M. Larson, *Cancer*, 1991, <u>67</u>, 1253-1260.

17.   S.M. Larson, *J. Nucl. Med.*, 1985, <u>26</u>, 538-545.

18.   R.M. Sharkey, F.A. Kaltovich, L.B. Shih, I. Fand, G. Govelitz and D.M. Goldenberg, *Cancer Res.*, 1988, <u>48</u>, 3270-3275.

19.   Y-C.C. Lee, L.C. Washburn, T.T.H. Sun, B.L. Bird, J.E. Crook, E.C. Holloway and Z. Steplewski, *Cancer Res.*, 1990, <u>50</u>, 4546-4551.

20.   L.C. Washburn, Y.C.C. Lee, T.T.H. Sun, B.L. Bird, E.C. Holloway, J.E. Cook and Z. Steplewski, *Antibod. Immunoconj. Radiopharm.*,1991, <u>4</u>, 729-728.

21.   D.J. Buchsbaum, T.S. Lawrence, P.L. Roberson, D.B. Heidorn, R.K. TenHaken and Z. Staplewski, *Int. J. Radiation Oncology Biol. Phys.*, 1993, <u>25</u>, 629-638.

22. H. Schmidberger, D.J. Buchsbaum, B.R. Blazer, P. Everson and D.A. Vallera, *Cancer Res.*, 1991, <u>51</u>, 1883-1890.

23. J.L. Klein, T.H. Nguyen, P. Laroque, K.A. Kopher, J.R. Williams, B.W. Wessels, L.E. Dillehay, J. Frincke, S.E. Order and P.K. Leichner, *Cancer Res.*, 1989, <u>49</u>, 6383-6389.

24. J.A. Williams, J.L. Klein, M.D. Wharam, B.W. Wessels and S.E. Order, *J. Neurosurg.*, 1989, <u>70</u>, 312A.

25. B.A. Parker, A.A. Vassos, S.E. Halpern, R.A. Miller, H. Humpf, D.G. Amox, J.L. Simoni, R.J. Starr, M.R. Green and I. Royson, *Cancer Res. (suppl.)*, 1990, <u>50</u>, 1022s-1028s.

26. S.J. DeNardo, E.L. Kramer, C.M. Richman, Q.A. Salako, E.A. Perez, L.F. O'Grady, M.B. Rippon, S.D. Glenn, G.M. Butchko, J.C. Couto, R.L. Ceriani and G.L. DeNardo, *J. Nucl. Med.*, 1993, <u>34</u>, 53P.

27. D.J. Hnatowich, M. Chinol, D.A. Siebecker, M. Gionet, T. Griffin, P.W. Doherty, R. Hunter and K.R. Base, *J. Nucl. Med.*, 1988, <u>29</u>, 1428-1434.

28. D.J. Hnatowich, G. Mardirossian, P.G. Rose et. al., *Antibod. Immunoconj. Radiopharm.*, 1991, <u>4</u>, 359-371.

39. R.E. O'Mara, J.G. McAfee and G. Subramanian, *J. Nucl. Med.*, 1968, <u>10</u>, 49-51.

30. J. Jowsey, R.E. Rowland and J.H. Marshall, *Rad. Res.*, 1958, <u>8</u>, 490-501.

31. J.R. Morphy, D. Parker, R. Alexander, A. Bains, A.F. Carne, M.A.W. Eaton, A. Harrison, A. Millican, A. Phipps, S.K. Rhind, R. Titmas and D. Weatherby, *J. Chem. Soc., Chem. Commun.*, 1988, 156-158.

32. A. Harrison, C.A. Walker, D. Parker, K.J. Jankowski, J.P.L. Cox, A.S. Craig, J.M. Sansom, N.R.A. Beeley, R.A. Boyce, L. Chaplin, M.A.W. Eaton, A.P.H. Farnsworth, K. Millar, A.T. Millican, A.M. Randall, S.K. Rhind, D.S. Secher and A. Turner, *Nucl. Med. Biol.*, 1991, <u>**18**</u>, 469-476.

33. D.J. Hnatowich, W.W. Layne, R.L. Childs, D. Lanteigne, M.A. Davis, T.W. Griffin and P.W. Doherty, *Science* 1983, <u>220</u>, 613.

34. S.J. Mather, D.M. Tolley and G.W. White, *Eur. J. Nucl. Med.*, 1989, <u>15</u>, 307-312.

35. D. Parker, *Chemistry in Britain*. October 1990, 942-945.

36. D.J. Hnatowich, F. Virzi and P.W. Doherty, *J. Nucl. Med.*, 1985, <u>26</u>, 503-509.

37. L.C. Washburn, T.T.H. Sun, Y-C.C. Lee, B.L. Byrd, E.C. Holloway, J.E. Crook, J.B. Stubbs, M.G. Stabin, M.W. Brechbiel, O.A. Gansow and Z. Steplewski, *Nucl. Med. Biol.*, 1991, <u>18</u>, 313-321.

38. M. Roselli, J. Schlom, O.A. Gansow, A. Raubitschek, S. Mirzadeh, M.W. Brechbiel and D. Colcher, *J. Nucl. Med.*, 1989, <u>30</u>, 672-682.

39. R.W. Kozak, A. Raubitschek, S. Mirzadeh, M.W. Brechbiel, R. Junghaus, O.A. Gansow and T.A. Waldmann, *Cancer Res.*, 1989, <u>49</u>, 2639-2644.

40. W.T. Anderson-Berg, R.A. Squire and M. Strand, *Cancer Res.*, 1987, <u>47</u>, 1905-1912.

41. L. Camera, S. Kinuya, K. Garmestani, C. Wu, H.W. Brechbiel, L.H. Pai, T.J. McMurry, O.A. Gansow, I. Pastan, C.H. Paik and J.A. Carrasquillo, *J. Nucl. Med.*, 1994, <u>35</u>, 882-889.

42. M.F. Loncin, J.F. Desreux and E. Merciny, *Inorg. Chem.*, 1986, <u>25</u>, 2646-2648.

43. W.P. Cacheris, S.C. Quay, and S.M. Rocklage, *Magn. Reson. Imaging*, 1990, <u>8</u>, 467-481.

44. M.K. Moi, S.J. DeNardo and C.F. Meares, *Cancer Res.*, 1990, <u>suppl. 50</u>, 789s-793s.

45. J.P.L. Cox, K.J.Jankowski, R. Kataky, D. Parker, N.R.A. Beely, B.A.Boyce, M.A.W. Eaton, K. Miller, A.T. Millican, A. Harrison and C.A. Walker, *J. Chem. Soc. Chem. Commun.*, 1989, 797-789.

46. C.J. Broan, J.P.L. Cox, A.S. Craig, R. Kataky, D. Parker, A.Harrison, A. Randall, and G. Ferguson, *J. Chem. Soc. Perkin Trans. 2*, 1991, 87-99.

47. K.P. Pulukkody, T.J. Norman, D. Parker, L. Royle, and C.J. Broan, *J. Chem. Soc. Perkins Trans. 2*, 1993, 605-620.

48. M. Kodama, T. Koite, A.B. Mahatma and E. Kimura, *Inorg. Chem.*, 1991, <u>30</u>, 1270-1273.

49. S.V. Deshpande, S.J. DeNardo, D.L. Kukis, M.K. Moi, M.J. McCall, G.L. DeNardo and C.F. Meares, *J. Nucl. Med.*, 1990, <u>31</u>, 473-479.

50. G.L. DeNardo, L.A. Kroger, S.J. DeNardo, L.A. Miers, Q. Salako, D.L. Kukis, I. Fand, S. Shen, O. Renn and C.F. Meares, *Cancer*, 1994, <u>73</u>, 1012-1022.

51. *'CRC Handbook of Chemistry and Physics'*, 74th edition, 1993-94, Ed. D.R. Lide.

52. C.A. Chang, K. Kumar, J.M. Garrison, H.G. Brittain, M.F. Tweedle, *Soc. Mag. Res. in Medicine, 9th Annual Conference*. 1990, 729.

53. D. Parker, *Chem. Soc. Rev.*, 1990, <u>**19**</u>, 271-291.

CHAPTER FOUR

GALLIUM AND INDIUM MACROCYCLE COMPLEXES.

4.1. INTRODUCTION

4.1.1. Radioisotopes of Gallium and Indium.

There has been considerable interest in the application of several gallium and indium isotopes in nuclear medicine . The different physical characteristics of each radioisotope determine its usefulness in different nuclear medicine applications (table 4.1). Gallium-67 has a half life of 78 hours which is convenient for multi-step preparations. This half life also allows in vivo studies to be carried out over several days. Indium-111 has a similar half life of 67 hours, imparting it with the same advantages as gallium-67. Both of these isotopes are cyclotron-produced enabling them to be obtained essentially carrier-free. The favourable energies of their γ photons make them ideal isotopes for detection by single photon emission tomography (SPECT). The absence of any particle emissions from these isotopes keeps the radiation dose to the patient to a minimum.

Two shorter lived, carrier free, generator produced isotopes are ^{113m}In and ^{68}Ga with half lives of 100 and 68 minutes respectively. The short half lives makes these isotopes suitable for quick scanning methods, and the generator system has the advantage of producing the isotopes on site. Gallium-68, a positron emitter, is suitable for use with positron emission tomography (PET). Its 511 keV annihilation photons are emitted at 180° to each other enabling a much sharper image to be obtained with PET than with SPECT. However the short half life of gallium-68 limits its use to those radiopharmacuticals which do not require lengthy preparations or in vivo targeting times.

Gallium-72 (half life of 14.1 hours) was the first gallium radioisotope to be investigated in man[1] but is not at all suitable as an imaging agent due to its β^- emission and high energy gamma rays which are too energetic for efficient detection by an Anger camera. Gallium-69 or -71, stable isotopes of gallium, have potential for use in nuclear

magnetic resonance imaging due to their nuclei possessing a
magnetic moment.

Table 4.1. *Isotopes of Gallium and Indium*[2,3].

Isotope	Half life	Method of decay	Maximum particle energy MeV	Principle gamma energies/ intensities MeV (%)	Method of production
^{67}Ga	78 hr	E.C.	none	0.093(38%) 0.185(21%) 0.300(17%)	^{68}Zn(p,2n) cyclotron
^{68}Ga	68 min	β+(90%) E.C.(10%)	1.83	0.511(178%) 1.077(3%)	^{68}Ge generator. Parent half life 272 days
^{72}Ga	14.1 hr	β^-	3.99	0.630(25%) 2.201(26%) 2.508(13%)	^{71}Ga(n,γ) nuclear reactor
^{111}In	67 hr	E.C.	none	0.171(91%) 0.245(94%)	^{111}Cd(p,n) cyclotron
^{113m}In	100 min	I.T.	none	0.392(64%) 0.364(29%)	^{113}Sn generator Parent half life 115 days.

E.C.= Orbital electron capture

I.T.= Isomeric transition from upper to lower isomeric state.

4.1.2. Gallium.

Investigations into the use of radiogallium in medicine
began in 1949 when studies by Dudley and Maddox[1] showed ^{72}Ga
(given as gallium lactate) deposited in bone. Gallium-72 ($t^1/_2$
14 hr, β^- and γ), was produced in a nuclear reactor from
stable ^{71}Ga and consequently contained considerable amounts of
stable carrier. When the cyclotron produced, essentially

carrier-free ^{67}Ga ($t^1/_2$ 78 hr, E.C. γ) was administered[4], a different biodistribution was found. When carrier free [$^{67}Ga.Citrate$] was administered alone, low bone uptake was observed[5] along with higher retention in other tissues such as liver. But, when stable gallium was administered along with the [$^{67}Ga.Citrate$] to increase the total dose of gallium, the radioisotope was taken up by the bone as had been observed with ^{72}Ga. This biodistribution of carrier-free [$^{67}Ga.Citrate$] was found to be due to the binding of ^{67}Ga to blood proteins[6]. The gallium III ion resembles the ferric ion in ionic radius and charge, and binds strongly to iron-binding macromolecules[6]. These include transferrin, lactoferrin[7], ferritin and sideophores[8] (the iron-binding protein of bacteria). At tracer levels in blood, gallium is exclusively bound to and transported by transferrin[9].

It was in 1969 that Edward and Hayes first described the localisation of ^{67}Ga in human tumours[10] after intravenous injection of [$^{67}Ga.Citrate$]. Since then [$^{67}Ga.Citrate$] has been shown to accumulate in a wide variety of tumours as well as in areas of inflammation[11,12]. The mechanism by which this accumulation of gallium takes place is controversial[9]. However, it is clear that transferrin plays an important role in the gallium uptake of tumours, although other mechanisms of uptake could be at work in different tumours. Suggestions such as the gallium being transferred from transferrin in the blood to lactoferrin in the tumour [7] have been made. Also studies on hypotransferrinemic mice[13] suggest that although transferrin may mediate the uptake of gallium by most normal soft tissues, transferrin independent factors can contribute towards the uptake of gallium by bone and some tumours. The most gallium-avid tumours are the lymphomas and these tumours are known to possess high levels of transferrin receptors[13]. The most popular theory at present is that gallium gains access to the tumour via transferrin and transferrin receptors on the tumour[13].

[^{67}Ga-Citrate] is used widely for imaging tumours and abscesses by SPECT. This is of particular use in the management of the treatment of patients with tumours such as

lymphomas. In these cases the [^{67}Ga-Citrate] complex acts as a viability agent for the detection of residual tumour, as fibrotic or necrotic tissues do not accumulate the ^{67}Ga label[14,15]. The action of gallium-citrate as an imaging agent is dependent on the fact that the gallium-citrate complex is unstable and that gallium-transferrin is formed very quickly in vivo. In the development of any further gallium labelled pharmaceuticals for imaging it is of great importance that these gallium complexes are stable if these pharmaceuticals are to direct the pharmacokinetics of the label.

Gallium labelled drugs currently under investigation for clinical use include:- ^{68}Ga-[Desferrioxamine B-Succinyl-(D)Phe^1]-Octroetide, a somatostatin analogue, for the imaging of somatostatin positive tumours[16]; ^{68}Ga labelled Iron hydroxide colloid as a liver imaging agent[17]; ^{68}Ga-oxine labelled red cells and platelets for imaging blood pools and assessing areas of platelet accumulation[18]; several ^{68}Ga labelled myocardial imaging agents[19-22]; and ^{67}Ga labelled antibodies[23]. Other complexes of ^{67}Ga which form highly stable complexes in vivo, such as Ga-HBED, Ga-PLED, Ga-EHPG[24-26] and complexes based on 9N3[27-30] are being investigated as potential imaging agents for renal or hepatic clearance and possibly for brain imaging.

4.1.3. Indium.

Like gallium, indium has two isotopes suitable for use in nuclear medicine. Indium-111 or indium-113^m administered as the chloride or citrate complex is rapidly taken up by transferrin in the blood[31] as with gallium. As such, indium has been used for tumour localisation and bone marrow imaging[32]. Indium labelled colloidal ferric hydroxide has been used for lymph node scanning[33], and larger aggregates used for lung scintigraphy[34]. ^{111}In-DTPA is used for studying cerebral spinal fluid dynamics[35]. The lipid soluble ^{111}In-oxine complex is used to label cellular blood components[32,36] for the detection of a variety of disorders. ^{111}In-leukocytes accumulate in abscesses[37], ^{111}In-platelets in areas of

thrombosis[38], and ^{111}In-red blood cells are used to image the blood pool of the liver and spleen[32].

Certain ligands used to complex gallium are also being used with indium and the stability of these complexes is being evaluated. These include ^{111}In-octreotide[39,40], ^{111}In-HBED, ^{111}In-PLED, ^{111}In-EHPG[24-26] and ^{111}In-macrocycles based on 9N3[27-29]. However, the majority of present interest in ^{111}In in nuclear medicine is centred around the use of ^{111}In labelled antibodies[41]. Monoclonal antibodies which have been labelled with ^{111}In via DTPA have proved successful in imaging patients with metastatic melanoma[42], colorectal cancer[43] and metastatic breast cancer[44]. Bispecific monoclonal antibody mediated targeting of an ^{111}In-DTPA dimer has also been used to image thyroid[45] and colorectal[46] cancers. ^{111}In-DTPA labelled polyclonal human IgG has been successful as an agent for detecting sites of infection and inflammation in patients[47,48]. Because of the importance of the chelate stability of ^{111}In labelled antibodies, new bifunctional chelating agents using macrocycles are being developed[49,50,28] for their labelling.

4.1.4. Comparative Stability of Ga^{3+}, In^{3+} and Fe^{3+} Complexes.

The in vivo stability of any metal-ligand complex is of paramount importance as the loss of metal label can lead to toxic effects. This is of particular importance where radioactive metals are involved, as once the metal has lost the target specificity imparted on it by the ligand, it will go elsewhere in the body. This will result in a radiation dose to normal tissue and also give high background noise in imaging.

As already discussed in section 1.2.6, metal-ligand complexes are subject to attack from H^+, and certain anionic complexes are sensitive to attack from endogenous metal ions such as Zn^{2+}, Ca^{2+}, Mg^{2+} and Cu^{2+}. Some complexes may also be unstable with respect to dissociation following binding to natural ligands such as citrate and transferrin. The metal ions Ga^{3+} and In^{3+} resemble the ferric ion in size, charge and

character. As such they tend to form stable complexes with naturally occurring ligands which are produced to complex Fe^{3+} in the body. By far the most important of these natural ligands is transferrin, which occurs at a concentration of 0.25 mg/100 ml in blood[36]. The stability constants for transferrin with the metal ions Ga^{3+}, In^{3+} and Fe^{3+} are listed in table 4.2 together with the metal ions ionic radii. Indium and iron exhibit high stability constants with transferrin, whereas gallium forms a weaker complex with transferrin. This means that indium is more likely than gallium to undergo transchelation to transferrin from a complex in vivo.

Table 4.2. *Stability Constants (Log K) of Ga^{3+}, In^{3+} and Fe^{3+} Complexes.*

Stability Constant (Log K, 298K, I=0.1)

Complex	Ga^{3+}	In^{3+}	Fe^{3+}
Transferrin[23]	23.7	30.5	30.3
DTPA[23]	25.5	29.0	28.6
EDTA[24]	21.7	24.9	25.0
PLED[25]	36.35	36.89	36.91
HBED[24]	39.57	39.66	39.68
P-HBED[23]	33.6	33.0	33.9
EHPG[24]	33.6	33.0	33.9
9N3[51]	30.98	26.2	28.3
Ionic radius[2]	0.62	0.80	0.65

The stability constants for some other complexes are also listed in table 4.2. The most commonly used chelates, DTPA and EDTA, have lower stability constants with indium than does transferrin. The most common method of attaching ^{111}In to proteins such as antibodies for imaging is via a bifunctional DTPA complexing agent[43,44,47,48,52,53]. Gallium-DTPA has a similar stability constant to gallium-transferrin. However,

studies on the in vitro and in vivo stability of both gallium and indium labelled DTPA-albumin (involving an amide-linkage to the protein) have shown losses of 9% per day of radiometal to transferrin in vitro, and 6% loss to transferrin in vivo within $3^1/_2$ hours[54].

It is clear that more stable complexes for both gallium and indium need to be developed. Current approaches being investigated are with ligands based on two different chemical backbones. (1), the acyclic ligand N,N'-bis[2-hydroxybenzyl]ethyienediamine-N,N'-diacetic acid (HBED), and (2), the macrocyclic ligand 1,4,7-triazacyclononanetriacetate (9N3).

4.1.5. HBED and Related Ligands.

Mathias, Welch et al are developing ligands based on the HBED backbone as chelating agents for gallium and indium[24-26,55,56]. Figure 4.1 lists the structures of HBED, P-HBED (propionic acid-HBED), t-butyl HBED, PLED EHPG and TMPHPG. These ligands form complexes with Ga^{3+}, In^{3+} and Fe^{3+} which have higher stability constants than the metal-transferrin complexes (table 4.2). However, the in vivo stability of a complex is not simply a reflection of the thermodynamic stability constant, but relies much more on the kinetic properties of the complex. This is demonstrated by the in vitro and in vivo stability of these acyclic complexes. [In.P-HBED] loses all of its indium within 2 hours[94] when incubated in human serum with equimolar Fe^{3+}. Under similar conditions [Ga.P-HBED] surrenders 6.6% of its gallium over 48 hours. In vivo this is seen as slower blood clearance of the label[23]. This slower blood clearance is also seen for gallium and indium complexes of EHPG[26] and TMPHPG[55], with the indium complexes losing more metal to transferrin than the gallium complexes. Biodistribution studies on gallium and indium complexes of HBED show more blood retention from the indium complex than the gallium complex at 1 hour[24], although no retention studies were carried out to assess longer term complex stability. Serum stability studies on [Ga.HBED] show a

loss of 2.7% of the gallium in 24 hours[24]. The indium and gallium complexes of PLED show higher blood levels at 1 hour than the HBED complexes indicating that they are less stable in vivo than the HBED complexes[24].

Figure 4.1. *Chemical Structures of HBED Related Ligands.*

HBED

P-HBED

t-butyl HBED

PLED

EHPG

TMPHPG
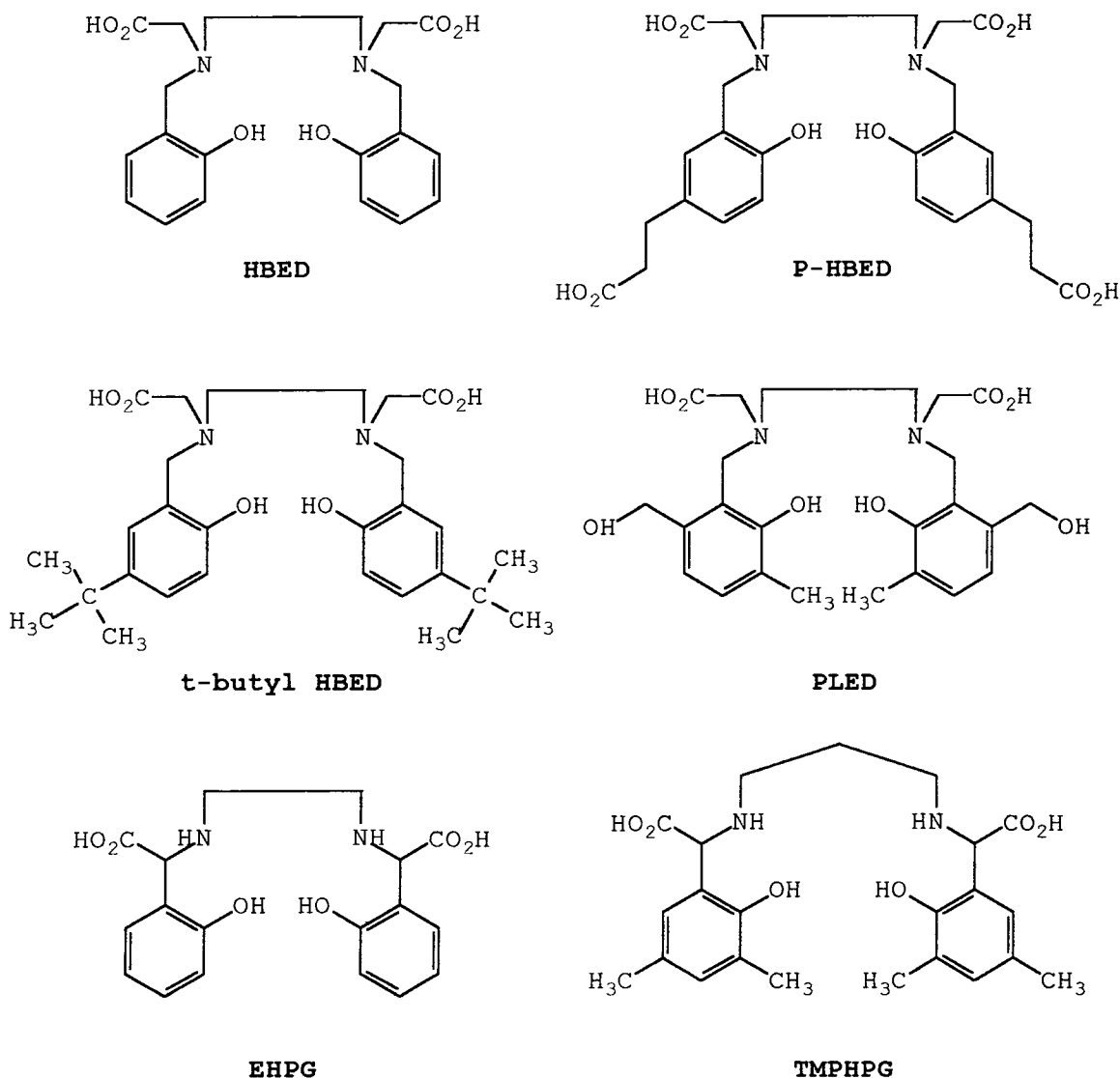
By altering the ring substituents on HBED, structurally related ligands with a range of lipophilicities have been produced. The effect of these changes on the pharmacokinetics of the complexes have been evaluated. For instance, the lipophilic ligand t-butyl-HBED shows hepatobiliary excretion rather then the renal excretion shown by the less lipophilic ligands[24]. It had been hoped that these small (molecular

weights 450-650), neutral, lipophilic complexes would cross
the blood-brain barrier to enable them to be used in SPECT
imaging of the brain. Although the cut off point for crossing
the blood-brain barrier had been estimated to be in the range
of 400 to 600 daltons, none of these HBED analogues crossed
the blood-brain barrier[24].

4.1.6. 9N3 and Related Ligands.

The second approach to developing stable indium and
gallium complexes has been with macrocyclic ligands (figures
4.2 and 4.3). The major advantage of metal complexes with
macrocycles over the ligands discussed previously (pages 155-
6), is their high kinetic stability. As was discussed in
section 1.2.6 for the stability of gadolinium macrocycles,
metal macrocycle complexes are highly inert, kinetically, to
acid or cation promoted attack. These metal-9N3 complexes are
expected to be even more resistant to acid or cation attack
than metal-DOTA(12N4) complexes as they have a neutral charge.
The thermodynamic stability constants listed in table 4.2 show
high values for the 9N3 complexes, but the stability constants
for PLED, HBED and EHPG are higher. However, in vivo, due to
their kinetic inertness, the macrocyclic 9N3 complexes are
more stable than the HBED type acyclic ligands.

When the acid-catalysed dissociation of [Ga.9N3] was
measured in 6M HNO_3 by ^{71}Ga NMR, no dissociation was observed
by 60 days[57]. This high stability is reflected in the in vivo
studies[58]. [In.9N3] is also resistant to acid-catalysed
dissociation, but not as much as [Ga.9N3]. When monitored by
^{13}C NMR in the pH range 0 to -0.7, [In.9N3] dissociated with a
second order rate constant[57] of 1.8×10^{-4} dm^3 mol^{-1} s^{-1}. In
vivo studies have shown that [In.9N3] is entirely cleared from
the body in a few hours[49]. The structurally related gallium
and indium 9N3P3Me3 and 9N3C3Me3 complexes also display high
resistance to in vitro acid-catalysed dissociation[28,58].

This high kinetic stability of the metal macrocycle
complexes is due to the compact arrangement of the donor
oxygen and nitrogen atoms around the centrally located

trivalent ion, and the overall rigidity of the structure. The stability of the complex is dependent on the fit of the metal ion in the macrocycle cavity. Two parameters which play an important role in this are the size-match selectivity and the steric efficiency of the ligand[59]. Size-match depicts the size of metal ion which is best matched to the macrocycles cavity and hence forms the most stable complex[60-62]. Steric efficiency is when the steric strain on the ligand is kept to the minimum whilst conforming to the preferred co-ordination geometry of the metal ion.

The gallium ion has a smaller radius than indium and adopts approximately octahedral co-ordination with the ligands 9N3[56] and 9N3P3Ph3[27]. Indium adopts the geometry of a distorted trigonal prism in the complex with the ligand 9N3Me3C3[58] and a pentagonal bipyramidal geometry in the hepta co-ordinate chloroindium complex of 9N3. Thus the favourable ionic size and co-ordination geometry of gallium with these 9N3 type macrocycles contributes to their higher stability over the indium complexes.

The high in vivo stability of these gallium and indium 9N3 complexes has lead to the development of functionalised ligands for the attachment to monoclonal antibodies for use in tumour detection[28,49-51].

Two further 9N3 analogues being studied are TX-TACN and TS-TACN by Moore, Welch at al[30,63,64] (figure 4.2). The gallium complexes of both these ligands exhibit slightly distorted octagonal geometry similar to that reported by Parker et al for the other 9N3 analogues[56,27]. The lipophilic indium complex of TX-TACN shows high liver and blood retention in vivo[63] indicating possible hepatobiliary clearance and instability of this complex. In vivo studies on the gallium complexes, which are likely to be more stable, have not yet been reported. The ligand TS-TACN has been designed to be smaller than TX-TACN whilst remaining lipophilic in the hope that it can cross the blood-brain barrier[64].

Figure 4.2. *Chemical Structures of TX-TACN and TS-TACN.*

TX-TACN   TS-TACN
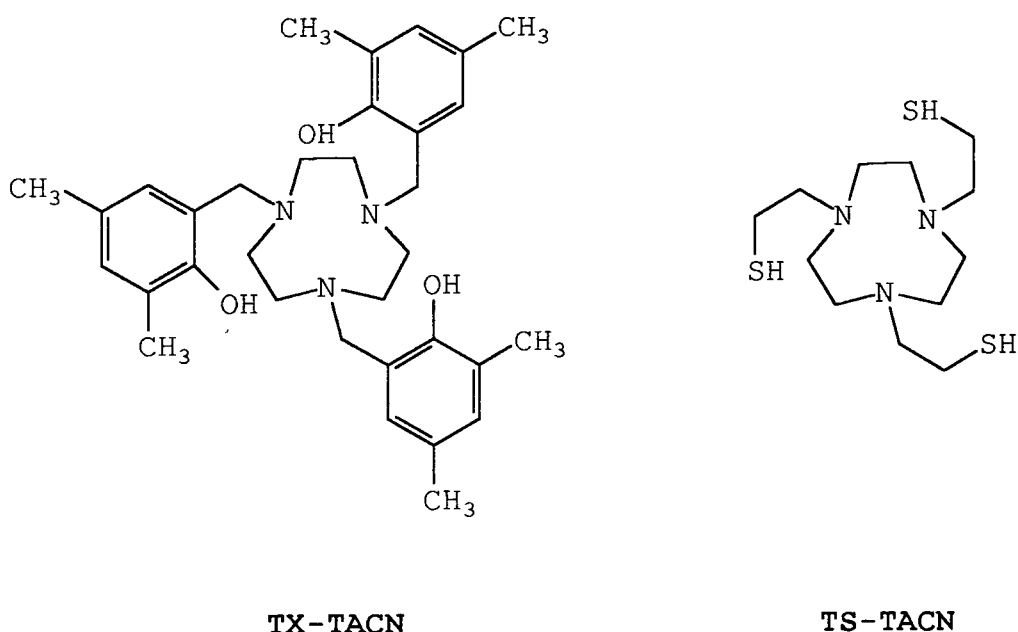
4.1.7. The Scope of the Work in This Chapter.

In this chapter a series of seven structurally related ligands (figure 4.3) are studied as complexes with gallium or indium. The effect of the different substituents added to the 9N3 core is evaluated. The in vivo stability and routes of excretion are examined, as well as the overall biodistributions of the complexes. Partition coefficients are measured for the indium complexes to try and correlate changes in lipophilicity of the complexes to changes in their pharmacokinetics. Gallium and indium 9N3 complexes are further studied as possible tumour localisation agents, as is a gallium-9N3-misonidazole conjugate. The gallium-71 complex of 9N3 is also investigated for its suitability in NMR imaging.

Figure 4.3. *Chemical Structures of the Ligands Used to Complex Gallium and Indium*

9N3
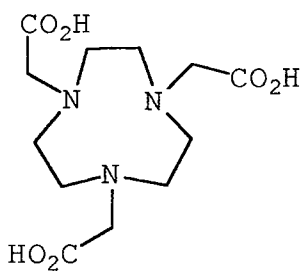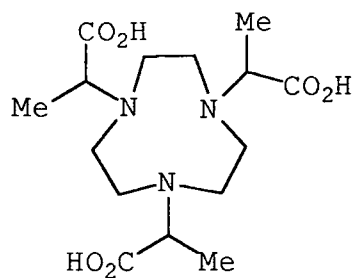
9N3C3Ph3

9N3Me3C3

9N3P3Me3

9N3P3iPr3

9N3P3Ph3
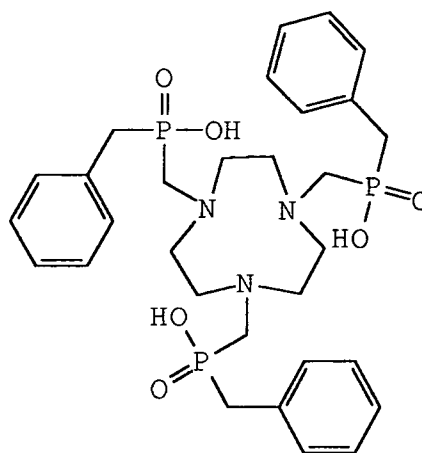
9N3P3Bz3

4.2. BIODISTRIBUTION OF GALLIUM COMPLEXES.

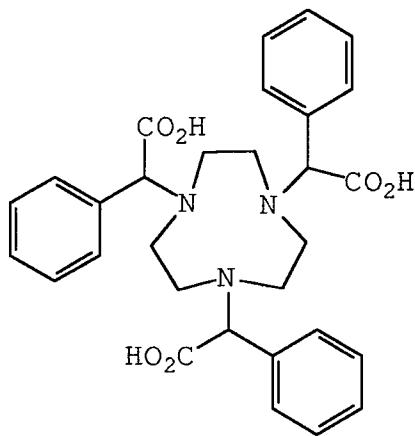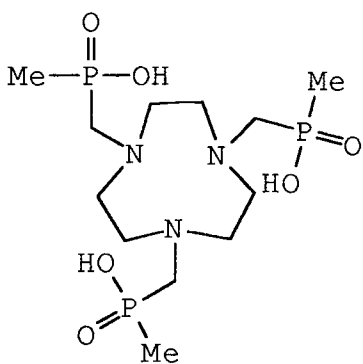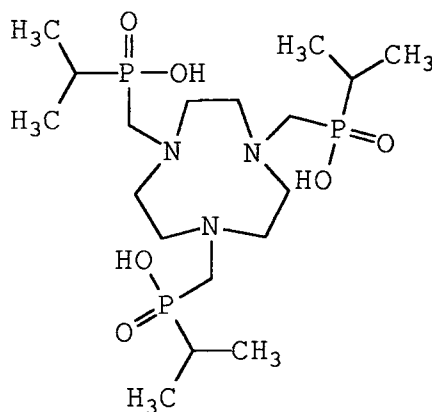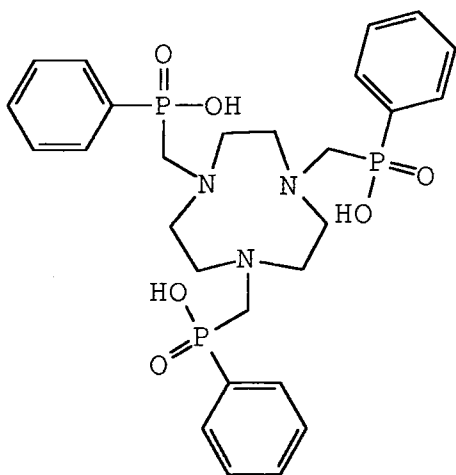The aims of this study were to determine the principle route of excretion (hepatobiliary or renal) of the 7 gallium complexes and to assess their in vivo stability.

Presentation of Results

The gallium complexes have been divided into two groups for the biodistribution studies. Group I are aza-carboxylic acids, and group II are aza-phosphinic acids.

Figures 4.4 and 4.5 show the % dose in 5 tissues at 1 hour post injection for the groups I and II. These 5 tissues are blood, kidneys, liver, gall bladder and gut, where the gut represents the intestinal tract (with contents) from the stomach to the large intestine inclusive. Figures 4.6 and 4.7 show the % dose in the tissue at 24 hours post injection for these groups. However at this time the % dose in the gall bladder was too low to be detected, but the % Dose in the skeleton is shown. More precise data for individual tissues are given in figures 4.8 to 4.17, these figures each show the % dose for each of the 7 complexes in a single tissue.

Key to Figures in this Section.

Number in Figures	Group	Complex
1.	I	[Ga.9N3]
2.	I	[Ga.9N3Me3C3]
3.	I	[Ga.9N3C3Ph3]
4.	II	[Ga.9N3P3Me3]
5.	II	[Ga.9N3P3iPr3]
6.	II	[Ga.9N3P3Ph3]
7.	II	[Ga.9N3P3Bz3]

4.2.1. Biodistribution Data for the Two Groups of Gallium Complexes.

Figure 4.4. *Biodistribution of Group I Aza-carboxylic Acids at 1 Hour.*
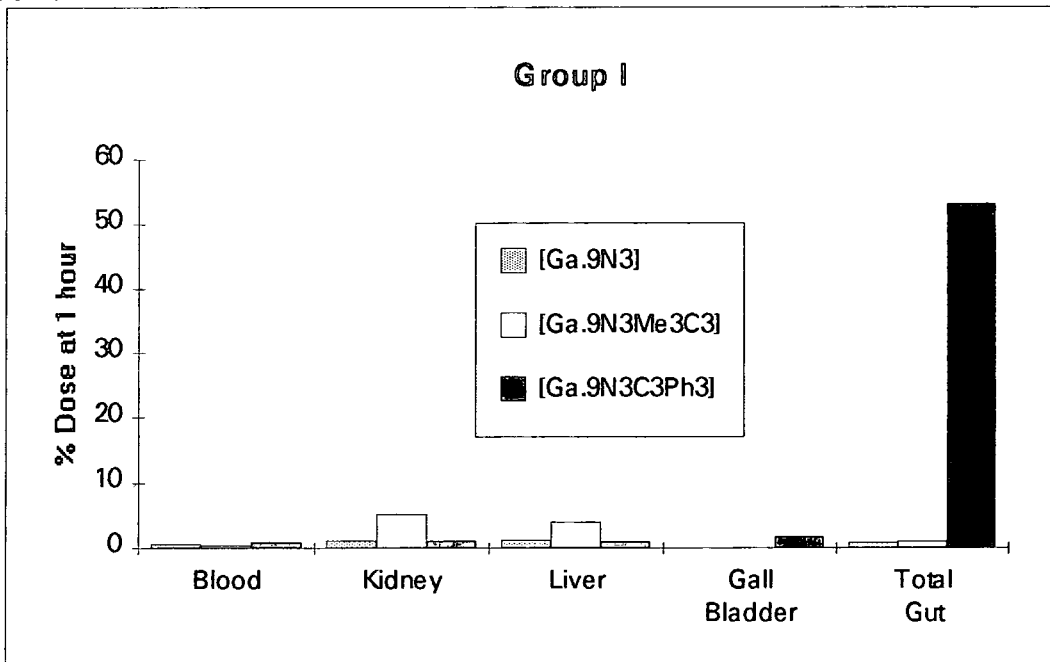
Figure 4.5. *Biodistribution of Group II Aza-phosphinic Acids at 1 Hour.*
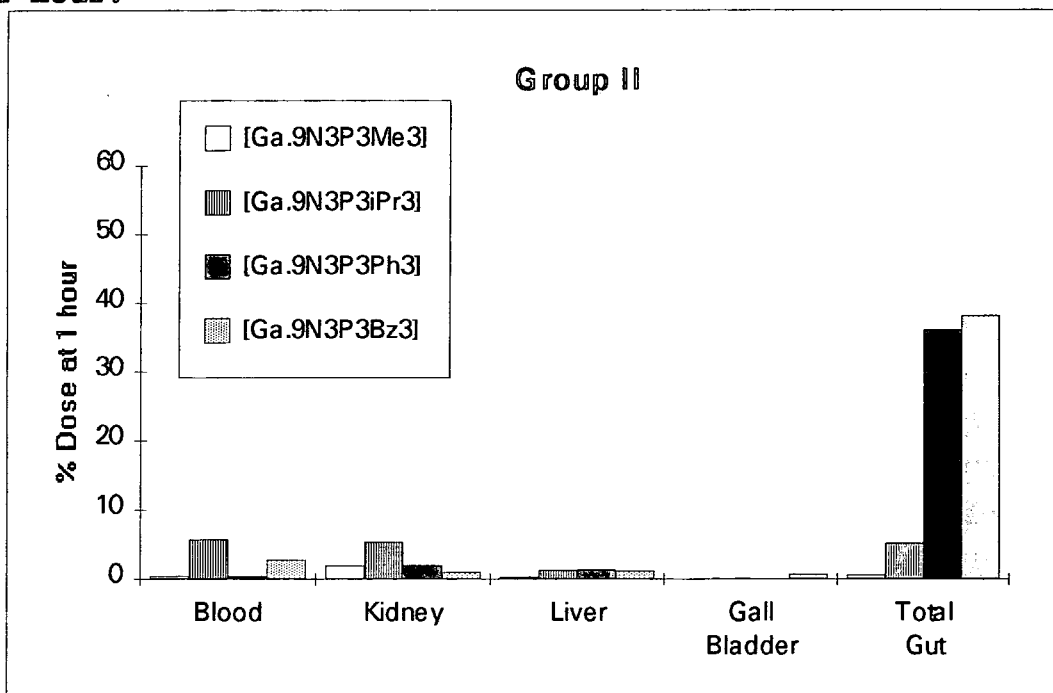
Figure 4.6. *Biodistribution of Group I Aza-carboxylic Acids at 24 Hours.*
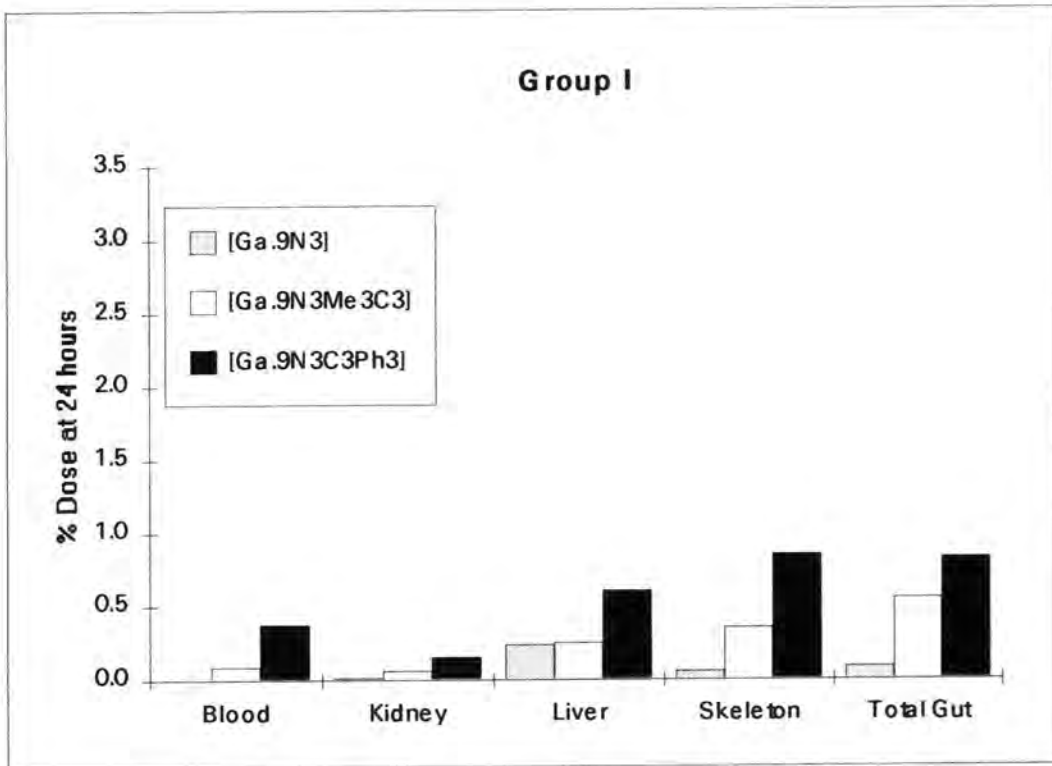
Figure 4.7. *Biodistribution of Group II Aza-phosphinic Acids at 24 Hours.*
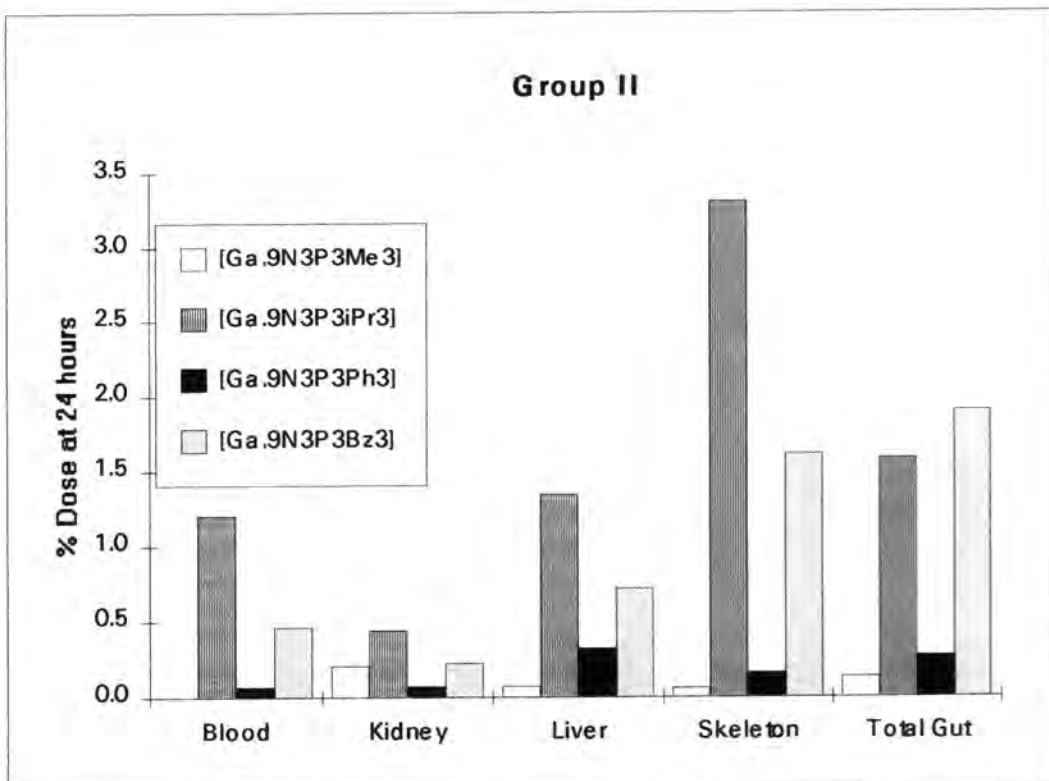
% Dose of ^{67}Ga in Blood.

Figure 4.8. *% Dose ^{67}Ga in Blood at 1 Hour.*

% Dose in Blood at 1 hour
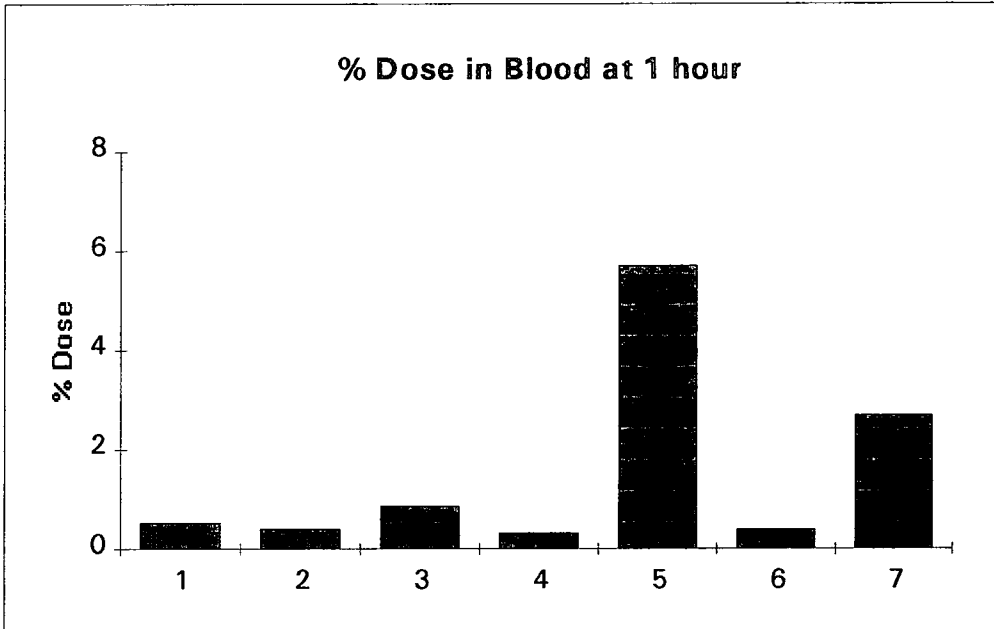
Figure 4.9. *% Dose ^{67}Ga in Blood at 24 Hours.*

% Dose in Blood at 24 hours
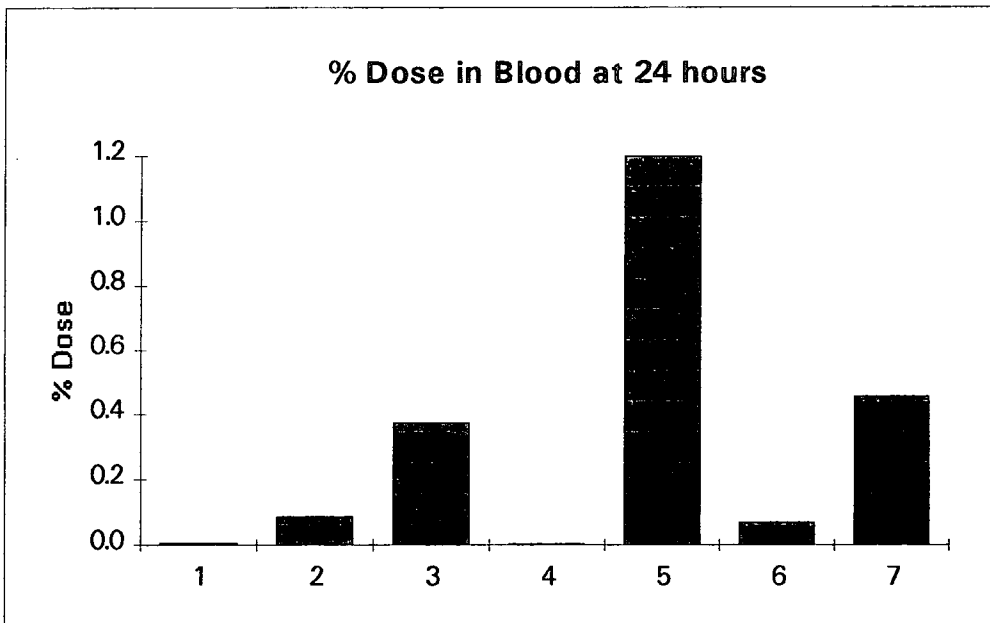
% Dose ^{67}Ga in Kidneys

Figure 4.10. *% Dose ^{67}Ga in Kidneys at 1 Hour.*

% Dose in Kidney at 1 hour
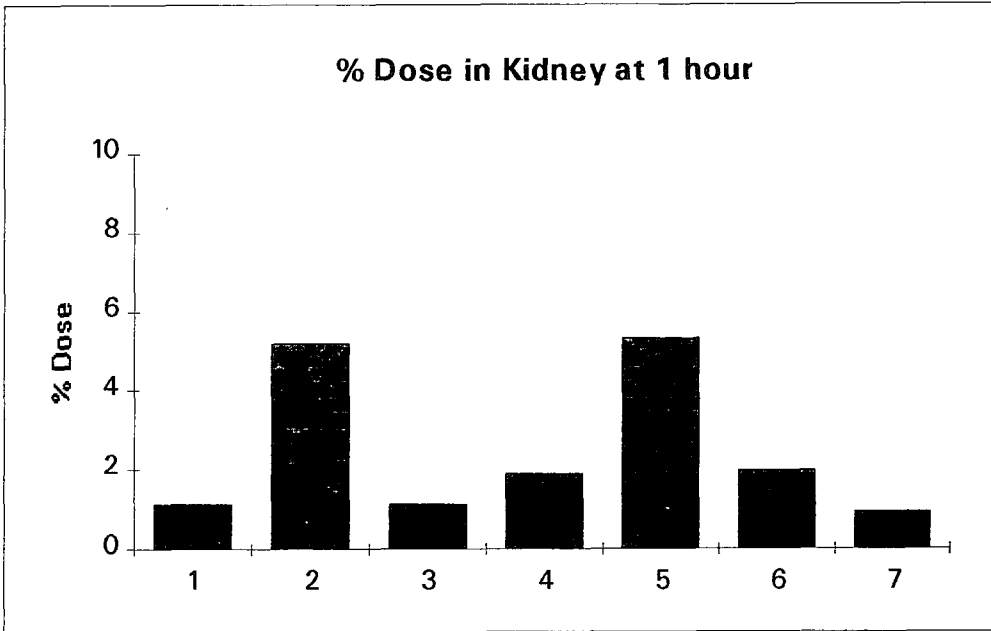
Figure 4.11. *% Dose ^{67}Ga in Kidneys at 24 Hours.*

% Dose in Kidney at 24 hours
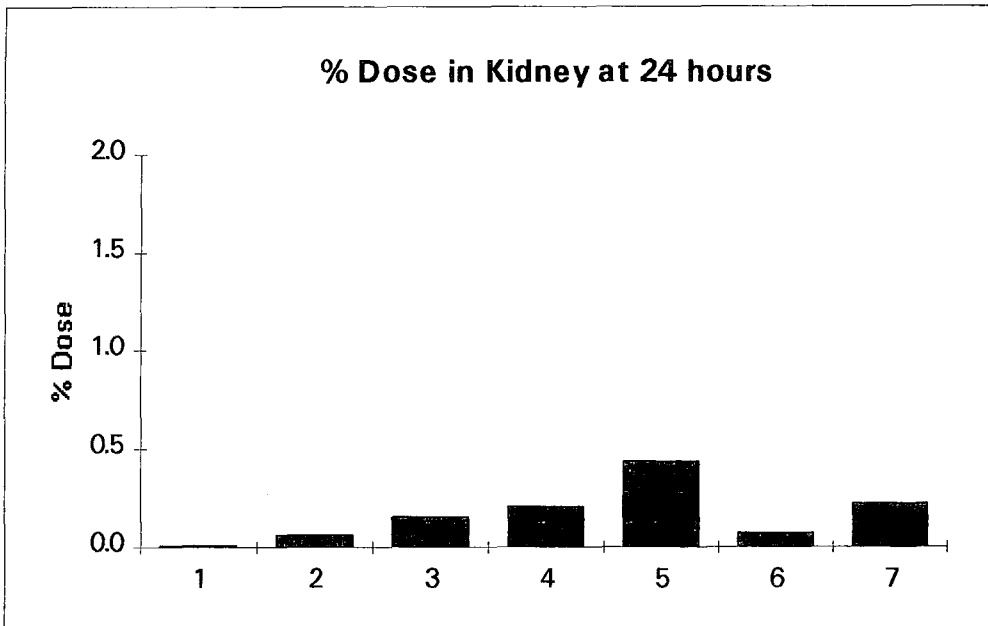
% Dose ^{67}Ga in Liver

Figure 4.12. % *Dose* ^{67}*Ga in Liver at 1 Hour.*
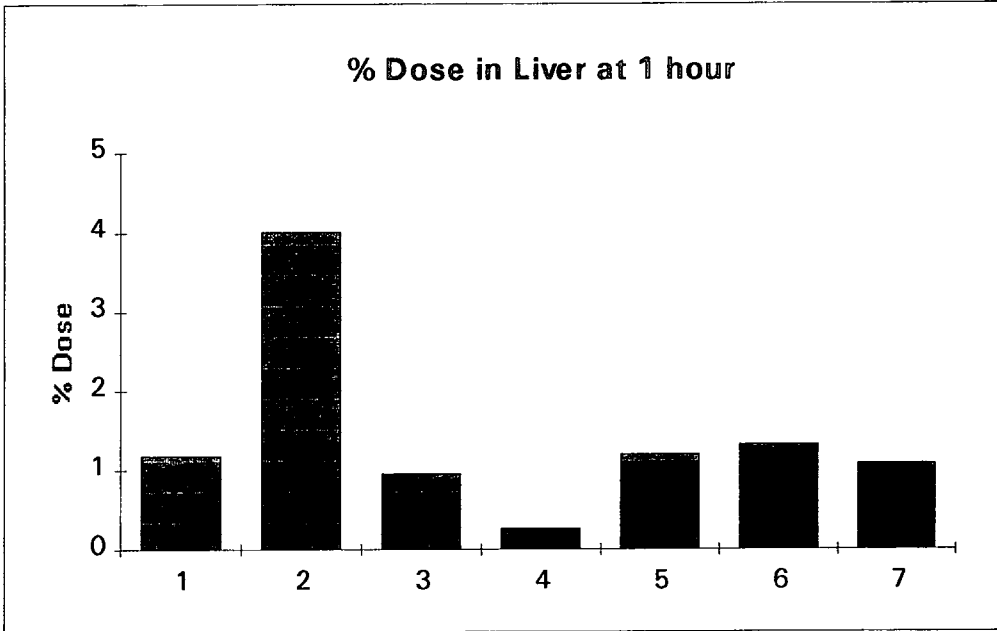
Figure 4.13. % *Dose* ^{67}*Ga in Liver at 24 Hours*
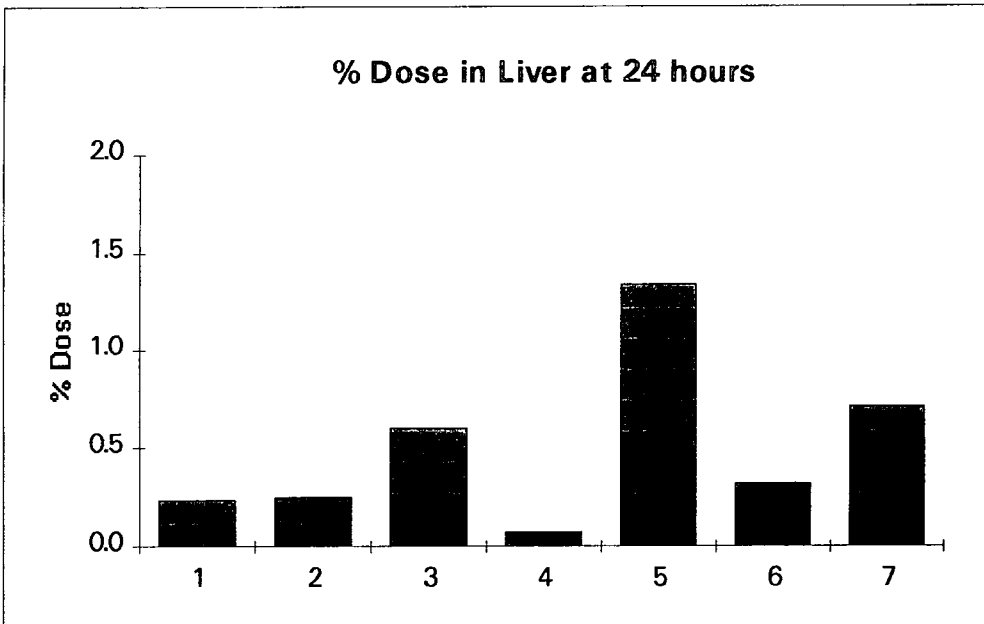
% Dose ^{67}Ga in Gall Bladder.

Figure 4.14. *% Dose ^{67}Ga in Gall Bladder at 1 Hour.*
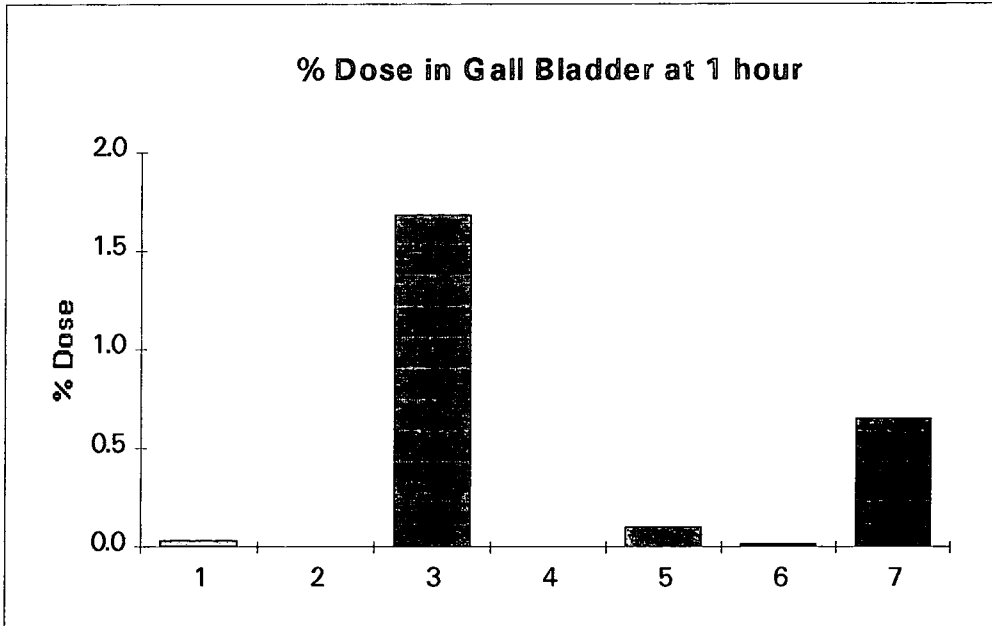
% Dose ^{67}Ga in Skeleton.

Figure 4.15. *% Dose ^{67}Ga in Skeleton at 24 Hours*
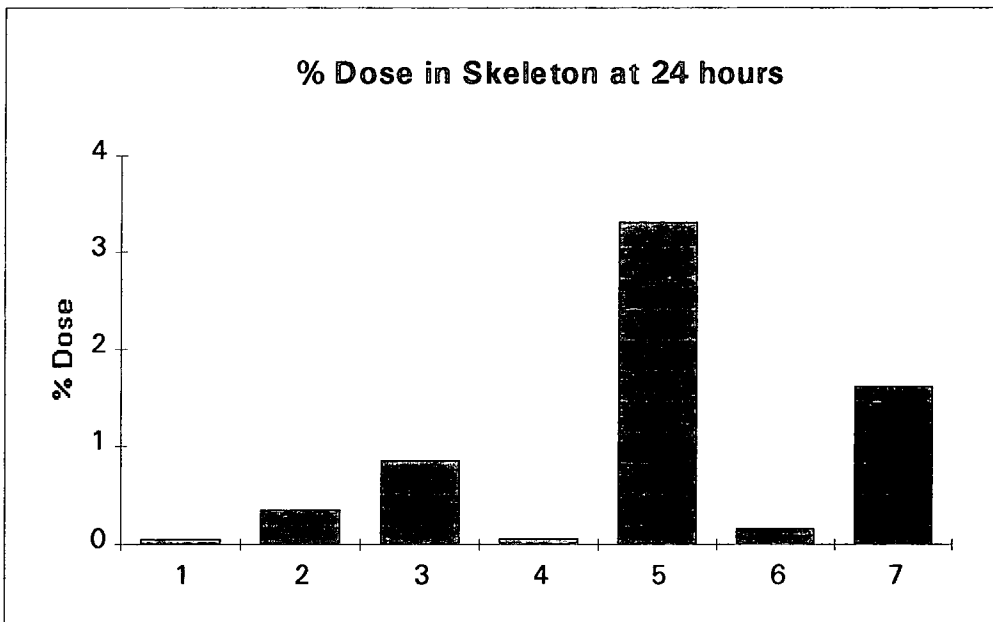
% Dose ^{67}Ga in the Gut.

Figure 4.16. *% Dose ^{67}Ga in Total Gut at 1 Hour*

% Dose in Total Gut at 1 hour
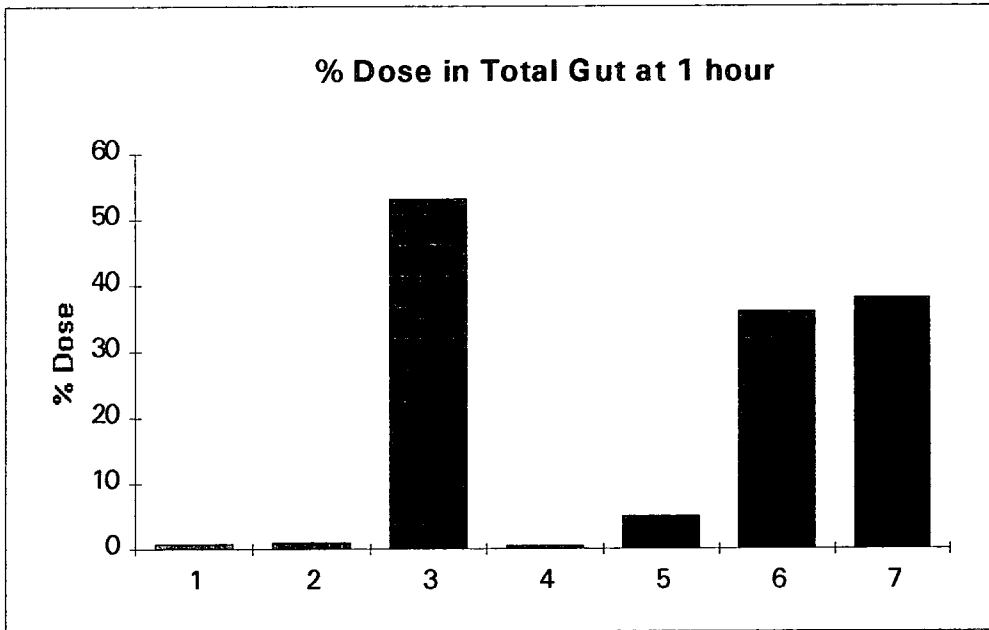
Figure 4.17. *% Dose ^{67}Ga in Total Gut at 24 Hours*
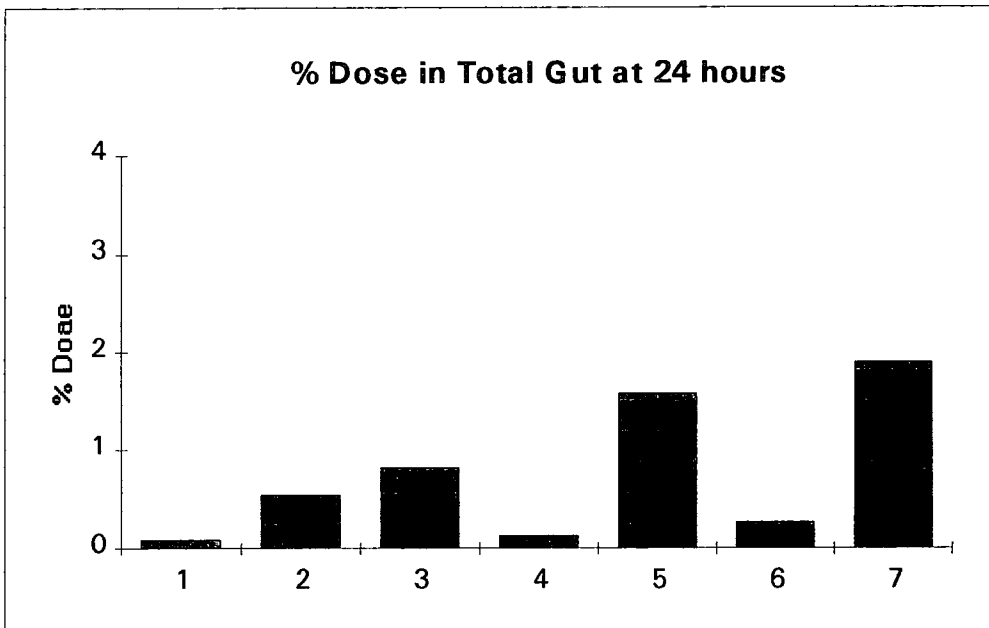
% Dose in Total Gut at 24 hours

Other Tissues

The % dose/g was also measured in the following tissues:- brain, lung, heart muscle, skeletal muscle, salivary glands and spleen. When the % dose/g in these tissues was compared to that of blood, there was some concentration of the complexes [Ga.9N3], [Ga.9N3Me3C3] and [Ga.9N3P3Me3] in the lung, salivary glands and spleen at 24 hours. Although there was 2 to 10 times the concentration of gallium in these tissues in comparison to the blood, they were very low absolute amounts. There was no concentration of gallium from any of the macrocycles measured in the brain, heart muscle or skeletal muscle.

4.2.2. Summary of the Gallium Biodistribution Data.

Clearance Pathways

Group I

Figure 4.4 gives the overall view of the biodistribution of these neutral gallium aza-carboxylic acids at 1 hour.

The complex [Ga.9N3] (number 1) is being cleared exclusively by the renal system. The rate of clearance is such that the majority of the complex has already left the body by 1 hour, (unlike complexes which are cleared via the hepatobiliary pathway which are still present in the gut at 1 hour).

The complex [Ga.9N3Me3C3] (number 2) is also cleared via the renal system. Although there is little evidence of this complex in the gut, there is a 4% dose in the liver (figure 4.12) at 1 hour. As this liver dose has been cleared by 24 hours (figure 4.13), it is likely to represent a small amount of hepatobiliary handling rather than deposition of uncomplexed gallium.

The lipophilic complex [Ga.9N3C3Ph3] (number 3) is being cleared primarily by the hepatobiliary system. This is apparent from the high (53%) dose in the gut at 1 hour (figure

4.16). Already by 1 hour there is little of the complex left
in the liver (figure 4.12), although there is still some in
the gall bladder on its way to the gut.

Group II

Figure 4.5 gives the overall picture of the
biodistribution of these neutral gallium aza-phosphinic acids
1 hour post injection.

The complex [Ga.9N3P3Me3] (number 4) is the only complex
in this group which exhibits exclusively renal clearance. The
slightly more lipophilic complex [Ga.9N3P3iPr3] (number 5) has
5% dose in the gut at 1 hour (figure 4.16), but is still being
cleared primarily via the renal pathway.

The two lipophilic complexes [Ga.9N3P3Ph3] and
[Ga.9N3P3Bz3] (numbers 6 and 7) are both cleared
preferentially via the hepatobiliary pathway with 36% and 38%
dose respectively in the gut at 1 hour (figure 4.16). The
amount of dose from these complexes present in the liver at 1
hour was not very high (figure 4.12) with only [Ga.9N3P3Bz3]
having any dose still in the gall bladder (figure 4.14). These
two lipophilic gallium complexes, like the complex
[Ga.9N3C3Ph3], are transported through the hepatobiliary
system and into the gut by 1 hour post injection.

In Vivo Stability of Gallium Macrocycles

Group I

Figure 4.6 gives the overall picture of the 24 hour
biodistributions of the aza-carboxylic acids.

The complex [Ga.9N3] (number 1) demonstrates very little
overall retention at 24 hours with only 0.05% dose remaining
in the skeleton (figure 4.15) and less than 0.002% dose in the
blood (figure 4.9). This is consistent with a high in vivo
stability.

[Ga.9N3Me3C3] (number 2) also has very little overall
retention at 24 hours. Although there is a higher retention in

the skeleton than for [Ga.9N3] (0.35% compared to 0.05% dose) this complex still exhibits good overall stability.

[Ga.9N3C3Ph3] (number 3) has the highest overall retention of the complexes in this group. The skeletal value of 0.85% dose and blood value of 0.37% dose at 24 hours is indicative of a low level of dissociation.

Group II

Figure 4.7 gives the overall picture of the 24 hour biodistributions of the gallium aza-phosphinic acids.

The renally excreted complex [Ga.9N3P3Me3] (number 4) shows the least retention of all the complexes in this group at 24 hours. The very low skeletal (0.06%) and blood (0.004%) doses (figures 4.15 and 4.9) are indicators of the high in vivo stability of this complex.

The complex [Ga.9N3P3iPr3] (number 5) has high levels of retention at 24 hours, particularly in the blood and skeleton, indicating that this complex is dissociating in vivo.

Complex number 7, [Ga.9N3P3Bz3], has 1.6% dose in the skeleton at 24 hours and elevated doses in the blood and liver. Although there still appears to be some hepatobiliary clearance occurring at 24 hours (figure 4.7), there is clearly some in vivo dissociation of this complex.

[Ga.9N3P3Ph3] (number 6) appears to be the most stable of all of the hepatobiliary cleared complexes from both groups. With only 0.15% dose in the skeleton and 0.07% dose in the blood at 24 hours. This makes [Ga.9N3P3Ph3] the most promising of these neutral gallium complexes for further study of hepatobiliary handling.

4.3. BIODISTRIBUTION OF INDIUM COMPLEXES.

The biodistribution of 7 indium complexes was examined in order to assess their principle route of excretion (hepatobiliary or renal) and in vivo stability. These were the same groups of aza-carboxylic and aza-phosphinic acids as were studied in section 4.2 complexed with gallium.

172

Presentation of Results

The indium complexes have been divided into the same two groups as the gallium complexes (section 4.2) for the biodistribution studies. Group I are aza-carboxylic acids, and group II are aza-phosphinic acids.

Figures 4.18 and 4.19 show the % dose in 5 tissues at 1 hour post injection for the groups I and II. These 5 tissues are blood, kidneys, liver, gall bladder and gut, where the gut represents the intestinal tract (with contents) from the stomach to the large intestine inclusive. Figures 4.20 and 4.21 show the % dose in 5 tissues at 24 hours post injection for these groups. However at this time the % dose in the skeleton is shown and not the gall bladder. More precise data for individual tissues are given in figures 4.22 to 4.31, these figures each show the % dose for each of the 7 complexes in a single tissue.

Key to Figures in this Section.

Number in Figures	Group	Complex
1.	I	[In.9N3]
2.	I	[In.9N3Me3C3]
3.	I	[In.9N3C3Ph3]
4.	II	[In.9N3P3Me3]
5.	II	[In.9N3P3iPr3]
6.	II	[In.9N3P3Ph3]
7.	II	[In.9N3P3Bz3]

4.3.1. Biodistribution Data for the Two Groups of Indium Complexes.

Figure 4.18. *Biodistribution of Group I Aza-carboxylic Acids at 1 Hour.*
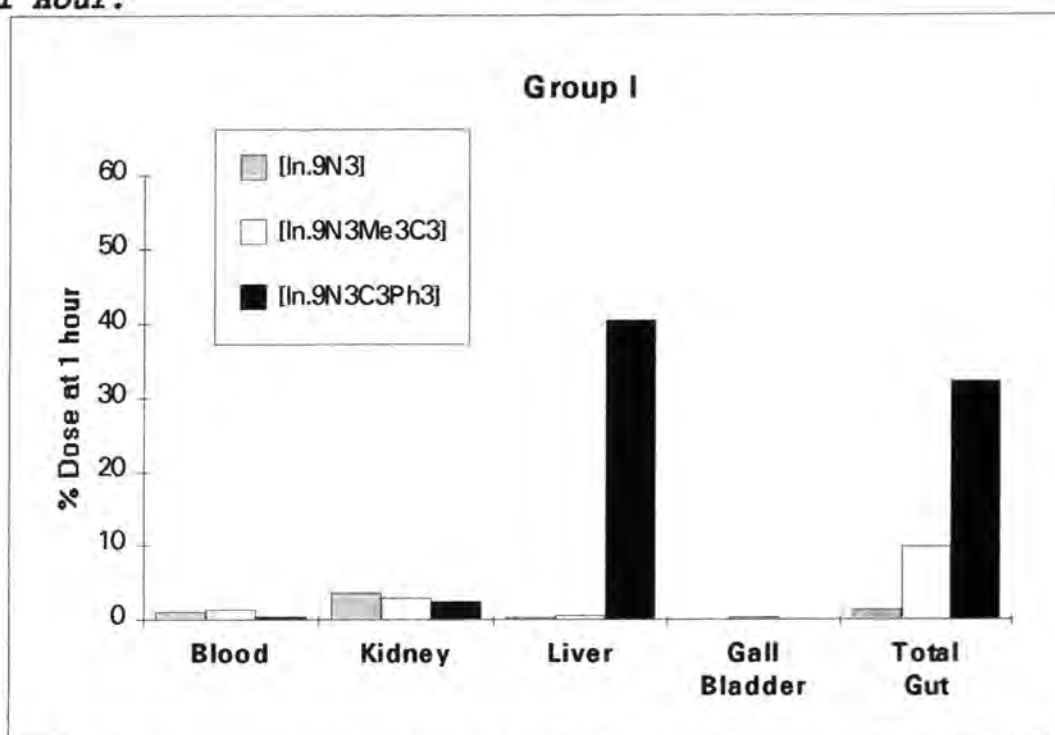
Figure 4.19. *Biodistribution of Group II Aza-phosphinic Acids at 1 Hour.*
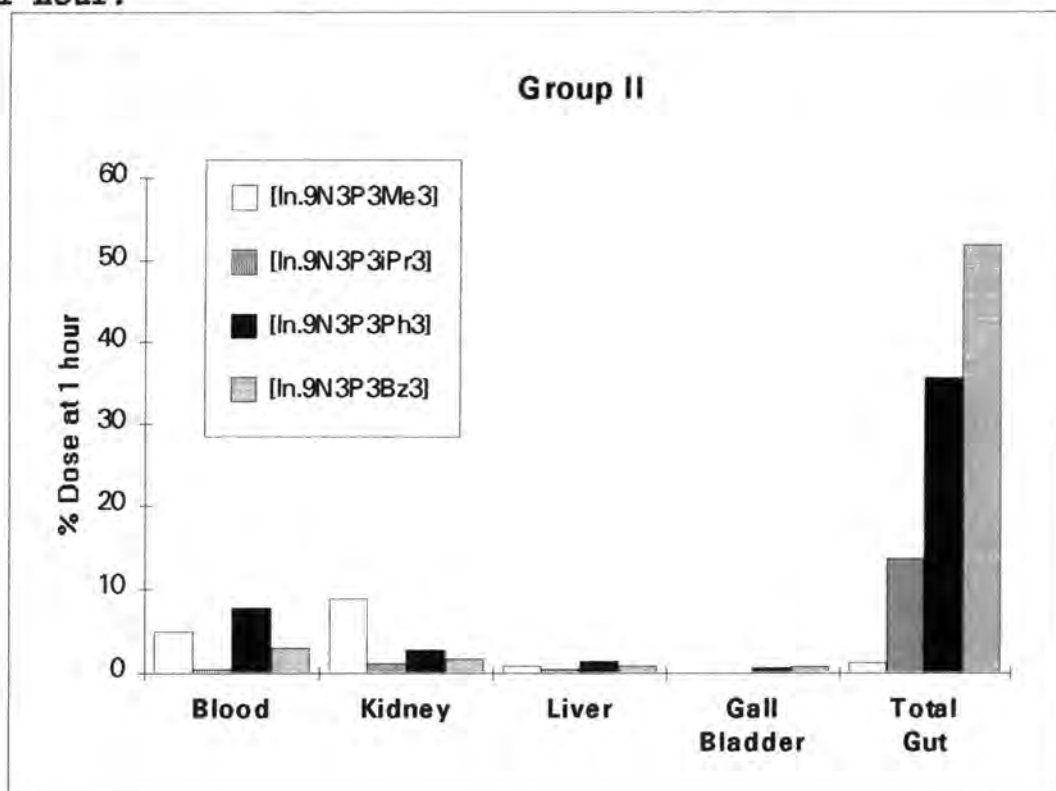
Figure 4.20. *Biodistribution of Group I Aza-carboxylic Acids at 24 Hours.*
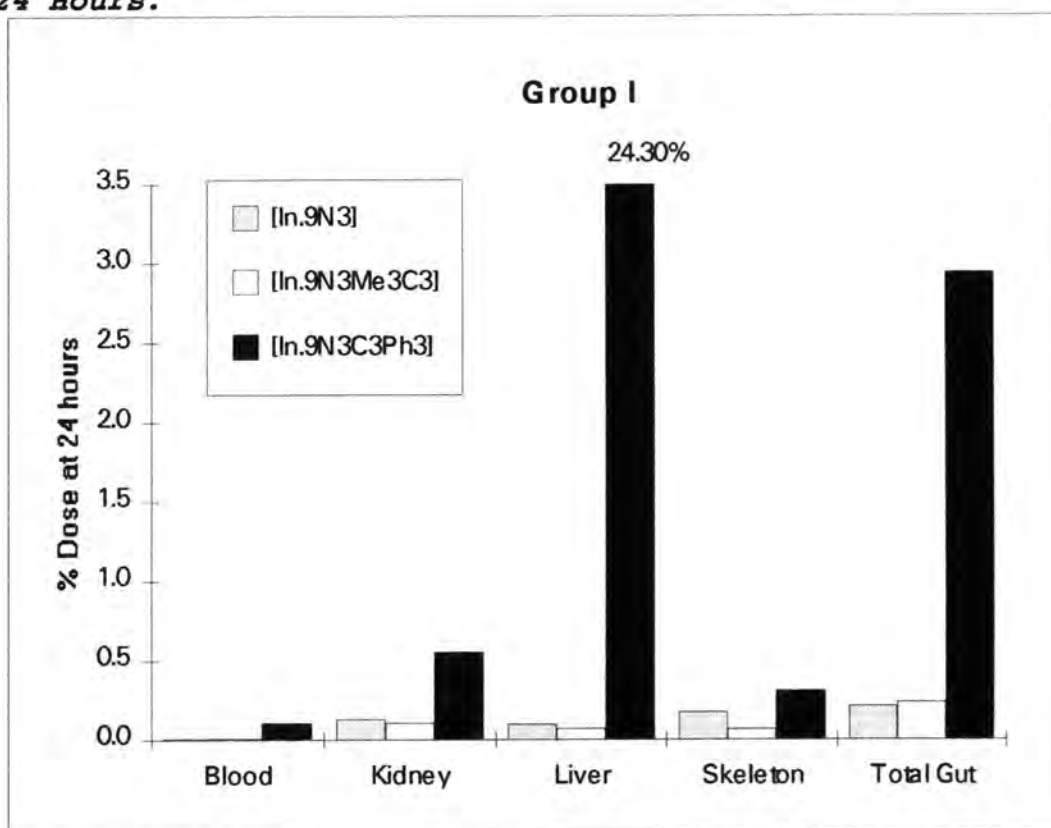
Figure 4.21. *Biodistribution of Group II Aza-phosphinic Acids at 24 Hours.*
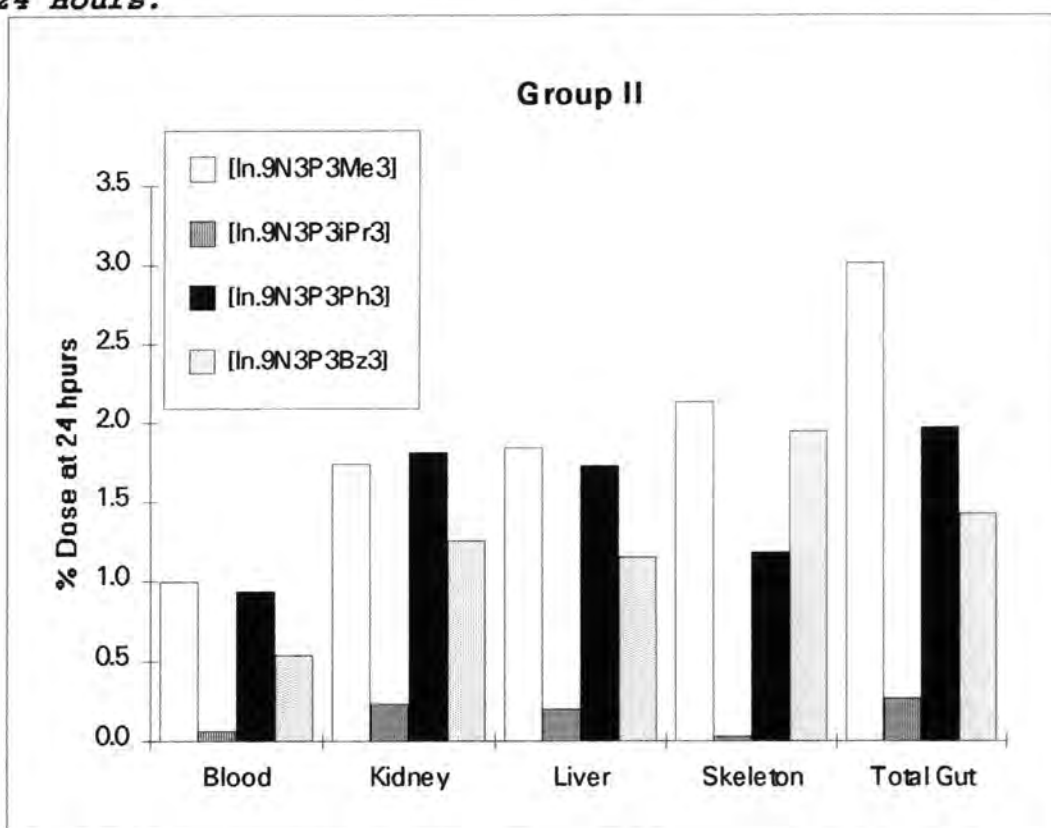
% Dose of ^{111}In in Blood.

Figure 4.22. % Dose ^{111}In in Blood at 1 Hour.
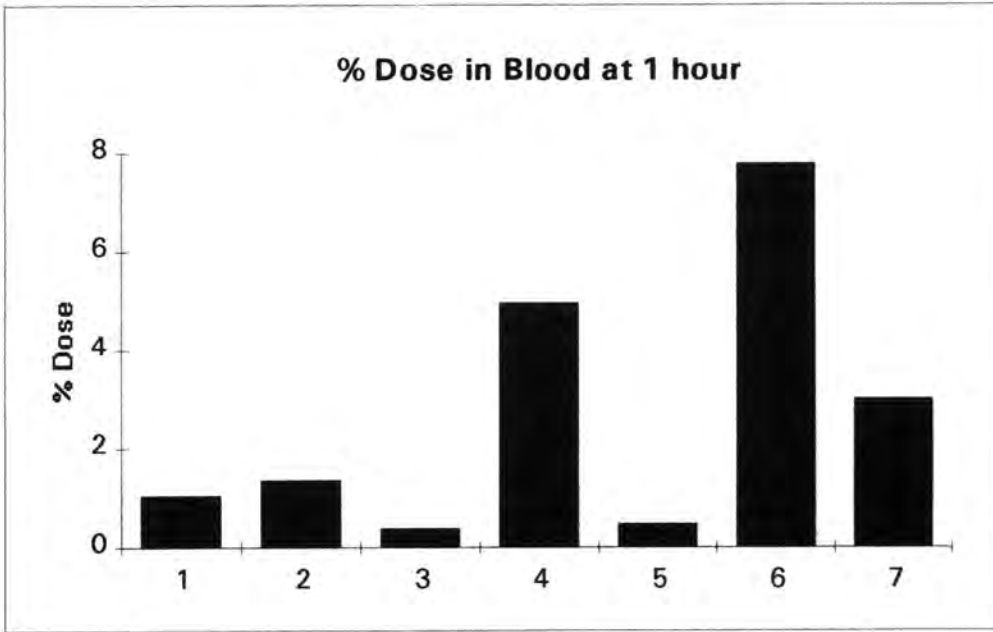
Figure 4.23. % Dose ^{111}In in Blood at 24 Hours.
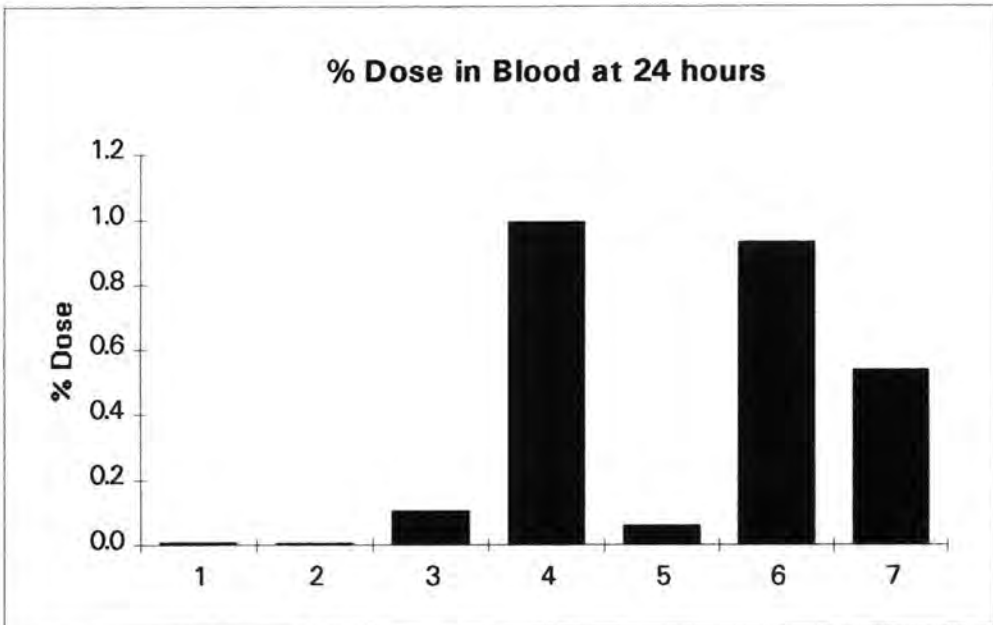
% Dose of ^{111}In in Kidneys

Figure 4.24. % Dose ^{111}In in Kidneys at 1 Hour.

% Dose in Kidney at 1 hour
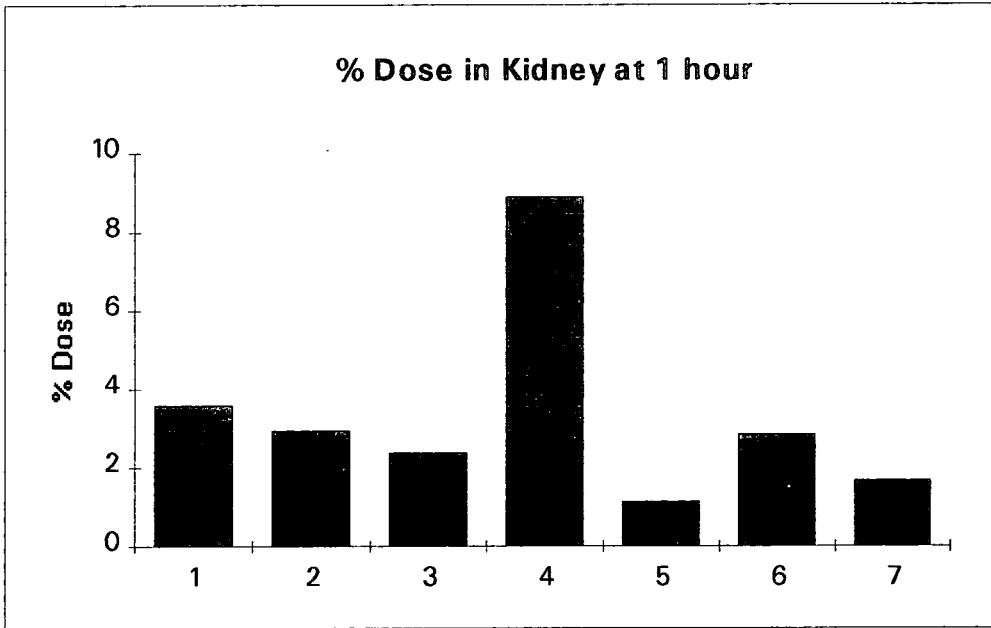
Figure 4.25. % Dose ^{111}In in Kidneys at 24 Hours.

% Dose in Kidney at 24 hours
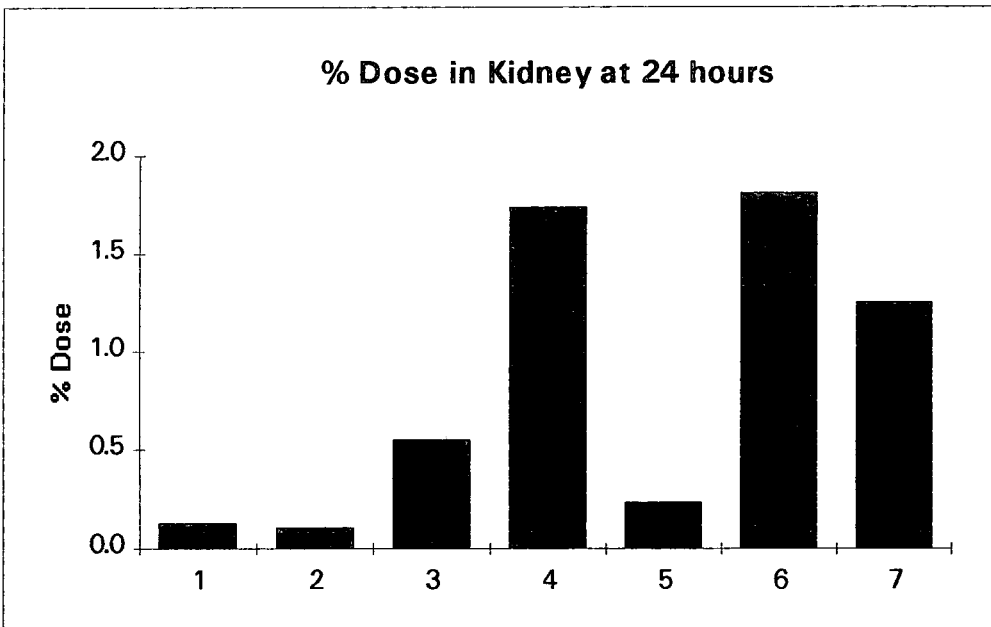
% Dose of ^{111}In in Liver

Figure 4.26. % Dose ^{111}In in Liver at 1 Hour.

% Dose in Liver at 1 hour
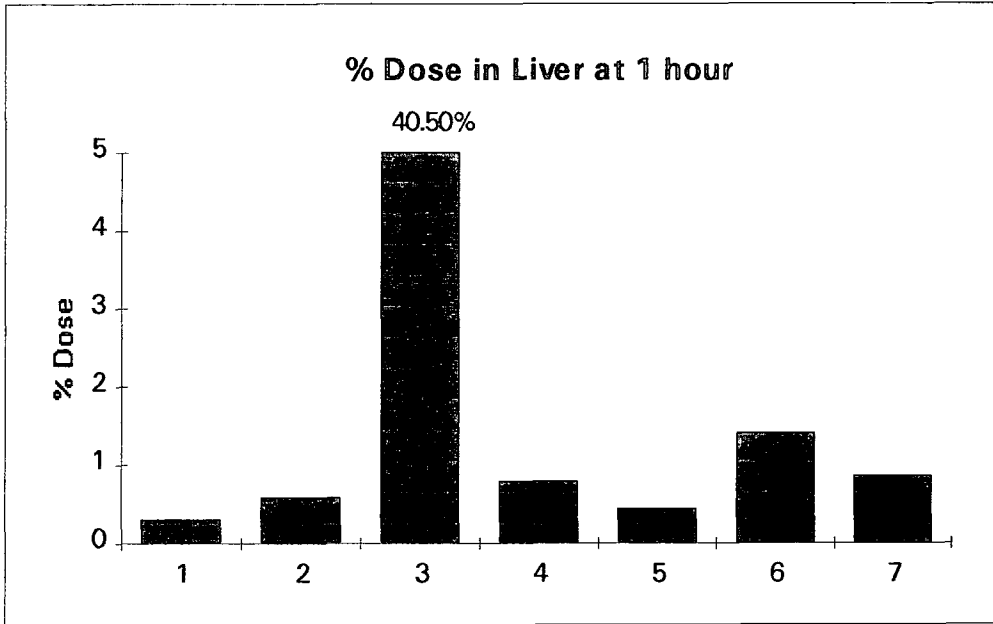
Figure 4.27. % Dose ^{111}In in Liver at 24 Hours

% Dose in Liver at 24 hours
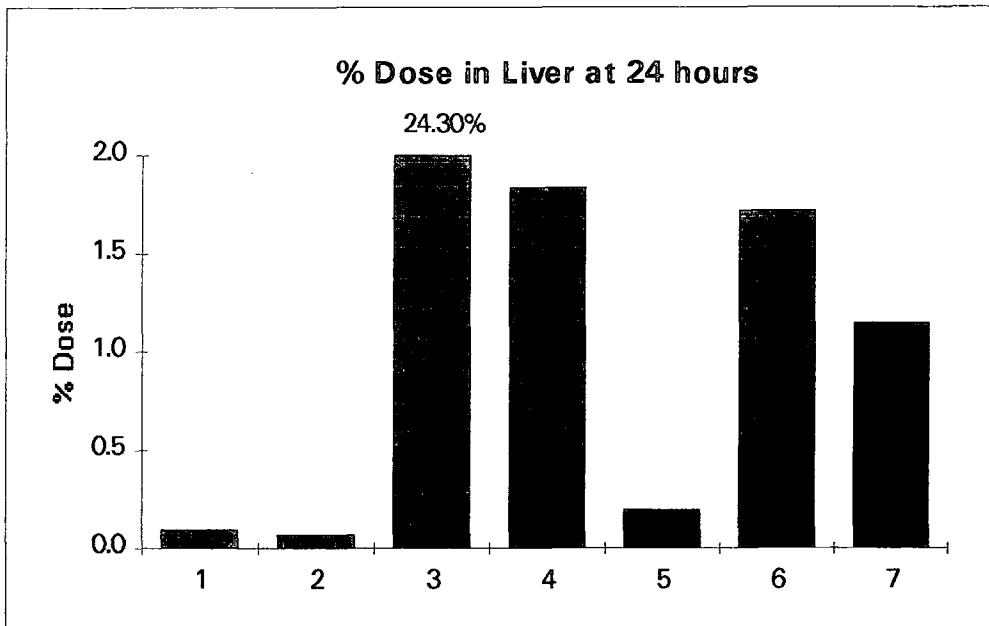
% Dose of ^{111}In in Gall Bladder.

Figure 4.28. % Dose ^{111}In in Gall Bladder at 1 Hour.

% Dose in Gall Bladder at 1 hour
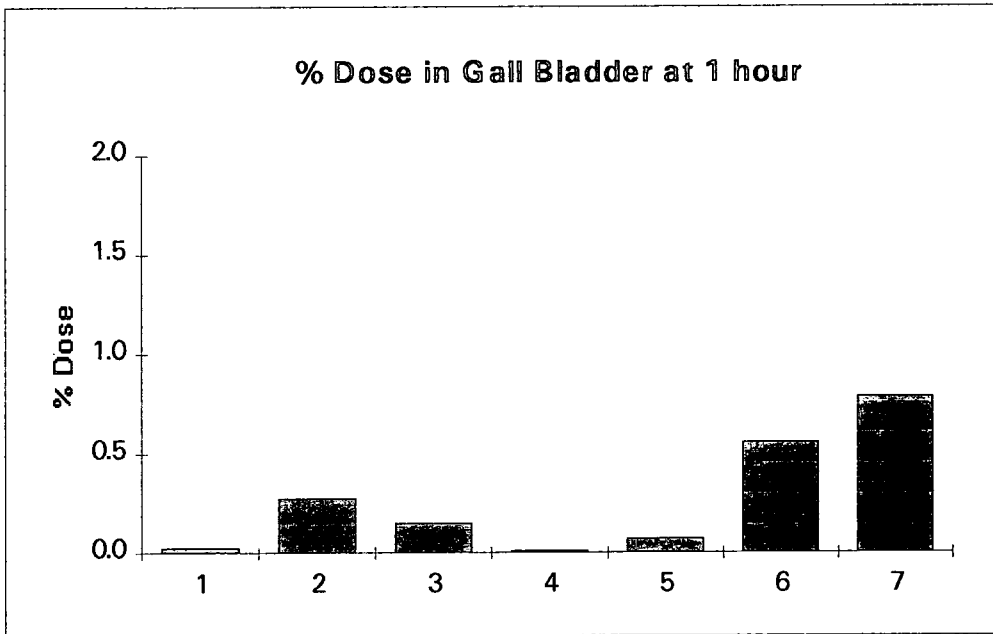
% Dose of ^{111}In in Skeleton.

Figure 4.29. % Dose ^{111}In in Skeleton at 24 Hours

% Dose in Skeleton at 24 hours
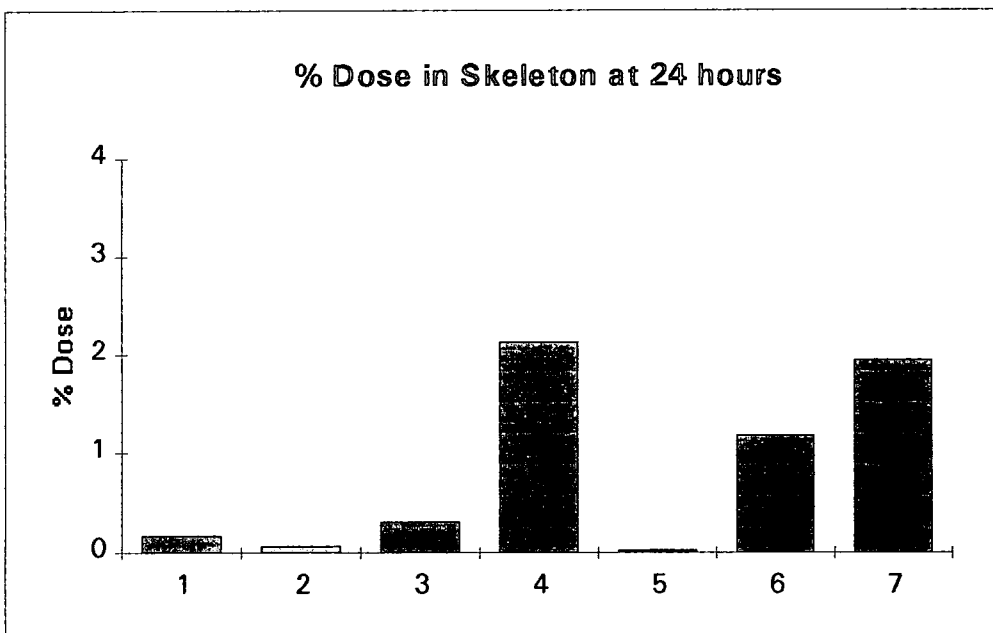
% Dose of ^{111}In in the Gut.

Figure 4.30. *% Dose ^{111}In in Total Gut at 1 Hour*

% Dose in Total Gut at 1 hour
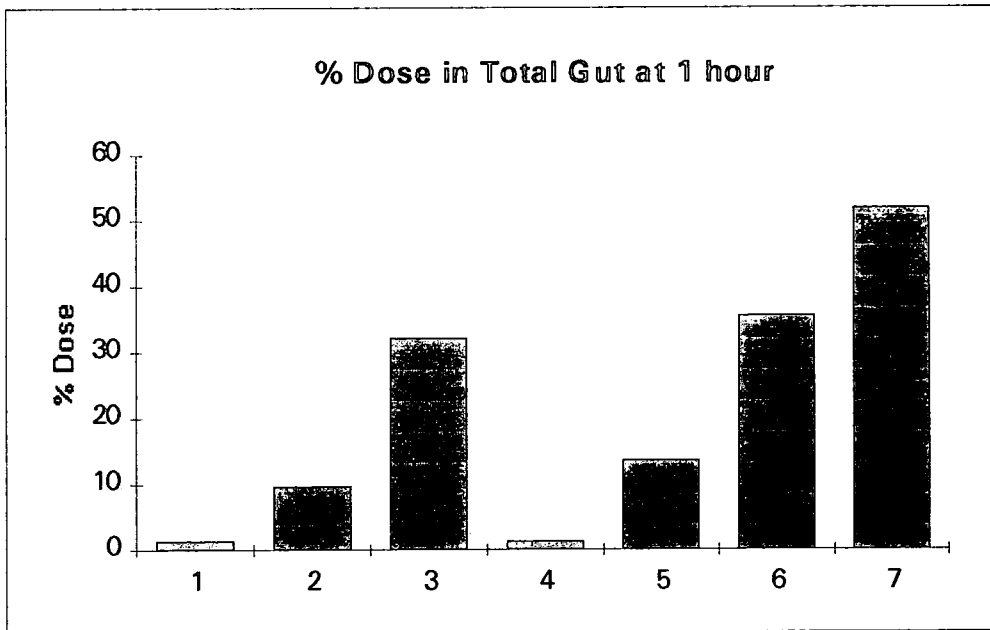
Figure 4.31. *% Dose ^{111}In in Total Gut at 24 Hours*
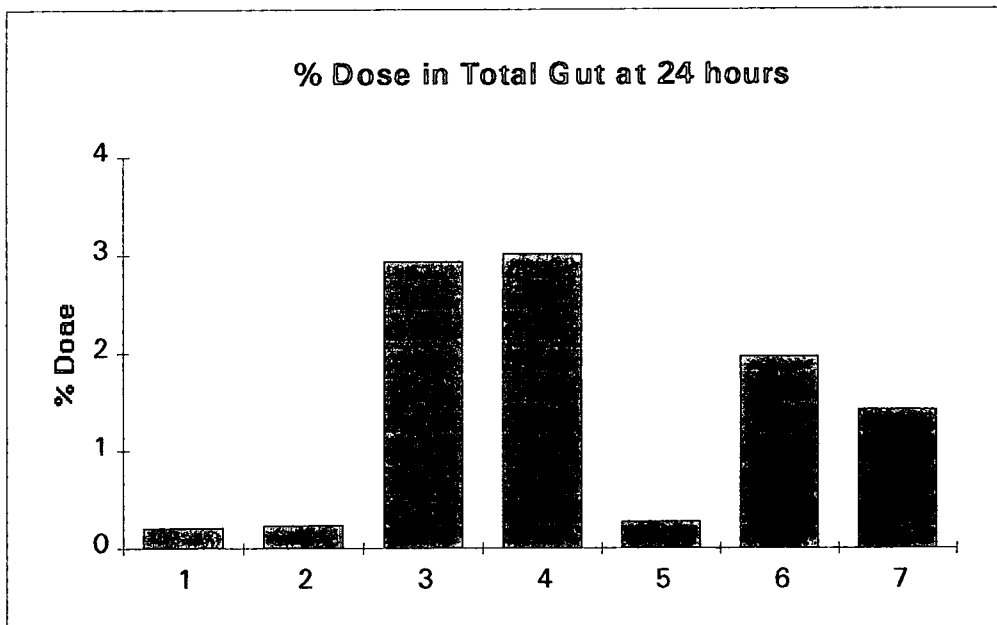
% Dose in Total Gut at 24 hours

Other Tissues

The % dose/g was also measured in the following tissues:-brain, lung, heart muscle, skeletal muscle, and spleen. When the % dose/g in these tissues was compared to that of the blood, there was about twice the concentration of indium in the lung and spleen at 24 hours from all the complexes. There was no concentration of indium in the brain, heart muscle or skeletal muscle from any of the complexes measured.

4.3.2 Summary of Biodistribution Data for Indium Macrocycles .

Clearance Pathways

Group I

Figure 4.18 gives the overall view of the biodistribution of the neutral indium aza-carboxylic acids at 1 hour post injection.

The complex [In.9N3] (number 1) is being cleared entirely by the renal system. After 1 hour the majority of the complex has already been cleared from the body via the renal system.

[In.9N3Me3C3] (number 2) is showing some hepatobiliary clearance, 10% at 1 hour (figure 4.30). Nevertheless the majority of this complex is still being handled by the renal system.

The third complex [In.9N3C3Ph3] has very high doses in both the liver (41%) and gut (32%) at 1 hour. This indicates a high amount of hepatobiliary clearance, however at 24 hours (figure 4.27) there is still 24% dose in the liver. This suggests the accumulation of decomplexed indium in the liver (see next page :-in vivo stability of indium macrocycles).

Group II

The biodistribution of the neutral indium aza-phosphinic acids at 1 hour post injection are given in figure 4.19.

The complex [In.9N3P3Me3] (number 4) has very little dose in the gut at 1 hour indicating that it is eliminated via the renal pathway.

The other 3 complexes in this group [In.9N3P3iPr3], [In.9N3P3Ph3] and [In.9N3P3Bz3] (numbers 5, 6 and 7) demonstrate increasing doses in the gut at 1 hour of 14, 36 and 42% respectively. The more lipophilic the phosphorus substituent on the complex the more hepatobiliary clearance is shown by the indium complex.

In Vivo Stability of Indium Complexes.

Group I

Figure 4.20 gives the overall view at 24 hours for the aza-carboxylic acid complexes.

The % dose in the skeleton at 24 hours is very low for all three complexes (<0.5% dose). The % dose in the blood is also low, less than 0.01% for [In.9N3] and [In.9N3Me3C3] (numbers 1 and 2), and 0.1% for [In.9N3C3Ph3] (number 3). This together with the low liver retention for the complexes [In.9N3] and [In.9N3Me3C3] is an indicator of high in vivo stability for these two complexes. The % dose in the liver for the complex [In.9N3C3Ph3] is however very high, 24% at 24 hours. Although there is still a little gut clearance of 3% dose, this level of liver deposition is indicative of dissociation of this particular complex.

Group II

Figure 4.21 gives the overall view at 24 hours for the indium aza-phosphinic acids.

The only complex in this group to show low tissue retention at 24 hours is number 5 [In.9N3P3iPr3]. This indium complex appears to be stable in vivo.

The other 3 complexes, [In.9N3P3Me3], [In.9N3P3Ph3] and [In.9N3P3Bz3] (numbers 4, 6 and 7) all show high tissue

retention at 24 hours. This is particularly evident from the %
doses in the skeleton of 2.1, 1.2 and 1.9% respectively. Even
if the high blood dose is taken into account, the skeleton has
at least twice as much dose/g as the blood. All three
complexes [In.9N3P3Me3], [In.9N3P3Ph3] and [In.9N3P3Bz3] are
dissociating in vivo.

From the indium macrocycles studied here, the only
complexes which are stable in vivo are number 1 [In.9N3],
number 2 [In.9N3Me3C3] and number 5 [In.9N3P3iPr3]. Of these
[In.9N3] is cleared solely by the renal pathway. [In.9N3Me3C3]
and [In.9N3P3iPr3] show limited hepatobiliary clearance of 10
and 14% dose respectively at 1 hour post injection.

4.4 PARTITION COEFFICIENTS OF INDIUM MACROCYCLE COMPLEXES

Log P values were determined for 6 of the 7 indium
complexes studied in vivo (section 4.3.). The complex
[In.9N3C3Ph3] was highly unstable in vivo and was omitted.

A high (more positive) Log P value is correlated with
increased lipophilicity. Lipophilic compounds are more likely
to be eliminated from the body via the hepatobiliary route
than the renal route. Therefore it was hoped to establish a
correlation between the Log P value of the complex and its
route of elimination from a mouse.

Table 4.3. *Partition Coefficients of Indium Macrocycles[a]*

Indium Complex		Log P Octanol/ water	Octanol/ PBS	Butanol/ water	Butanol/ PBS
1	9N3	-4.92	-4.51	-2.54	-2.98
2	9N3Me3C3	-3.38	-3.62	-1.79	-2.22
4	9N3P3Me3	-3.80	-3.68	-1.88	-2.06
5	9N3P3iPr3	-1.92	-1.89	-0.98	-0.99
6	9N3P3Ph3	0.33	0.24	0.63	0.49
7	9N3P3Bz3	0.13	0.10	0.54	0.34

a) PBS is phosphate-buffered saline, pH 7.4.

Figure 4.32. *Log P values for Indium Complexes.*
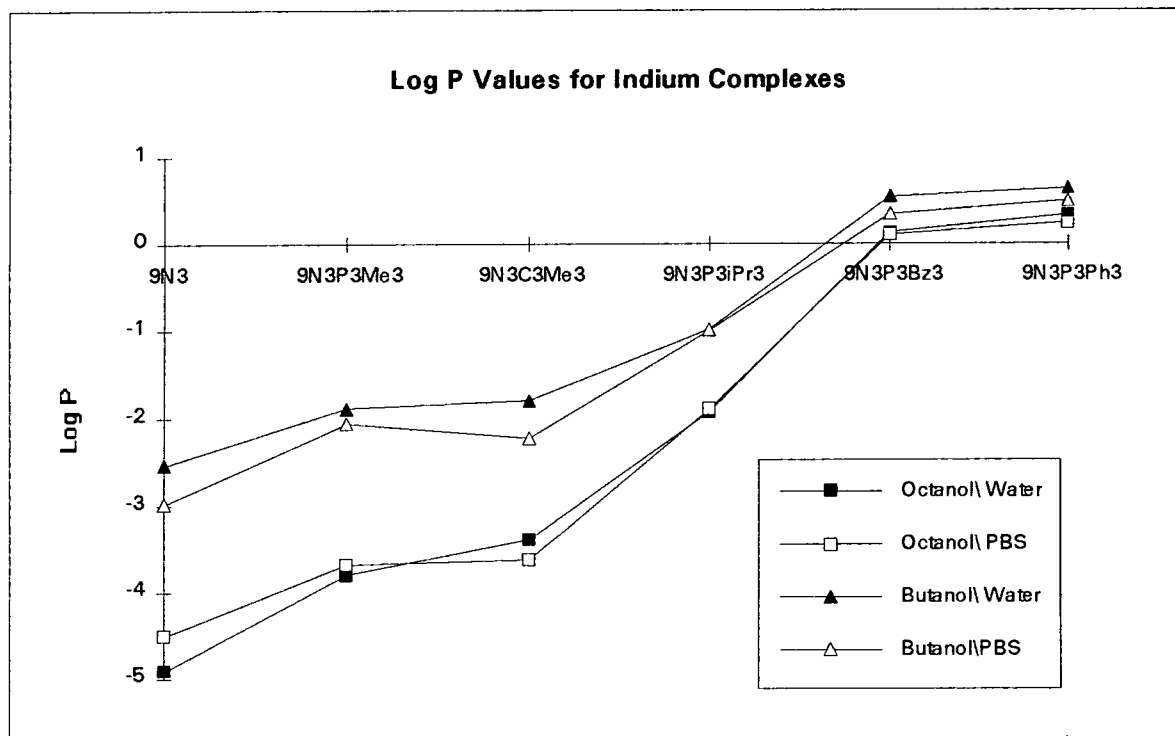
Figure 4.33. *Plot of Butanol/Water Log P Values vs. % Dose of Indium Macrocycle in the Total Gut at 1 Hour Post Injection.*
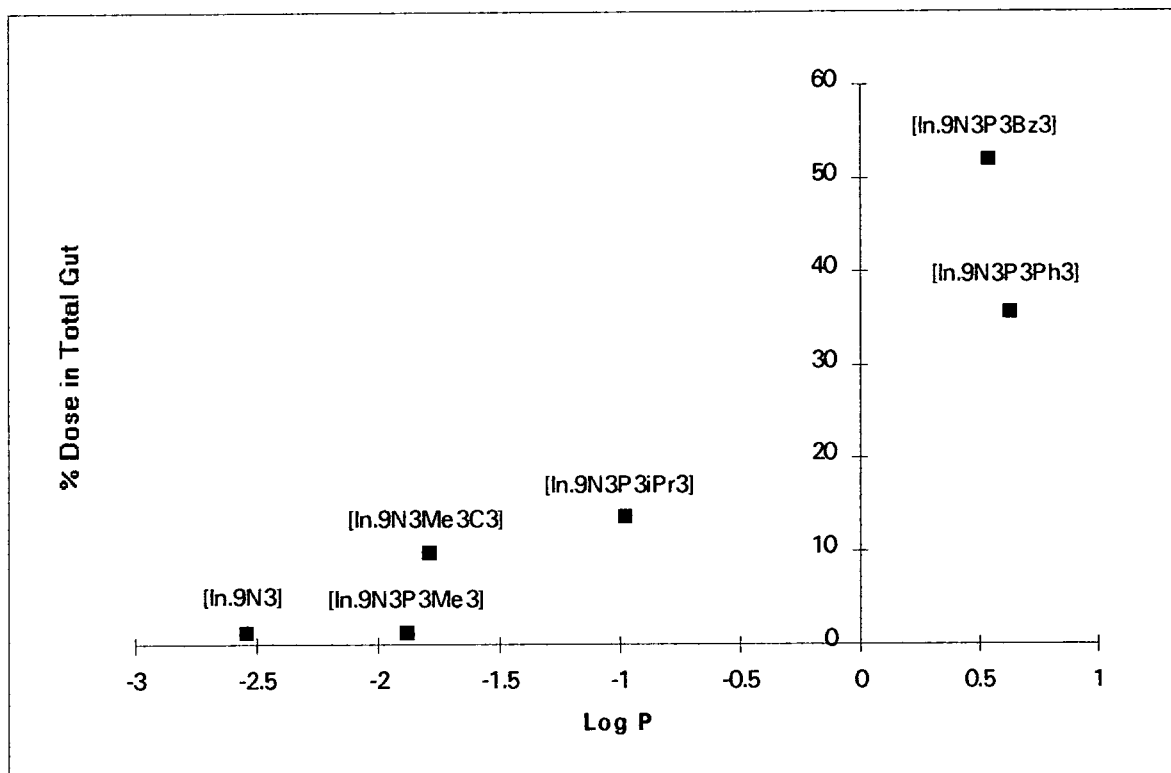
For all the indium complexes there is no significant difference between the Log P values in water or PBS (phosphate-buffered saline), indicating that the buffering action of the PBS has no great effect on the Log P value. The complexes follow the same pattern of solubility in both octanol and butanol, with generally higher Log P values in butanol. The two complexes [In.9N3P3Ph3] and [In.9N3P3Bz3] both have positive Log P values. These same two complexes are those which exhibit the highest percentage hepatobiliary clearance in mice. A plot of the relationship between the Log P value in butanol/water and the % dose in the total gut at 1 hour post injection for the six indium macrocycles (figure 4.33.) reveals a correlation (R^2 by linear regression) of 0.89. Thus for these neutral indium complexes the higher their lipophilicity the greater the hepatobiliary clearance. This agrees with the pattern seen for the gadolinium complexes (section 2.5). However, it would be expected that these

neutral indium complexes are using a different transporter site in the hepatocytes from the 'anionic transporter' used by BSP and $[Gd.12N4P4Bz4]^-$.

4.5. COMPARISON OF CLEARANCE PATHWAY AND IN VIVO STABILITY OF GALLIUM AND INDIUM MACROCYCLE COMPLEXES.

The 7 macrocycles listed below were complexed with either gallium (III) or indium (III). The full biodistribution data for these complexes has been given in sections 4.2 and 4.3. Here only the total gut dose at 1 hour and the blood, liver and skeletal doses at 24 hours are examined. Figures 4.34 to 4.37 give the comparative % doses in these tissues for both the gallium and indium complexes.

Key to Figures in this Section.

Number in Figures	Macrocycle
1.	9N3
2.	9N3Me3C3
3.	9N3C3Ph3
4.	9N3P3Me3
5.	9N3P3iPr3
6.	9N3P3Ph3
7.	9N3P3Bz3

From figures 4.34 to 4.37 and table 4.4 it can be seen that the amount of complex which clears via the hepatobiliary pathway follows a similar pattern for both the gallium and indium complexes.

Figure 4.34. *Comparison of the % Dose in the Total Gut at 1 Hour.*
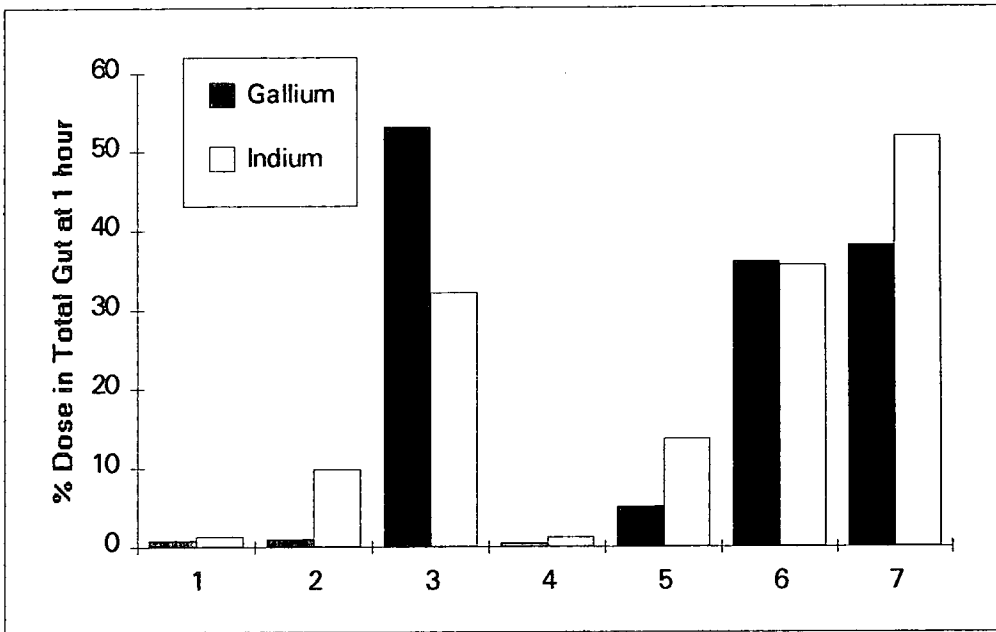
Figure 4.35. *Comparison of the % Dose in the Blood at 24 Hours.*
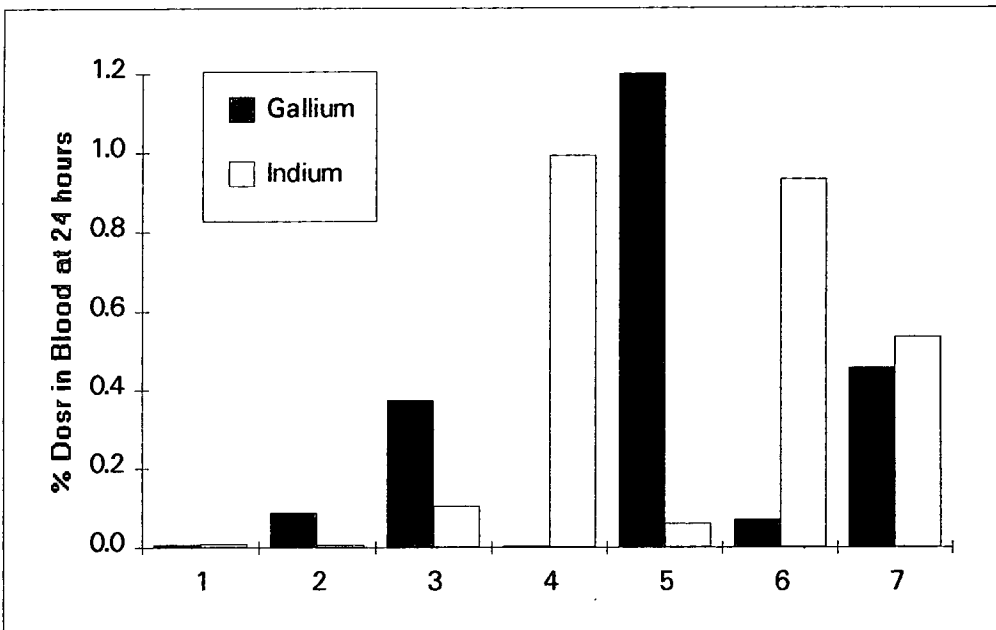
Figure 4.36. *Comparison of the % Dose in the Liver at 24 Hours.*
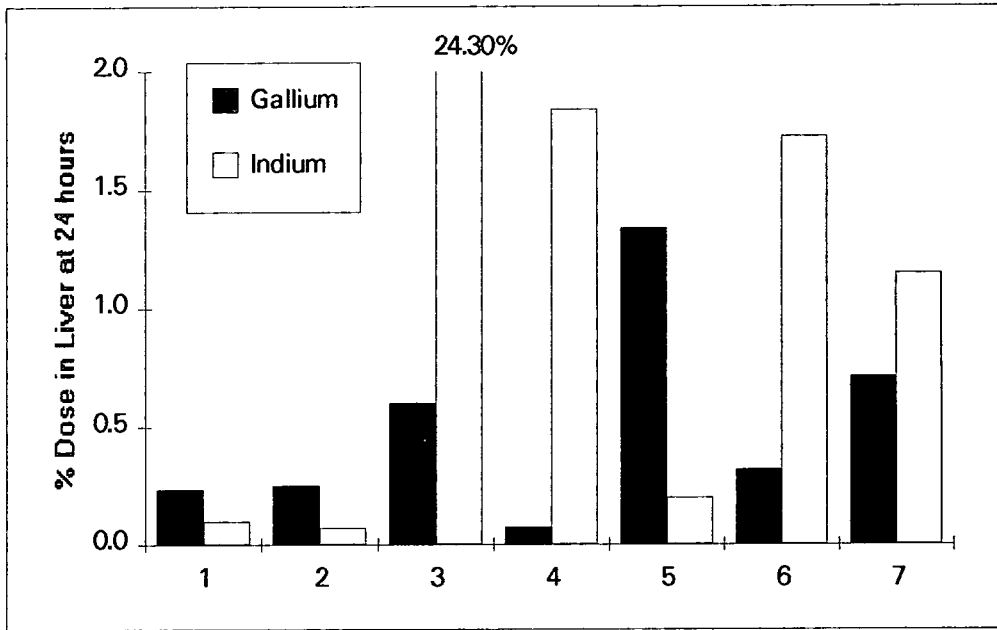
Figure 4.37. *Comparison of the % Dose in the Skeleton at 24 Hours.*
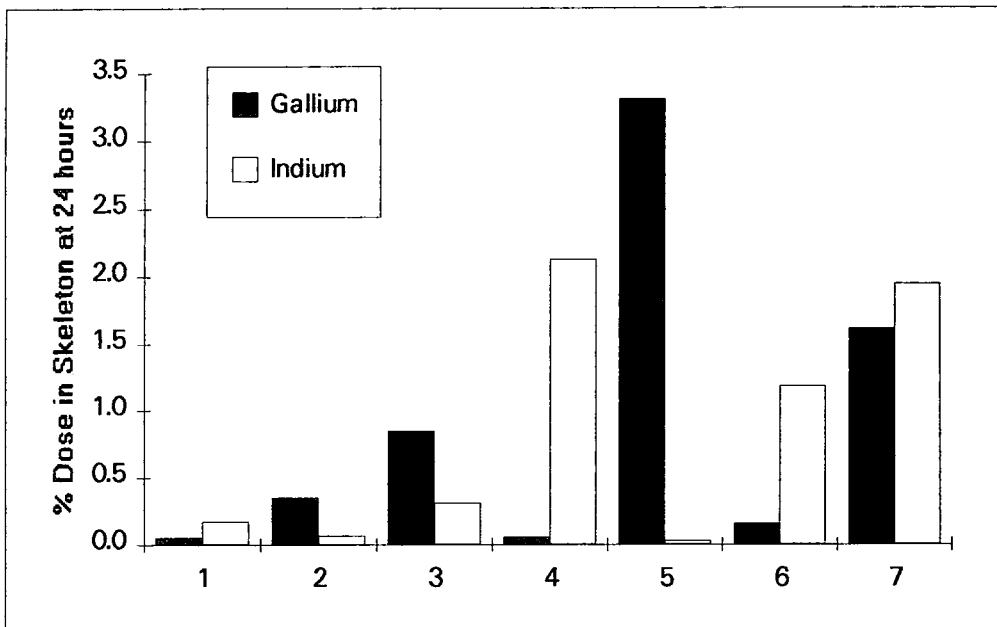
Table 4.4. *Summary of In Vivo Clearance and Stability of Gallium and Indium Complexes.*

Complex Number		Hepatobiliary Clearance		In Vivo Stability	
		Ga	In	Ga	In
1.	9N3	0	0	+++	+++
2.	9N3Me3C3	0	+	+++	+++
3.	9N3C3Ph3	+++	+++	-	---
4.	9N3P3Me3	0	0	+++	---
5.	9N3P3iPr3	+	+	---	+++
6.	9N3P3Ph3	+++	+++	+++	---
7.	9N3P3Bz3	+++	+++	---	---

The in vivo stability measurements show that the gallium and indium complexes with the ligands 9N3 and 9N3Me3C3 are stable in vivo. [Ga.9N3C3Ph3] shows some dissociation in vivo but is more stable than the [In.9N3C3Ph3] complex. [Ga.9N3P3Me3] and [Ga.9N3P3Ph3] are both stable in vivo whereas the corresponding indium complexes are not. Both the gallium and indium complexes of 9N3P3Bz3 are unstable in vivo.

These in vivo measurements agree well with previous in vitro measurements (see section 4.1.6). [Ga.9N3], [In.9N3], [Ga.9N3P3Me3] and [Ga.9N3Me3C3] having shown high resistance to acid-catalysed dissociation[28,57,60]. The general trend that gallium forms more stable complexes with 9N3 type ligands than indium (see sections 4.1.4 to 4.1.6) also holds with the exception of 9N3P3iPr3.

In conclusion, the complexes [Ga.9N3], [Ga.9N3Me3C3], [Ga.9N3P3Me3], [In.9N3] and [In.9N3Me3C3] are all stable neutral complexes with potential for in vivo imaging. The complex [Ga.9N3P3Ph3] is the most promising candidate for hepatobiliary imaging with a high in vivo stability. [67]Ga or ^{111}In labelled complexes are potentially useful with SPECT, ^{68}Ga with PET or [71]Ga in NMR imaging.

4.6. TUMOUR LOCALISATION OF GALLIUM AND INDIUM MACROCYCLE COMPLEXES.

4.6.1. Introduction

In this section the biodistribution and tumour uptake of gallium and indium macrocycle complexes are examined in mice bearing xenografts of the human melanotic melanoma HX118.

The γ-emitting isotopes of gallium and indium (^{67}Ga and ^{111}In) utilised here for the determination of biodistributions have the potential of tumour imaging in vivo by SPECT. There is also the possibility of using other isotopes of gallium for alternative imaging techniques. For example, radioactive ^{68}Ga for PET, or stable ^{71}Ga for nuclear magnetic resonance imaging.

For the visualisation of tumour tissue by any of these imaging techniques it is the contrast between the concentration of the labelled complex in the tumour to that of the surrounding tissues (particularly blood) which is important, rather than just the total amount of tumour uptake. To this end it is the % dose/g of tissue and particularly the ratio of the tumour % dose/g to the blood % dose/g which is of significance in this study.

The biodistribution and tumour uptake of the gallium 9N3 complex is studied at 1, 2, 4, 8, and 24 hours post injection (figures 4.38 and 4.39). The corresponding indium 9N3 complex is studied at 1, 2 and 4 hours post injection (figures 4.40 and 4.41). Biodistribution and tumour uptake of two further gallium complexes, [Ga.9N3P3Me3] and [Ga.9N3C3Ph3], together with [Ga.Citrate] are also examined at 4 hours post injection (figures 4.42 and 4.43).

A comparison of the tumour to blood ratios for all 5 complexes is given in figure 4.44. Finally a comparison of [Ga.9N3] biodistribution in both normal and HX118 tumour bearing mice is made (figure 4.45).

4.6.2. Biodistribution of Complexes in HX118 Tumour Bearing Mice.

[Ga.9N3]

The biodistribution of [Ga.9N3] in HX118 tumour bearing mice is given in figures 4.38 and 4.39. The fastest drop in % dose/g of tissue with time is for the blood. The slower rate of loss of [Ga.9N3] from the tumour tissue leads to a high tumour to blood ratio (figure 4.44.). Between 2 and 24 hours post injection the tumour to blood ratio for [Ga.9N3] is in excess of 12, peaking to a value of 22 at 4 hours and then slowly declining with time. At 4 hours the ratios kidney to blood and liver to blood are about twice that of tumour to blood.

Figures 4.45 (a), (b) and (c) compare the biodistribution data for [Ga.9N3] in both normal and HX118 tumour mice at 1, 4 and 24 hours. Differences between the two groups in the amount of dose present in the kidney, liver and gut can be attributed to the variation in excretion rate between individual animals. The most important comparison is at 24 hours (figure 4.45 (c)), this shows that the % dose in the skeleton is as low in the tumour mice as in normal mice confirming the high in vivo stability of [Ga.9N3].

[In.9N3]

Figures 4.40 and 4.41 show the biodistribution of [In.9N3] over 1, 2 and 4 hours. As was seen for [Ga.9N3], the tumour to blood ratio is greatest at 4 hours post injection (figure 4.44). However, this tumour to blood ratio of 12 is only about half the concentration achieved with [Ga.9N3]. The [In.9N3] does have a lower tumour to liver ratio than [Ga.9N3], with a concentration of about 3 times more complex in the tumour than in the liver at 4 hours.

A comparison of the % dose/g at 4 hours with that of the other complexes examined (figure 4.42) demonstrates that [In.9N3] has a larger % dose/g in the tumour than any of the

other complexes except [Ga.Citrate]. However with [Ga.Citrate] this is also true for the % dose in the skeleton demonstrating the much more unstable nature of this complex.

[Ga.9N3P3Me3], [Ga.9N3C3Ph3] and [Ga.Citrate].

The biodistribution at 4 hours of [Ga.9N3P3Me3], [Ga.9N3C3Ph3] and [Ga.Citrate] are plotted in figures 4.42 and 4.43 along with that of [In.9N3] and [Ga.9N3].

By 4 hours [Ga.9N3P3Me3] has virtually cleared from all the tissues except for small amounts in the kidney and gut. The % dose/g tumour is the lowest of all the complexes. The tumour to blood ratio is also low (figure 4.44).

The majority of the complex [Ga.9N3C3Ph3] is being cleared by the hepatobiliary route, however the blood level at 4 hours is still high reflecting the low in vivo stability of this complex as already demonstrated in section 4.2. The % dose in the tumour and the tumour to blood ratio for [Ga.9N3C3Ph3] are both very low.

The highly unstable complex [Ga.Citrate] has high blood, tumour and gut levels. When the tumour to blood ratio is calculated (figure 4.44), this value is the lowest seen.

4.6.3. Conclusion.

Of the complexes measured [Ga.9N3] gives the best tumour to blood contrast. This is obtained at 4 hours post injection when a tumour to blood ratio of 22 is seen. At this time the concentration of [Ga.9N3] in the tumour exceeds that in all the other tissues examined with the exception of the kidney and liver.

The fast blood clearance and low % dose in the skeleton at 24 hours are indicators of the high in vivo stability of the [Ga.9N3] complex. Thus the concentration of gallium seen in the tumour must be due to differential retention of the complex rather than from uptake of uncomplexed gallium as is utilised in gallium citrate imaging (see section 4.1.2).

Figure 4.38. % Dose/g of [Ga.9N3] in HX118 Tumour Bearing Mice 1 to 24 Hours Post Injection.
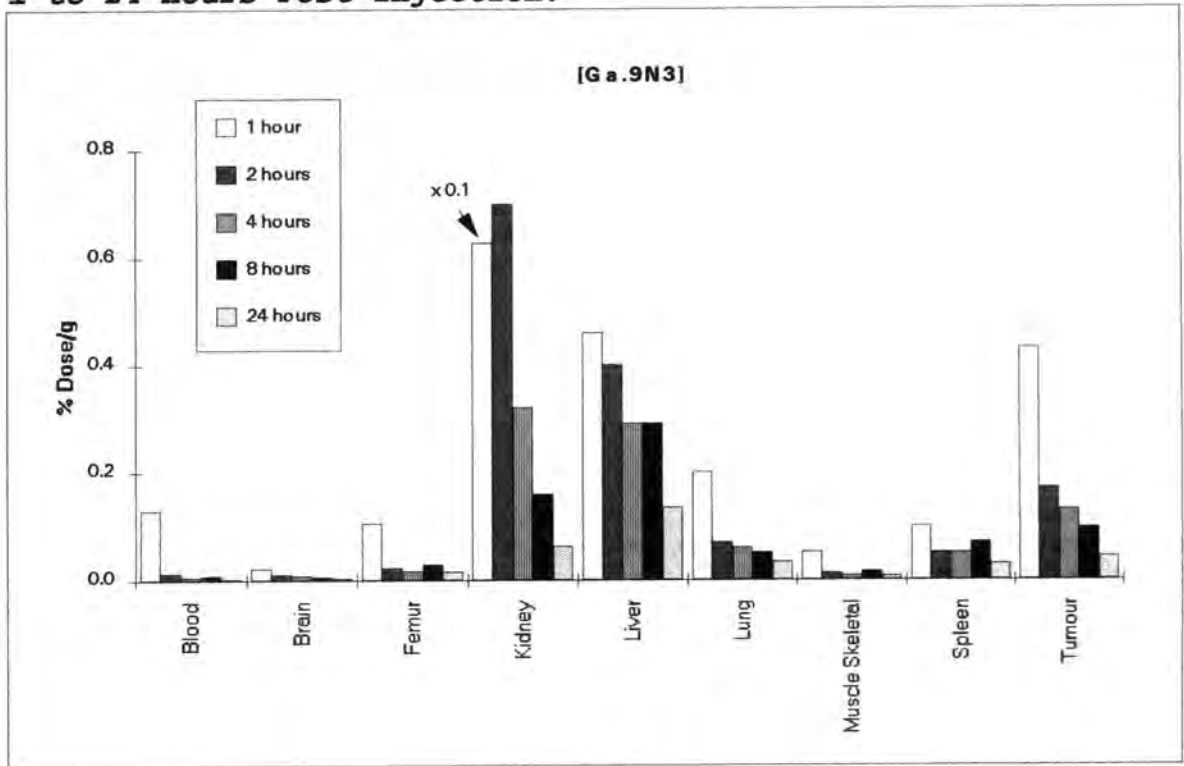
Figure 4.39. % Dose of [Ga.9N3] in HX118 Tumour Bearing Mice 1 to 24 Hours Post Injection.
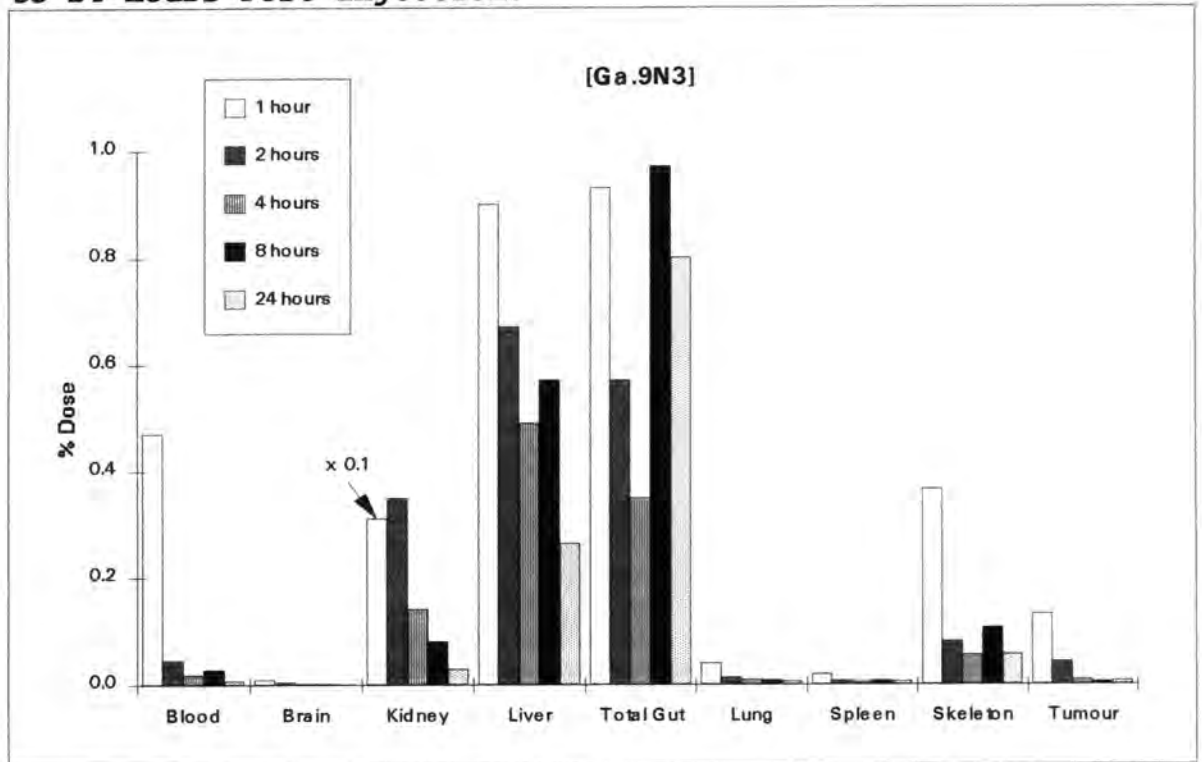
Figure 4.40. % Dose/g of [In.9N3] in HX118 Tumour Bearing Mice 1 to 4 Hours Post Injection.
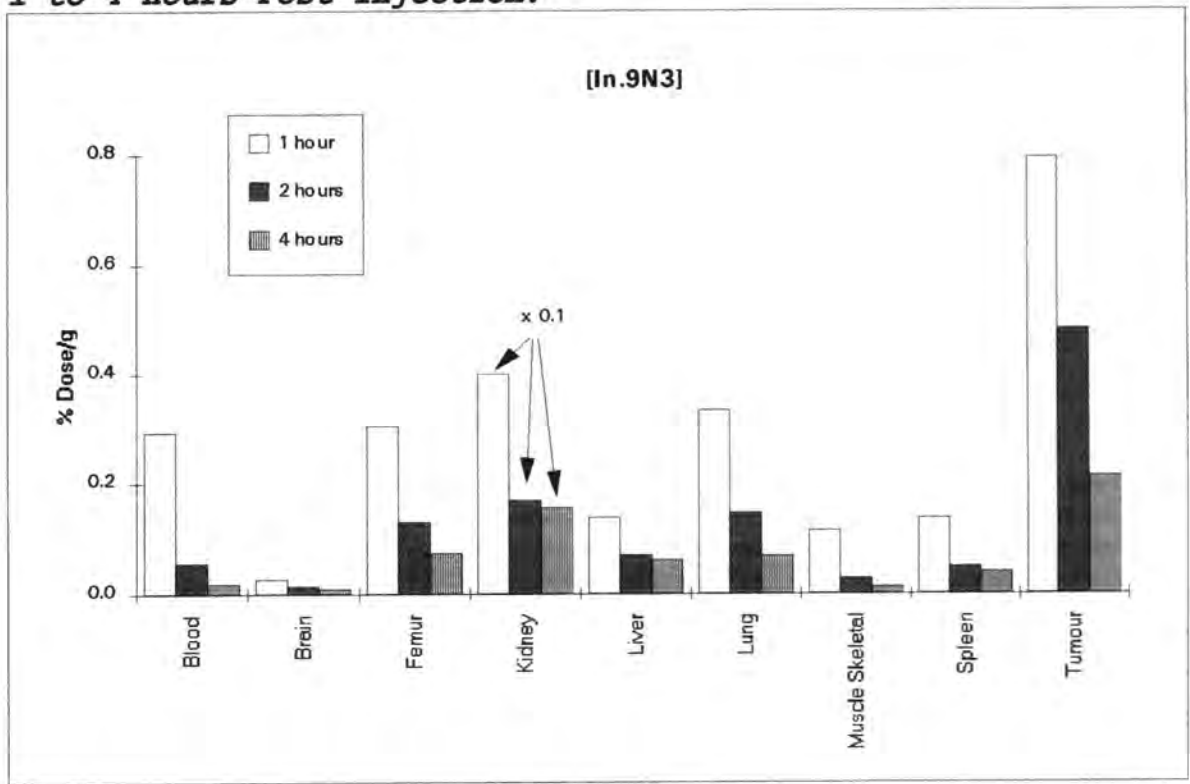
Figure 4.41. % Dose of [In.9N3] in HX118 Tumour Bearing Mice 1 to 4 Hours Post Injection.
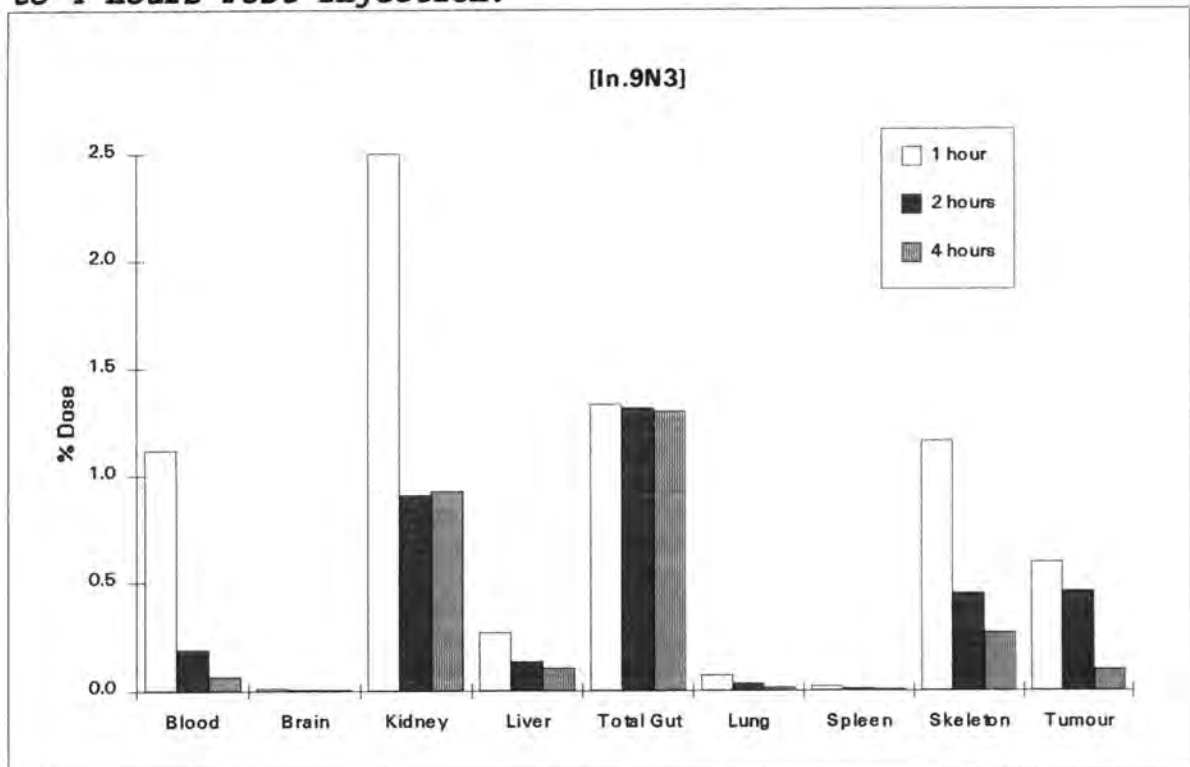
Figure 4.42. *% Dose/g of Gallium and Indium Macrocycles in HX118 Tumour Bearing Mice at 4 Hours Post Injection.*
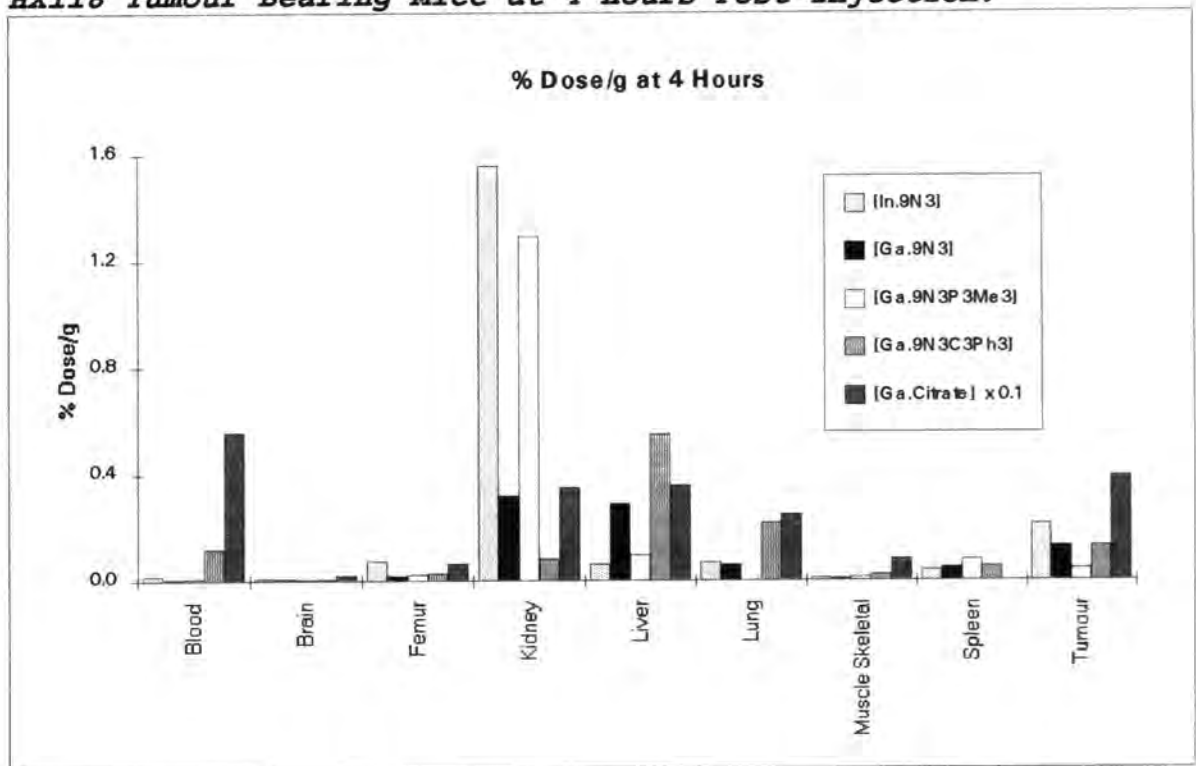
Figure 4.43. *% Dose of Gallium and Indium Macrocycles in HX118 Tumour Bearing Mice at 4 Hours Post Injection.*
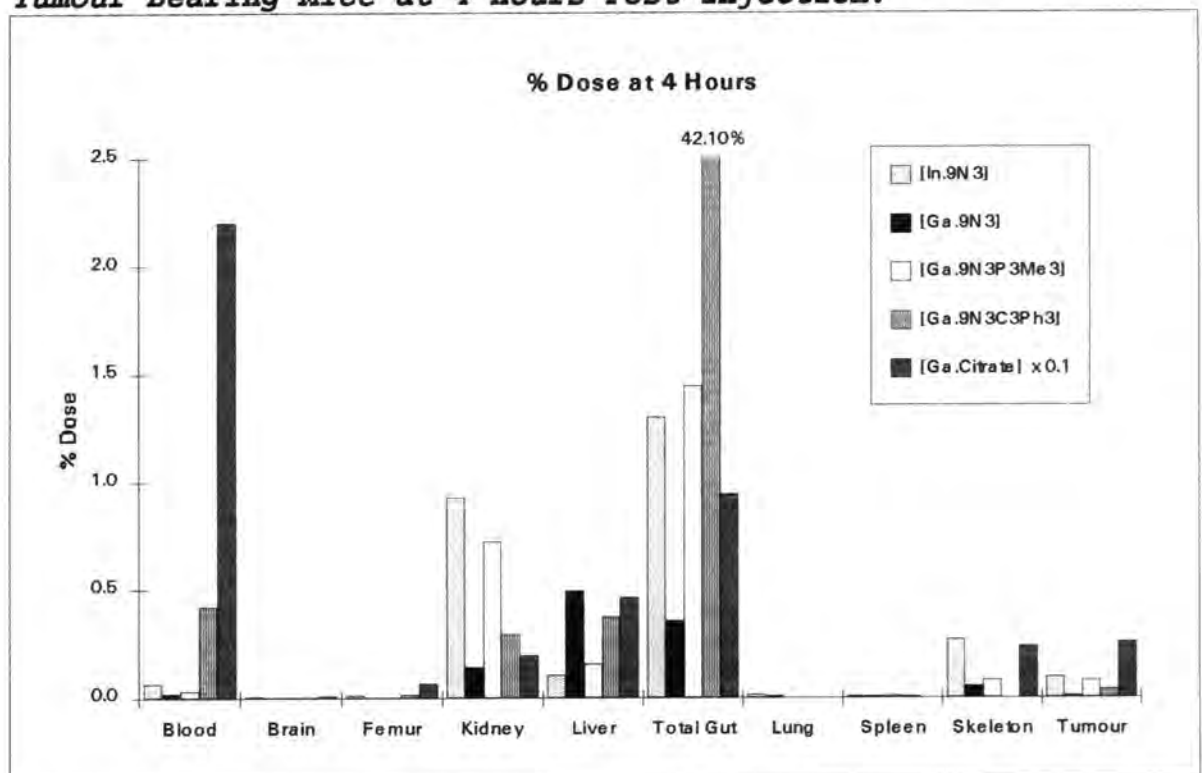
Figure 4.44. *Tumour to Blood Ratios of % Dose/g of Gallium and Indium Macrocycles.*
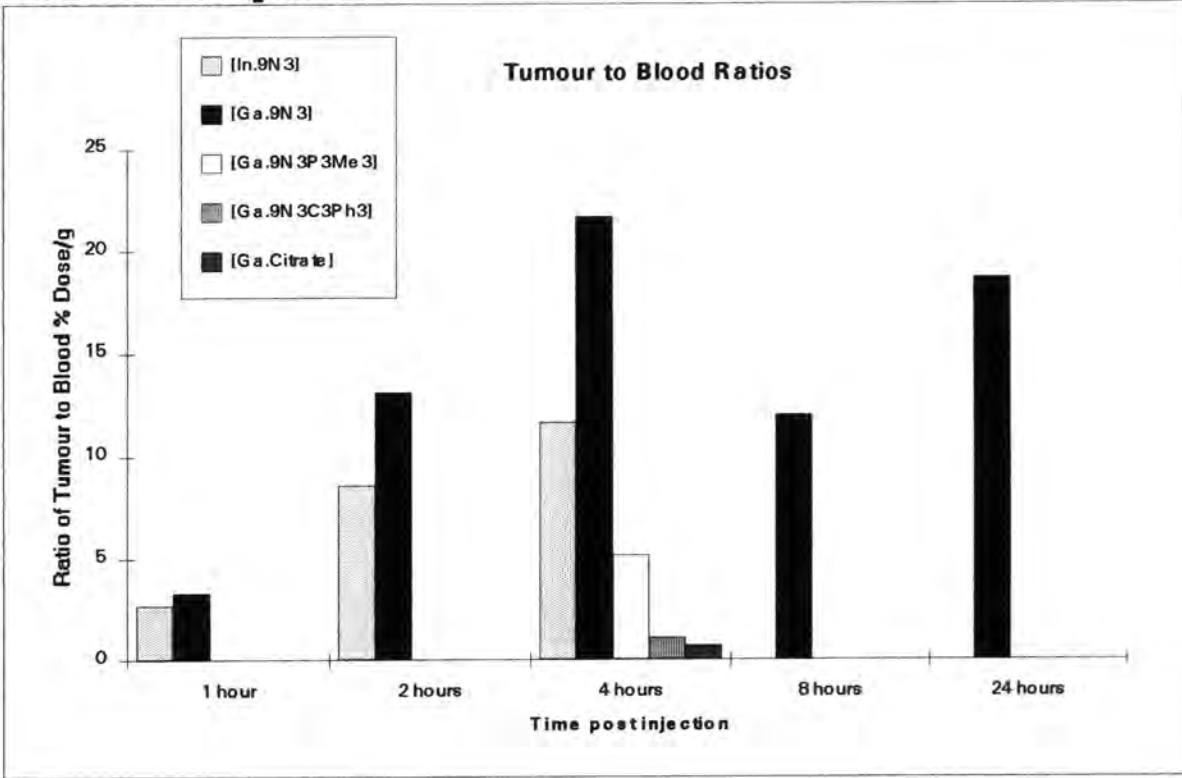
Figure 4.45 (a). *Comparison of % Dose/g and % Dose of [Ga.9N3] in Normal and HX118 Tumour Bearing Mice at 1 Hour Post Injection.*
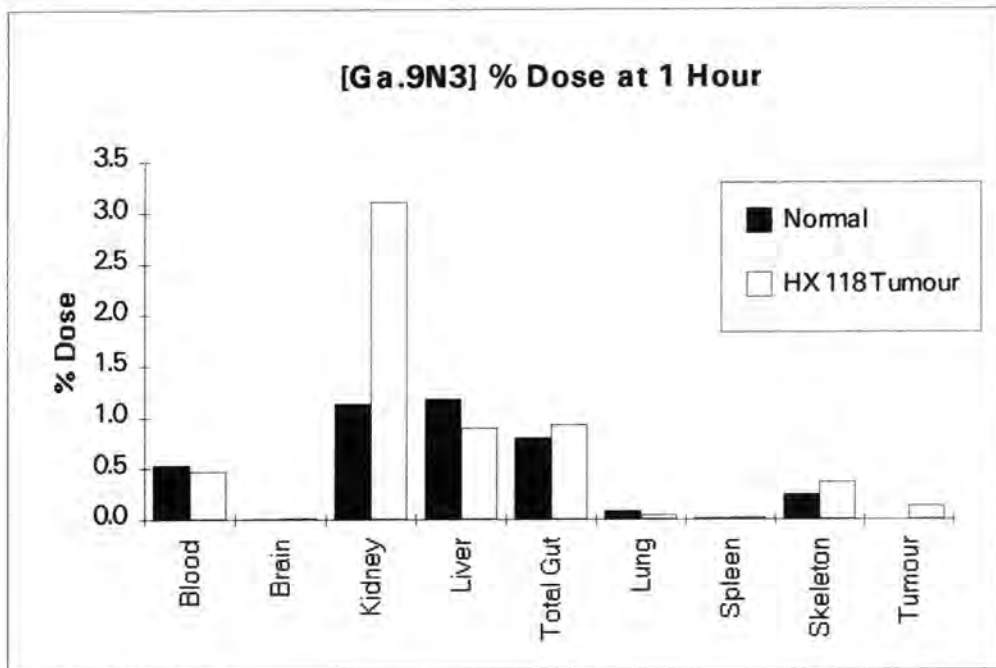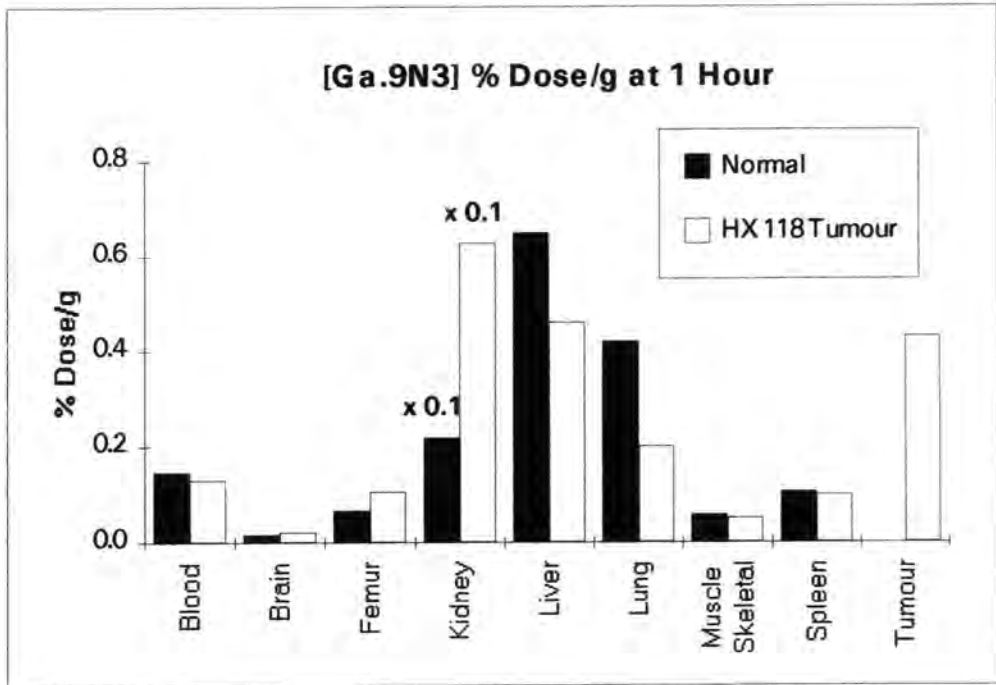
Figure 4.45 (b). Comparison of % Dose/g and % Dose of [Ga.9N3] in Normal and HX118 Tumour Bearing Mice at 4 Hours Post Injection.
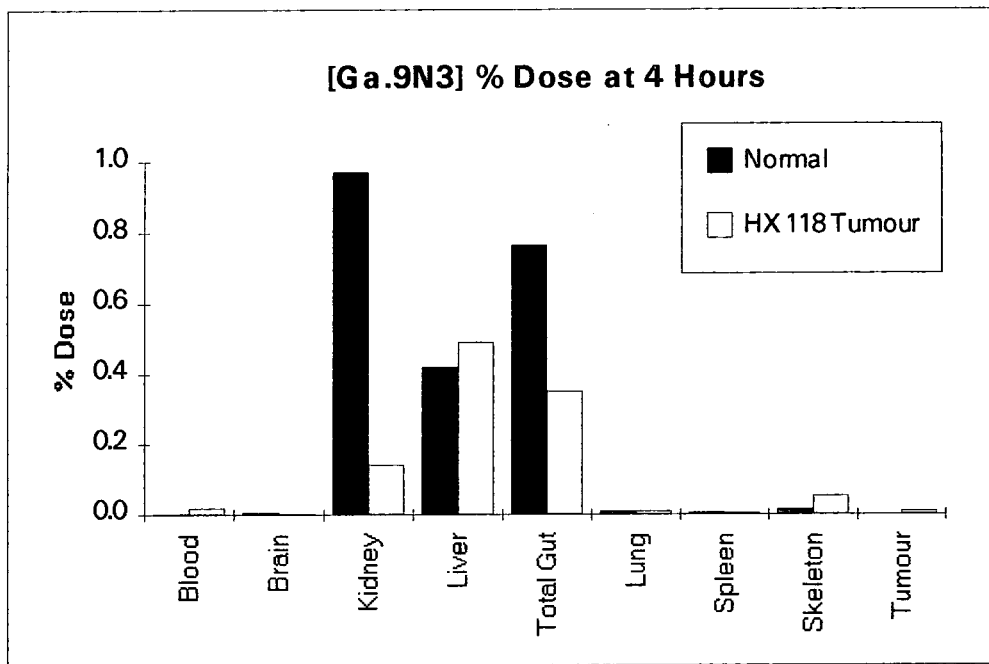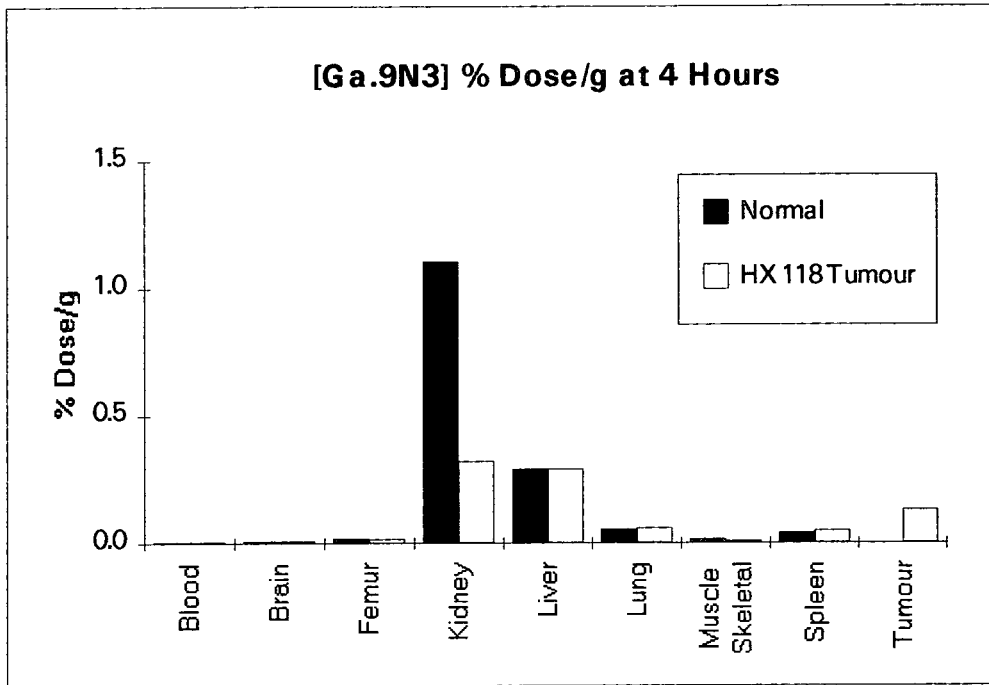
Figure 4.45 (c). *Comparison of % Dose/g and % Dose of [Ga.9N3] in Normal and HX118 Tumour Bearing Mice at 24 Hours Post Injection.*
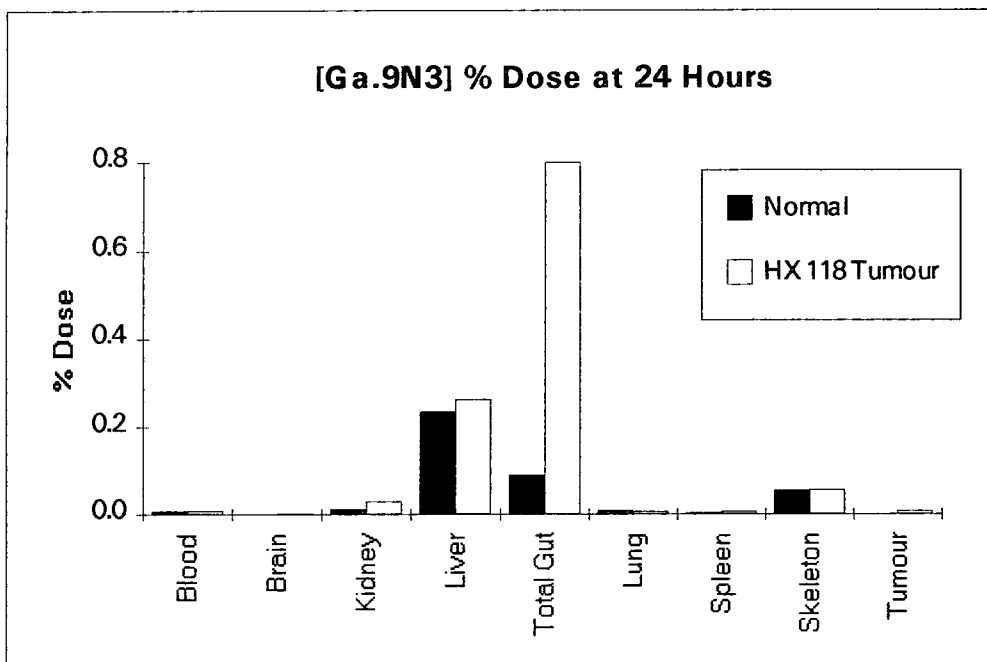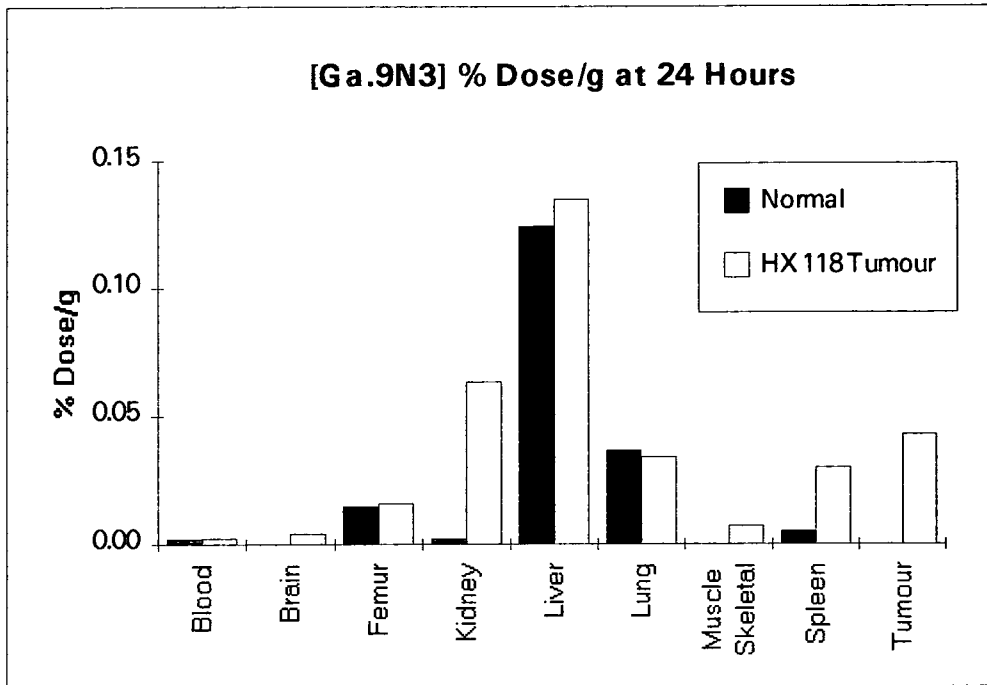
4.7. THE BIODISTRIBUTION OF [Ga.9N3.MISO] IN NORMAL AND TUMOUR BEARING MICE.

4.7.1. Introduction.

Drugs based on 2-nitroimidazoles such as Misonidazole (Miso) (figure 4.46), are well known for localising in areas of hypoxia (low oxygen) in malignant and normal tissues[65]. This localisation arises from the enzymatic reduction of Miso which, at low oxygen levels, forms a metabolite which reacts with and covalently binds to adjacent macromolecules[66]. The radiolabelling of Miso with a γ emitting isotope such as ^{67}Ga or [99m]Tc[67,68] could potentially lead to the imaging of hypoxic areas within the body, in particular the hypoxic regions of tumours. Also by labelling the Miso with a therapeutic isotope, such as the β^- emitter ^{90}Y, there is the possibility of tumour therapy.

In this section the labelling of Miso with [[67]Ga.9N3] is investigated. The tumour used for these experiments is the human melanotic melanoma HX118. This tumour has been shown to accumulate 2-nitroimidazoles[69]. Experiments by L.M. Cobb et al using ^{14}C and ^{3}H labelled Miso[70] showed accumulation of Miso in normal tissues such as the oesophagus, eye lids, liver and lungs in addition to tumour tissue. Normal tissues would not be expected to have areas of hypoxia, except for the liver, and the accumulation of Miso is ascribed to the high levels of reductase activity in these tissues[70].

In these experiments a range of tissues are examined to determine whether the labelled [Ga.9N3.Miso] (figure 4.46) shows any behaviour characteristic of the 2-nitroimidazole moiety. The ability to detect tumours is the ultimate aim of these investigations, therefore the complex [Ga.9N3] is compared to the [Ga.9N3.Miso] as the former complex has already demonstrated high tumour to blood contrast (section 4.6).

Figure 4.46. *Chemical Structures of 9N3.Miso and Misonidazole*
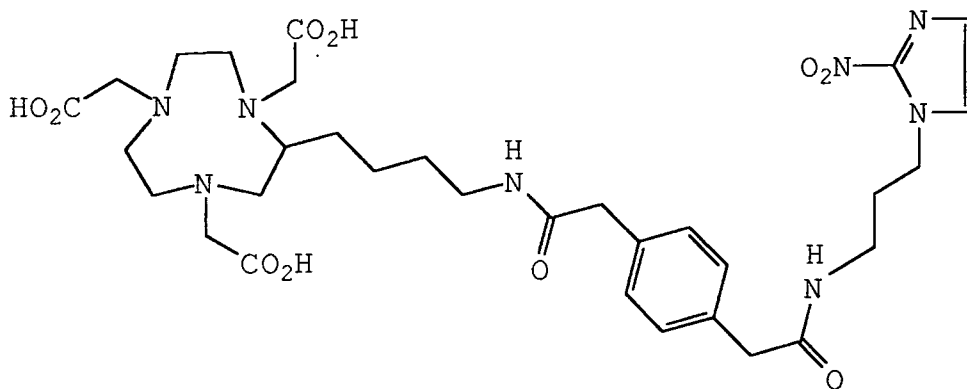
9N3.Miso
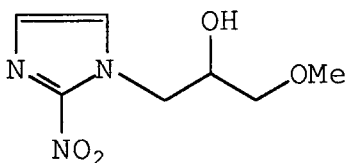
Misonidazole

Presentation of Results.

Figures 4.47 to 4.52 give the % dose and % dose/g from both [Ga.9N3] and [Ga.9N3.Miso] at 4, 8 and 24 hours in mice bearing xenografts of the human melanotic melanoma HX118. Figures 4.53 to 4.56 give the % dose and % dose/g from both [Ga.9N3] and [Ga.9N3.Miso] in normal mice. Tissue to blood ratios are given in figures 4.57 to 4.61.

Figure 4.47. % Dose/g of [Ga.9N3.Miso] and [Ga.9N3] in HX118 Tumour Bearing Mice 4 Hours Post Injection.
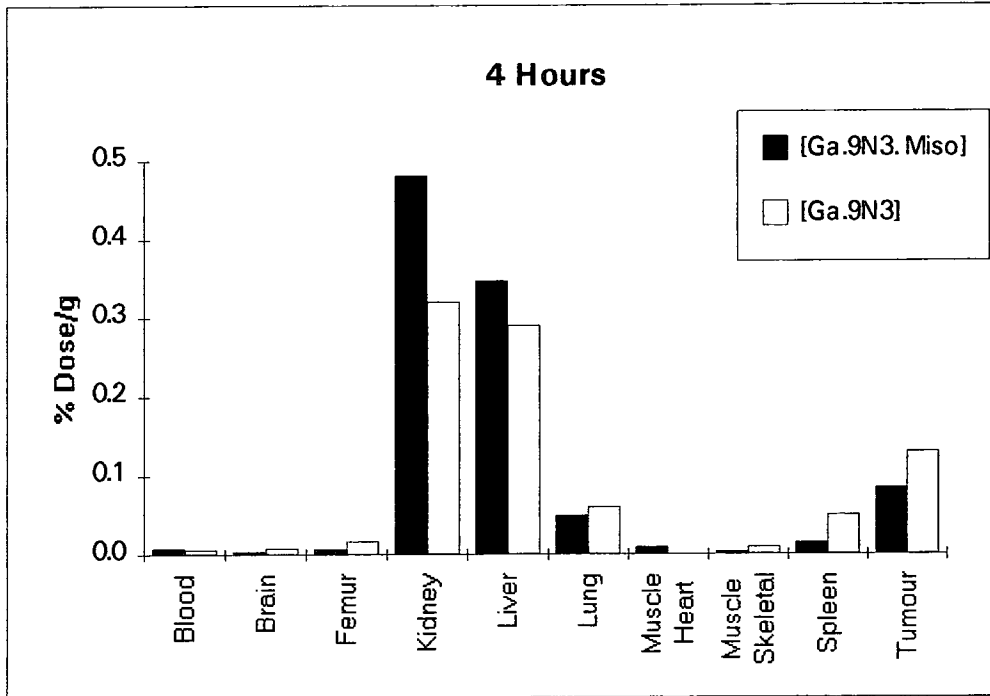
Figure 4.48. % Dose of [Ga.9N3.Miso] and [Ga.9N3] in HX118 Tumour Bearing Mice 4 Hours Post Injection.
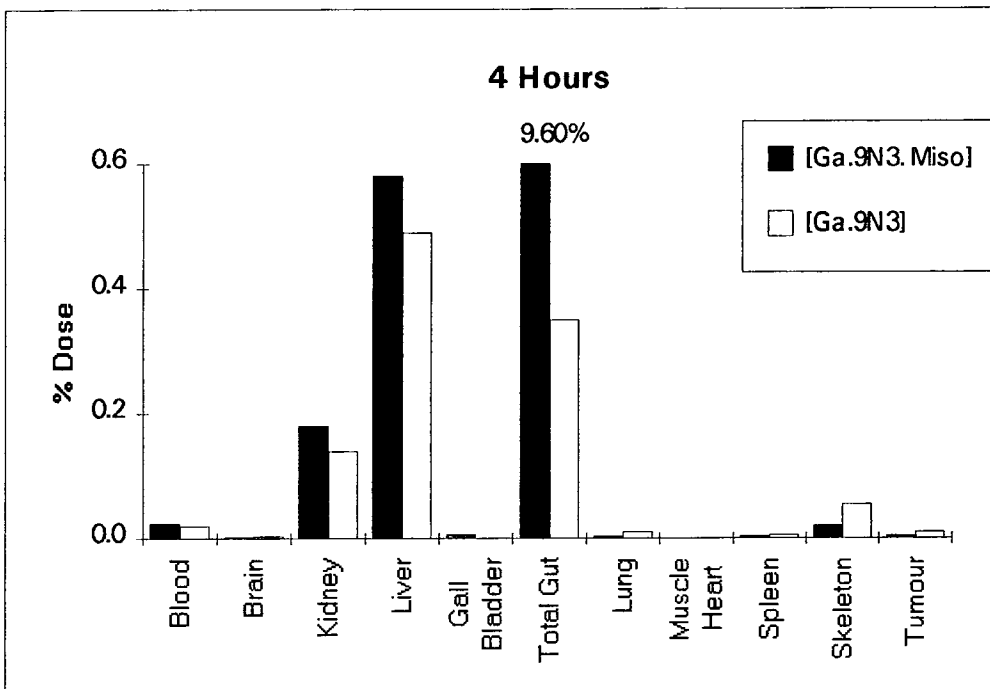
Figure 4.49. % Dose/g of [Ga.9N3.Miso] and [Ga.9N3] in HX118 Tumour Bearing Mice 8 Hours Post Injection.
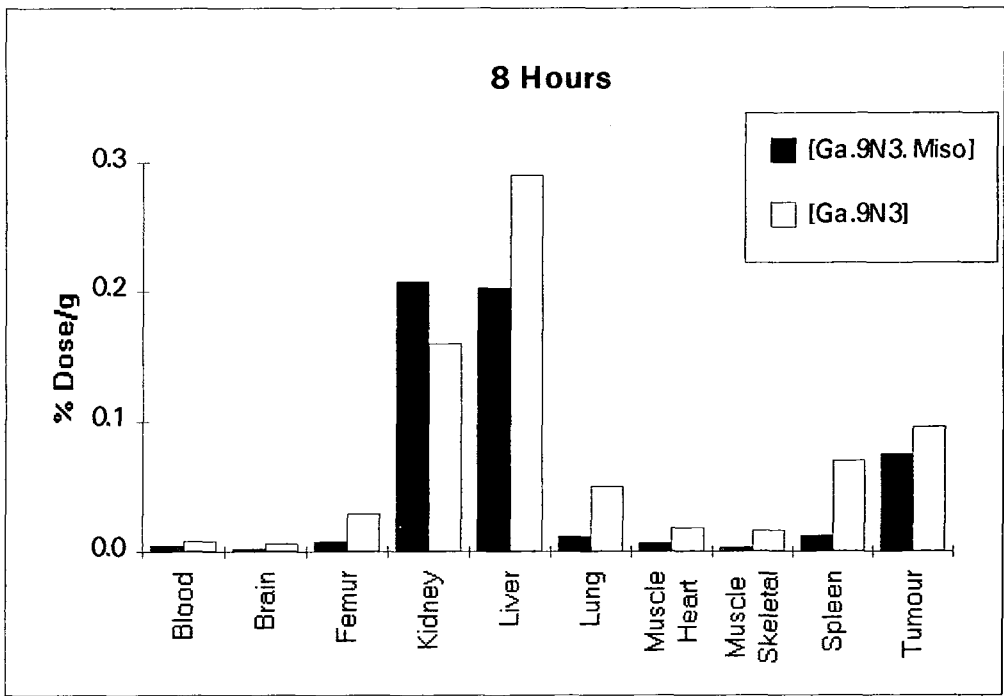
**Figure 4.50. % Dose of [Ga.9N3.Miso] and [Ga.9N3] in HX118 Tumour Bearing Mice 8 Hours Post Injection.**
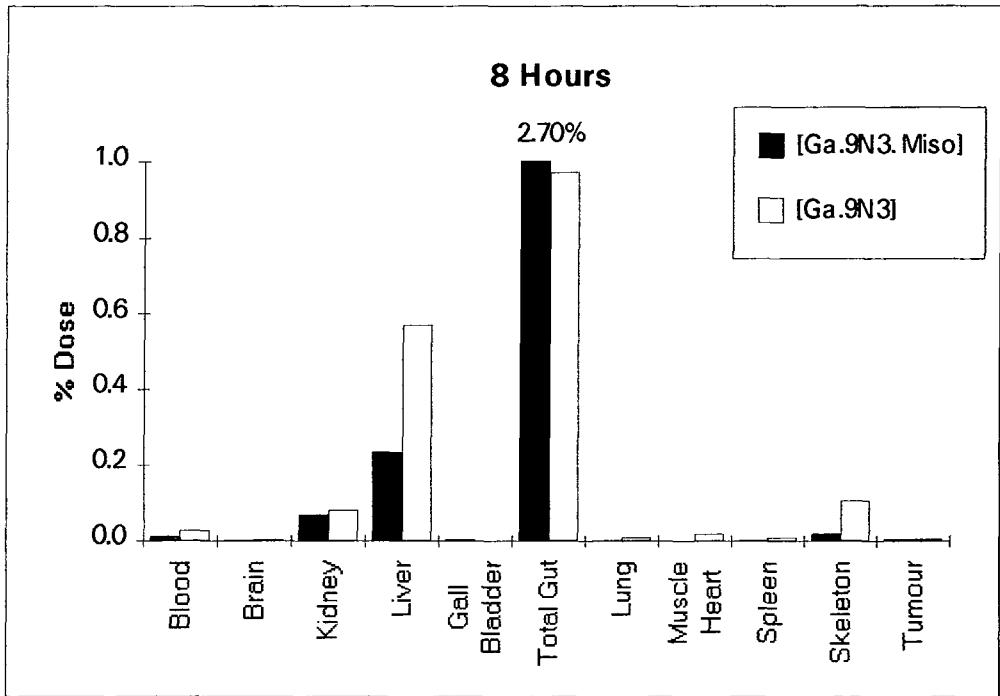
Figure 4.51. *% Dose/g of [Ga.9N3.Miso] and [Ga.9N3] in HX118 Tumour Bearing Mice 24 Hours Post Injection.*
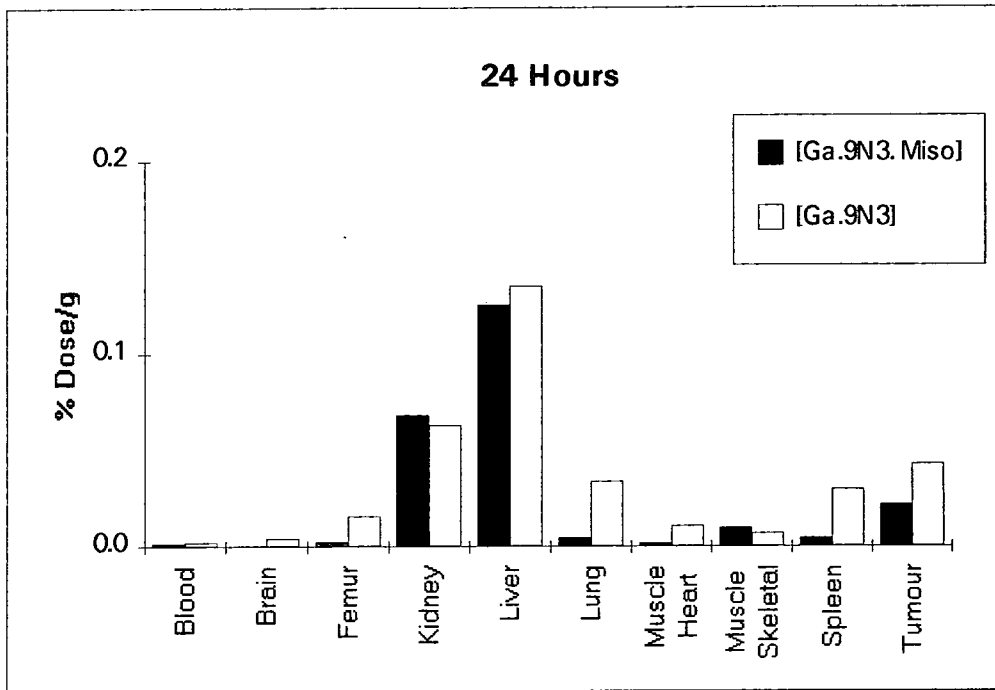
Figure 4.52. *% Dose of [Ga.9N3.Miso] and [Ga.9N3] in HX118 Tumour Bearing Mice 24 Hours Post Injection.*
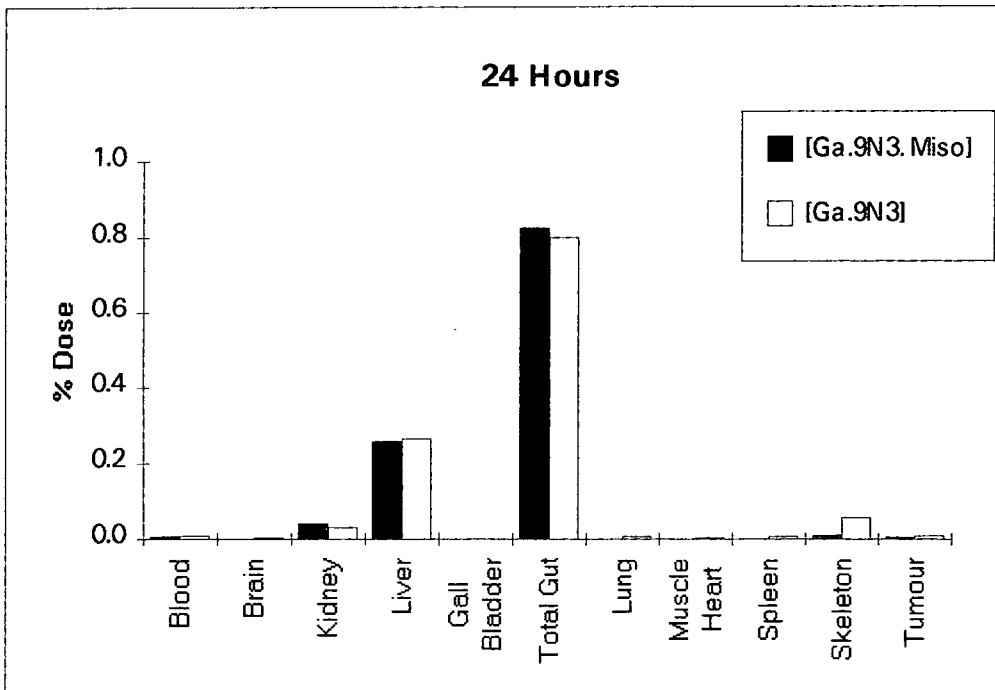
Figure 4.53. % Dose/g of [Ga.9N3.Miso] and [Ga.9N3] in Normal Mice 1 Hour Post Injection.
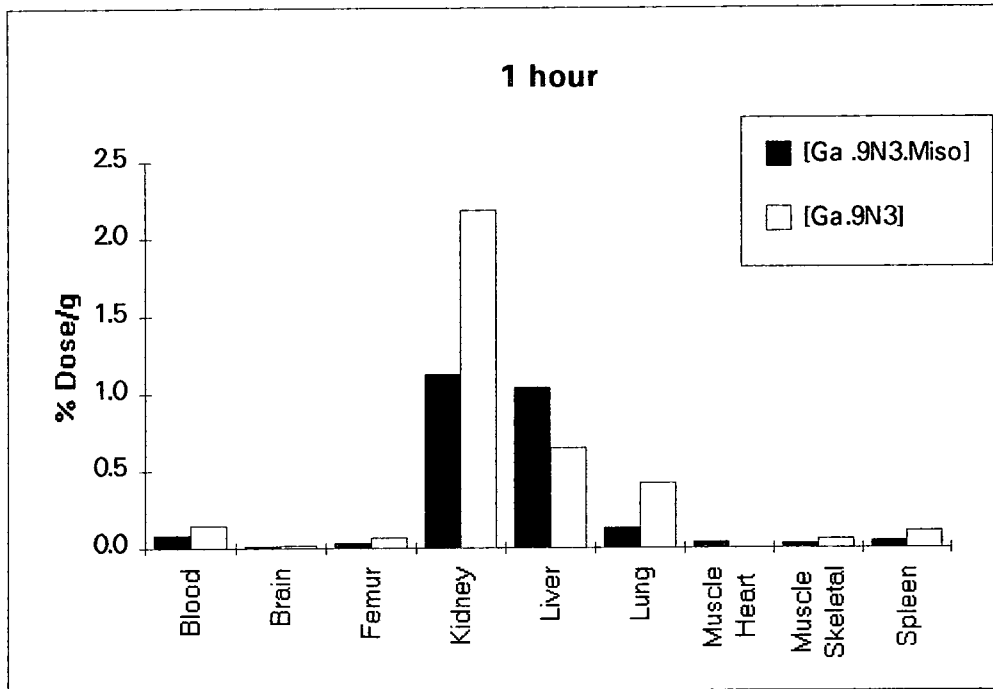
Figure 4.54. % Dose of [Ga.9N3.Miso] and [Ga.9N3] in Normal Mice 1 Hour Post Injection.
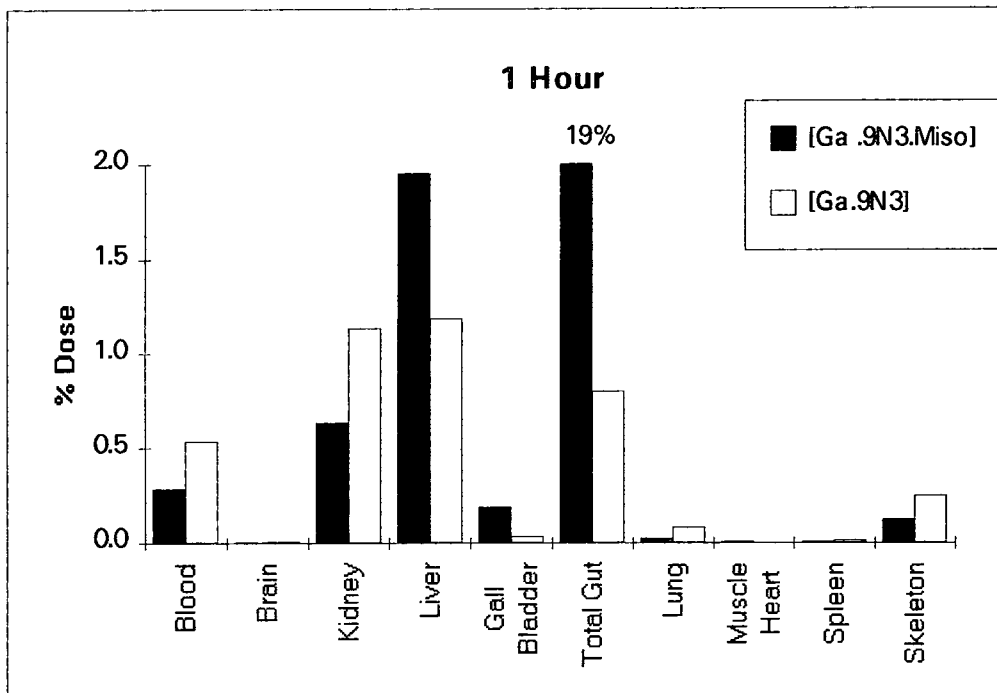
Figure 4.55. *% Dose/g of [Ga.9N3.Miso] and [Ga.9N3] in Normal Mice 24 Hours Post Injection.*
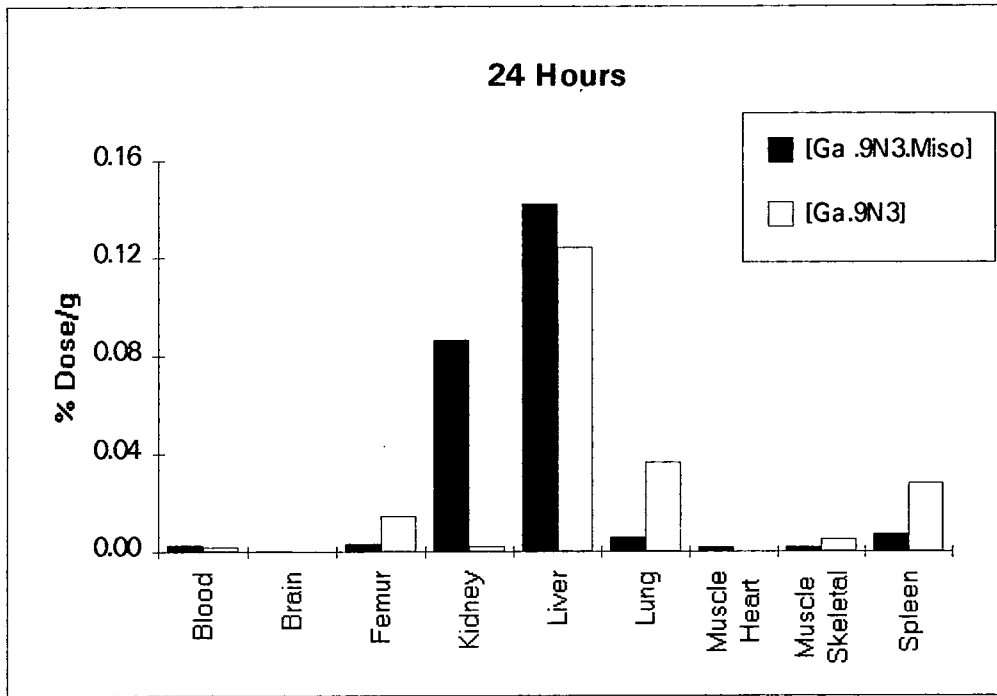
Figure 4.56. *% Dose of [Ga.9N3.Miso] and [Ga.9N3] in Normal Mice 24 Hours Post Injection.*
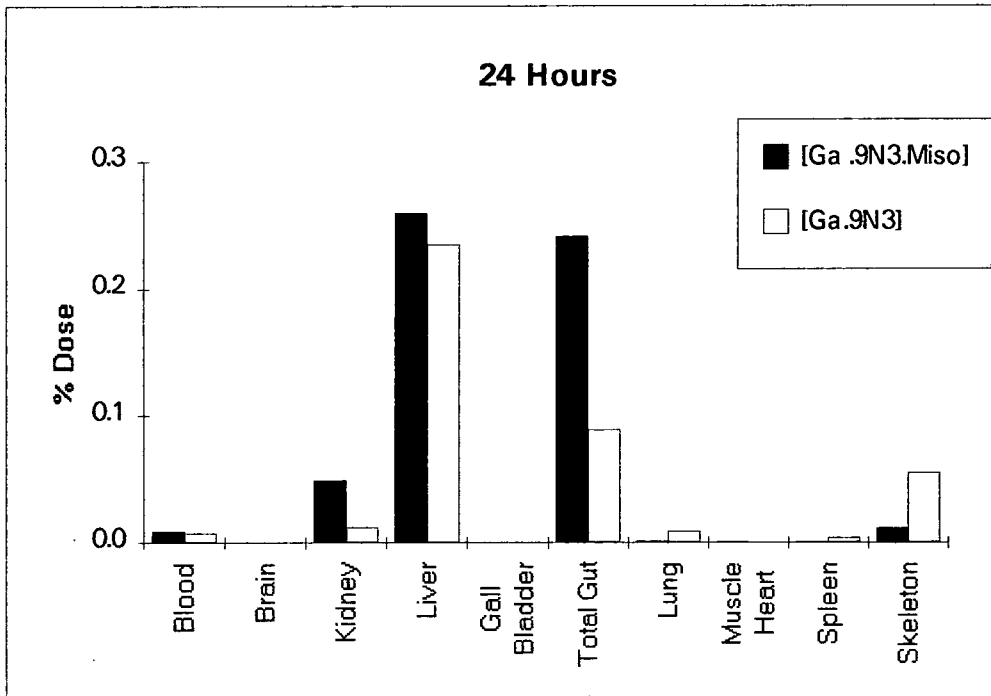
Figure 4.57. *Tissue to Blood Ratio at 4 Hours in HX118 Tumour Bearing Mice.*
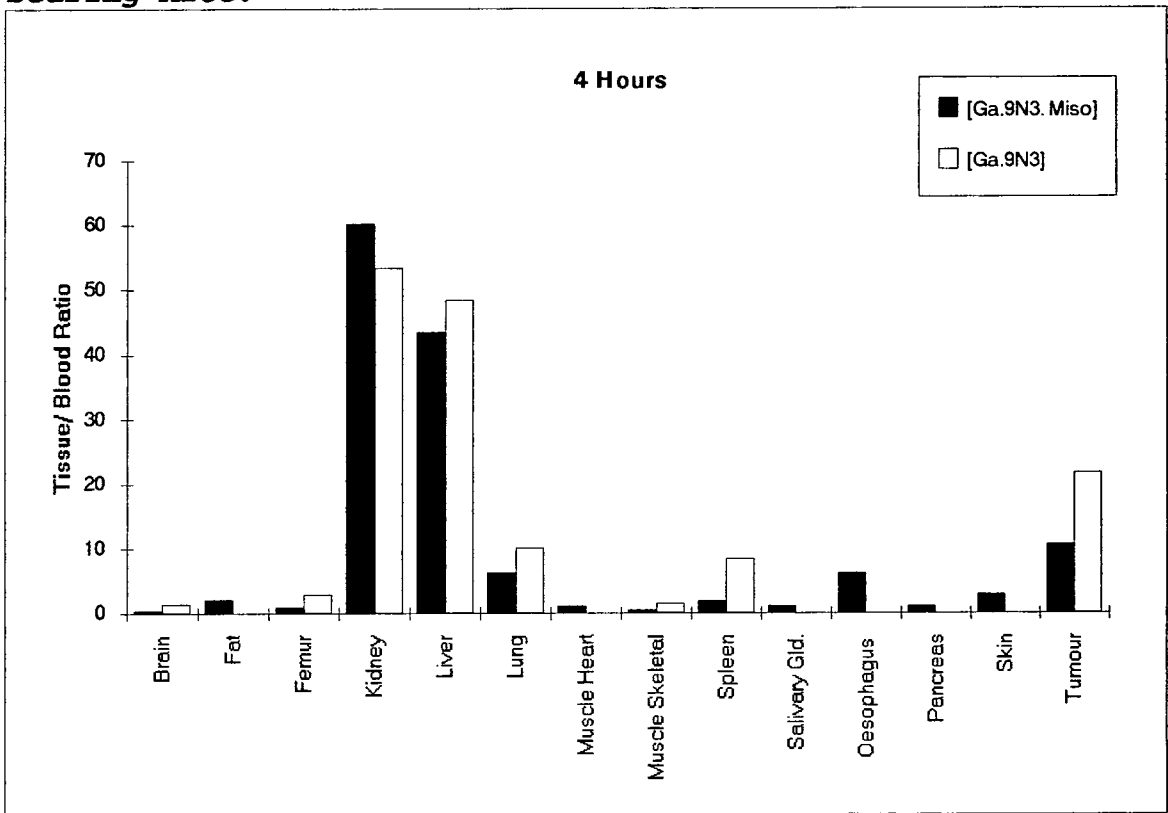
Figure 4.58. *Tissue to Blood Ratio at 8 Hours in HX118 Tumour Bearing Mice.*
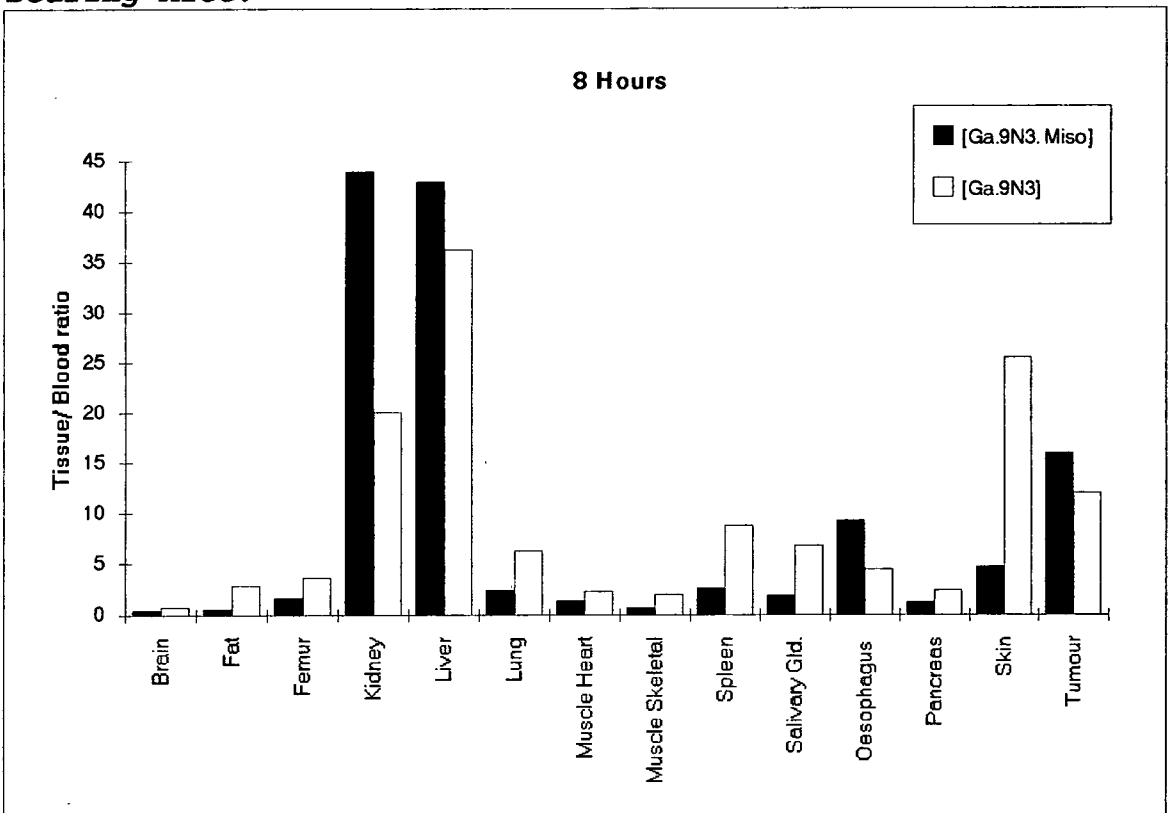
Figure 4.59. *Tissue to Blood Ratio at 24 Hours in HX118 Tumour Bearing Mice.*

24 Hours

Legend:
- [Ga.9N3. Miso]
- [Ga.9N3]

Y-axis: Tissue/ Blood Ratio

X-axis categories: Brain, Fat, Femur, Kidney, Liver, Lung, Muscle Heart, Muscle Skeletal, Spleen, Salivary Gld., Oesophagus, Pancreas, Skin, Tumour
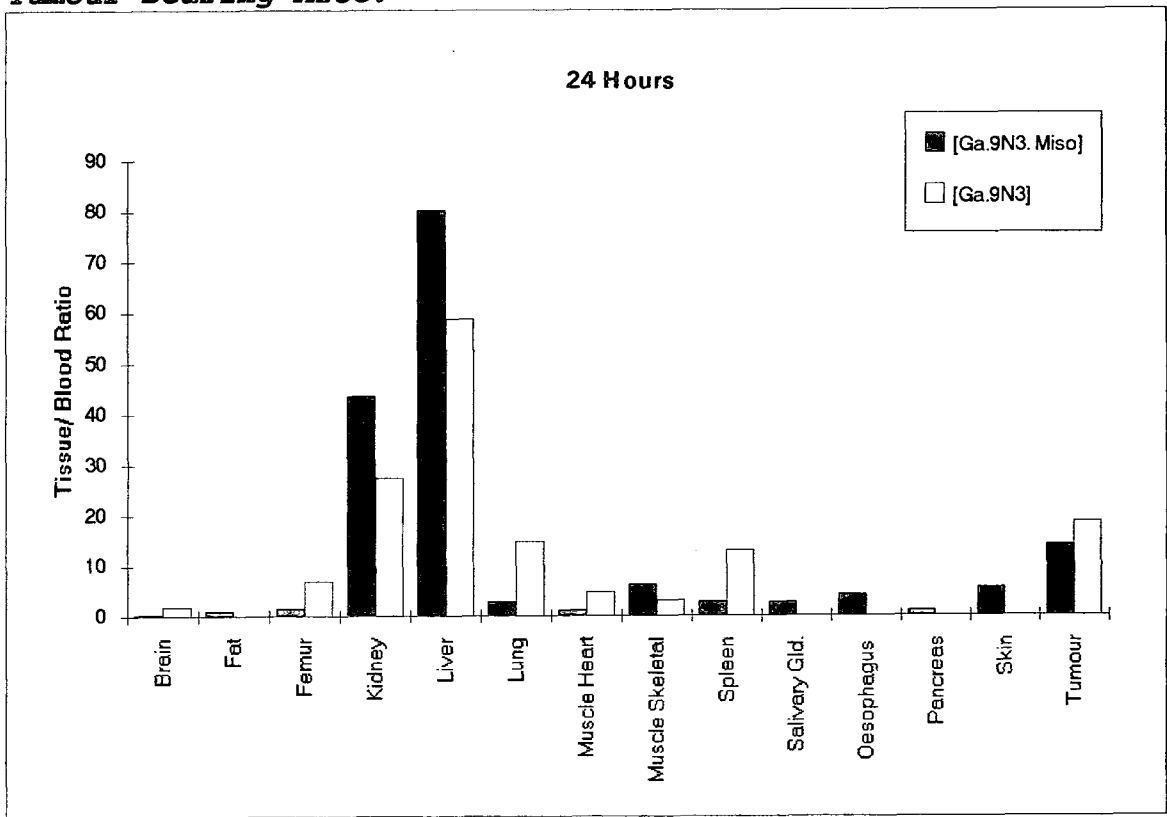
Figure 4.60. *Tissue to Blood Ratio at 1 Hour in Normal Mice.*

1 Hour

Legend:
- [Ga.9N3. Miso]
- [Ga.9N3]

Y-axis: Tissue/ Blood Ratio

X-axis categories: Brain, Fat, Femur, Kidney, Liver, Lung, Muscle Heart, Muscle Skeletal, Spleen, Salivary Gld., eye balls, eye lids, Oesophagus, Pancreas, Skin
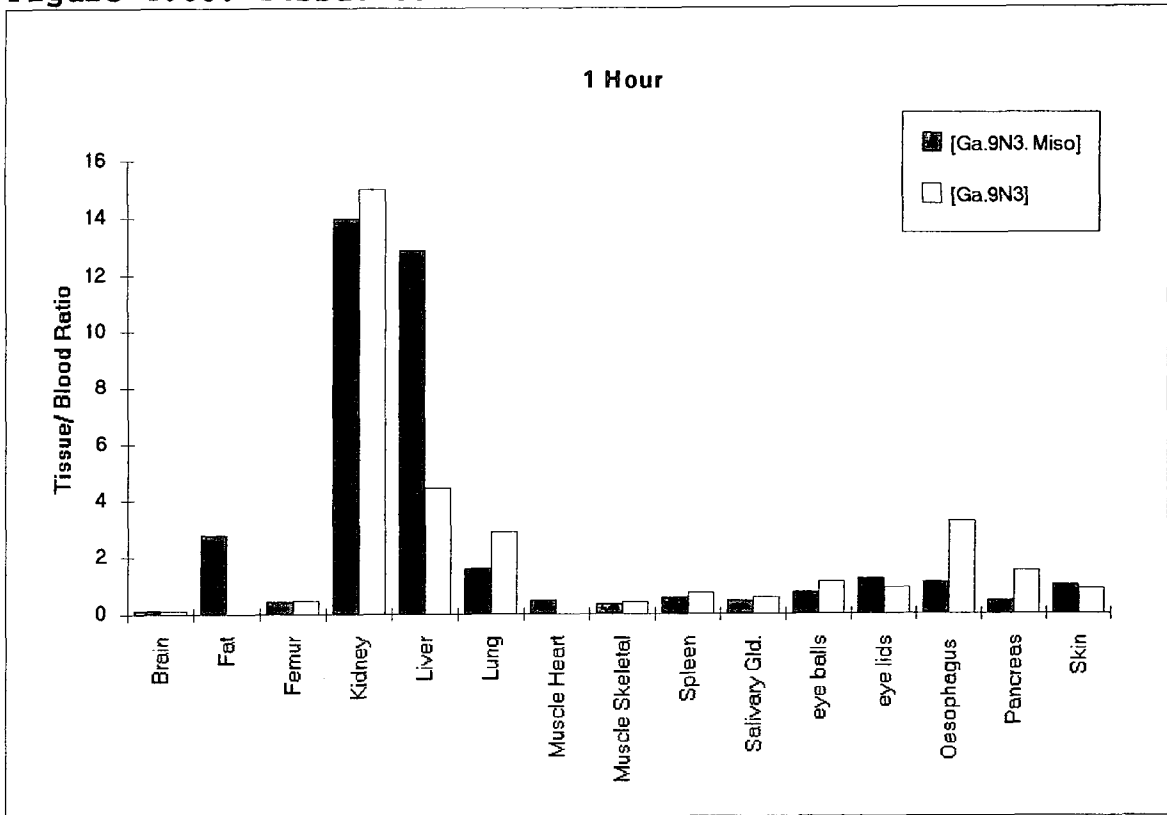
Figure 4.61. *Tissue to Blood Ratio at 24 Hours in Normal Mice.*
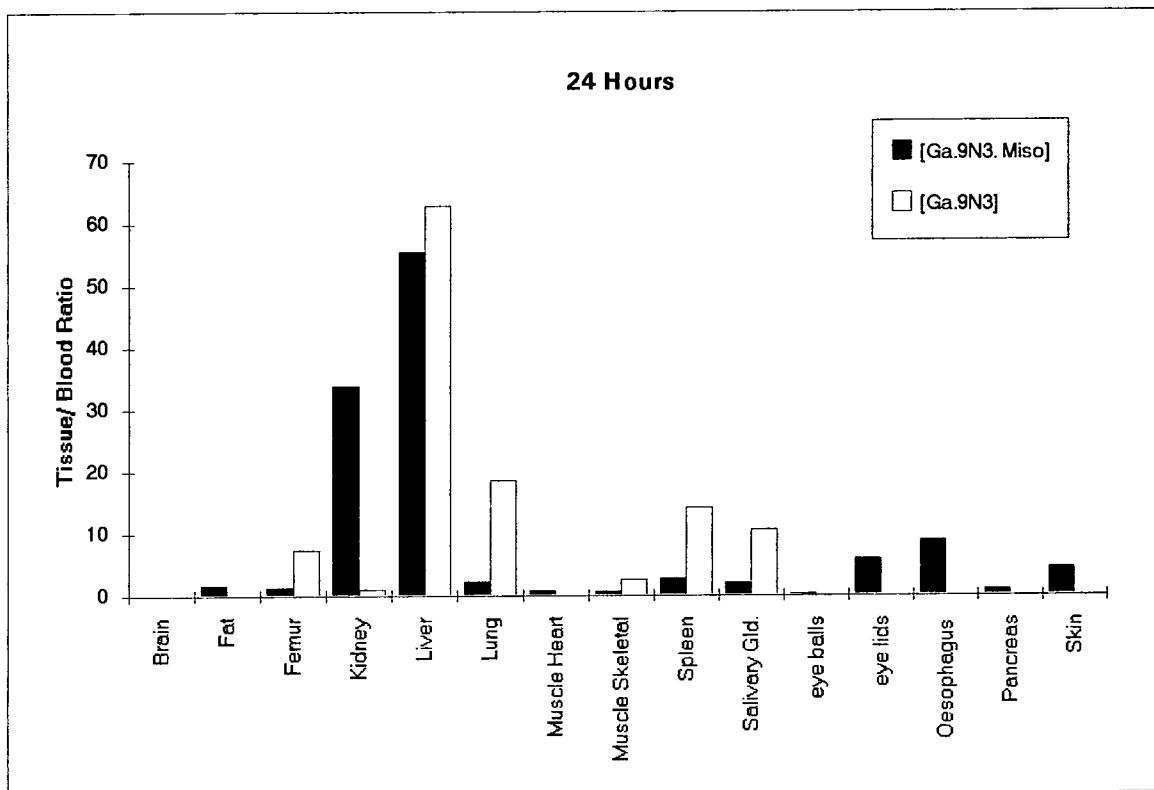
4.7.2. Results

From the information reported in figures 4.47 to 4.56 it can be concluded that the major difference between the biodistribution of [Ga.9N3] and [Ga.9N3.Miso] is that [Ga.9N3.Miso] is eliminated from the mouse by hepatobiliary as well as renal excretion. This is in line with the findings of L.M. Cobb et al, that both ^{14}C and ^{3}H labelled Miso are cleared from the mouse by the hepatobiliary as well as renal routes. After 24 hours in both tumour bearing and normal mice (figures 4.51 and 4.55) there is less dose left in the femur, lung, spleen and tumour tissues from [Ga.9N3.Miso] than from [Ga.9N3]. This may be due to the quicker drop in blood dose (figure 4.54) for [Ga.9N3.Miso]. The low skeletal dose from [Ga.9N3.Miso] also reflects the high in vivo stability of this gallium macrocycle complex.

In order to assess whether any concentration of [Ga.9N3.Miso] was taking place in hypoxic tissues such as the

tumour, oesophagus or eyes, the tissue to blood ratios were calculated from the % dose/g values. These are plotted in figures 4.57 to 4.59 for mice bearing HX118 tumour and figures 4.60 and 4.61 for normal mice. The best tumour to blood contrast obtained is that at 4 hours from [Ga.9N3], this give a tumour to blood ratio of 22. The highest tumour to blood ratio obtained from [Ga.9N3.Miso] is a value of 16 at 8 hours.

The actual amounts of [Ga.9N3.Miso] retained after 24 hours in tissues such as the oesophagus, eye lids and lungs are very low, but figures 4.59 and 4.61 indicate that there is some retention of [Ga.9N3.Miso] over that in the blood. This together with the observed hepatobiliary excretion, is in agreement with the expected biological properties as seen for ^{14}C and ^{3}H Miso[74]. However, the only occasion where [Ga.9N3.Miso] shows any increased tissue to blood ratios over those of [Ga.9N3] is at 8 hours post injection where there are slightly higher tissue to blood ratios for the tumour and oesophagus (figure 4.58).

In conclusion, better tumour imaging can be obtained from the use of [Ga.9N3] without attaching it to Misonidazole.

4.8. [^{71}Ga.9N3] FOR NMR.

The principles of nuclear magnetic resonance imaging have been discussed in chapter 1 (section 1.3). Although it is the protons of water which are the most often studied in MRI, any nuclei which possess spin and a magnetic moment are suitable for detection by NMR. The ^{71}Ga isotope of gallium is suitable for detection by NMR at high strength fields. The chemical shift of the gallium nucleus is a sensitive probe of the symmetry and co-ordination environment of complexes of gallium. The complexation of ^{71}Ga to the macrocycle 9N3 generates a neutral complex of high solubility, low osmolality and high in vivo stability. The chemical shift of this complex in water is +172 ppm, with a relatively narrow linewidth of 200 Hz.

Figure 4.62. *NMR Spectra.*

(a) 100 μl of 20 mM [^{71}Ga.9N3] in PBS.
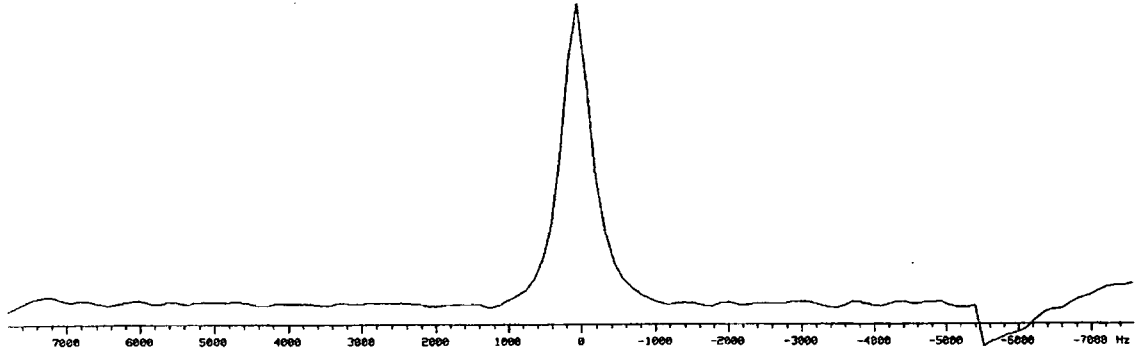
(b) HX 118 Tumour Mass.
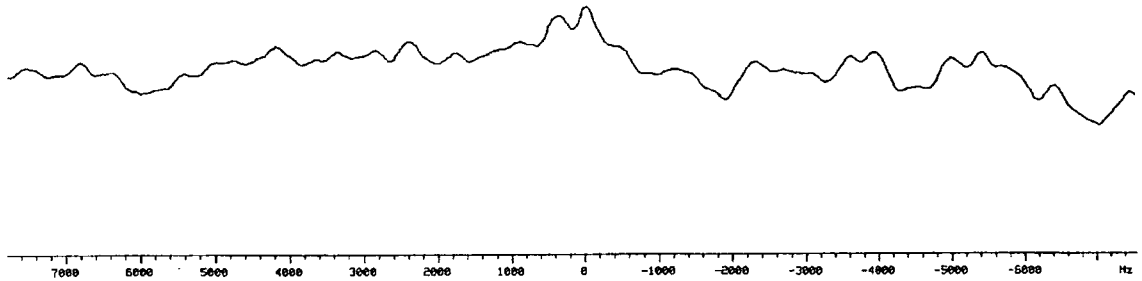
(c) 500 μl of Urine from the Mouse Post Injection of [^{71}Ga.9N3].
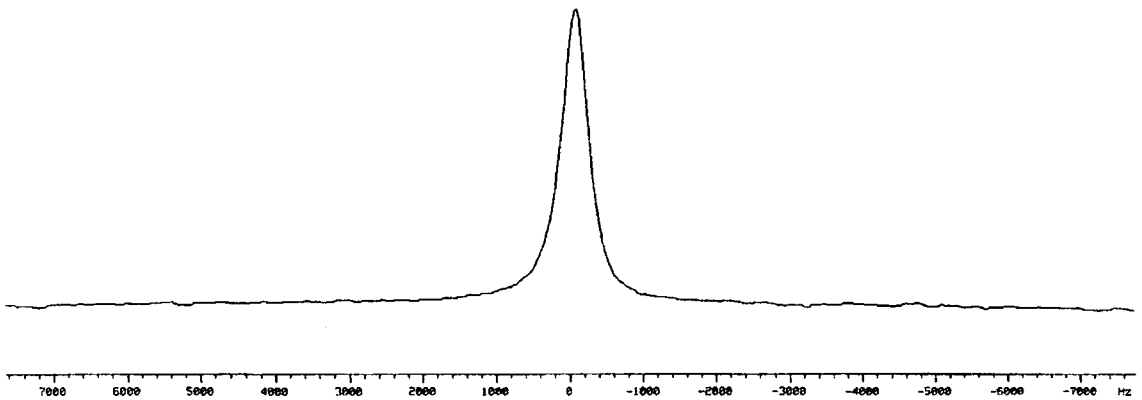
(d) [^{71}Ga.9N3] and ^{71}GaCl$_3$ reference standard
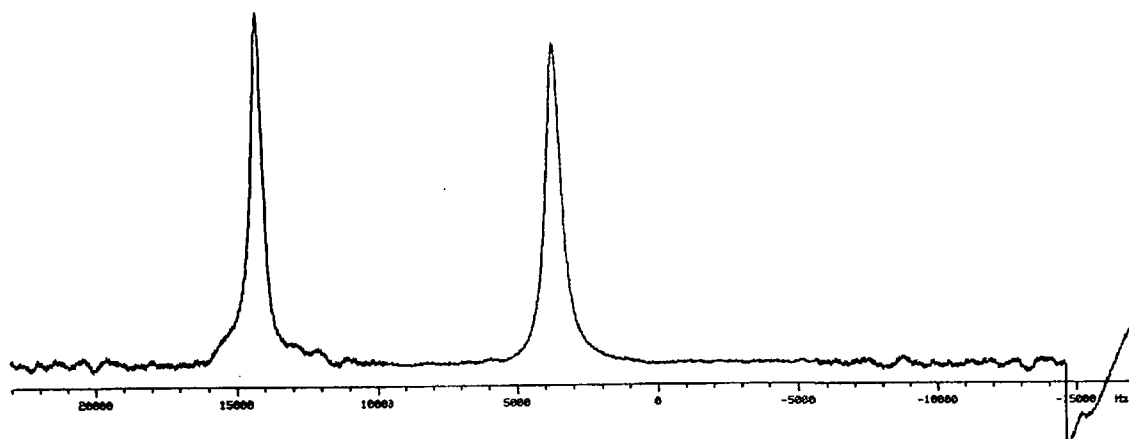
The [Ga.9N3] complex has already been shown to clear rapidly from the mouse via the kidneys (section 4.2), and to concentrate in xenografts of the human melanotic melanoma HX118 (section 4.6). In this experiment, a mouse bearing a xenograft of HX118 was injected with 250 μl of 20 mM [^{71}Ga.9N3] in PBS. After about 1 hour NMR spectra were obtained via a sample coil sitting either around the sample (liquid in a small vial) or directly above the tumour (still in situ in an anaesthetised mouse). Spectra were obtained for the following:-

(a) 100 μl of 20 mM [^{71}Ga.9N3] in PBS.

(b) HX 118 tumour mass.

(c) 500 μl of urine excreted from the mouse post injection of [^{71}Ga.9N3].

(d) Both [^{71}Ga.9N3] and ^{71}GaCl$_3$ as reference standards.

212

Conclusions

For the HX 118 tumour there was insufficient concentration of [^{71}Ga.9N3] to allow for proper detection, although there is a possible peak at the resonant frequency expected for [^{71}Ga.9N3], at 172 ppm, (δ_{Ga} = 0 ppm, for Ga(H$_2$O)$_6^{3+}$).

The urine sample has a clear signal for [^{71}Ga.9N3] as opposed to ^{71}GaCl$_3$ indicating that the gallium complex has been excreted intact.

4.9. GALLIUM AND INDIUM EXPERIMENTAL.

Throughout the following experimental procedures, gold label quality chemicals and metal free plastic ware were used to reduce any metal contamination. The suppliers of apparatus and reagents used, together with the purity of reagents are listed in Appendix I. Gallium-67 was supplied as gallium chloride in 0.04M HCl carrier free, >10 mCi/mg Ga.(>370 MBq/mg Ga), t1/2= 78 hours, γ's= 93, 185 and 300 KeV. Indium-111 was supplies as indium chloride in 0.04M HCl carrier free. t^1/$_2$= 67 hours, γ's= 171 and 245 KeV.

4.9.1. Preparation of Gallium and Indium Macrocycle Complexes for Biological Use

The methods of preparation of the gallium and indium macrocycle complexes were very similar. The radioactive solutions of both gallium-67 and indium-111 were both essentially carrier free. The ^{67}Ga was >10 mCi/mg Ga, i.e. a 100 μCi sample of ^{67}Ga contained <10 ng of stable Ga (<0.014 nmoles). The ^{111}In was also >10 mCi/mg In, i.e. a 100 μCi sample of ^{111}In contained <10 ng of stable In (<0.009 nmoles).

Maximum labelling efficiency was achieved with the addition of 10% carrier to the reaction mixture. The amount of contaminating cations present in the reaction mixtures was

kept to the minimum by the use of high purity (e.g. Aldrich 'gold label') chemicals and metal free plastics throughout.

The metal macrocycle complexes were purified by HPLC after the addition of DTPA to bind any unreacted gallium or indium. Formation of the $[Ga.DTPA]^{2-}$ or $[In.DTPA]^{2-}$ complex not only prevented contamination of the HPLC column with radioactivity, but also provided the means by which the percentage labelling of gallium or indium macrocycle complex could be measured accurately. A 10 fold molar excess of DTPA over macrocycle was sufficient to complex all unreacted Ga^{3+}, In^{3+} or any other cations which may have been present. When testing very small amounts e.g. 1 μl of 2 mM macrocycle solution, a 50 times molar excess of DTPA over macrocycle was used to complex any small absolute amounts of contaminating cations.

All the gallium and indium complexes were prepared by methods similar to those employed for the preparation of [Ga.9N3]. For the indium complexes, ^{111}In and $InCl_3$ carrier were used. This method is set out below with any variations used in the other preparations listed in Table 4.5 and 4.6.

Preparation of [Ga.9N3]

250 μl of a solution containing 200 mM ammonium acetate pH 5.0, 2 mM 9N3, 0.2 mM $GaCl_3$ (10% carrier) + 100-200 μCi ^{67}Ga, was incubated at 310K (37°C) for 30 minutes.

The formation of [Ga.9N3] and other complexes was measured at 30 minutes by adding 1 μl of the reaction mixture to 50 times molar excess of DTPA over macrocycle (2 μl of 100 mM DTPA). This was then made up to 100 μl with HPLC running buffer (0.2 M ammonium acetate pH 6.8, 10% acetonitrile with AX300 column, or 0.15 M ammonium acetate pH 6.8 with Poros Q/M column) and incubated for 5 minutes. The percentage labelling was then analysed by anion exchange HPLC. If the % of [Ga.9N3] or of the other complexes was >90% the reaction mixture was quenched with DTPA. If the labelling was less than 90% the reaction mixture was incubated for a further period at 37°C and the percentage complex formation re-

examined. When there was no further increase in complex formation the reaction mixture was quenched by adding 10 μl of 500 mM DTPA (10 times molar excess over macrocycle). This mixture was then separated by HPLC, the [Ga.9N3] (or other complex) peak being collected manually (dropwise into a polyethylene tube).

For [Ga.9N3] and [In.9N3] the labelling efficiency was usually greater than 98%. On an AX300 anion exchange column run at 1 ml/min with 0.2 M ammonium acetate pH 6.8, 10% acetonitrile running buffer, [Ga.9N3] elutes at 3.9 min followed by [Ga.DTPA]$^{2-}$ at about 17 minutes.

On a Poros Q/M anion exchange column run at 2 ml/min with 0.15 M ammonium acetate pH 6.8 running buffer, [In.9N3] elutes at 1.0 min followed by [In.DTPA]$^{2-}$ at 2.1 minutes.

Table 4.5. *Preparation of Gallium Complexes.*

Gallium Complex	Variation from [Ga.9N3] prep.	% labelling	Elution time (min) AX300	Poros Q/M
9N3		99	3.9	
9N3Me3C3	no carrier	99	4.1	
9N3C3Ph3		93	4.3	1.0
9N3P3Me3		99	3.6	
9N3P3iPr3		88		0.9
9N3P3Ph3		86	4.6	
9N3P3Bz3		86		1.0
DTPA			17	2.1
9N3.Miso	4mM 9N3.Miso 50% carrier	95	4.4	

Table 4.6. *Preparation of Indium Complexes.*

Indium Complex	Variation from [In.9N3] prep.	% labelling	Elution time (min) AX300	Poros Q/M
9N3		98		1.0
9N3Me3C3		98		1.0
9N3C3Ph3	3 hour incubation	70	4.3	1.1
9N3P3Me3		94		0.9
9N3P3iPr3	1 hour incubation	75		0.9
9N3P3Ph3		79		1.0
9N3P3Bz3	18 hour incubation	76		1.1
DTPA				2.1

4.9.2. Partition Coefficients of Indium Complexes

The indium macrocycle complexes were prepared as described in section 4.9.1.

The method followed for the measurement of partition coefficients was the same as that for the gadolinium complexes in section 2.6.3.

A typical data set is given below for [In.9N3P3Ph3]

	P	Log P		P	Log p
Octanol/Water	2.44	0.39	Octanol/PBS	1.71	0.23
0.5 ml/0.5 ml	2.67	0.43	0.5 ml/0.5 ml	1.74	0.24
Octanol/Water	0.98	-0.01	Octanol/PBS	0.82	-0.08
0.75 ml/0.25 ml	1.09	0.04	0.75 ml/0.25 ml	0.87	-0.06
Octanol/Water	3.46	0.54	Octanol/PBS	3.44	0.54
0.25 ml/0.75 ml	4.04	0.61	0.25 ml/0.75 ml	3.56	-0.55
Average	2.45	0.33	**Average**	2.02	0.24
SD	*1.23*	*0.26*	SD	*1.21*	*0.28*

	P	Log P		P	Log p
Butanol/Water	4.63	0.67	Butanol/PBS	2.96	0.47
0.5 ml/0.5 ml	4.79	0.68	0.5 ml/0.5 ml	3.00	0.48
Butanol/Water	2.21	0.34	Butanol/PBS	1.74	0.24
0.75 ml/0.25 ml	2.38	0.38	0.75 ml/0.25 ml	1.75	0.24
Butanol/Water	7.13	0.85	Butanol/PBS	5.58	0.75
0.25 ml/0.75 ml	7.57	0.88	0.25 ml/0.75 ml	5.91	0.77
Average	4.78	0.63	**Average**	3.49	0.49
SD	*2.27*	*0.23*	SD	*1.84*	*0.23*

Table 4.7. *A Summary of Partition Coefficients for Indium Macrocycles.*

Indium Complex	Octanol \Water LOG P	SD	Octanol \PBS LOG P	SD	Butanol \Water LOG P	SD	Butanol \PBS LOG P	SD
9N3	-4.92	*0.29*	-4.51	*0.46*	-2.54	*0.04*	-2.98	*0.04*
9N3Me3C3	-3.38	*0.07*	-3.62	*0.21*	-1.79	*0.03*	-2.22	*0.01*
9N3P3Me3	-3.80	*0.11*	-3.68	*0.31*	-1.88	*0.02*	-2.06	*0.01*
9N3P3iPr3	-1.92	*0.02*	-1.89	*0.04*	-0.98	*0.12*	-0.99	*0.13*
9N3P3Ph3	0.33	*0.26*	0.24	*0.28*	0.63	*0.23*	0.49	*0.23*
9N3P3Bz3	0.13	*0.22*	0.10	*0.21*	0.54	*0.20*	0.34	*0.21*

4.9.3. Biodistribution Studies

Biodistribution studies were carried out on 7 gallium and 7 indium complexes whose preparations are described in section 4.9.1. All complexes had their purity checked by HPLC before injection into animals.

The biodistributions were conducted on congenitally athymic nude male mice (MFI-nu/nu/Ola/Hsd) aged 13 to 16 weeks with an average weight of 36 g. Between three and five mice were killed for each complex at each time point.

Gallium or indium complexes were administered intra venously via the tail vein at a dose of approx. 0.1 μmol/kg, 7.5 μCi/mouse.

Mice were killed by an intra-peritoneal injection of pentobarbitone. A sample of cardiac blood was taken and the following tissues dissected:- brain, both femurs, both kidneys, liver, gall bladder, lungs, heart muscle, salivary glands, spleen, stomach, small intestine (from the pyloric sphincter to the start of the caecum), caecum, large intestine, samples of fat, skeletal muscle and skin.

All samples were weighed with the exception of the gut. For calculations of total tissue dose, the mass of both the blood and the skeleton were taken as 10% of the body weight. Tissue samples were assayed by the same methodology as used for ^{153}Gd samples in section 2.6.3.

Summary tables are presented in Chapter 4.2 and 4.3.

4.9.4. Tumour Localisation studies.

The mice used for these studies were congenitally athymic nude mice (MFI-nu/nu/Ola/Hsol) as used in the above studies. Mice aged 8 to 10 weeks were injected subcutaneously in each flank with a suspension of cells from the regularly passaged human melanotic melanoma HX 118. After 6 to 8 weeks when the tumours had grown to a size of at least 0.05 ml, they were used for tumour localisation studies. Gallium or indium complexes were injected via the tail vein at a dose of 10 to 25 μCi per mouse. Mice were killed at set times after

administration of the labelled complex by intraperitoneal injection of pentobarbitone. Blood and tissue samples were taken and analysed as previously.

4.10. REFERENCES

1.   H.C. Dudley, G.E. Maddox and H.C. LaRue, *J. Pharm. Exp. Ther.*, 1949, <u>96</u>, 135-138.

2.   *'CRC Handbook of Chemistry and Physics'*, 74th edition, 1993-94, Ed. D.R. Lide.

3.   *'Radionuclide Transformations'.Annals of the ICRP*, publication 38, 1983, Vol 11-13.

4.   H.D. Bruner, R.L. Hayes, J.D. Perkinson, *Radiology,* 1953, <u>61</u>, 602-611.

5.   R.L. Hayes, J.E. Carlton and B.L. Byrd, *J. Nucl.Med.*, 1965, <u>6</u>, 605-610.

6.   P. Hoffer, *J. Nucl. Med.*, 1980, <u>21</u>, 282-285.

7.   P.B. Hoffer, J. Huberty and H. Khayam-Bashi, *J. Nucl.Med.*, 1977, <u>18</u>, 713-717.

8..   S.M. Moerlein, M.J. Welch and K.N. Raymond, *J. Nucl.Med.*, 1982, <u>23</u>, 501-506.

9.   S.R. Vallabhajosula, J.F. Harwig, J.K. Siamsen and W. Wolf, *J. Nucl. Med.*, 1980, <u>21</u>, 650-656.

10.   C.L. Edwards and R.L. Hayes, *J. Nucl. Med.*, 1969, <u>10</u>, 103-105.

11.   T. Higasi, Y. Nakayama, A. Murata, K. Nakamura, M. Sugiyama, T. Kawaguchi and S. Suzuki, *J. Nucl. Med.*, 1972, <u>13</u>, 196-201.

12.   M. Hayward and G. Sing,. *Nucl. Med. Comm.*, April 1986.

13.   M-H. Sohn, B.J. Jones, J.H. Whiting, Jr., F.L. Datz, R.E. Lynch and K.A. Morton, *J. Nucl. Med.*, 1993, <u>34</u>, 2135-2143.

14. O. Israel and D. Font, *J. Nucl. Med.*, 1993, <u>34</u>, 1330-1331.

15. W.D. Kaplan, M.S. Jochelson, T.S. Herman, L.M. Nadler, P.C. Stomper, T. Takvorian, J.W. Andersen and G.P. Canellos, *J. Clinical Oncology*, 1990, <u>8</u>, 1966-1970.

16. P.M. Smith-Jones, B. Stolz, C. Bruns, R. Albert, H.W. Reist, R. Fridrich and H.R. Mäcke, *J. Nucl. Med.*, 1994, <u>35</u>, 317-325.

17. B. Kumar, T.R. Miller, B.A. Siegel, C.J. Mathias, J. Markham, G.J. Ehrhardt and M.J. Welch. *Am. J. Roentgenol.*, 1981, <u>136</u>, 685-690.

18. M.J. Welch, M.L. Thakur, R.E. Coleman, M. Patel, B.A. Siegel and M.M. Ter-Pogossian. *J. Nucl. Med.*, 1977, <u>18</u>, 558-562.

19. H.F. Kung, B.L. Lui, D. Mankoff, M.P. Kung, J.J. Billings, L. Francesconi and A. Alavi, *J. Nucl. Med.*, 1990, <u>31</u>, 1635-1640.

20. M.A. Green, M.J. Welch, C.J. Mathias, K.A.A. Fox, R.M. Knabb and J.C. Huffman, *J. Nucl. Med.*, 1985, <u>26</u>, 170-180.

21. M.A. Green, C.J. Mathias, W.L. Neumann, P.E. Fanwick, M. Janik and E.A. Deutsch, *J. Nucl. Med.*, 1993, <u>34</u>, 228-233.

22. B.W. Tsang, C.J. Mathias and M.A. Green, *J. Nucl. Med.*, 1993, <u>34</u>, 1127-1131.

23. J. Schuhmacher, R. Matys, H. Hauser, W. Maier-Borst and S. Matzku, *Eur. J. Nucl. Med.*, 1986, <u>12</u>, 397-404.

24. C.J. Mathias, Y Sun, M.J. Welch, M.A. Green, J.A. Thomas, K.R. Wade and A.E. Martell, *Nucl. Med. Biol.*, 1988, <u>15</u>, 69-81.

25. M.A. Green, M.J. Welch, C.J. Mathias, P.Taylor and A.E. Martell, *Int. J. Nucl. Med. Biol.*, 1985, <u>12</u>, 381-386.

26. S.L. Madsen, C.J. Bannochie, A.E. Martell, C.J. Mathis and M.J. Welch, *J. Nucl. Med.*, 1990, <u>31</u>, 1662-1668.

27. E. Cole, D. Parker, G. Ferguson, J.F. Gallagher and B. Kaitner, *J. Chem. Soc., Chem. Commun.*, 1991, 1473-1475.

28. C.J. Broan, K.J. Jankowski, R. Kataky and D. Parker, *J. Chem. Soc., Chem. Commun.*, 1990, 1738-1739.

29. D. Parker, *Chem. Soc. Rev.*, 1990, 19, 271-291.

30. D.A. Moore, P.E. Fanwick and M.J. Welch, *Inorg. Chem.*, 1989, 28, 1504-1506.

31. D.J. Hnatowich, *Int.J. App. Radiat. and Isotopes*, 1977, 28, 169-181.

32. M.L. Thakur, *Int.J. App. Radiat. and Isotopes*, 1977, 28, 183-201.

33. D.A. Goodwin, R.A. Finston, L.G. Colombetti, J.E. Beaver and H. Hupf, *Radiology*, 1970, 94, 175-178.

34. D.A. Goodwin, *J. Nucl.Med.*, 1971, 12, 580-582.

35. D.A. Goodwin, C. Hun Song, R. Finston and P. Matin, *Radiology*, 1973, 108, 91-98.

36. M.J. Welch and S. Moerlein, *Inorg. Chem. Biol. Med.*, 1980, 7, 121-140.

37. M.B. Doherty, J.T. Bushberg, M.J. Lipton *et al.*, *Clinical Nucl.Med.*, 1978, 3, 108.

38. M.L. Thakur, M.J. Welch, J.H. Joist and R.E. Coleman, *J. Nucl.Med.*, 1976, 17, 561.

39. E.P. Krenning, W.H. Bakker, P.P.M. Kooij, W.A.P. Breeman, H.Y. Oei, M. de Jong, J.C. Reubi, T.J. Visser, C. Bruns, D.J. Kwekkwboom, A.E.M. Reijs, P.M. van Hagen, J.W. Koper and S.W.J. Lamberts, *J. Nucl. Med.*, 1992, 33, 653-658.

40. M. De Jong, W.H. Bakker, W.A.P. Breeman, M.E. van der Pluijm, P.P.M. Kooij, T.J. Visser, R. Docter and E.P. Krenning, *J. Nucl. Med.*, 1993, 34, 2025-2030.

41. M.W. Brechbiel, O.A. Gansow, R.W. Atcher, J. Schlom, J. Esteban, D.E. Simpson and D. Colcher, *Inorg. Chem.*, 1986, 25, 2772-2781.

42. J.A. Carrasquillo, P.G. Abrams, R.W. Schoff, *et al.*, *J. Nucl. Med.*, 1988, 29, 39-47.

43. W.B. Webster, S.J. Harwood, R.G. Carroll and M.A. Morrissey, *J. Nucl. Med.*, 1992, 33, 498-504.

44. E. Lipcon Kramer, S.J. DeNardo, L. Liebes, *et al.*, *J. Nucl. Med.*, 1993, 34, 1067-1074.

45. P. Peltier, C. Curtet, J-F. Chatal, *et al.*, *J. Nucl. Med.*, 1993, 34, 1267-1273.

46. J-M. Le Doussal, A. Chetanneau, A. Gruaz-Gruyon, *et al.*, *J. Nucl. Med.*, 1993, 34, 1662-1671.

47. J.R. Buscombe, W.J.C. Oyen, A. Grant, R.A.M.J. Claessers, J. van der Meer, F.H.M. Corstens, P.J. Ell and R.F. Miller, *J. Nucl. Med.*, 1993, 34, 1621-1625.

48. F.L. Datz, C.E. Anderson, R. Ahluwalia, *et al.*, *J. Nucl. Med.*, 1994, 35, 74-83.

49. A.S. Craig, I.M. Helps, K.J. Jankowski, D. Parker, N.R.A. Beeley, B.A. Boyce, M.A.W. Eaton, A.T. Millican, K. Miller, A. Phipps, S.K. Rhind, A. Harrison and C. Walker, *J. Chem. Soc., Chem. Commun.*, 1989, 794-796.

50. J.P.L. Cox, A.S. Craig, I.M. Helps, K.J. Jankowski, D. Parker, M.A.W. Eaton, A.T. Millican, K. Millar, N.R.A. Beeley and B.A. Boyce, *J. Chem. Sos. Perkins, Trans. 1*, 1990, 2567-2576.

51. E.T. Clarke and A.E. Martell, *Inorganica Chimica Acta*, 1991, 181, 273-280.

52. J.A. Greager, T-C. Chao, M.J. Blend, R.W. Atcher, O.A. Gansow, M.W. Brechbiel and T.K. Das Gupta, *J. Nucl. Med.*, 1990, 31, 1378-1383.

53. S.J. Wagner and M.J. Welch, *J. Nucl.Med.*, 1979, 20, 428-433.

54. S.L. Madsen, C.J. Bannochie, M.J. Welch, C.J. Mathias and A.E. Martell, *Nucl. Med. Biol.*, 1991, 18, 289-294.

55. Y. Sun, C.J. Mathias, M.J. Welch, S.L. Madsen and A.E. Martell, *Nucl. Med. Biol.*, 1991, 18, 323-330.

56. A.S. Craig, D. Parker, H. Adams and N.A. Bailey, J. Chem. Soc., Chem. Commun., 1989, 1793-1794.

57. C.J. Broan, J.P.L. Cox, A.S. Craig, R. Kataky, D. Parker, A. Harrison, A. Randall, and G. Ferguson, *J. Chem. Soc. Perkin Trans. 2*, 1991, 87-99.

58. R.C. Matthews, D. Parker, G. Ferguson, B. Kaitner, A. Harrison, and L. Royle, *Polyhedron*, 1991, <u>10</u>, 1951-1953.

59. R.D. Hancock and A.E. Martell, *Chem. Rev.*, 1989, <u>89</u>, 1875-1914.

60. E. Brucher and A.D. Sherry, *Inorg. Chem.*, 1990, <u>29</u>, 1555-1559.

61. K. Shomäcker, G.J. Beyer, W.G. Franke and S.K. Shukla, *Isotopenpraxis*, 1990, <u>26</u>, 145-149.

62. W.P. Cacheris, S.K. Nickle and A.D. Sherry, *Inorg. Chem.*, 1987, <u>26</u>, 958-960.

63. D.A. Moore, M.J. Welch, K.R. Wade, A.E. Martell and R.J. Motekaitis, *J. Labelled Compd. Radiopharm.*, 1989, <u>26</u>, 362-363.

64. D.A. Moore, P.E. Fanwick and M.J. Welch, *Inorg. Chem.*, 1990, <u>29</u>, 672-676.

65. J.D. Chapman, J. Lee and B.E. Meeker, *Int. J. Radiat. Oncology Biol. Phys.*, 1989, <u>16</u>, 911-917.

66. L.M. Cobb, J. Nolan and T. Hacker, *Br. J. Cancer*, 1990, <u>61</u>, 524-529.

67. K.E. Linder, J. Cyr, Y.M. Chan, N. Raju, K. Ramalingam, D.P. Nowotnik and A.D. Nunn, *J. Nucl. Med.*, 1992, <u>33</u>, 919.

68. R.J. Di Rocco, A. Bauer, B.L. Kuczynski, J.P. Pirro, K.E. Linder, R.K. Narra and A.D. Nunn, *J. Nucl. Med.*, 1992, <u>33</u>, 865.

69. J.M. Walling, J. Deacon, S. Holliday and I.J. Stratford, *Cancer Chemother. Pharmacol.* 1989, <u>24</u>, 28-32.

70. L.M. Cobb, J. Nolan and S. Butler, *Int. J. Radiat. Oncology Biol. Phys.*, 1990, <u>18</u>, 347-351.

APPENDIX I

REAGENTS

Radioisotopes

Radioisotopes were purchased from Amersham International plc.

Gadolinium-153 as Gadolinium chloride in 0.1M HCl, 0.5-5
    mCi/mg Gd.(18.5-185 MBq/mg Gd), t1/2= 242 days, γ= 97-103
    KeV, X-rays= 41-47 KeV.

Yttrium-90 as Yttrium chloride in 0.02M HCl carrier free.
    $t^1/_2$= 64 hours, β^- average energy 0.935 MeV.

Gallium-67 as Gallium chloride in 0.04M HCl carrier free, >10
    mCi/mg Ga.(>370 MBq/mg Ga), t1/2= 78 hours, γ's= 93, 185
    and 300 KeV.

Indium-111 as Indium chloride in 0.04M HCl carrier free.
    $t^1/_2$= 67 hours, γ's= 171 and 245 KeV.

Reagents used in the preparation of ligand-metal complexes

All chemicals used were of high purity ;-
Acetic acid 99+%, gold label, (Aldrich).
Ammonium acetate 99+%, gold label, (Aldrich).
BOPTA, donated by Bracco Industria Chimica, SpA, Milan,
    Italy.
Citric acid anhydrous 99+%, gold label, (Aldrich).
DTPA anhydride, (Sigma).
Gadolinium(III) chloride hexahydrate 99.999%, gold label,
    (Aldrich).
Gallium(III) chloride 99.99+%, gold label, (Aldrich).
Hydrochloric acid 35.0%, <1ppm Fe, Aristar, (BDH).
Indium(III) chloride 99.999%, gold label, (Aldrich).

Macrocycles and DTPA(NHBz)$_2$ were synthesised in the Chemistry
   Department of Durham University by Professor D Parker, Dr
   K Pulukkody, Mr T Norman, Miss F Smith and Mr R Matthews.
9N3.Miso, Miss F Smith Durham University.
Potassium hydroxide pellets 99.99%, gold label (Aldrich).
Water was purified by a Milli Q system, (Millipore).
Yttrium chloride anhydrous 99.9%, gold label, (Aldrich).

Additional reagents

Acetonitrile, HPLC grade, (Aldrich).
Aldrithiol (Dithiodipyridine), (Aldrich).
Ammonium Acetate 98.0%, AnalaR grade,(BDH).
B72.3 monoclonal antibody, (Celltech Ltd.).
Butan-1-ol 99.5%, AnalaR grade, (BDH).
N ethyl maleimide, (Sigma).
[Gd.12N4P4Me4]$^-$, Dr.B. Boyce Celltech Ltd.
[Gd.12N4P4Bz4]$^-$, Dr K Pulukkody Durham University.
2-Iminothiolane.HCl [Trauts Reagent], (Pierce and Warriner
   (UK) Ltd).
Octan-1-ol 99%, GPR, (BDH).
Pentobarbitone, (Veterinary Drugs Co. PLC).
PBS, Phosphate Buffered Saline, Dulbeccos'A' tablets,(Oxoid).
Sodium dihydrogen orthophosphate, anhydrous, >99.0%, (Sigma)
Di-sodium hydrogen orthophosphate anhydrous, >99.0%, (Sigma).

APPARATUS

   All metal complexes were purified by HPLC performed on a
Hewlett Packard HPLC system consisting of a H.P.85B HPLC
controller, H.P. HPLC pump unit (HP 1090) connected to a
Beckman radioisotope detector (model 170) and an LKB chart
recorder. Columns used were SynChropak AX300 4.6 x 250 mm
analytical column (Hichrom Ltd.) or Poros Q/M 4.6 x 100 mm
analytical column (PerSeptive Biosystems).
   HPLC analysis of radiolabelled protein-macrocycle
conjugates was performed on an LKB HPLC system consisting of

an LKB 2150 HPLC pump, an LKB 2152 LC controller, an LKB 2158 UVICORD SD with a 280 nm filter to monitor protein concentration and a Beckman radioisotope detector (model 170) connected to an LKB chart recorder. Du Pont Bio Series GF-250 columns 9.4 x 250 mm were used (Hichrom Ltd.).

Ultra free-Mc Durapore 0.22 μm filters (Millipore(UK) Ltd.) were used for filtering high concentration macrocycle complexes before injection into mice.

All pipette tips (Anachem) and micro test tubes (BioRad Labs.) [500 μl and 1.5 ml] were metal free.

2 ml screw capped eppendorf tubes (Sarstendt) were used for partition coefficient experiments.

5 ml polyethylene vials (Hughes and Hughes) were used to hold radioactive samples for measurement on the LKB compugamma .

An eppendorf centrifuge 5415 (Anderman) was used to centrifuge all reaction mixtures.

Spectrophotometric measurements were made on a Beckman DU-50 series spectrophotometer.

Mini-monitors (Mini-instruments) were used to detect β and γ radioactivity.

A Compugamma (LKB Wallac) equipped with a 3" NaI(Tl) well type crystal was used to measure radioactivity in individual samples.

The pH of solutions was measured using a Whatman pH μ sensor, a Horiba compact pH meter C-1 (Whatman Scientific Ltd), or BDH pH strips. The pH strips had the advantage that samples as small as 0.5 μl could be removed and applied to the strip for measurement.

ADDRESSES OF SUPPLIERS.

Aldrich Chem. Co. Ltd. The Old Brickyard, New Road, Gillingham, Dorset. SP8 4JL.

Anderman and Co. Ltd. Central Ave, East Molesey, Surrey. KT8 0QZ.

Anachem. Charles St., Luton, Beds. LU2 0EB.

Amersham International plc. Lincoln Place, Green End, Aylesbury, Bucks. HP20 2TP.

Beckman Industrial. Queensway Industrial Estate, Glenrothes, Fife. KY7 5PU.

BDH. Merck Ltd., Hunter Boulevard, Magna Park, Lutterworth, Leics. LE17 4XN.

BioRad Labs. Ltd., BioRad House, Maylands Ave. Hemel Hempstead, Herts. HP2 7TD.

Celltech Ltd., 216 Bath Rd., Slough, Berks. SL1 4EN.

Hewlett Packard Ltd. Miller Ho. The Ring, Bracknell, Berks. RG12 1XN.

Hichrom. 1, The Markham Centre, Station Rd., Theale, Reading, Berks. RG7 4PE.

Hughes & Hughes. Unit 1F, Lowmoor Industrial Estate, Tonedale, Wellingon, Somerset. TA21 0A2

LKB (Wallac). Davy Ave., Knowlhill, Milton Keynes. MK5 8PH.

Millipore(UK) Ltd. The Boulevard, Blackmoor Lane, Watford, Herts. WD1 8YW.

Mini Instruments. 8, Station Industrial Estate, Burnham on Crouch, Essex. CM0 8RN.

Oxoid. Unipath Ltd, Basingstoke, Hampshire.RG24 0PW.

PerSeptive Biosystems. 38, Sidney St., Cambridge, Mass.02139, USA. UK supplier :- Progressive Research Systems Ltd., 7, Lonsdale, Linton, Cambridge. CB1 6LT.

Pharmacia LKB Biotechnology. Davy Avenue, Knowlhill, Milton Keynes. MK5 8PH.

Pierce & Warriner(UK) Ltd. 44, Upper Northgate St, Chester. CH1 4EF.

Sarstendt Ltd. 68, Boston Rd., Beaumont Leys, Leicester. LE4 1AW.

Schering Health Care Ltd., Burgess Hill, West Sussex. RG15 9NE.

Sigma Chemical Co. Ltd. Fancy Rd., Poole, Dorset. BH17 7BR.

Veterinary Drugs Co. PLC. Common Rd., Dunnington, York. YO1 5RU.

Whatman Scientific Ltd. St. Leonard's Rd., 20/20 Maidstone, Kent. ME16 0LS.

APPENDIX II

PUBLICATIONS

Matthews, R.C., Parker, D. Ferguson, G., Kaitner, B., Harrison, A., Royle, L., *Polyhedron*, 1991, <u>10</u>, 1951-1953.

Harrison, A., Walker, C.A., Pereira, K.A., Parker, D., Royle, L., Matthews, R.C., Craig, A.S., *Nuc. Med. Commun.*, 1992, <u>13</u>, 667-672.

Parker, D., Pulukkody, K., Norman, T.J., Harrison, A., Royle, L., Walker, C., *J.Chem. Soc. ,Chem. Comm.*, 1992, 1441-1443.

Pulukkody, K., Norman, T.J., Parker, D., Royle, L., Broan, C.J., *J. Chem. Soc., Perkin Trans. 2* ,1993, 605-620.

Harrison, A., Walker, C.A., Pereira, K.A., Parker, D., Royle, L., Pulukkody, K., Norman, T.J., *Magn.. Reson. Imaging*, 1993, <u>11</u>, 761-770.

Norman, T.J., Smith, F.C., Parker, D., Harrison, A., Royle, L., Walker, C.A., *Supramolecular Chemistry*, 1995, <u>4</u>, 305-308.